The University Of Sheffield.

Characterisation of the interaction of the cytoskeleton protein BacM and the Ras GTPase MglA of *Myxococcus xanthus*

A thesis submitted to the

Department of Molecular Biology and Biotechnology

University of Sheffield

Mohsen Almakrami

May 2023

Abstract

MglA is the master regulator of A- and S-motility, and one of three RasGTPases, MXAN_1925 (MglA), MXAN_6703 (SofG), and MXAN_2495 of the soil bacterium *Myxococcus xanthus*. Besides motility, MglA plays key roles in cell division, polarity, fruiting body formation, and sporulation. Recent research has revealed that MglA and SofG specifically interact with bactofilin cytoskeletal proteins, suggesting that this interaction has important functional implications. Using a novel luciferase-based protein-protein two-hybrid system, it was shown that two out of four tested MglA-BacM pairs from the non-myxobacterial prokaryotes, *Leptothrix mobilis* and *Bdellovibrio bacteriovorus*, interacted specifically with each other in *M. xanthus*. This indicates that RasGTPase binding to bactofilins is a broadly conserved function. Importantly, a previously reported SofG-BacP interaction could not be confirmed, as SofG only bound to BacM in the luciferase assay.

To understand how MglA controls these different processes, its cellular localization was studied using differently tagged versions of the protein. Unfortunately, N- and C-terminal eYFP-tagged MglAs were either unable to complement the *ΔmglA* phenotype or only able to restore motility at single-cell but not colony level. Full complementation, including colony-level motility, was only observed using MglA tagged with the small six-amino-acid-long TC tag. Using fluorescence light microscopy, the TC-tagged MglA also showed the previously described characteristic intracellular distribution, a large unipolar cluster with smaller lateral clusters. Expression of eYFP-MglA in yeast cells resulted in mitochondrial staining, suggesting that MglA may bind to cardiolipin-containing membranes, which are also found at the poles of *M. xanthus* cells.

Various bacterial and eukaryotic MglA homologues were used to test their ability to restore motility, colony expansion, fruiting body formation, and sporulation in *ΔmglA*. With the exception of the 99% identical $MglA_{stigm}$ from the closely related myxobacterium *S. aurantiaca*, no other tested pro- or eukaryotic homologue, including mutated versions, was able to complement *ΔmglA*. Importantly, in contrast to an earlier report, Sar1 from yeast was unable to rescue fruiting body spore formation, but instead formed glycerol spores upon starvation. Finally, mutated MglA was unsuccessfully used to detect potential post-translational modifications, indicating that other methods such as mass spectrometry may have to be employed in the future.

Acknowledgements

I thank Allah with deep gratitude who gave me the opportunity to do this thesis.

First, I would like to express my gratitude and appreciation to my supervisor Dr Egbert Hoiczyk for his efforts and guidelines and the inspiration to work on this project I appreciate his patience, enthusiasm, motivation and the knowledge that help me in my research and thesis writing.

Secondly, I would like to thank Koen Semeijn for his time, support, training, advice that help me day by day through my PhD journey. I do appreciate that.

Thirdly I would like to thank the lab members on the Hoiczyk lab Jeffery So, Harry B Mcdowell Asim AS Alsenani, Eleojo A Nwokeoji , Shuang Li. for all their valuable support and assistance during my time in the lab.

I would like also to thank member of the Hettema lab for their help and assistance, in particular Abdulaziz alqahtani and Ibrahim Somily. Last but not the least I would like to thank Nick Mackey for proofreading my English.

Finally, my gratitude goes to my family, the soul of my father Mansour and my mom Wafg, my wife Jood, kids Myar, Mansour, Ibrahim and Ward as well as all my brother and sisters. I would like to thank them for their pray, support, motivation and patience.

Table of contents

List of figures:

List of tables

List of abbreviations

aa: Amino acid

ATP: Adenylate triphosphate

A-motility: Adventurous motility

BLAST: Basic local alignment tool

Cryo-EM: Cryo-electron microscopy

COPI: Coat protein complex I

COPIl: Coat protein complex II

CFP: Cyan fluorescent protein

CTPM: Casitone, tris, magnesium sulphate, and potassium phosphate media

CTT: Casitone, tris media

ddH2O: Double-distilled water

EM: Electron microscopy

FAC: Focal adhesion complex

eYFP: Enhanced yellow fluorescent protein

GAP: GTPase-activating protein

GDP: Guanosine diphosphate

GEF: Guanine exchange factor

GFP: Green fluorescent protein

GTP: Guanosine triphosphate

GTPase: GTP hydrolysing enzyme

HD: Host-dependent

HI: Host-independent

kDa: Kilo Dalton

LB: Lysogeny broth

Lg-bit: Large-bit luciferase

Sm-bit: Small-bit luciferase

MglA: Mutual gliding motility protein A

MglB: Mutual gliding motility protein B

MCS: Multiple cloning site

OD: Optical density

PCR: Polymerase chain reaction

RLU: Relative light units

Rom: Required for motility response regulator

SDS: Sodium dodecyl sulphate

S-motility: Social motility

SofG: Social motility function GTPase

T4P: Type IV pili

Sm-bit: Small bit luciferase fragment

TPM: Tris, potassium phosphate, magnesium sulphate media

TC: Tetra cysteine

WT: Wild-type

YFP: Yellow fluorescent protein

α5-helix: Alpha 5 helixes

β0β1- sheets: Beta 0 Beta 1 sheet

Introduction

Myxococcus xanthus is a Gram-negative bacterium that belongs to the phylum *Myxococcota* (Waite et al., 2020). The rod-shaped cells of this bacterium form swarms that consist of hundreds of thousands of individual cells that predate other bacteria or feed on decomposing organic matter (Copenhagen et al., 2020). As a soil bacterium, *M. xanthus* lives in a very diverse habitat and uses two types of motilities to move on different substrates. On moist substrates, the cells rely on S-motility, a type IV pili-powered form of motility, while on drier surfaces the cells use A-motility, a form of motility for which the motor is currently not clearly identified. Importantly, the only known protein that is essential for both, A- and S-motility is MglA, the master regulator of myxobacterial motility. MglA belongs to a class of proteins called small Ras GTPases that in eukaryotic cells are important regulators of various cellular functions including cell division, polarity and motility. In total, *M. xanthus* possesses three Ras GTPases, MglA, SofG and MXAN_2495. While the function of MglA in motility is well documented, SofG has been proposed to form a complex with the bactofilins BacN, BacO and BacP to control cell division and type IV pili activity, while the function of MXAN_2495 is currently unknown (Bulyha et al, 2013). Importantly, the precise mechanism with which MglA controls motility in *M. xanthus* is not well understood.

In a previous study in the laboratory protein-protein interaction assays had revealed that MglA binds to the cytoskeletal protein BacM (Semeijn, 2019). Therefore, this study aimed at investigating the interaction of MglA with BacM homologs from the following different four bacteria: *Bdellovibrio bacteriovorus*, *Leptothrix mobilis*, *Collimonas fungivorans,* and *Xanthomonas bromi*. These bacteria were selected because they represent evolutionary different phyla and possess both BacM and MglA homologes similar to *M. xanthus.* Moreover, various fluorescently tagged versions of these different non-myxobacterial MglAs were generated and used to study the localization of these protein in *M. xanthus* as well as their ability to complement the non-motile phenotype of a Δ*mglA* strain.

Chapter I: General introduction

1.1 The bacterial model organism *Myxococcus xanthus*

Myxococcus xanthus is a Gram-negative bacterium that belongs to the newly created phylum *Myxococcota* (Waite et al., 2020). The individual cells of this bacterium are long, flexible, rod-shaped cells that exist in multi-cellular swarms numbering in the hundreds of thousands of individual cells (Spormann, 1999; Copenhagen et al., 2020). Each *M. xanthus* cell has a diameter of about 0.5 μm, a length of about 4-8 μm and moves at a speed of about 2-4 μm/min across the surface of substrates (**Fig. 1**). During swarming, *M. xanthus* secretes lytic enzymes and toxic secondary metabolites that can either degrade organic macromolecules or stun and lyse a wide range of Gram-negative and Gram-positive bacteria to release nutrients for growth (Keane and Berleman, 2016). Interestingly, predation in *M. xanthus* is a facultative behaviour and occurs only when the organism is in proximity to potential prey cells (Thiery and Kaimer, 2020). Predation also helps to satisfy *M. xanthus'* peculiar need for valine, leucine, and isoleucine, as the organism lacks the biosynthetic pathways necessary to synthesize these three crucial amino acids. Vegetative cells of *M. xanthus* move as coordinated swarms, a behaviour that increases the efficiency of utilising insoluble nutrients better than single cells. This increase in efficiency is due to the fact that the cells of a swarm can pool hydrolytic enzymes and metabolites, thereby increasing their concentration within the environment, a strategy that has often been linked to the technique of wolf pack hunting.

While motility is important for swarming and hunting, it also plays a major role during developmental differentiation (**Fig. 1**). This important phase of the life cycle of *M. xanthus* is initiated when the cells run out of nutrients. Upon starvation, the cells start to drastically change their motility-driven behaviour. They initiate the synthesis of the hyperphosphorylated guanosine derivatives (p)ppGpp, stop swarming, and start instead moving towards each other.

This reversed movement results in the formation of large clumps of cells, called aggregation centres, which, over time through the attraction of more cells become fully formed mature fruiting bodies (Copenhagen et al., 2020). Inside the haystack-shaped fruiting bodies, approximately 80% of the aggregated *M. xanthus* cells will eventually lyse to liberate nutrients so that about 15% of the remaining cells can develop into spherical spores (Van Gestel et al., 2015), while the remaining 5% of cells differentiate into so-called peripheral rods that are highly motile cells scouting for nutrients to jump-start the formation of a new swarm. In contrast to other spore-forming bacteria, such as *Bacillus subtilis*, *M. xanthus* cells do not undergo cell division during spore formation, but the entire rod-shaped cell converts into an environmental stress-resistant spore. As a consequence, the spherical spores are diploid in contrast to the vegetative cells that possess only one chromosome (Tzeng and Singer, 2005; Harms et al., 2013). One possible reason for this peculiar strategy is that upon encountering nutrients, the germinated *M. xanthus* cells do not have to duplicate their chromosome during their first cell division and, therefore, can start their complex life cycle faster.

Overall, fruiting body formation is a highly complex form of developmental differentiation and depends on regulated changes in gene expression, intercellular communication, cell-to-cell signalling, regulation of the cell cycle, and motility. This complex social predatory and developmental lifestyle has made *M. xanthus* a model organism for investigating factors and processes that control and enable organisational complexity in bacteria (Zusman et al., 2007).

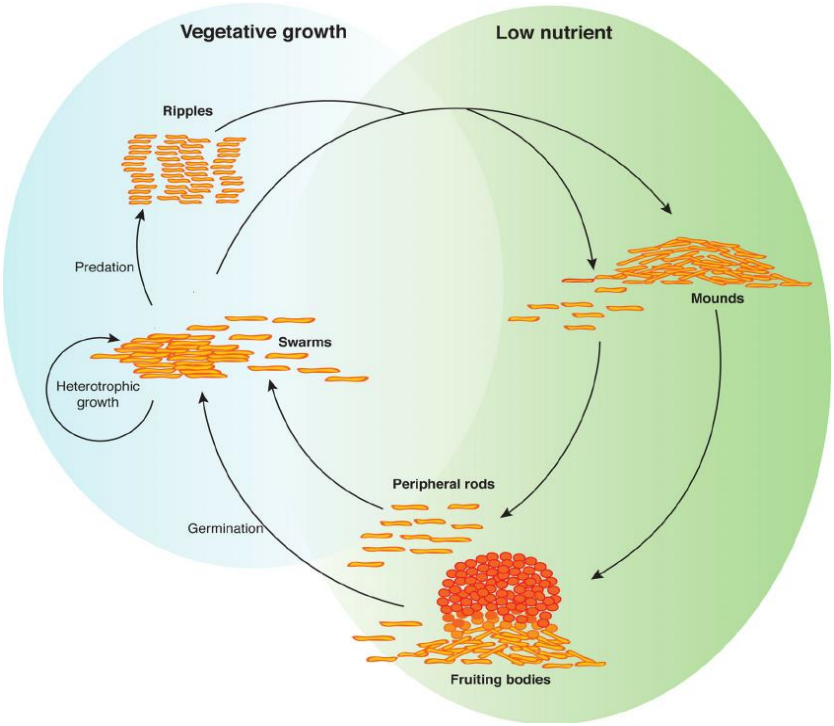

Figure 1: Life cycle of *M. xanthus*.
During its vegetative phase, *M. xanthus* cells forms large swarms that feed on decaying organic matter or prey on other bacteria (left). Upon starvation, the development phase is initiated, culminating in the formation of fruiting bodies filled with spores that are resistant to desiccation and heat. Image from Mauriello et al. (2010).

1.1.1 Motility systems of *M. xanthus*

M. xanthus possesses two distinct but coordinated forms of locomotion for its surface-associated motility. Social (S-) motility is powered by type IV pili (T4P) (Kaiser, 1979), while adventurous (A-) motility relies on an, as of yet not unequivocally identified, molecular motor (Wolgemuth et al., 2002; Nan and Zusman, 2011). Although both motility systems allow movement across substrates, they differ in important aspects. For example, S-motility requires cell-cell contacts and is used by groups of cells, while A-motility enables single-cell movement that allows individual cells to explore their surroundings (Schumacher and Søgaard-Andersen, 2017). Another important difference is the ability of these two systems to enable motility on very different substrates. While the S-motility system is essential for cell movement on soft and wet substrates, A-motility enables gliding motility of cells on hard and dry surfaces (Shi

and Zusman, 1993). Importantly, although A- and S-motility are coordinated, they are mechanistically independent. Mutant studies revealed that motile cells deficient in either A- or S-motility still retain wild type characteristics of the other motility system. However, double mutants (A^-S^-) are non-motile, suggesting that one or both systems are required for successful locomotion (Spormann, 1999).

1.1.1.1 A- and S- motility system

S-motility-driven locomotion is initiated when T4Ps are assembled at the leading pole of the cell, bind to exopolysaccharides, and then retract (Li et al., 2003). This retraction pulls the cells forward and enables locomotion on wet solid surfaces, independent of flagella (Shi and Sun, 2002). Usually, S-motility is stimulated when cells are in proximity to each other. As the extension and retraction of T4P are powered by the ATPases PilB and PilT, respectively, S-motility is ATP-dependent and contingent on the functionality of genes involved in the synthesis, processing, export, assembly, and function of the T4P machinery (Spormann, 1999; Chang et al., 2016). Genes identified to be associated with the S-motility system include the *pil* genes, but also a number of non-*pil* genes such as *frzA, mglA, tgl* etc. In *M. xanthus*, all *pil* genes have been identified and annotated with putative functions (**Fig. 2**) (Spormann, 1999; Chang et al., 2016).

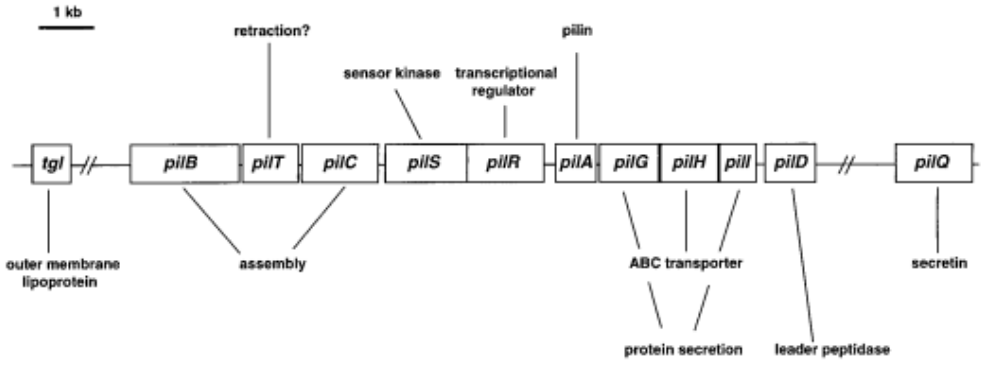

Figure 2: Schematic overview of genes involved in the S-motility system.
In *M. xanthus*, various *pil, frzA, mglA, tgl* genes, and others have been identified and annotated based on their putative functions. The majority of the pilus filament is made up of the pilin protein which is encoded by the *pilA* gene. The two-component regulatory system, PilS, and PilR, controls the regulation of this gene. PilR serves as a transcriptional activator, facilitating *pilA* expression, whereas the sensor kinase PilS is believed to impede it. In addition, *pilA* expression is autoregulated. Although *pilA* expression is activated under high-nutrient conditions and developmental circumstances, it does not depend on PilS or R. Figure from Spormann (1999).

In contrast to the S-motility system, the A-motility system is not linked to the activity of T4P or any other obvious molecular motor structure(s) and, therefore, is currently less well understood. Two principally different models have been proposed to account for A-motility: The focal adhesion (Mignot et al., 2007) and the slime nozzle model (Wolgemuth et al., 2002).

The focal adhesion model was initially developed by studying the behavior of the YFP-tagged protein AglZ in *M. xanthus*. Although AglZ is an essential protein for A-motility, it is not necessary for S-motility. Using time-lapse video microscopy of *M. xanthus* cells expressing AglZ-YFP, it was found that the tagged Ag1Z formed fluorescent clusters along the cell length that were localised at transient adhesion sites that stayed stationary, while the cell moved in the opposite direction (Mignot et al., 2007). This initial observation, together with genetic and protein-protein interaction studies, led to the discovery of the multi-protein Agl-Glt trans-envelope machinery. This machinery is thought to attach to the substratum using the peptidoglycan carbohydrate strands of the cell wall as helical tracks to move on. As the adhesion sites are fixed to the substratum, the movement of the intracellular parts of the complexes then moves the cells forward using the carbohydrate strands as tracks. Whereas the

S-motility machinery is polarly arranged, the Agl-Glt machinery is distributed along the entirety of the cell. Interestingly, motile cells which lacked S-motility moved at speeds unrelated to the length of the cell, which was even true when cells were artificially elongated using the antibiotic cephalexin. Hence, the number of A-motility clusters observed in cells appears to correlate with the speed of locomotion, supporting the idea that the focal adhesion sites generate the power for A-motility (Mignot et al., 2007).

According to the slime nozzle model, A-motility is powered by the secretion and swelling of a polyelectrolyte slime that is secreted from polarly arranged pores located in the outer membrane and part of a trans-envelope "nozzle" apparatus (Wolgemuth et al., 2002). Electron microscopy of isolated *M. xanthus* cell envelopes has shown that these nozzles are highly concentrated at both poles of the cells but also, more sparsely, present along the entire cell length (Wolgemuth et al., 2002). Light microscopy has confirmed that all cells capable of A-motility secrete slime, and that this secretion occurs at the lagging pole of the cells, which could explain how secretion can push the cells in the opposite direction. Moreover, *M. xanthus* mutant strains that are unable to move using A- motility either secrete no slime or slime from both the leading and lagging poles simultaneously (Yu and Kaiser, 2007). Finally, mathematical calculations support the plausibility of the slime nozzle model as the secretion and swelling of slime physically generate sufficient force to move the cells at the observed speeds (Wolgemuth et al., 2002).

So far, no consensus model has emerged, and it is currently unclear whether the two proposed model could be integrated into one general model for A-motility or whether only one of the two is correct (Nan, 2017). In part, progress on this subject has been hampered as important aspects of the two models are either speculative or simply unknown. For example, it is currently unclear how the outer membrane part of the focal adhesion complex binds to the carbohydrate strands of the peptidoglycan and how the cells would ensure that the movement

of this part is unidirectional from the front to the rear of the cell. As the carbohydrate strands are relatively short no real “tracks” exist that are long enough to guide the focal adhesion complexes along the entire length of the cells. Similarly, important aspects of the slime nozzle model are currently not known. To start, the chemical nature of the slime is currently unknown as the material has defied isolation and purification so far. Therefore, it is not only unclear whether the slime has the adhesive and expansive properties the model proposes, but research has not yet been able to generate a true slime-minus mutant that could shed light on the overall role of slime secretion in A-motility.

1.2 The bacterial cytoskeleton

The cytoskeleton is an intricate, dynamic network of interconnected protein filaments found in the cytoplasm of all cells. Initially discovered in eukaryotes, cytoskeletons are also present in bacteria and archaea, controlling the temporal and spatial organization of these cells. In their simplest form, cytoskeletons are scaffolds that support the cell's physical structure and distribute macromolecular complexes to particular subcellular locations.

Bioinformatics and comparative genomics have revealed that bacteria contain a wide range of polymer-forming proteins that play roles in cell polarity, morphogenesis, DNA segregation, and cell division. The best studied polymer-forming cytoskeletal proteins in bacteria are FtsZ and MreB, which are homologous to eukaryotic tubulin and actin, respectively, suggesting that the eukaryotic cytoskeleton can trace its evolutionary origins to bacterial and, more likely, to archaeal ancestors (Graumann, 2004; Pogliano, 2008; Thanbichler and Shapiro, 2008). In addition to FtsZ and MreB, bacterial cytoskeletal proteins include the intermediate filament-like protein crescentin, as well as proteins that have no counterparts in eukaryotes, such as Walker AB type ATPases and bactofilins.

The tubulin homologue FtsZ polymerizes into a contractile ring near the location of future cell divisions, emphasizing its significance in cytokinesis. During cell division, the FtsZ ring acts as a scaffold for the assembly of a multi-protein machinery called the divisome that executes cell divisions in bacteria (Bi and Lutkenhaus, 1991; Goehring and Beckwith, 2005). In contrast, the actin homologue MreB (and its various paralogues) is responsible for maintaining the specific shape of rod-like bacteria like *Escherichia coli* and *B. subtilis*. To do so, MreB polymerizes into short fibres that line the cytoplasmic membrane and serve to control the spatial distribution of peptidoglycan synthesizing enzyme complexes, responsible for the synthesis of the peptidoglycan sacculus in these bacteria. Initial light microscopic investigation suggested that MreB forms a solid cable-like helix spanning from the front to the rear of the cell (Jones et al, 2001). However, more recent research has shown that this appearance of a solid cable was an optical artefact, and that MreB forms instead about 200 nm long fibres that are sparsely distributed across the circumference of cells. Interestingly, MreB in some bacteria has also been implicated in chromosome segregation and cell polarity (Jones et al, 2001; Carballido-Lopez, 2006).

The third intensely studied bacterial cytoskeleton protein is crescentin, a coiled-coil protein closely related to eukaryotic intermediate filament proteins (Izard et al., 1999; Ausmees et al., 2003; Bagchi et al., 2008). Crescentin forms a polymeric cable at the concave side of *Caulobacter crescentus* cells and is responsible for the distinctive crescent shape of the organism (Ausmees et al., 2003). Unlike MreB, it appears to act purely mechanically by constraining longitudinal extension of the cell wall, resulting in uneven cell growth and bending (Cabeen et al., 2009). Interestingly, intermediate filament-like cytoskeleton proteins like crescentin polymerize differently compared to tubulin/actin-like proteins (FtsZ and MreB). While the latter polymerise dynamically in the presence of nucleotide cofactors, intermediate filament proteins assemble spontaneously to form stable filamentous structures both *in vitro*

and *in vivo* (Ausmees et al. 2003; Bagchi et al. 2008; Carballido-Lopez and Errington, 2003; Charbon et al. 2009; Mukherjee and Lutkenhaus, 1998).

1.2.1 Bactofilins: A new family of cytoskeletal proteins

Somewhat surprisingly, bacterial cytoskeleton proteins exhibit greater diversity than their eukaryotic counterparts, encompassing molecular structures and folds that have not yet been found in higher cells. One such class of bacterial cytoskeletal proteins is bactofilins. Bactofilins are widespread and conserved in bacteria, and although they polymerize nucleotide-independently into fibres, these structures are distinct from intermediate filament-like proteins such as crescentin (Kühn et al., 2010; Deng et al., 2019). Biochemically, bactofilins can be easily identified by their conserved DUF583 domain, which forms the major part of the filamentous protein and is flanked by variable, usually short N- and C-terminal regions. Recently, the atomic structure of the DUF583 domain has been determined by combining solid-state NMR and electron microscopic data. These studies revealed that the DUF583 domain adopts a right-handed β-helix architecture, in which 18 β-strand segments are arranged in six turns surrounding a hydrophobic triangular core (Vasa et al., 2015; Shi et al., 2015). Functional investigations using different bacteria have revealed that bactofilins play important roles in cell morphology, motility, and possible cell division.

The first ever identified bactofilin was CcmA (**c**urved **c**ell **m**orphology protein **A**) of *Proteus mirabilis* (Hay et al., 1999). This bactofilin was found during a transposon-based genetic screen that identified cells with morphological and motility defects. Importantly, this early study failed to recognize the cytoskeletal nature of CcmA but helped identify the conserved DUF583 domain, later found as a common structural motif in a large number of small proteins found across many bacteria. Moreover, the work in *P. mirabilis* also established

a possible role of bactofilins in motility, as both the transposon mutant and a *ccmA* null mutant produced elongated, irregular-shaped cells that could not swarm (Hay et al., 1999). Importantly, the cytoskeletal nature of bactofilins was later established when a number of CcmA homologs in various bacteria, including *Helicobacter pylori, C. crescentus*, and *M. xanthus* were investigated in more detail (Kühn et al., 2010; Sycuro et al., 2010; Koch et al., 2011). These later studies also consolidated the initial finding that bactofilins play a major role in cell shape maintenance.

For example, in *H. pylori,* the CcmA homolog is essential for the cell's characteristic helical cell shape, which is important for the bacterium's colonization of the stomach (Sycuro et al., 2010). As this bactofilin, like all others, lacks any enzymatic domain, it became clear that its morphological function appears to be indirect, most likely by interacting with other proteins, such as Csd1-3, and particularly Csd5, an endopeptidase that could change the cell's peptidoglycan structure through the cleavage of peptide bridges (Sycuro et al., 2010, Blair et al., 2018).

More recent research has revealed more direct evidence of bactofilin's role in motility. For example, the assembly of the flagellar hook and filaments in *B. subtilis* and *Treponema pallidum* is facilitated by the presence of bactofilins. In *B. subtilis,* the two conserved genes, *yhbE* and *yhbF,* encode bactofilins that, like their paralogs from *T. pallidum,* interact with FliY and FliS, two proteins crucial for flagella production (Rajagopala et al., 2007). While FliY is found in the flagellum's basal body complex, FliS serves as chaperone for flagellin, the structural protein component that forms the hollow cylinder-shaped filament of the flagellum. Importantly, deletion of both bactofilins reduced motility, probably by impairing formation or functionality of the flagella (Rajagopala et al., 2007).

A more specific morphological function of bactofilins was identified in *C. crescentus* (Kühn et al., 2010). In this bacterium, two bactofilins, BacA and BacB, form membrane-associated polymeric sheets that recruit PbpC (penicillin binding protein C) to the stalk, an elongated tube-like outgrowth of the cell body. The presence of PbpC at the stalk then further supports the continuous elongation of this characteristic cell structure.

1.2.2 Bactofilins in *M. xanthus*

One key organism that has been extensively used to study the function of bactofilins is *M. xanthus*. Intriguingly, this bacterium possesses not only one but four different bactofilins, namely BacM (MXAN_7475), BacN, BacO, and BacP (MXAN 4637-4635), that are located in two separate operons (Koch et al., 2011). Early work in the Hoiczyk laboratory revealed the importance of BacM for the cell shape maintenance of *M. xanthus*, as the loss of this bactofilin resulted in a recognizable "crooked" cell shape. Moreover, this work also showed that the morphological change was not simply a deformation of the peptidoglycan, but had a more complex effect on the structure of the cell wall polymer, as the BacM deletion mutant also showed greater susceptibility to antibiotics that affect peptidoglycan synthesis (Koch et al., 2011).

Biochemically, BacM is a 150-amino acid-long protein that exists in the cell in two different forms: a full-length version and a shorter one that is cleaved at the amino acid Ser28. Electron microscopy of natively isolated BacM fibres showed 3 nm wide structures that, based on the NMR structure of bactofilins, represent bundles of multiple, probably three individual fibres. Like MreB, fluorescent light microscopy has indicated that BacM forms large cell-spanning helical structures. However, it is currently unclear whether this observation is an optical artefact like the initial descriptions of MreB helices and whether higher resolving

microscopy techniques will eventually show small patch-like distributions of the protein inside cells. In addition, light microscopy also revealed a thicker, polarly arranged rod-like structure in a subset of cells (Koch et al., 2011). As this structure is found in all cells upon overexpression of BacM, it may represent a storage form of excess BacM. Intriguingly, isolated native BacM fibres are only formed by the shorter version of BacM starting at Ser28, which could indicate that the two different forms are differently distributed in the cell and therefore may play different roles. Based on work on the bactofilin from *Thermus thermophilus*, the full-length version may attach to the cytoplasmic membrane, while the shorter version may be distributed in the cytosol.

Labelling of BacM with mCherry changed BacM's structure and distribution inside the cell. Instead of the normally visible helix, the fusion protein forms a distinct thick corkscrew-like structure that attaches to one pole of the cell and, eventually, in some cells can reach the opposite pole. A comparison of the cellular distribution of MreB and BacM in *M. xanthus* demonstrated that their geometry differed with respect to the pitch and overall structure of their helices. Interestingly, this specific distribution of the BacM fusion protein mirrors the observed structure and distribution of mCherry- and GFP-fused crescentin, and, unsurprisingly, in both cases, the fusion proteins are unable to complement the morphological defect of the lack of the native version of those proteins (Cabeen et al. 2009; Koch et al., 2011). BacM and crescentin also share their high propensity to polymerise *in vivo* and *in vitro* as both proteins form spontaneously filaments when overexpressed in *E. coli* or reconstituted after denaturation with urea (Kühn et al., 2010; Koch et al., 2011).

1.3 Ras-like GTPases

Ras-like GTPases form an ancient protein superfamily of GTPase that play important roles in the production of proteins, transmembrane signalling through receptor-mediated processes, protein translocation, cytoskeleton formation, regulation of vesicular traffic, cell differentiation, and growth. Moreover, GTPases have also been studied due to their involvement in cancer and the pathogenesis of infectious diseases through their mutations and as targets of toxins, respectively (Verstraeten et al., 2011). While eukaryotic GTPases are functionally highly divers, all globally conserved bacterial GTPases have been linked to protein synthesis or ribosome assembly. In fact, the largest class of bacterial ribosome assembly factors are GTPases (Karbstein, 2007). In bacterial ribosomes, GTPases play diverse and crucial roles. Their functions encompass facilitating the recruitment or displacement of ribosomal proteins during ribosome assembly, the regulation of assembly factors, and the inhibition of early binding of ribosomal proteins (Britton, 2009). Beyond their involvement in ribosome assembly and function, bacterial GTPases are involved in a range of biological processes, including DNA replication, cell division, stress response, sporulation, as well as contributing to pathogenesis and bacterial motility.

The characteristics of members of the Ras-like GTPase superfamily are exemplified by the protoypical GTPase Ras, after which the superfamily was named. Structurally, Ras is a 20 kDa large globular protein containing six beta strands (β1-β6) and five alpha helices (α1-α5) (Wittinghofer and Vetter, 2011). Together, these structural elements form two domains: the G domain, with 166 amino acids, responsible for guanosine nucleotide-binding, and the CAAX-COOH domain, modified by farnesyl transferase, RCE1, and ICMT, directing membrane targeting. These two domains of Ras share a conserved architecture, GTP-binding, and hydrolysis motifs with other GTPases like Rho, despite differences in their primary amino acid sequences (Mishra and Lambright, 2016).

The Ras protein's G domain features five G motifs, which are crucial for the individual steps of the binding, activation, and hydrolysis of GTP to GDP. Notably, the P-loop or G1 motif binds to the beta phosphate of both GTP and GDP. While the G2 motif, known as Switch I (SW1), interacts with a magnesium ion and the terminal phosphate of GTP, facilitating the coordination of nucleotide binding (**Fig. 3**). Crucially, the GTPase conformation is vital for effector protein binding, and this is modulated by the different nucleotide states. The G3, G4, and G5 motifs ultimately determine the specificity of Ras for GTP. The G3 motif, also known as Switch II (SW2), contains the DXXGQ motif, in which Asp57 plays a key role in selectively binding guanine over adenine, while Gln61 activates a water molecule, facilitating GTP hydrolysis to GDP. In the G4 motif, the preference for guanine over adenine is mediated through the sequence LVGNKxDL, while in the G5 motif the consensus sequence SAK features Ala146, which is crucial for selectivity. Ultimately, the G2 and G3 motifs undergo conformational changes upon GTP hydrolysis, defining the molecular switch transition between the GTP-bound "on" and the GDP bound "off" state **(Fig. 3)**. Overall, G-proteins exhibit specificity for GTP hydrolysis, guanine base selectivity, and GDP release due to their unique conformation and amino acid sequences (Cherfils and Zeghouf, 2013). In contrast, NTP-binding proteins possess the distinct Walker A motif (G1 motif) with the signature sequence GxxxxGK[TS], while guanine base binding specificity, as described, is mostly determined by the combination of the G4 motif [NT]KxD and the G5 motif xAx. Importantly, the O6 of the guanine forms a bond with Ala146, while Asp57 with its side chain establishes bifurcated hydrogen bonds with guanine. Conformational changes occur in the switch I (1-2 loop) and switch II (3-2 loop) regions during the GTP-GDP hydrolysis. As described by Mishra and Lambright (2016) and Wittinghofer and Vetter (2011), the G2 motif's conserved xTx threonine stabilizes the phosphate in GTP by interacting with Mg^{2+}, and DxxGQ in the G3 motif is critical for GTP hydrolysis, mediating contact between water and the phosphate of

GTP. Additionally, the aspartate in the Walker B motif contributes to the water-mediated magnesium coordination. Relaxation of ordered switch regions in the GTP-bound form post-GTP hydrolysis has also been observed (Gerwert et al., 2017).

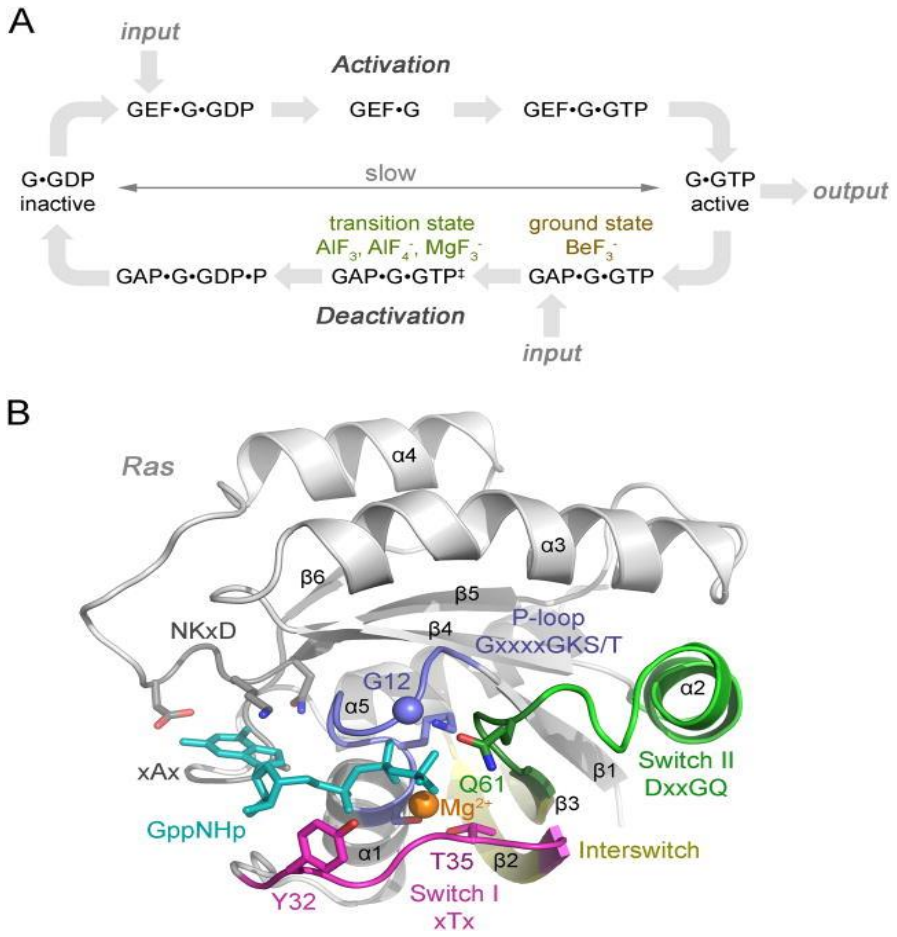

Figure 3: Small GTPase Ras cycle and X-ray structure.
(A) The cycling of GDP/GTP is tightly regulated by specific proteins known as regulatory proteins. Among them, Guanine nucleotide exchange factors (GEFs) and GTPase-activating proteins (GAPs) are the two primary types of regulatory proteins involved in this process. GEFs facilitate the transformation of the inactive GDP-bound state into the active GTP-bound state, while GAPs facilitate the opposite transformation from the active GTP-bound state to the inactive GDP-bound state. **(B)** Structure of the prototypical small GTPase Ras in the active conformation. The Ras GTPase protein consists of five G motifs and a conformational change region that are essential for its proper functioning. The importance of conformational changes in the Ras GTPase protein underscores its key feature as nucleotide-dependent molecular switch highlighting its significance in biological processes (Mishra and Lambright, 2016).

1.3.1 Ras superfamily

The discovery of Ras started in the early 1980s during investigations into oncogenes induced by a rat sarcoma virus (Han et al., 2017). Nearly two decades later, the human version of the Ras-GTPase was identified. All members of the Ras protein superfamily are small GTP-binding proteins with molecular weights typically ranging from 21–25 kDa. In eukaryotes, these Ras-GTPases control numerous signalling cascades crucial to various biological functions (Han et al., 2017). Historically, the Ras protein superfamily has been divided into five major subclasses - Ras, Rho, Arf/Sar1, Rab, and Ran - based on their biological roles and amino acid sequences (Touchot et al., 1987).

Broadly speaking, Ras-like GTPases serve as nucleotide-dependent molecular switches in cellular signalling, exerting profound influences on cell growth, differentiation, morphology, and apoptosis. The multiple roles they play underscore their key importance in maintaining proper cell function (Yamamoto, 1999; Overmeyer, 2011).

1.3.1.1 Rho protein family

Rho (Ras homologous) proteins play important roles as regulators within signalling networks that mediate external stimuli, orchestrating the organization of actin, gene transcription, development, and the cell cycle (Etienne-Manneville and Hall, 2002). Among these proteins, Rac is associated with hematopoiesis, cytoskeletal organization (Heasman and Ridley, 2008), and cell polarity (Park and Bi, 2007; Schlessinger et al., 2009). The Rho family encompasses approximately twenty members, with RhoA, Rac1, and Cdc42 being the most extensively studied (Boureux et al., 2007).

Mammalian Rho primarily functions in the regulation and reorganization of the actin cytoskeleton. In contrast, Rac1 stimulates lamellipodium growth and membrane ruffling, while

RhoA prompts focal adhesion emergence and actin stress fibres, and Cdc42 induces the development of actin microspikes and filopodia (Sayyad et al., 2016). Additionally, Rho GTPases are involved in regulating exocytosis and endocytosis, as well as modifying cell polarity, motility, shape, and interactions with the environment and other cells (Ridley, 2001). The extensive involvement of RhoA, Rac1, and Cdc42 proteins in a wide range of cellular processes is underscored by their regulation by a diverse array of GEFs and GAPs, as well as their utilization of various downstream effectors (Moon and Zheng, 2003; Moon and Hall, 2002; Schmidt and Hall, 2002).

All Rho-family proteins share a Rho-type GTPase-like domain, with a distinctive Rho insert domain within the small GTPase domain, setting them apart from other small GTPases. Noteworthy within the Rho proteins is the Miro subfamily, initially classified as atypical Rho GTPases due to their lack of the Rho insert domain. Subsequently, they have been reclassified as the Miro subfamily of the Ras superfamily (Wennerberg and Der, 2004). Miro proteins consist of an N-terminal GTPase domain containing two EF-hand motifs and a C-terminal GTPase-like domain (Wennerberg and Der, 2004). They are crucial for maintaining the integrity of mitochondria, exhibiting a specific localization to these organelles without association with the cytoskeleton, unlike any other Rho GTPases.

1.3.1.2 Arf/Sar protein family

The Arf protein family plays a crucial role in regulating vesicular transport and exhibits similarities with the Rab protein family. Among its members, Arf1 has been extensively studied (Memon, 2004; Wennerberg et al., 2005). The Arf GDP/GTP cycle is tightly regulated by various GEFs and GAPs. During this cycle, Arf proteins interact with numerous effectors, including coat complex proteins like COP, AP-1, and AP-3, lipid-modifying enzymes such as

phosphatidylinositol 4-kinase, PLD1, phosphatidylinositol 4 and 5-kinase, and vesicle coat proteins that bind to the active GTP-bound Arf (Nie et al., 2003). Distinct conformations in the switch I and II domains and the N-terminal region are exhibited by the two nucleotide-bound forms of Arf during their activity cycle. These conformational changes enable Arf proteins to interact with membranes effectively (Pasqualato et al. 2002). Arf1, in particular, plays a key role in cargo sorting, vesicle production, and release. These activities involve interaction with and stimulation of coat proteins within the Arf-coat-protein complex during various stages of exocytosis and endocytosis (Nie et al., 2003; Memon, 2004).

The Arf-coat-protein complex consists of Arf bound to GTP and the donor cell membrane. Dissociation of this complex and subsequent fusion with acceptor membranes require the activity of GAP, which converts GTP-bound Arf into its GDP-bound form. Unlike Rab proteins, Arf proteins can perform multiple functions simultaneously at different stages of membrane trafficking. For instance, Arf1 stimulates the production of immature secretory vesicles, the association of endosomes with the clathrin/adapter protein 1 (AP1) complex in the trans-Golgi network (TGN), and the retrograde transport of COPI-coated vesicles between the Golgi and ER.

While Arf1 has been extensively studied, some members of the Arf family, such as Arf6, exhibit unique functions in endocytosis and actin cytoskeleton remodelling, distinct from conventional Arf1 roles. Additionally, Sar1, another member of the Arf family, regulates COPII-coated vesicle assembly in the ER, similar to Arf1. Generally, Arf1 is associated with membrane trafficking, while other Arf family members have diverse or poorly understood cellular roles.

1.3.1.3 Rab family

The regulation of vesicle transport, fusion, uncoating, and budding of vesicles in various cell types is primarily regulated by Rab GTPases – an important and large family within the Ras superfamily (Srikanth et al., 2017). This family, vital for cellular processes, has notable expanded throughout evolution *via* gene duplication. In the vertebrate genome, including humans, 66 Rab family genes have been identified. The orchestration of intracellular vesicular transport and the movement of proteins between organelles within endocytotic and secretory pathways is a fundamental role of the Rab family members (Zerial and McBride, 2001). During these processes is the unique functionality of each Rab family member intricately tied to its specific cellular location, emphasizing the critical role of spatial distribution (Stenmark, 2009).

The functional cycle of Rab involves the GDP-dissociation inhibitor (GDI) and the GTPase-activating proteins (GAPs) catalyzing GTP hydrolysis. This cycle is pivotal in recycling Rab back to the donor compartment (Li and Martin, 2015). Conformational changes in the switch regions (I and II) of Rab proteins, induced by the binding of GTP or GDP, facilitate their dynamic interconversion between active and inactive states (Homma et al., 2021).

Beyond their central role in intracellular membrane transport, Rab proteins are involved in diverse cellular processes including signalling and autophagy. For instance, Rab5 plays a crucial role in recruiting the signalling molecules APPL1 and APPL2 to early endosomes, modulating Akt's phosphorylation specificity for GSK-3 rather than TSC2 (Zhu et al., 2007; Schenck et al., 2008).

1.3.1.4 Ran family

Ran, a 25-kDa protein known as ras-related nuclear protein, is an important member of the Ras superfamily. It plays a crucial role in facilitating the translocation of RNA and proteins through the nuclear pore complex (Dingwall et al., 1995). Similar to other small GTP-binding proteins, Ran undergoes cycles between an active (GTP-bound) and inactive (GDP-bound) state. However, it distinguishes itself by lacking the CAAX motif at their C-terminus, which typically facilitates plasma membrane localization during trafficking between the nucleus and the cytoplasm (Boudhraa et al., 2020).

The intricate regulation of Ran involves its interaction with the regulator of chromosome condensation 1 (RCC1) protein for nuclear localization and the GTPase-activating protein RanGAP1 in the cytosol (Ki and Ying, 2009). The compartmentalization of RanGAP1 in the cytoplasm and RCC1 in the nucleus results in an asymmetric distribution of Ran-GTP and Ran-GDP across the nuclear envelope (Lonhienne et al., 2009). This asymmetry is fundamental for nucleocytoplasmic transport as it mediates the assembly and disassembly of import and export complexes through interaction with the nuclear import machinery (Lonhienne et al., 2009).

RCC1, situated in the nucleus, generates a high local concentration of Ran-GTP around chromatin and within the nucleus. This localised concentration induces the nucleation of microtubules and exerts control over nuclear transport (Izaurralde et al., 1997). The nuclear import process is facilitated by the interaction of Ran-GTP with importin-beta, leading to the release or displacement of the cargo into the nucleus (Lange et al., 2007).

Conversely, the nuclear export complex comprises exportin1 and Ran-GTP. Upon reaching the cytoplasm, Ran-GTP is hydrolysed to Ran-GDP by RanGAP1, and exportin1 is subsequently recycled (Lonhienne et al., 2009). Beyond its role in nucleocytoplasmic transport, Ran participates in various other processes and biological functions through interactions with

diverse proteins. Consequently, Ran has been implicated in diseases such as cancer and Kennedy's disease.

1.4 Ras-like GTPases in *M. xanthus*

As described above, small Ras-like GTPases are commonly found in eukaryotes and are used for wide range of cellular functions, including cell signalling and motility. In contrast, bacterial GTPases that are not involved in ribosomal functions are relatively rare (Keilberg and Søgaard-Andersen, 2013). Notably, these non-ribosomal bacterial Ras-like GTPases have similar functions to their eukaryotic counterparts, playing, among others roles, a crucial part in determining cell polarity and motility (Mauriello, 2010; Zhang et al., 2010). Maintaining bacterial cell polarity is crucial for the assembly and function of polarly arranged cellular structures such as flagella and pili and for bacterial behaviours like cell attachment and motility.

As has been described in detail, in *M. xanthus*, bidirectional surface motility is regulated by two types of motilities: social (S-) motility and adventurous (A-) motility. Importantly, both require the mutual gliding motility locus (*mgl*), consisting of two genes, *mglA* and *mglB*, in which the RasGTPase MglA (Mxan_1925) is the master regulator of A- and S-motility, while MglB (MXAN_1926) is a GTPase-activating protein (GAP) regulating MglA activity (**Fig. 4a**). Research has shown that GTP-bound MglA and MglB have incompatible localization patterns, with the majority of MglA-GTP localizing at the leading pole and MglB at the lagging pole (Figure 4**b**; Miertzschke et al., 2011; Leonardy et al., 2010). This specific distribution is stable but dynamic due to MglB's function as GAP. GTP-bound MglA, which may bind to the lagging pole, is instantaneously converted into GDP-MglA. The resulting GDP-MglA is no longer able to bind to the lagging pole, thereby ensuring exclusive MglA accumulation at the leading pole.

In *M. xanthus*, MglA is a crucial determinant of motility, controlling both A- and S-motility systems and the localization of T4P at only one, the leading pole at any given time. When cells undergo a polarity reversal, the polarities of both motility systems shift in relation to the pole where T4P form, and the leading pole becomes the lagging one. This process is possible, as MglA's GTPase activity is enhanced by MglB, an interplay that is important for suppressing cellular reversals so that wild-type cells can move in a single direction for several cell lengths before reversing (Bulyha et al., 2013, Zhang et al., 2010).

As described above, in the absence of MglA, *M. xanthus* cells are non-motile. This supports the idea that the polarly arranged MglA is responsible for controlling both the activities of the T4P and the proteins involved in the A-motility engine, both of which appear to operate in a polar fashion. For MglA-controlled A-motility, this switch may be achieved through the interaction of MglA with its partner protein RomR, which is activated by signals received from the Frz chemosensory system (**Fig. 4b**). In turn, RomR then controls cellular reversals in *M. xanthus* (Keilberg et al., 2012).

Although most functionally relevant domains and amino acid residues of Ras-like GTPase are usually conserved, MglA differs with respect to a number of distinct features. Within the conserved G-domain of MglA, all amino acid residues necessary for guanine binding and GTP hydrolysis are present, but the aspartate residue in the G4 motif is replaced by threonine. Moreover, the extra-long switch I region in MglA surprisingly suggests a closer relationship to the Arf subfamily of GTPases than to any of the eukaryotic Ras-like GTPases that are in involved in motility or cytoskeletal protein function like i.e. Rho (Miertzschke et al., 2011).

Interestingly, *M. xanthus* possesses two more non-ribosomal small Ras-like GTPases, SofG (MXAN_6703) and MXAN_2694. SofG plays an important role in S-motility by

controlling the polarly localization of PilB and PilT, two ATPases that are crucial for the proper functioning of T4P (**Fig. 4c**). PilB and PilT power T4P-driven S-motility through cycles of extensions and retractions of the PilA-formed pilus filament at the leading pole, which in turn pulls the cells forward (Bulyha et al., 2013; Chang et al., 2016). Although SofG has been shown to play a crucial role in pilus functioning, its precise contribution to the polarly arrangement of PilB and PilT is not completely understood. Finally, *M. xanthus* possesses a third non-ribosomal Ras-like GTPase, the protein MXAN_2694. The function of this protein has not been elucidated so far, but investigations of MXAN_2694 mutant and deletion strains did not reveal any obvious phenotypes, indicating at least that this RasGTPase is not involved in *M. xanthus* motility or polarity (Bulyha et al., 2013).

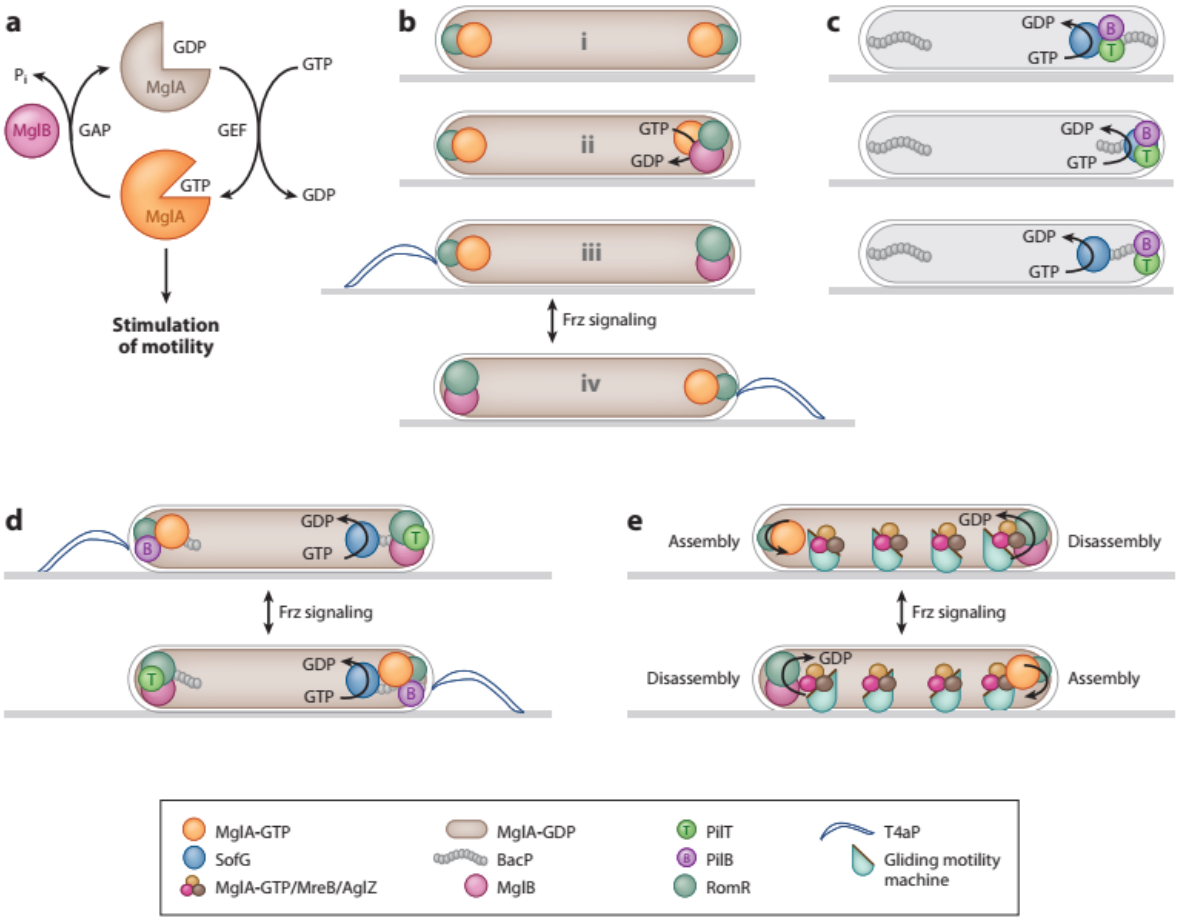

Figure 4: Polarity of the motility system of *M. xanthus* is regulated by three protein modules. MglA/MglB/RomR, SofG/BacP, and Frz. (*a*) GTPase cycle of MglA regulated by MglB. (*b*) The MglA/MglB/RomR polarity module. RomR recruits MglA-GTP to the poles. MglB localized to one pole sets up MglA-GTP asymmetry by stimulating GTP hydrolysis by MglA to form MgIA-GDP, which loses its ability to bind to the pole. (*c*) The SofG/BacP module for polar localization of PilB and PilT. SofG is shuttled over the BacP patch resulting in polar localization of PilB and PilT. (*d*) Dynamic polar localization of PilB and PilT is established by the three protein modules: SofG/BacP, MglA/MglB/RomR, and Frz. (*e*) Polarized assembly and disassembly of the gliding motility machine at the leading and lagging cell poles, respectively. At the leading cell pole, MglA-GTP stimulates assembly of the gliding motility machine. MglB at the lagging pole stimulates disassembly of the machine. Image from Schumacher and Søgaard (2017).

1.5 The Scope of the work

Recent research in the lab had shown that the master regulator of *M. xanthus* S- and A-motility, MglA, binds to the cytoskeletal protein BacM (Semeijn, 2019), not MreB, as had been previously reported (Mauriello, 2010). Separate work has shown that another *M. xanthus* Ras-like GTPase, the protein SofG, binds to BacP to control S-motility (Leonardy et al., 2010).

Therefore, the initial scope of this work was to investigate whether interactions between bacterial Ras-like GTPases like MglA/SofG and bactofilins also occur in other bacteria. Bioinformatics was used to identify bacteria from various phyla that contained both an MglA and a BacM homologue. Necessary protein-protein interaction studies between the various protein combinations were conducted in *M. xanthus* using a newly developed luciferase-based two-hybrid system (Semeijn, 2019).

Next, attempts were made to determine the precise cellular localization of MglA inside *M. xanthus* cells, as well as in a non-bacterial organism, the yeast *S. cerevisiae*. Previously published research had relied on variously fluorescently tagged versions of MglA to localize the protein and to demonstrate that the tag did not interfere with the function of MglA. In these experiments, the restoration of A-motility of individual cells of complemented *ΔmglA M. xanthus* strains was used to confirm the functionality of the tagged MglA (Leonardy et al., 2010; Mauriello, 2010; Patryn et al., 2010). Interestingly, the position of the tags in these experiments switched between the C-terminus and the N-terminus, as the latter positioning appeared to rescue A-motility better, indicating that the position of the tag unsurprisingly influenced the ability to recover A-motility. However, while these experiments had shown a rescue of A-motility in a *ΔmglA* mutant of *M. xanthus* on a single-cell level, no data indicating a rescue of colony spreading on agar was reported (Leonardy et al., 2010; Mauriello, 2010; Patryn et al., 2010). As our investigation showed a lack of such rescue, the next goal of the thesis was to systematically develop and test variously tagged versions of MglA with the aim to identify a construct that fully complements the phenotype, thereby improving the interpretation of localization studies for this important protein. This part of the thesis showed that the introduction of a longer highly flexible linker between MglA and the fluorescent fusion protein is crucial for achieving full complementation of the *ΔmglA* phenotype. Using this new construct, its localisation in *M. xanthus* as well as *S. cerevisiae* was investigated. These experiments

showed that in *M. xanthus* the protein forms small dispersed clusters, while in *S. cerevisiae* it appears to specifically associate with mitochondria, a compartment that is rich in cardiolipins. Intriguingly, cardiolipins are also highly enriched at bacterial cell poles where they enable membrane curvature, indicating that MglA may find its intracellular location through its interaction with cardiolipins.

Finally, the motility of *ΔmglA M. xanthus* cells was studied to investigate whether the loss of the master regulator prevented motility *per se*, as often described in the literature, or resulted in a hyper-reversing phenotype that prevents cell locomotion (Spormann and Kaiser, 1999). Lack of motility would support the idea that MglA is part of the currently unknown A-motility motor, while hyper-reversing would indicate a more likely regulatory function in motility. Observations of *in vivo* motility of *ΔmglA M. xanthus* cells on agar patches clearly showed small displacement motility of the cells supporting a regulatory function for MglA.

Together, the results of these studies should result in a better understanding of the function of MglA, an important motility-associated protein of *M. xanthus* that shows homology to eukaryotic Ras-like GTPases.

Chapter II: Development of luciferase system in *M. xanthus*

2.1 Introduction

Luciferases are a diverse group of enzymes found in various organisms that are capable of emitting light during the oxidation of their small molecule substrates collectively called luciferins (Hastings, 1998). This production and emission of light by living organisms is referred to as bioluminescence and found in numerous organisms ranging from unicellular bacteria and dinoflagellates to fungi, insects, jelly fish, and higher, often marine, animals (Widder, 2010). As light can be easily detected and quantified, research has early on focused on developing luciferase-based assays for a wide variety of purposes. One of the earliest examples were simple luciferase reporter gene-based expression assays that allowed to measure the expression level of a protein of interest by quantifying the emitted light of the fusion protein (Wood, 1991; Hall et al., 2012). Using such transgenic luciferase gene constructs, protein expression levels have been successfully studied for thousands of proteins across a broad range of organisms and cell types (Hampf and Gossen, 2006). The most commonly used luciferases for these assays were from the firefly beetle (*Photinus pyralis*, Pluc) and the cnidaria sea pansy (*Renilla reniformis*, Rluc) and used due to their high sensitivity, which is in the low pico-gram range. This high sensitivity is, however, only one of many attractive features that bioluminescence-producing luciferase-based assays offer. Other advantages are the linearity of the produced light signal that in most studied cells allows accurate quantification across several orders of magnitude or the fact that no external excitation light is necessary to generate bioluminescence. Consequently, luciferase-based assays show minimal autofluorescence and are virtually free of any interfering background emission (Hampf and Gossen 2006). For high throughput and industrial applications, the low-cost aspect of these assays can also be of interest. However, luciferase-based assays are not without drawbacks. One particularly important one is that the cells have to be permeable for the relevant luciferin substrate, which,

dependent on the type of luciferase, can have a molecular weight ranging from 280 to over 400 g/mol. Therefore, during measurements using the bitlucopt system, the cells are lysed to allow access of the substrate to the luciferase enzyme, a necessity that prevents e.g. long-term or dynamic *in vivo* studies of biochemical or physiological processes (Semeijn, 2019).

While research initially relied mostly on the firefly luciferase (Fluc, 61kDa) and the sea pansy luciferase (Rluc, 36 kDa), the recent search for alternative sources of luciferases, particularly from marine organisms, has greatly expanded our repertoire of luciferases adding among others e.g. emission or substrate variability. Among these newly discovered luciferases are e.g. those from the bioluminescent copepods *Gaussia princeps* (20 kDa) and *Metridia longa* (24 kDa) (Inouye et al. 2000; Markova et al. 2004; Nakajima et al. 2004; Suzuki et al. 2005; Tannous et al. 2005). Other organisms include the ostracod *Cypridina noctiluca* (61 kDa), the dinoflagellate *Pyrocystis lunula* (40 kDa), and the deep-sea shrimp *Oplophorus gracilirostris* (106 kDa; **Fig. 5**). Over time, this increasing number of available luciferases has concomitantly expanded the scope and objectives of luciferase-based assays. Besides of the initial reporter gene-based assays studying expression levels, newer assays use luciferase-protein fusions as intracellular biosensors to track the metabolism and interactions of these proteins with e.g. their substrates, co-factors or ions (Perroy et al., 2004; Smirnova et al., 2011). Yet another type of application relies on splitting luciferase into two parts with each part being fused to a different protein thereby allowing to identify and track protein-protein interactions (PPI) *in vivo* between the two proteins of interest (Remy and Michnick, 2006). Importantly, bioluminescence-based PPIs allow the study not only of individual interactions but of complex cell- or even organism-wide PPI networks called interactomes that are often at the core of physiologic and system-wide responses of organisms to changes in their environment (Braun et al., 2009). Therefore,

understanding PPIs is at the centre of our understanding of virtually all cellular, physiological, biochemical, and immunological functions of living cells (Jia et al., 2011).

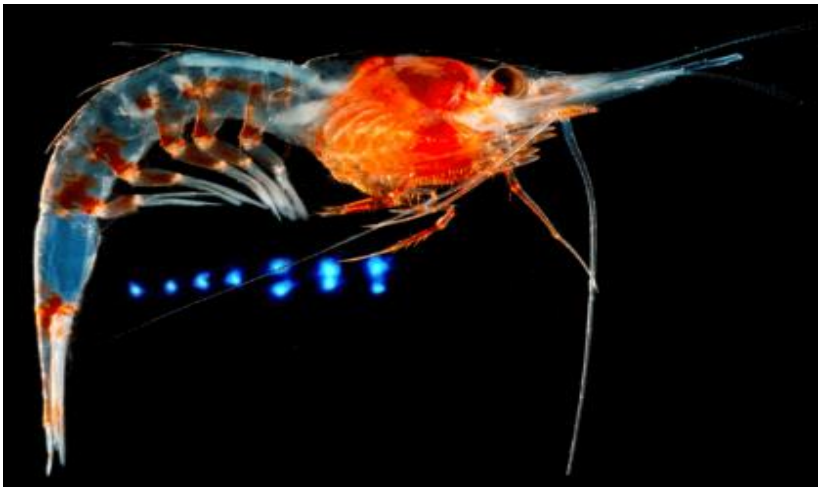

Figure 5: Typical morphology of the bioluminescent deep-sea shrimp *Oplophorus gracilirostris*.
Deep-sea shrimps have photophores, which are specialized organs that emit bioluminescence and are located throughout their bodies. (Heather , 2020).

Examples of large-scale high-throughput applications are LUMIER (**LU**minescence-based **M**ammalian Int**ER**actome) or LuMPIS (**Lu**minescence-based **M**altose-binding protein **P**ull-down **I**nteraction **S**creening System). These studies used a combination of Luc- and Flag-tagged proteins or maltose-binding fusion proteins to quantitatively measure and recover interacting protein pairs in a human embryonic kidney 293T cell line and infected cells with varicella-zoster virus. (Vizoso Pinto et al., 2009; Barrios-Rodiles et al., 2017). Other commonly used luciferase reporter assays simultaneously analyse the relative protein expression levels of two different proteins using the dual luciferase reporters (DLRs) Fluc and Rluc. The Fluc and Rluc reporter assays measure and quantify these interactions in a single sample, making it a quick, simple, sensitive, and quantitative tool (Sherf et al., 1996). The abovementioned high

sensitivity and bright bioluminescence of the DLRs is hereby essential to achieve the necessary high signal to background ratio which is key for the sensitivity of this assay (Hall et al., 2012).

As has been described above the various luciferases from different organisms show large variance of their molecular weights ranging from ca. 20 kDa in the marine copepods to over 100 kDa in the shrimp *O. gracilirostris.* One reason for this large variance is that in some organisms, luciferase is present as a single polypeptide (e.g. copepods), while in others, such as *O. gracilirostris*, the physiologic form of luciferase is a large complex containing multiple 35 and 19 kDa-large polypeptides. Ideally of course, a luciferase for bioluminescence assays should be small, monomeric, and structurally stable under highly variable physiological and environmental conditions (Hall et al., 2012). Intriguingly, the luciferase of the deep-sea shrimp *O. gracilirostris* has just these desirable properties and therefore is widely used in currently employed luciferase assays (Hall et al., 2012). Although this luciferase is secreted by the shrimp as the described ca. 100 kDa-large multiprotein complex, its active luciferase is the small, only 19 kDa-large, subunit of this high weight molecular complex. Genetic analysis of chromosomal DNA (cDNA) clones revealed this surprising result (Inouye et al., 2000). This smaller 19 kDa-large subunit (Oluc-19; **Fig. 6**) contains 169 amino acid residues, including one cysteine residue, and does not show significant homology with any other luciferases including those that use similar imidazopyrazinone substrates (Thompson et al., 1989; Lorenz et al., 1991; Verhaegen and Christopoulos, 2002; Markova et al., 2004). In contrast, the second luciferase complex protein, which consists of 320 amino acid residues and has a molecular weight of 35 kDa, contains eleven cysteine residues and five leucine-repeat sequences. These repeats exhibit the consensus pattern (Leu/Ile)-Xaa-Xaa-Leu-Xaa-(Leu/Ile)-Xaa-Xaa-Asn-Xaa-(Leu/Ile)-Xaa-Xaa-Xaa-Pro, where Xaa represents any amino acid residue. Of note, this particular sequence is also found in multiple members of the leucine-rich repeat family of proteins (Reinke et al., 1988; Kobe and Deisenhofer, 1994; Buchanan and Gay, 1996). As the

35 kDa protein does not *per se* contribute to the observed bioluminescence, it appears to have a different, currently unknown, function. One possible function that has been proposed in the literature is the stabilisation of the 19 kDa-large luciferase protein (Inouye et al., 2000). However, other possibilities exist, such as increasing luminescence through the increase of the local concentration of luciferase in the secreted complexes or slowing down the dispersal of the secreted bright luminous clouds through aggregation. In nature, the shrimps use secreted material to protect themselves from predation (Hall et al., 2012). These luminous clouds appear to stun predators with their blue light (South et al., 2017). This light emission, which is produced through the ATP-independent oxidation of the imidazopyrazinone substrate coelenterazine, has a spectral maximum of 454 nm (Shimomura et al., 1978).

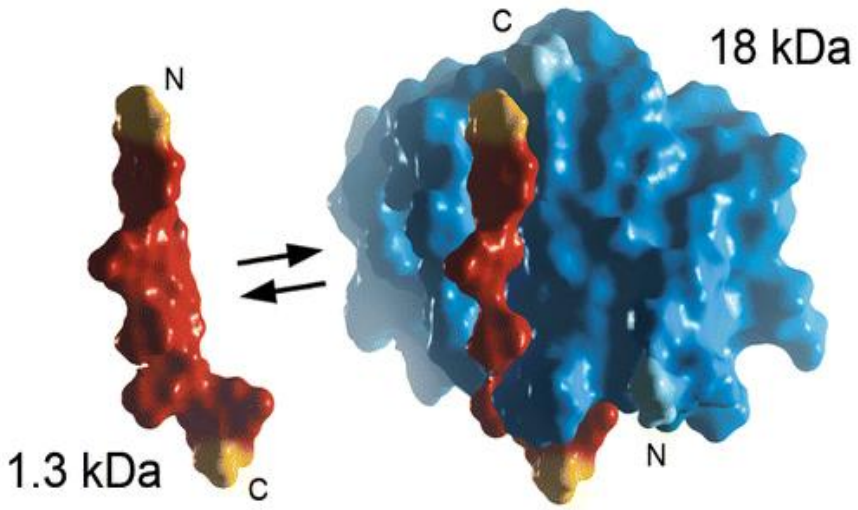

Figure 6: Dimeric structure of the engineered luciferase bitLucopt from *Oplophorus gracilirostris*.
For the engineered version, the native 19 kDa-large nanoluc luciferase is split into two parts: a small 1.3 kDa peptide and a larger 18 kDa polypeptide. These two parts have been selected so that they interact only very weakly with each other and therefore can be used for protein-protein interaction assays. Bioluminescence only occurs upon the interaction of the two target proteins which through their binding re-constitute the active bitLucopt luciferase. Hence, the brightness of the emitted signal is proportional to the strength of the protein-protein interaction of the two target proteins and can be used to accurately quantify this parameter (Dixon et al., 2016).

Due to its complex life style and unusually large proteome, *M. xanthus* has been used for numerous PPI studies. These studies have, because of the lack of a suitable *M. xanthus*-based

assay, either been done using *E. coli*-based bacterial two-hybrid (Nan et al., 2015) or yeast two-hybrid systems (Whitworth et al., 2008). One protein that has been particularly intensely studied is MglA, a 22 kDa-large cytoplasmic RasGTPase that plays a critical role in the bacterium's growth, development and motility (Kroos et al., 1988; Stephens et al., 1989; Hartzell and Kaiser, 1991). Homologues of MglA are present in all myxobacteria and have also been characterised in cell extracts of *Myxococcus virescens* and *Stigmatella aurantiaca*. (Hartzell and Kaiser, 1991).

Previous experiments in the Hoiczyk laboratory had aimed at identifying potential protein-protein interaction partners of the novel discovered cytoskeletal protein BacM (Kühn et al., 2010; Koch et al., 2011). For this purpose, a former postdoctoral, Dr David Zuckerman had performed pull-down assays using isolated purified BacM fibres as bait. These fibres were incubated overnight with *M. xanthus* cell lysate, harvested by centrifugation, and extensively washed with buffer before analysed using SDS-PAGE electrophoresis. BacM fibres lacking the polyproline-containing C-terminus were used as control bait. Mass spectrometry was used to identify bands that specifically interacted with full-length BacM but were absent from the $BacM_{\Delta C\text{-term}}$ sample. The most abundant BacM-interacting protein identified in these pull-downs was MglA (Zuckerman, unpublished). More recently, a PhD student in the lab, Koen Semeijn confirmed this MglA BacM interaction using a novel luciferase-based assay that he adapted for use in *M. xanthus* (Semeijn, 2019). Importantly, BacM and MglA are not the only bactofilin-RasGTPase interactions in *M. xanthus.* Previously, it had been shown that the bactofilin BacP interacts with the RasGTPase SofG (Bulyha et al., 2013). Together these results suggested that RasGTPase may generally be used in *myxobacteria* bactofilins as cellular binding partners and motivated the investigation whether these interactions also occur in other bacteria that possess bactofilins and RasGTPases (Bulyha et al., 2011; Wuichet and Søgaard-Andersen, 2014). Therefore, bioinformatics was used to select MglA and BacM homologues

from various bacterial species representing different classes of myxococcota, bdellovibrionia and proteobacteria (Waite et al., 2020). In particular, MglA BacM pairings from *Bdellovibrio bacteriovorus, Leptothrix mobilis, Collimonas fungivorans,* and *Xanthomonas bromi* were used for the PPI studies based on their homology (Wuichet and Søgaard-Andersen, 2014). The goal of this chapter was to explore the interaction of these four MglA BacM homologues in the *M. xanthus ΔmglA* strain using the lab-developed *M. xanthus*-based luciferase assay (Semeijn, 2019). These cells still contained their native BacM as previous work in the lab had shown that *mglA bacM* double deletions are lethal for *M. xanthus* cells (Semeijn, 2019). In addition, the luciferase PPI assay was also used to re-investigate possible interactions between the RasGTPase SofG and the four bactofilins of *M. xanthus*, BacM, BacN, BacO, and BacP (Koch et al., 2011). Finally, we wanted to test whether the expression of the various MglA homologues of the five bacteria would be able to rescue A- and/or S-motility in the *M. xanthus ΔmglA* strain.

2.2 Materials and methods:

2.2.1 Bacteria strains and growth condition

All *M. xanthus* cells including the wild-type DK1622 were cultivated and prepared as described in the literature (Kaiser 1979). Briefly, cultures were inoculated and grown in CTT medium, which contained 1% casitone, 8 mM $MgSO_4$, 1 mM K_2PO_4, and 10 mM Tris-HCl at pH 8.0. They were shaken at 250 rpm and incubated at a temperature of 32 °C until a density of approximately 4 x 10^8 cells/mL was achieved, corresponding to an approximate OD_{600} of 0.8. Cell motility was investigated using either CTT soft (0.5% agar) or hard agar (1.5% agar) plates for S- and A-motility respectively. For all cloning experiments, *E. coli* DH5α was used, which was cultivated using LB medium containing 5 g/L yeast extract, 10 g/L tryptone and 5 g/L NaCl. All *E. coli* cells were grown at 37°C either in liquid LB or on LB agar plates containing 1.5% agar. If necessary, the LB medium was supplemented with 50 µg/mL kanamycin to select for mutant strains. As the four bioinformatically selected bacterial species, *Bdellovibrio bacteriovorus* (DSM 50701), *Leptothrix mobilis* (DSM 10617), *Collimonas fungivorans* (DSM 17622), and *Xanthomonas bromi* (DSM 18804) are difficult to grow and only needed as a source for chromosomal DNA, no live cells were cultivated of these species. Instead, samples of genomic DNA were purchased for the listed type strains from the German Collection of Microorganisms and Cell Cultures (DSMZ).

2.2.2 PCR protocols

For most PCR reactions, a touchdown protocol was used. Briefly, for each PCR reactions the following components were pipetted into a PCR tube: 10-20 ng chromosomal or plasmid DNA, 12.5 µl Q5 Hot Start PCR Master Mix or Dreamtaq Master Mix, 0.5 µl DMSO, 0.25 µl of each of the primers and enough double distilled sterile water to reach a total volume

of 25 µl. Table 1 lists the primers used in this study. All touch down PCR reactions were run according to standard protocols using annealing temperatures between 60 °C and 50 °C depending on the melting temperature of the used primers. Q5 Hot Start PCR Master Mix was used for all reaction where the fidelity of the product was essential (e.g. cloning), while *E. coli* transformant colony PCR was done using the cheaper Dreamtaq Master Mix. With the exception of the M13 forward and reverse primers, all primers used in the study were either designed as part of this study or adapted from previous work done in the laboratory.

2.2.3 Cloning of *mglA*- and *bacM*-like genes for the luciferase-based PPI assay

For the expression of the luciferase system in *M. xanthus* the pMR3679 plasmid was used (Iniesta et al. 2012). Dr Semeijn, a former PhD student in the lab, designed four different luciferase fragments that were cloned into the multiple cloning site (MCS) of this plasmid (Semeijn, 2019). These lucif fragments allowed for both the N and C-terminal tagging of proteins with the small (Sm) and large (Lg) subunits of the bitLucopt luciferase. The plasmid allowing for N-terminal tagging of proteins was used for the interaction assays between Ras-GTPases and bactofilins. This was based on the observation, that the C-terminus of BacM is essential for the interaction with MglA. An overview of the Lucif fragment allowing for N-terminal tagging of proteins of interest is presented in (**Fig. 7 and 8).** At the start of the transcriptional unit is the vanillate-inducible promoter (purple). Both the Sm and Lg subunits are flanked by a ribosomal binding site (RBS, green), which allows for efficient and accurate translation of the mRNA. The Sm (yellow) and Lg (blue) are followed by a flexible linker (grey). This flexible linker is 15 amino acids long and consists of glycine and serine residues (GSSGGGGSGGGGSSG). The first HupA gene (orange) is flanked by *KpnI* and *BglII* restriction sites allowing for cloning of genes with an Sm-tag. The second HupA gene (orange) is flanked by *EcoRI* and *MluI* restriction sites allowing for cloning of genes with a Lg-tag. At

the end of the transcriptional unit a SlpA terminator region (red) was added to efficiently stop transcription.

The Ras-like genes were amplified using PCR and digested with KpnI and BglII. The bactofilins genes were amplified using PCR and digested using *EcoRI-HF* and *MluI-HF* (NEB). The plasmid was digested with these enzymes allowing for a two-step cloning of these genes at the Sm and Lg. As a positive control a plasmid containing the full-length luciferase was used. As a negative control a plasmid containing non-tagged Sm and Lg was used. In addition, for each PPI, constructs were made expressing a tagged protein with a non-tagged Sm or Lg. These controls are essential as they check for erroneous interactions between the protein of interest and the Sm-Lg complex.

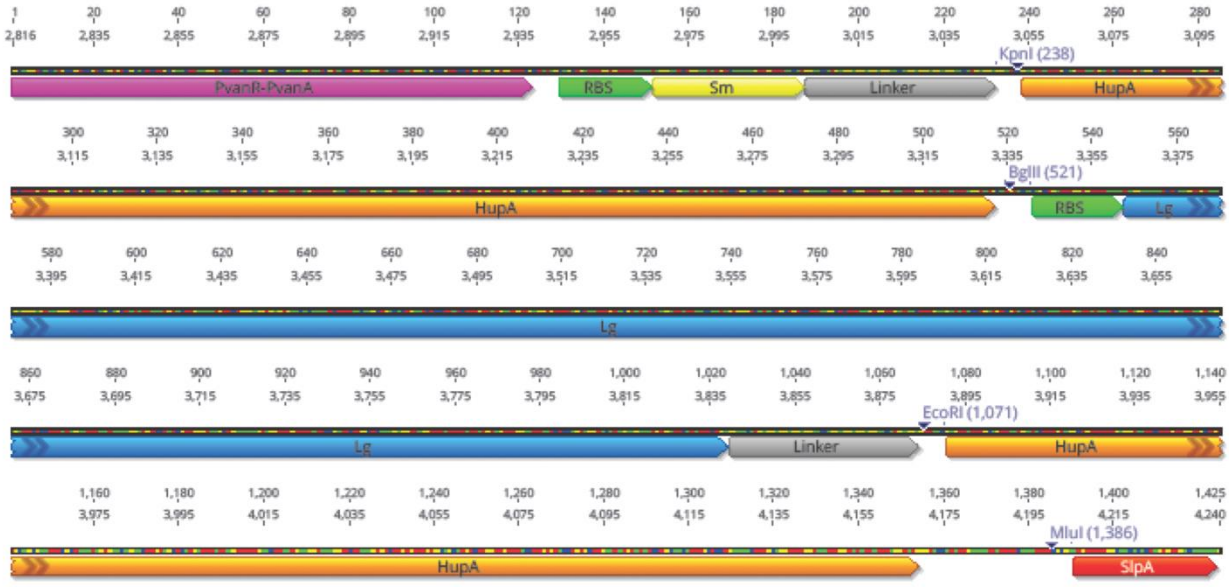

Figure 7: Transcriptional unit showing the genetic parts for N-terminal tagging of proteins of interest with Sm and Lg.
The colours highlight the following elements: vanillate promoter (purple), RBS sites (green), Sm (yellow), Lg (blue), linker regions (grey), HupA genes (orange) and the SlpA terminator region (red). Restriction sites are annotated in light purple above the sequence.

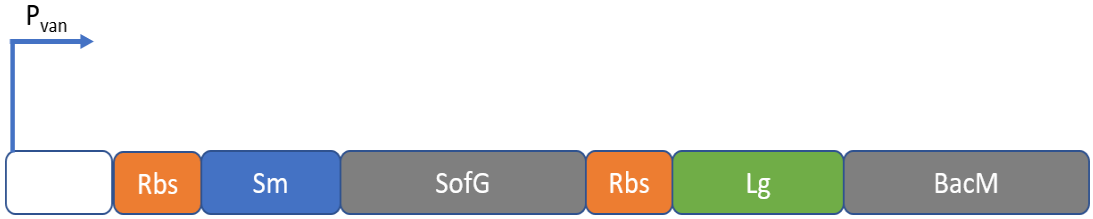

Figure 8:Schematic arrangements of the genetic elements of the plasmid-based bitLucopt system used for the PPI assays.
The following colour coding is used to highlight the different elements: ribosomal binding sites (Rbs, orange), the small fragment (Sm, blue), the large fragment (Lg, green), and the various investigated proteins (MglA, SofG, and BacM, grey).

Table 1: List of used primers.

Plasmid + gene	**Description** **Forward (F) and revers(R) primers**	**Sequence 5' to 3'**
pMR3679-lucif	Sm F MglA *X. bromi* + KpnI	TATATGGTACC ATGAGCCTTCCGGCCAAC
pMR3679-lucif	Sm R MglA *X. bromi* + BgIII	TATATCTAGATCT TCATGGTGATGCCCACCG
pMR3679-lucif	Sm F MglA *C. fungivorans* + KpnI	TATATGGTACC ATGGCTGGGCCGGAGCCG
pMR3679-lucif	Sm R MglA *C. fungivorans* + BgIII	TATATCTAGATCT TCATATTGTTATCAGCAG
pMR3679-lucif	Sm F MglA *B. bacteriovorus* + KpnI	TATATGGTACC ATGTCCTTTATTAACTAC
pMR3679-lucif	Sm R MglA *B. bacteriovorus* + BgIII	TATATCTAGATCT TTACAGAGTCGTTCCGCC
pMR3679-lucif	Sm F MglA *C. aggregans* + KpnI	TATATGGTACC ATGGGTCTGATCAATGTC
pMR3679-lucif	Sm R MglA *C. aggregans* + BgIII	TATATCTAGATCT CTACAATTTACTAATAAC
pMR3679-lucif	Sm F MglA *L. mobilis* + KpnI	TATATGGTACC ATGGCTCACAAAGACCAC
pMR3679-lucif	Sm R MglA *L. mobilis* + BgIII	TATATCGCGT TCAGGCGTCGGCCGTTTC
pMR3679-lucif	Lg F BacM *X. bromi* + EcoRI	TATATGAATTC ATGTTCGGAAACAAGTCC
	Lg R BacM *X. bromi* + MIuI	TATATCGCGT

pMR3679-lucif		TCAGGCGTCGGCCGTTTC
pMR3679-lucif	Lg F BacM *C. fungivorans* + EcoRI	TATATGAATTC ATGTTCAACCGTAAAGCA
pMR3679-lucif	Lg R BacM *C. fungivorans* + MIuI	TATATCGCGT TTAGGCAGATTGCGACAT
pMR3679-lucif	Lg F BacM *B. bacteriovorus* + EcoRI	TATATGAATTC ATGGCAGTAAACCTTTCC
pMR3679-lucif	Lg R BAcM *B. bacteriovorus* + Mlul	TATATCGCGT CTAAGACTTAGGCATGAT
pMR3679-lucif	Lg F BacM *C. aggregans* + EcoRI	TATATGAATTC ATGTTTGGTTCTAATCGC
pMR3679-lucif	Lg R BacM *C. aggregans* + MIuI	TATATCGCCT TCACGACTCTGATGATGA
pMR3679-lucif	Lg F BacM *L. mobilis* + EcoRI	TATATGAATTC ATGTTTGGTTCGAAGAAA
pMR3679-lucif	Lg R BacM *L. mobilis* + MIuI	TATATCGCGT TTACTTCGTGTCGTTGCC
pMR3679-lucif	Sm F SofG + kpnl	TATA-GGTACC GTGAGGAGCCGGATTTCG
pMR3679-lucif	Sm R SofG + BgIII	TATA_CTAGAT TCATCGCCCTTCTCCGCT
pMR3679-lucif	Lg F BacM - EcoR1	TATAT-GAATTC TCTGGTGAGGTCCAC
pMR3679-lucif	Lg R BacM - Mlul	TATAT-ACGCGT CTAGGCTTCTCCTTCTCGTCCACC

Table 2: Bacterial constructs used for the PPI studies in *M. xanthus*.

Constructs	plasmid	Expression	Reference
$MglA_{Sm}$ $BacM_{Lg}$ *X. bromi*	pMM*101*	*M. xanthus*	This study
$MglA_{Sm}$ $BacM_{Lg}$ *C. fungivorans*	pMM *102*	*M. xanthus*	This study
$MglA_{Sm}$ $BacM_{Lg}$ *B. bacteriovorus*	pMM*103*	*M. xanthus*	This study
$MglA_{Sm}$ $BacM_{Lg}$ *C. aggregans*	pMM*104*	*M. xanthus*	This study
$MglA_{Sm}$ $BacM_{Lg}$ *L. mobilis*	pMM*105*	*M. xanthus*	This study
$SofG_{Sm}$ $BacM_{Lg}$ *M. xanthus*	pMM*106*	*M. xanthus*	This study
$SofG_{Sm}$ $BacN_{Lg}$ *M. xanthus*	pMM*107*	*M. xanthus*	This study
$SofG_{Sm}$ $BacO_{Lg}$ *M. xanthus*	pMM*108*	*M. xanthus*	This study
$SofG_{Sm}$ $BacP_{Lg}$ *M. xanthus*	pMM*109*	*M. xanthus*	This study

2.2.4 Colony spreading assays

The spreading of *M. xanthus* cell colonies was measured on hard agar (1.5%) over a period of 1 to 3 days of growth at a temperature of 32 ˚C. Briefly, *M. xanthus ΔmglA* strains expressing MglA proteins from the five different bacterial species were grown in CTT medium until they reached the mid-log stage. After that the cells were diluted using fresh CTT medium to a cell density of ca. 5^{10} cells per ml, and 10 µl of the cell suspension was spotted onto the hard agar surface. To induce overexpression of the various MglA homologues, selected agar plates contained 500 µM vanillate. All agar plates were left for ten minutes to dry under the flow hood. Subsequently, the plates were wrapped with parafilm to prevent the agar from drying and placed for three days into the incubator at a temperature of 32 ˚C. The diameter of

the cell colonies in millimetres was measured daily, and from each strain, an average of three independent colonies were measured in this way.

2.2.5 Nano-Glo luciferase assay

For each generated construct, cells were taken from three separate colonies and incubated in liquid CTT overnight at 200 rpm and 32 °C. In the morning, the cells were induced for 3 hours by adding 250 µM vanillate, before they were used for the assay. Luciferase activity was measured by combining 50 µl of the cell culture with 50 µl of Nano-Glo lysis buffer (Promega N112A) before adding 1 µl of furimazine substrate (Promega, N113A). The addition of the furimazine substrate initiates the oxidation reaction that causes a measurable light output (**Fig. 9**). Measurements in triplicate were carried out in test tubes using a Berthold LuMat-3 luminometer to quantify the relative light units (RLUs). To compare measurements, the relative light units' output was normalized to the cultures optical densities measured at 600 nm (OD_{600}).

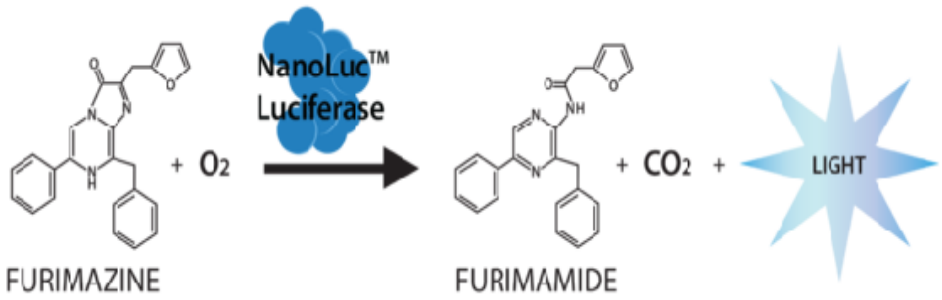

Figure 9: Chemical reaction of the optimised luciferase bitLucopt.
BitLucopt is composed of two fragments, Sm and Lg, which, when interacting, catalyse the oxidation and conversion of furimazine to furimamide. This oxidation leads to the measurable emission of light and the release of carbon dioxide. (Hall et al., 2012).

2.3 Result

2.3.1 Investigation of the interactions between MglA and BacM protein pairs of different bacteria using a luciferase-based interaction assay in *M. xanthus*

In this chapter, a previously in the lab developed novel luciferase-based protein-protein interaction assay for *M. xanthus* (Semeijn, 2019) was used to test possible interactions between small MglA-like RasGTPases and BacM-like bactofilins in a number of phylogenetically diverse bacteria. For this purpose, the two bitLucopt luciferase subunits, Sm and Lg, were fused to each of the selected RasGTPases and bactofilins, respectively and then pair-wise expressed in an *M. xanthus ΔmglA* strain background. The *ΔmglA* strain was used as background so that the cloned non-myxobacterial RasGTPases did not have to compete with $MglA_{myx}$ for bactofilin binding. Unfortunately, previous work in the lab had shown that *M. xanthus* does not tolerate the loss of both its RasGTPase MglA and its bactofilin BacM at the same time (Semeijn, 2019). Therefore, the used strain for the PPI study still contained the native BacM, which could have resulted in non-productive interactions with the cloned non-myxobacterial MglA homolog.

Each of the five selected bacterial strains, *B. bacteriovorus, L. mobilis, C. fungivorans, X. bromi,* and *C. aggregans* were used to generate an *M. xanthus* strain containing the corresponding RasGTPase-bactofilin pair. These expression strains were grown as biological triplicate and prepared according to the described protocol. After the cells of 50 µl culture volumes were lysed using the Nano-Glo lysis buffer, the substrate was added and after the light output reached its maximum the relative light units for each sample was measured. The results of these measurements showed that the RasGTPase-bactofilin pairs of *B. bacteriovorus* and *L. mobilis* showed high relative light outputs with RLU values of 22,000 RLU and 25,000 RLU,

respectively (**Fig. 10**). These data indicated that in these two bacteria the MglA homologues and bactofilins showed a positive interaction, when the Lg subunit was fused to the bactofilin while the Sm subunit was fused to the RasGTPase. Moreover, the measured relative light units were comparable to the ones measured for the original PPI of the MglA and BacM of *M. xanthus*. In contrast, when the position of the fusion was reversed, the light output fell to 10,000 and 3,000 RLUs, respectively indicating that the location of the fusion is an important factor that needs to be considered to achieve a successful and productive reconstitution of the luciferase. The absence of a PPI in the second combination was in line with a previous observation that MglA and BacM interact with their C-termini and therefore the unavailability of this part of the protein due to the fusion would prevent the PPI. No signs of interactions between the RasGTPase and bactofilins were observed for the two other investigated bacteria, *C. fungivorans* and *X. bromi*, in the *M. xanthus* background irrespectively of the used protein termini for the fusion. In these experiments the highest interaction values were 6,000 RLUs or below, values that were similar to the one seen for the Sm-Lg negative control. Even the positive RLU values in *L. mobilis and B. bacteriovorus* were much lower than the positive control of the optimised bitLucopt luciferase that reached RLU values of 1.4 million RLUs. Importantly, some of the negative control strains, such as $MglA_{Sm}$ *L. mobilis*$_{Lg}$, showed relative high interaction values of around 3,000 to 10,000 RLUs. Most likely this phenomenon is caused by the fact that the C-terminus of these MglA homologs play a critical role in their physiological interaction with their cognate output proteins including bactofilins. Overall, these results demonstrated the specificity and sensitivity of the luciferase system for detecting MglA-BacM protein-protein interactions using *M. xanthus* as host organism. More importantly, the data showed that RasGTPase bactofilin interactions are not limited to *M. xanthus* but also present in other bacterial species indicating that this interaction is a novel discovered key feature of these important cellular proteins.

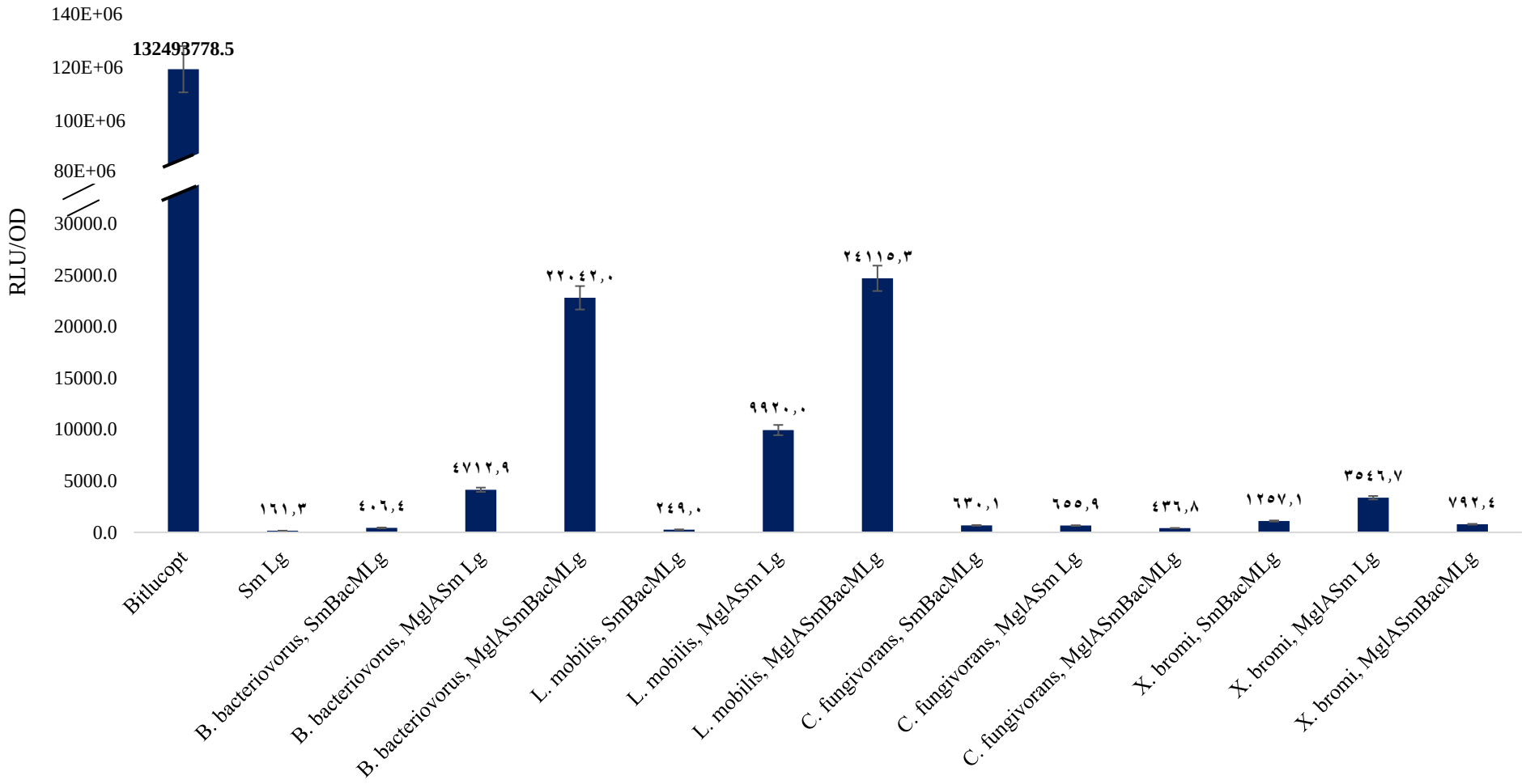

Figure 10: Results of the luciferase assay for the interaction of various bacterial RasGTPases and bactofilins in *M. xanthus*.
For two bacterial species, *L. mobilis* and *B. bacteriovorus* high RLU values confirmed the predicted interaction between the RasGTPase and bactofilin. For the two other species *C. fungivorans* and *X. bromi* no indication of a positive protein-protein interaction between the two tested proteins could be detected. The bitLucopt and Sm-Lg only constructs were used as positive and negative control, respectively.

2.3.2 Motility assay of Δ*mglA* cells expressing MglA and BacM homologs.

As described earlier, MglA is the master regulator for myxobacterial motility controlling both A- and S-motility (Hartzell and Kaiser, 1991). Although the underlying molecular mechanisms for this control function are currently unknown, we wanted to investigate whether non-myxobacterial MglA homolgues could rescue the non-motility phenotype of an Δ*mglA* strain. This plan was based on published data that indicated that the yeast GTPase Sar1 was able to partially rescue a Δ*mglA* phenotype in *M. xanthus* (Hartzell, 1997). Therefore, both A- and S-motility assays were carried out using hard and soft CTT agar plates to determine whether any of the non-myxobacterial MglA homologues could rescue the cell's ability to move using either A- or S-motility.

2.3.2.1 Restoration of A- or S-Motility in Δ*mglA* cells using various MglA and BacM homologs

The motility phenotypes of *M. xanthus* cells expressing $MglA_{Sm}$ and $BacM_{Lg}$ homologues of *B. bacteriovorus, X. bromi, C. fungivorans, and L. mobilis* were compared to the wild type strain DK1622 and *ΔmglA* cells. All strains containing MglA-BacM constructs were grown overnight in CTT liquid media, plated onto CTT hard agar plates (1.5% agar) containing either no or 250 μM vanillate and incubated at 32 °C for four days. As (**Fig. 11)** shows, no restoration of A-motility was observed for any of the construct-containing strains even when the expression of the MglA homologues were induced by adding 250 μM vanillate indicating that the investigated homologues appear not to interact with their cognate partners controlling the A-motility motor. Even after four days of incubation, the diameter of these

colonies on the agar plates remained fairly constant and similar to the one of the Δ*mglA* negative control strain; indicating that the various MglA homologues could not rescue A-motility in *M. xanthus* Δ*mglA* cells. In contrast, the diameter of the colony of the wild type of strain, as expected, gradually increased over the four-day period, showing the normally observed A-motility-dependent colony expansion **(Fig. 12)**.

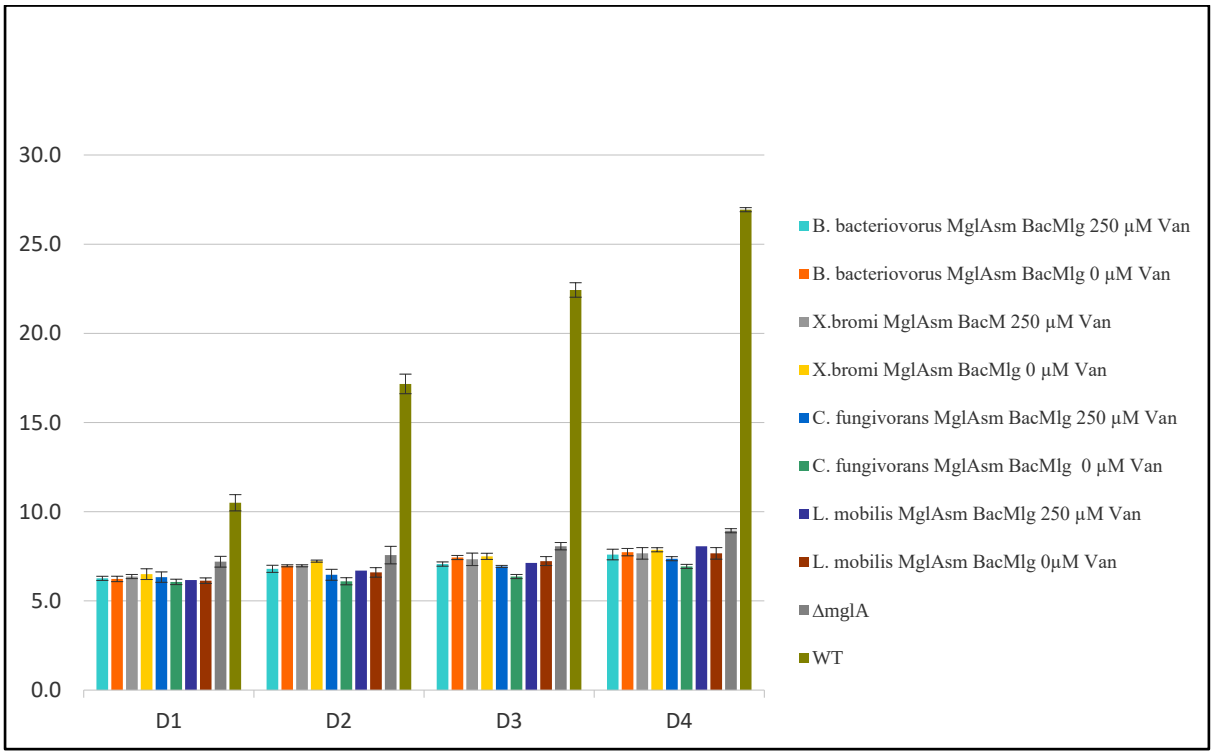

Figure 11: Restoration of A-motility of Δ*mglA* cells expressing various $MglA_{Sm}$ and $BacM_{Lg}$ homologs in an Δ*mglA* background.
The bars depict the diameters of the cell colonies on the hard agar surface. The X-axis represents the number of days of incubation, and the Y-axis shows the colony diameter in millimetres. Expression of the various bacterial MglA-BacM protein pairs in *M. xanthus* was induced through the addition of 250 µM vanillate and colony diameters were measured daily for a period of four days and normalised to a cell density of OD 0.1 for each measurement. All measurements are based on three biological replicates and shown with standard deviations.

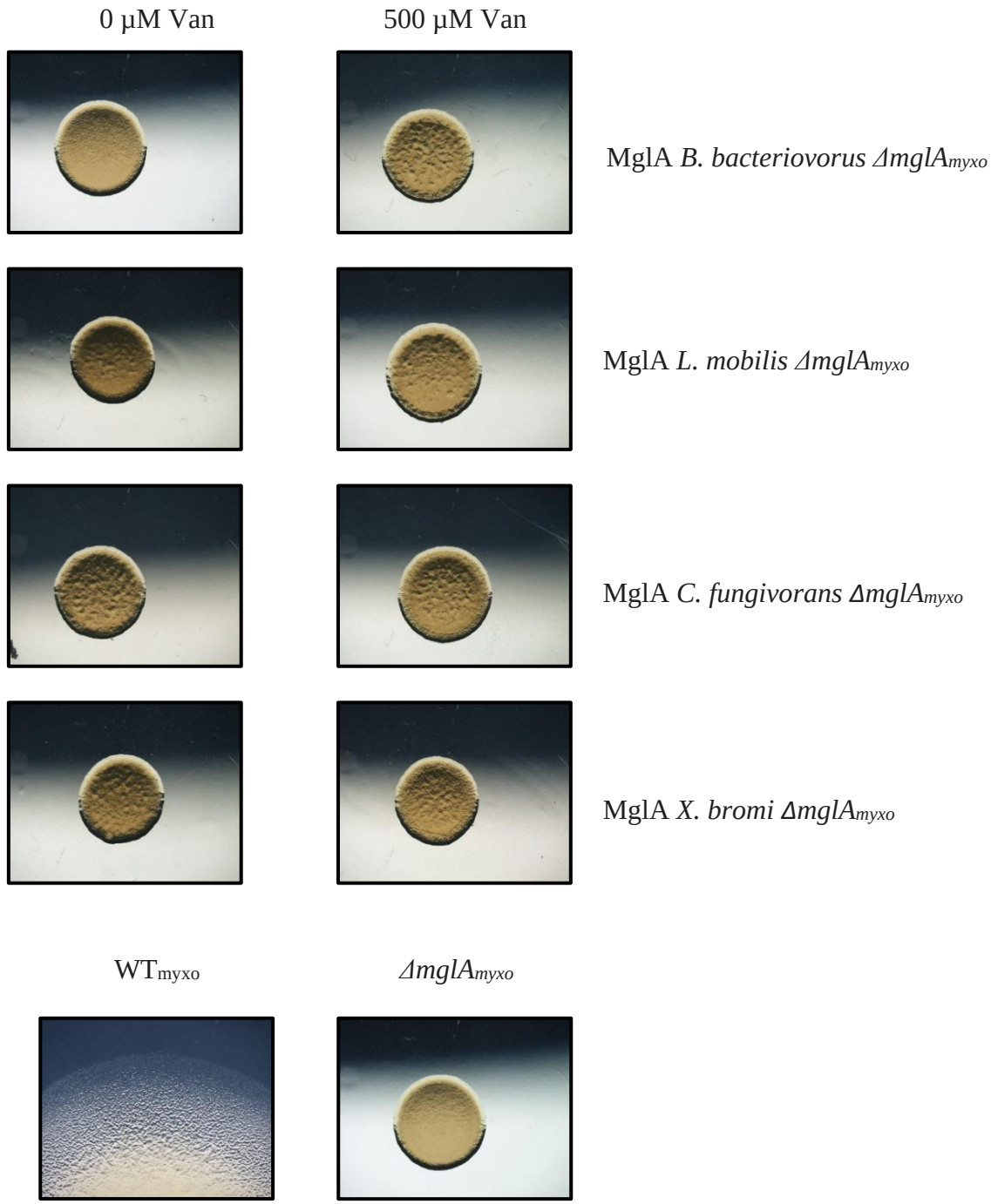

Figure 12: Morphology of Δ*mglA* cell colonies expressing various $MglA_{Sm}$ and $BacM_{Lg}$ homologs in an Δ*mglA* background on hard agar.

This experiment involved the expression of $MglA_{Sm}$ $BacM_{Lg}$ homologs from the bacteria *B. bacteriovorus, X. bromi, L. mobilis, and C. fungivorans* in ΔmglA cells on 1.5% soft agar. The MglA-expressing strains were induced using 500 µM of vanillate, and pictures were taken after four days of growth.

Next, we investigated whether the expressed MglA and BacM homologues of *B. bacteriovorus, X. bromi, C. fungivorans, and L. mobilis* could restore S-motility in *M. xanthus* Δ*mglA* cells. For these experiments CTT soft agar plates (0.5% agar) containing either 0 or 250 μM vanillate were incubated at 32 °C for four days. As negative and positive controls the parental *M. xanthus* Δ*mglA* strain (SA4420) and the wild type of strain DK1622 were used, respectively. For each construct, three colonies were spotted on a single plate, and the diameter of the colonies was measured over a four-day period. The results showed that none of the cloned MglA homologs was able to rescue S-motility and achieve a similar level of swarming as the wild type on soft agar (**Fig. 13 and 14**). Only the wild type showed the S-motility-dependent gradual increase in colony diameter during the four-day incubation period, while the parental *M. xanthus* Δ*mglA* strain (SA5910), like the tested constructs, did not show any S-motility. Overall, these results demonstrate that the various of non-native MglA homologues can neither restore A- nor S-motility of *ΔmglA* cells.

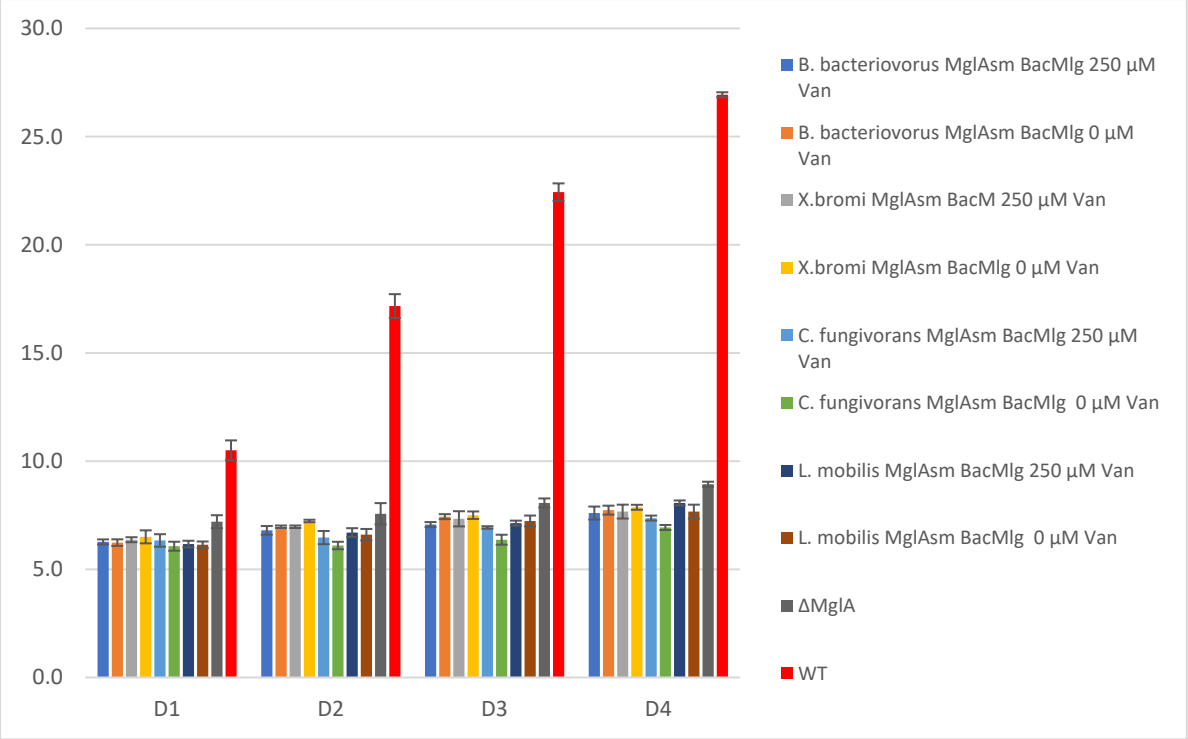

Figure 13: Restoration of S-motility of Δ*mglA* cells expressing various $MglA_{Sm}$ and $BacM_{Lg}$ homologs in an Δ*mglA* background.
The bars in the graph depict the diameters of the cell colonies on the soft agar surface. The X-axis represents the number of days of incubation, while the Y-axis shows the colony diameter in millimetres. Expression of the various bacterial MglA-BacM protein pairs in *M. xanthus* was induced through the addition of 250 µM vanillate and colony diameters were measured daily for a total of four days and normalised to a cell density of OD 0.1 for each measurement. All measurements are based on biological triplicates and shown with standard deviations.

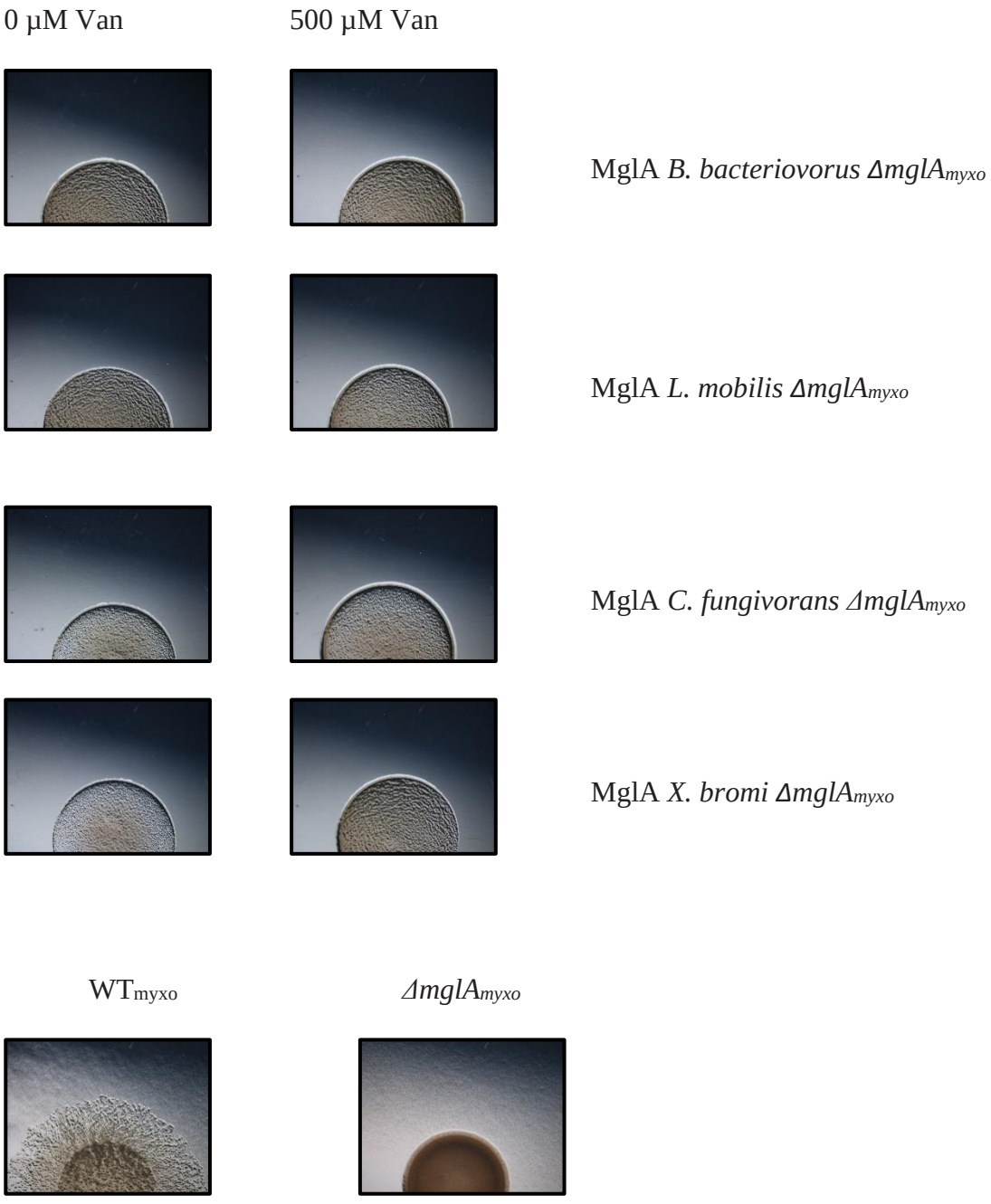

Figure 14: Morphology of Δ*mglA* cell colonies expressing various $MglA_{Sm}$ and $BacM_{Lg}$ homologs in an Δ*mglA* background on soft agar.
This experiment involved the expression of $MglA_{Sm}$ $BacM_{Lg}$ homologs from the bacteria *B. bacteriovorus*, *X. bromi*, *L. mobilis*, and *C. fungivorans* in Δ*mglA* cells on 0.5% soft agar. The MglA-expressing strains were induced using 500 µM of vanillate, and pictures were taken after four days of growth.

2.3.2.2 Restoration of S-motility in *M. xanthus* Δ*mglA* cells using the $MglA_{Sm}$ $BacM_{Lg}$ construct

Earlier work in the laboratory using the bitLucopt luciferase system had established that MglA binds BacM in *M. xanthus* (Semeijn, 2019). To investigate whether the fusion of Sm to MglA interfered with the function of MglA in S-motility, it was investigated whether the $MglA_{Sm}$ $BacM_{Lg}$ construct could restore S-motility in an *ΔmglA* background. Therefore, the *ΔmglA* $MglA_{Sm}$ $BacM_{Lg}$ strain was grown overnight in liquid CTT media and plated on 0.5% soft agar containing 0, 5, 50, 250 or 500 µM vanillate. Notably, a significant increase in the diameter of the colonies on soft agar was observed after induction of $MglA_{Sm}$ $BacM_{Lg}$ expression with vanillate, with the optimal concentration being 250 µM vanillate (**Fig. 15** and **16**). At this concentration, swarming closely resembled that of wild type cells, whereas a concentration of 500 µM did not further increase swarming, and at 5 µM and 50 µM swarming was reduced compared to the wild type. Importantly, in the absence of vanillate, no swarming was observed and the diameter of the colony during the four-day period did not increase. Of note, biochemical investigations indicated that the uninduced construct shows weak leaky expression which could result in the presence of small amounts of the protein. However, experiments with these uninduced cells demonstrate that these small amounts do not support any detectable A- or S-motility. Overall, the gradual increase in the diameter of the colonies at increasing vanillate concentrations indicated that the fusion of the Sm fragment to MglA did not interfere with the biological function of MglA in S-motility.

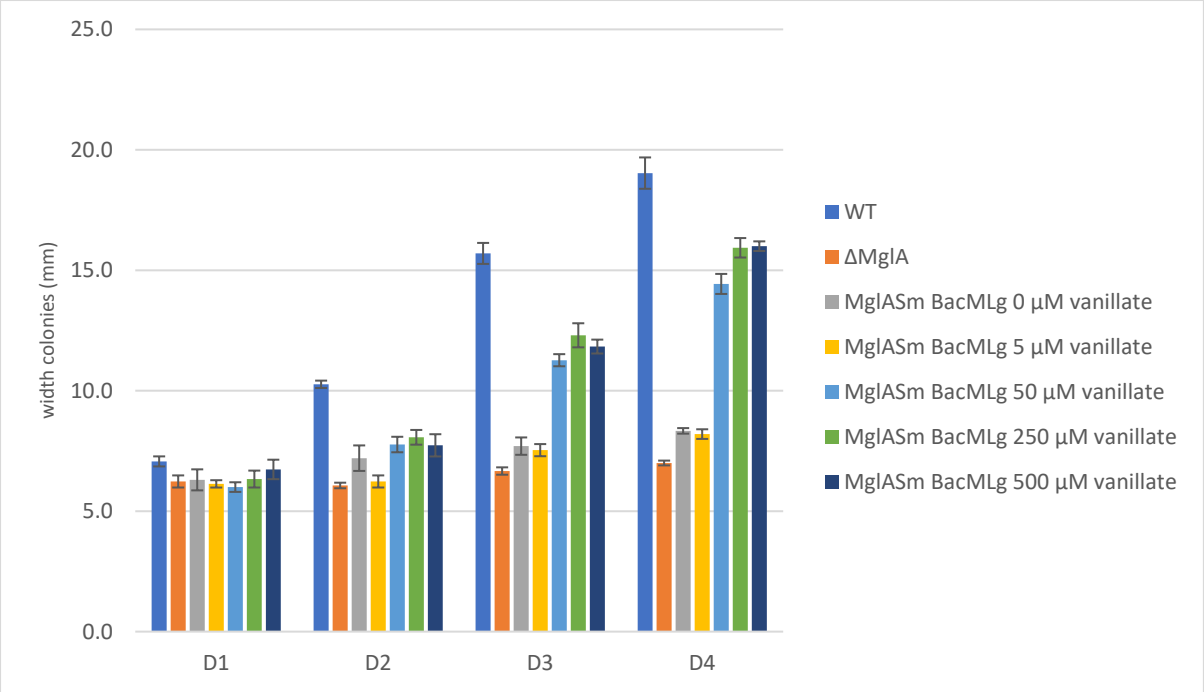

Figure 15: Restoration of S-motility in *M. xanthus* Δ*mglA* cells through the controlled expression of $MglA_{Sm}$ and $BacM_{Lg}$.
The ability of $MglA_{sm}$ $BacM_{lg}$-expressing *M. xanthus* Δ*mglA* cells to swarm was analysed on soft agar for four days. The X-axis represents the number of days of incubation, and the Y-axis shows colony diameter in millimetres. Cultures were induced with increasing vanillate concentrations. Colony diameter was measured daily using three biological replicates. For all measurements the standard deviation is shown.

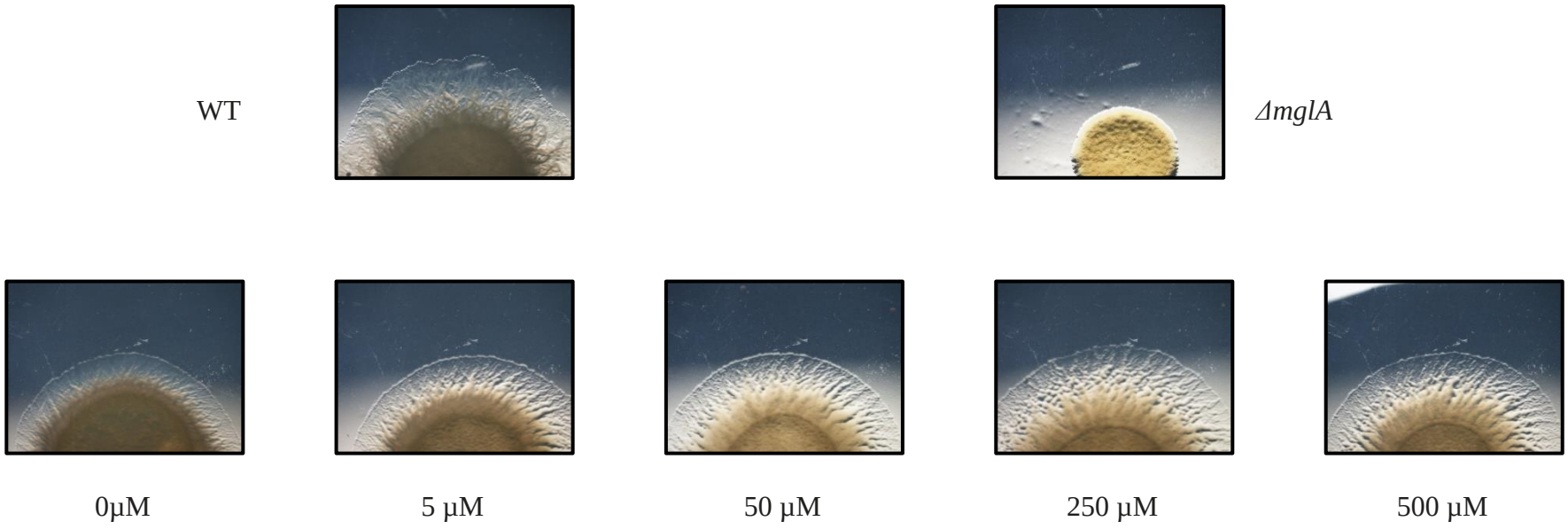

Figure 16: Swarming of Δ*mglA* cells expressing $MglA_{Sm}$ and $BacM_{Lg}$.
The cells were grown on 0.5% soft agar and induced with increasing concentrations of vanillate. Images were captured after four days of growth. The Δ*mglA* strain and the wild type DK1622 were used as negative and positive control, respectively.

2.3.2.3 Restoration of A-motility in *M. xanthus* Δ*mglA* cells using the $MglA_{sm}$ $BacM_{Lg}$ construct

M. xanthus ΔmglA cells expressing the $MglA_{Sm}$ $BacM_{Lg}$ construct were grown overnight in a liquid CTT medium and plated on hard agar containing increasing amounts of vanillate. Five different concentrations of vanillate ranging from 0, 5, 50, 250 and 500 µM were tested for their ability to restore A-motility. Similar to the recovery of S-motility, the optimal concentration of vanillate for the restoration of A-motility was 250 µM vanillate. At this concentration the A-motility-driven spreading of the cells on hard agar reached almost wild type level. Mirroring the S-motility recovery experiments, a further increase of vanillate above 250 µM did not result in a further increase of A-motility. Likewise, the leaky expression of the construct resulted already in a weak but detectable A-motility-driven colony expansion in the absence of vanillate. Similar to S-motility, A-motility restoration on hard agar correlated with the concentration of vanillate (**Fig. 17** and **18**), but overall was lower than the A-motility of the wild type during the four-day incubation period. The negative control, *ΔmglA*, was not affected by increasing vanillate concentrations during the four days of investigation. In contrast, there was a gradual increase in the diameter of the *ΔmglA* $MglA_{Sm}$ $BacM_{Lg}$ colonies as the concentration of vanillate increased from 0 µM to 500 µM following day 2. Overall, these results suggest that the vanillate-induced expression of $MglA_{Sm}$ fusion protein can rescue the A-motility defect of *ΔmglA* cells, and that the optimal vanillate concentration to do so is 250 µM on hard agar.

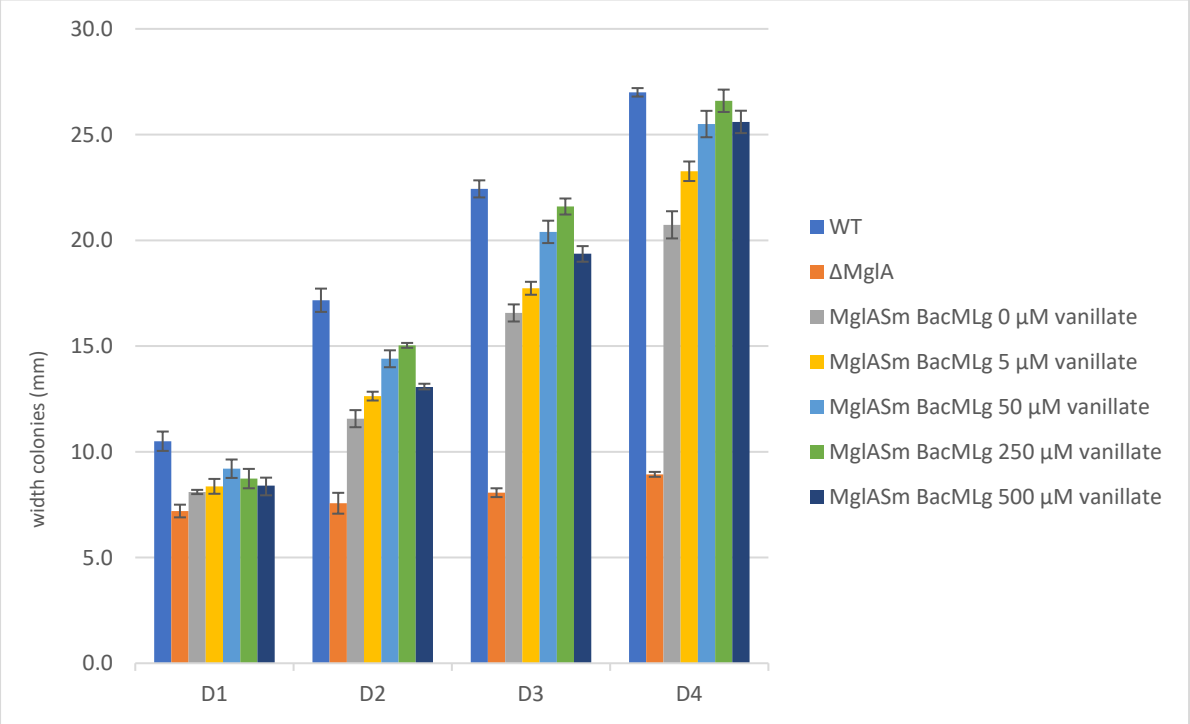

Figure 17: Restoration of A-motility in *M. xanthus* Δ*mglA* cells through the controlled expression of the $MglA_{Sm}$ $BacM_{Lg}$ construct.
The ability of $MglA_{Sm}$ $BacM_{Lg}$ expressing *M. xanthus* Δ*mglA* cells to move on hard agar using A-motility was analysed for four days. The X-axis represents the number of days of incubation, and the Y-axis shows colony diameter in millimetres. Cultures were induced with increasing vanillate concentrations. Colony diameters were measured daily using three biological replicates. For all measurements the standard deviation is shown

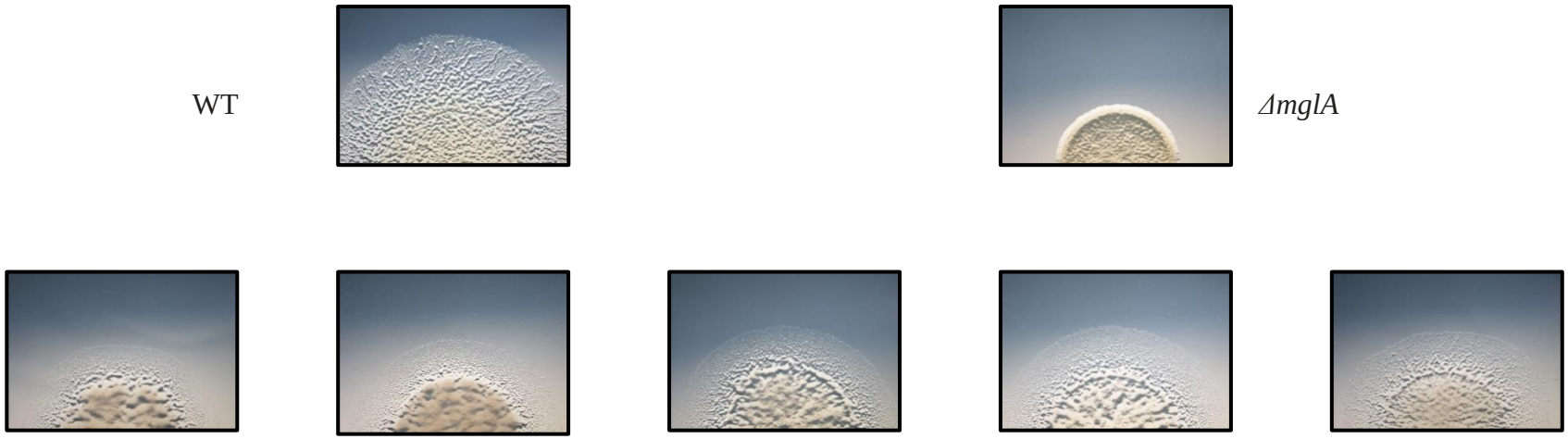

Figure 18: Colony morphology of *ΔmglA* expressing $MglA_{Sm}$ $BacM_{Lg}$
The cells were grown on 1.5% hard agar and induced with increasing concentrations of vanillate. Images were captured after four days of growth. The Δ*mglA* strain and the wild type DK1622 were used as negative and positive control, respectively.

2.3.3 Interaction between the Ras-like protein SofG and the bactofilins BacM, BacN, BacO and BacP

Previously, it had been reported that the Ras-like GTPase SofG is necessary for S-motility in *M. xanthus* and that SofG interacts with the bactofilin BacP (Bulyha et al. 2013). Intriguingly, research in the Hoiczyk lab had shown that the master regulator protein for myxobacterial A- and S-motility MglA also interacts with a bactofilin, namely BacM. This PPI had been demostrated using pull down assays (Zuckerman, unpublished) and a novel developed luciferase assay (Semeijn, 2019). In contrast, the interaction between SofG and BacP had been established using *in vitro* experiments utilizing a SofG protein that was fused to the maltose-binding protein MalE for solubilisation and purification purposes and a His_6-BacP. Therefore, we decided to repeat and expand the SofG bactofilin PPI studies and investigate possible interaction between a minimally changed SofG and all four *M. xanthus* bactofilins, BacM, N, O, and P using our luciferase assay. In this experiment, Sm was fused to the N-terminus of SofG, while Lg was fused to the N-termini of BacM, N, O and P as their C-termini are potentially involved in PPI. Each strain was grown in triplicate in CTT liquid medium overnight and then induced for 3 h using 250 μM of vanillate. This concentration of vanillate was chosen as it restored A- and S-motility to nearly wild type levels in our previous experiments. Our luciferase assay was used to measure the interaction between the proteins, and the RLU values were recorded , while the established interaction of $MglA_{Sm}$ $BacM_{Lg}$ was used as positive control (**Fig. 19**). Surprisingly, our *in vivo* assay showed that $SofG_{Sm}$ and $BacM_{Lg}$ interacted with each other resulting in the production of 21,000 RLU, a value half the measured RLU output for the $MglA_{Sm}$ $BacM_{Lg}$ PPI

(42,000 RLUs). However, all other combinations, SofG-BacN, SofG-BacO, and SofG-BacP showed no interactions, with most having RLU values below 3,000, a value similar to the one measured for the negative control Sm-Lg and Sm-BacM_{Lg}. Importantly, these data contradicted published reports suggesting that SofG interacts with BacP in *M. xanthus* (Bulyha et a., 2013).

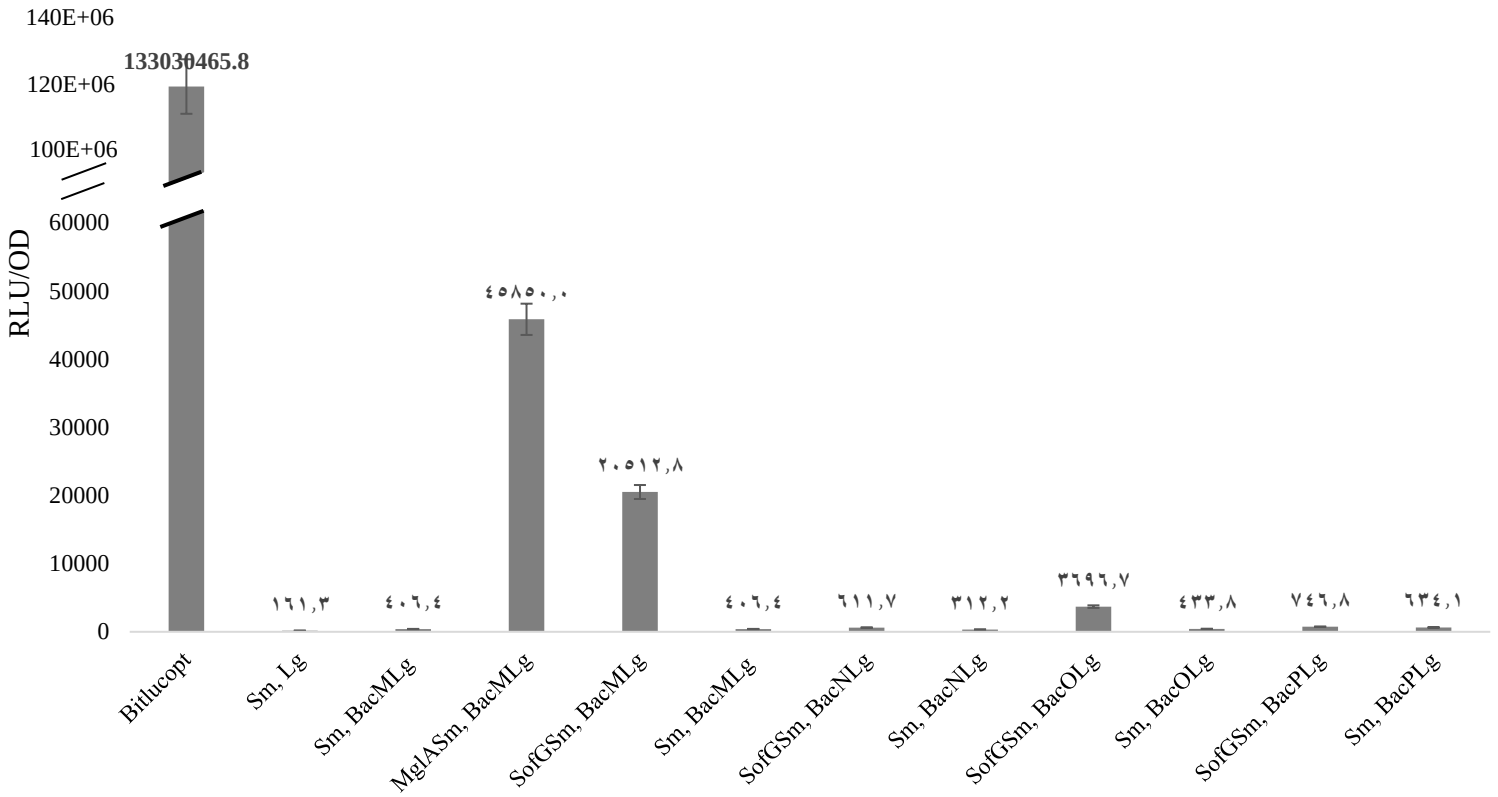

Figure 19: Luciferase assay measuring PPIs between SofG and the four bactofilins, BacM, N, O and P of *M. xanthus*.
The measurements show that only BacM interacts with SofG and that none of the other three bactofilins, including BacP, appear to interact with SofG contradicting published accounts (Bulyha et a., 2013).

2.3.4 Restoration of S-motility in Δ*sofG M. xanthus* cells using $SofG_{Sm}$ and $BacM_{Lg}$

To test whether the fusion of the Sm fragment of bitlucopt to the N-terminus of SofG would interfere with the biological function of this protein in swarming, the mutant strain's ability to restore S-motility was investigated. *M. xanthus ΔsofG* cells expressing the $SofG_{Sm}$ $BacM_{Lg}$ construct were grown overnight in liquid CTT medium and plated on soft agar. Five different concentrations of vanillate ranging from 0, 5, 50, 250 and 500 μM were tested for their ability to restore S-motility.0.5% soft agar at 32 °C with increasing concentrations of vanillate to establish the optimal concentration of the inducer. Notably, the results showed that up to a concentration of 250 μM vanillate the rate of swarming steadily increased, while a further increase of the inducer to 500 μM did not further improve the cell's ability to swarm (**Fig. 20** and **21**). Like in other rescue experiments, the wild type was used as a positive control, while the *ΔmglA* cells were used as a negative control, respectively. The diameter of every colony was measured each day for a total of four days.

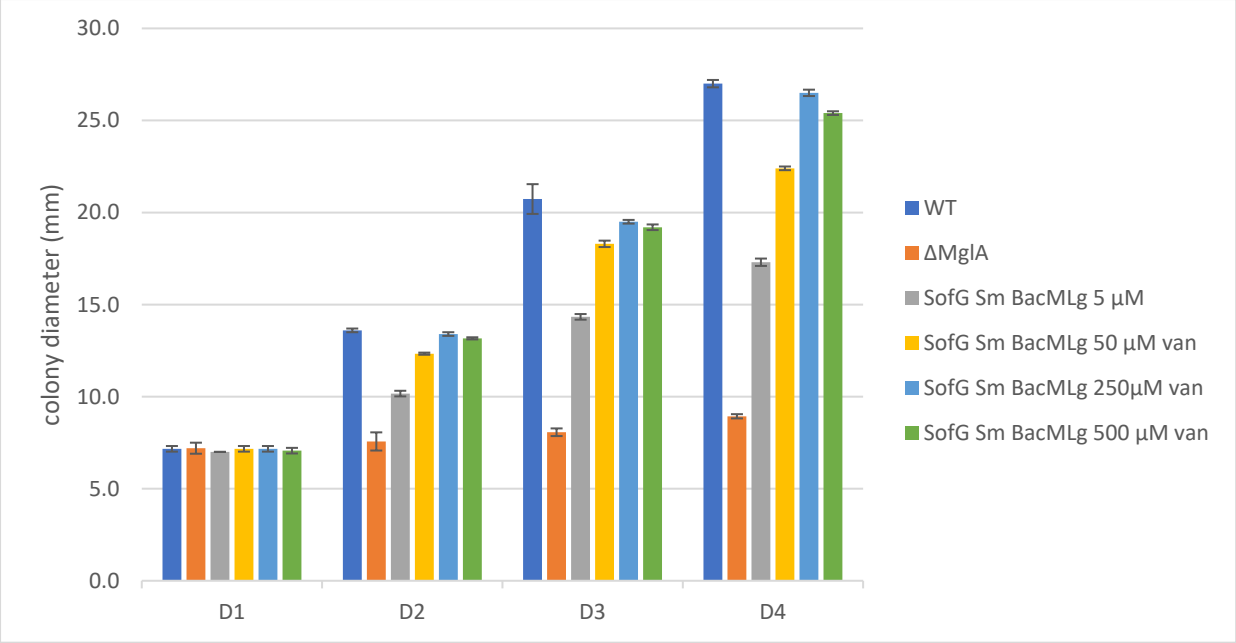

Figure 20: S-motility rescue on soft agar by expression of SofG in Δ*sofG*.
The graph displays the relationship between the number of days of incubation and the width of colonies in millimetres. The X-axis represents the number of days of incubation, and and the Y-axis represents the width of the colony in millimeters. The experiment involved inducing cultures with increasing concentrations of vanillate. The width of the colonies was measured daily over a period of four days, with a base optical density OD_{600} = 0.1. The measurement rates were determined by calculating the standard deviation based on the treplicates on each colony plate.

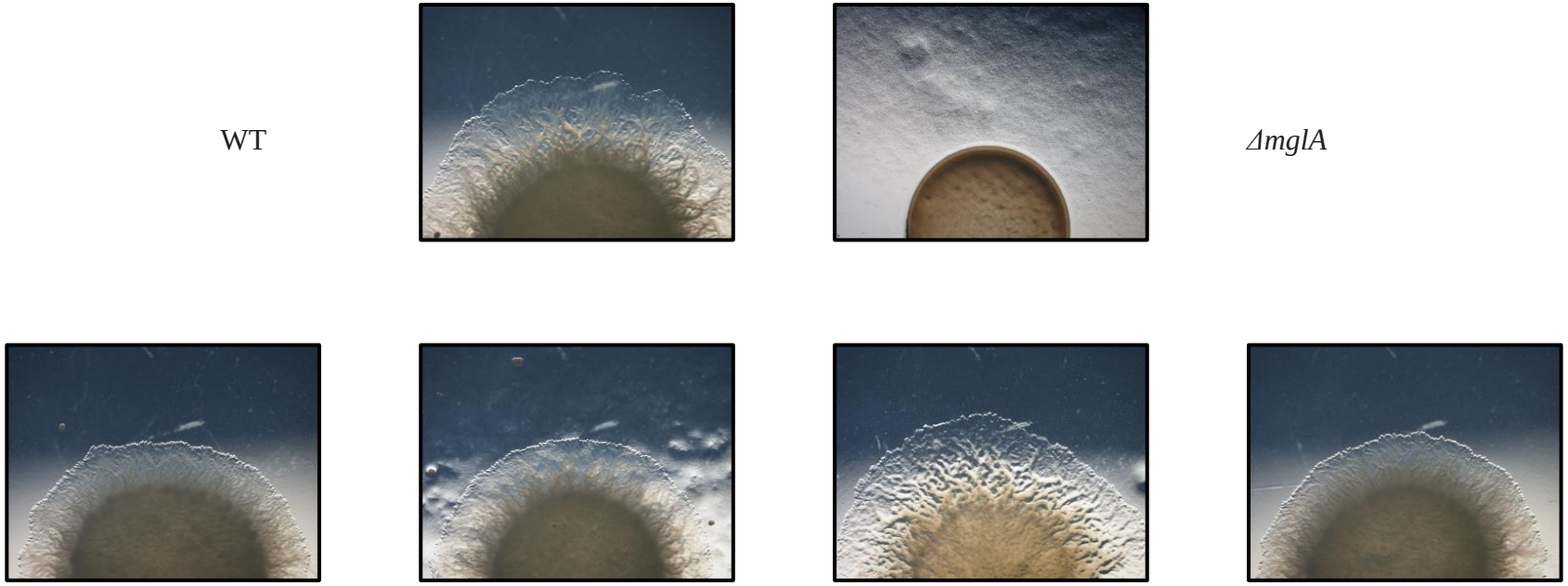

Figure 21: Spread of Δ*SofG* cells expressing of SofG.
The image displays the spread of colonies on hard agar 1.5 CTT with an increase in the concentration of vanillate. The photo was captured after four days of growth, and it visually demonstrates different colony spread at varying vanillate concentrations.

2.3.5 Investigation of the interaction of *B. bacteriovorus* $MglA_{bdv}$ and *S. cerevisiae* $Sar1_{yeast}$ with *M. xanthus* $BacM_{myx}$

Previously published results suggested that the RasGTPase Sar1 from *S. cerevisiae* can partially complement a *M. xanthus ΔmglA* phenotype (Hartzell, 1997). Moreover, our bioinformatic analysis had shown that the sequences of the *M. xanthus* and *B. bacteriovorus* MglAs show high homology (64% identity, 82% similarity). Therefore, this part of the study investigated possible interactions between $BacM_{myx}$ from *M. xanthus* and $MglA_{bdv}$ from *B. bacteriovorus* ($SmMglA_{bdv}$ $LgBacM_{myx}$) or $Sar1_{yeast}$ of *S. cerevisiae* ($SmSar1_{yeast}$ $LgBacM_{myx}$) using the bitlucopt luciferase assay. Each construct was examined using biological triplicates. For the actual luciferase assay, the triplicate constructs were grown overnight, induced with 250 µM vanillate and RUL measurements were made three hours post induction. BitLucopt luciferase and $Mgla_{bdv}$ $BacM_{bdv}$ were used as postive controls, while $SmMglA_{bdv}$ Lg and $SmSar1_{yeast}$-Lg constructs were used as negative controls to rule out that possible detected interactions were the result of the binding between the Sm-tagged protein and the Lg subunit of bitLucopt. Like in the previous reported experiments, the interaction between $SmMglA_{myx}$ and $LgBacM_{myx}$ resulted in a high positive RLU output of ca. 44,000, while $SmMglA_{myx}$ and $BacM_{bdv}$ had roughly half the output at 22,000 RLUs (**Fig. 22)**. However, no significant interaction was observed using the $SmMglA_{bdv}$ $LgBacM_{myx}$ or $SmSar1_{yeast}$ $LgBacM_{myx}$ constructs indicating that neither $SmMglA_{bdv}$ nor $SmSar1_{yeast}$ binds to $LgBacM_{myx}$. The measured values for these experiments, like for other non-interacting pairings, were all below 1,000 RLUs.

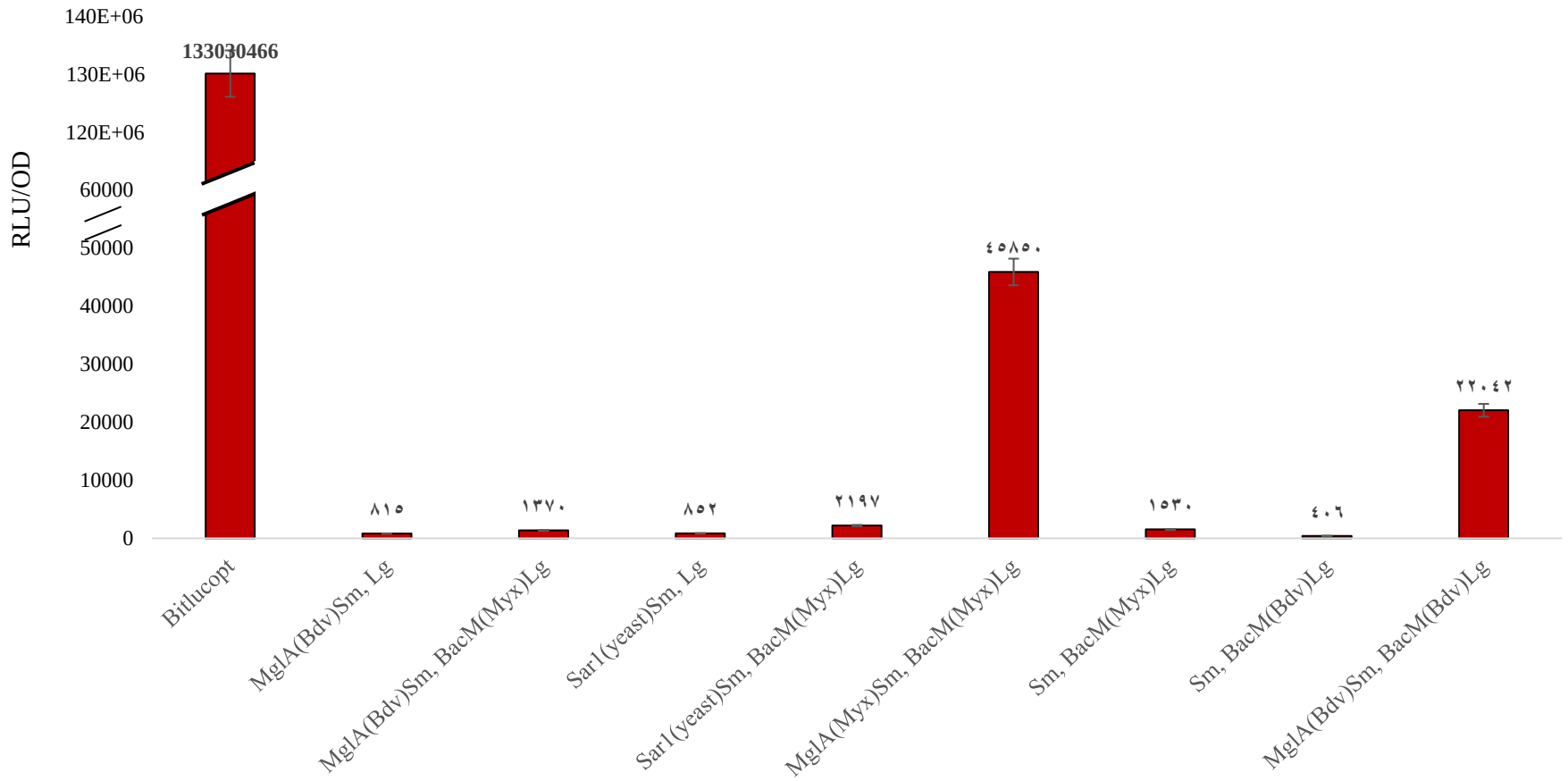

Figure 22: Luciferase assay measuring PPIs between $BacM_{myxo}$ and the MglA homologs *$SmMglA_{bdv}$* and SmSar1yeast in *M. xanthus*.
The measurements show positive PPIs between $SmMglA_{myx}$ and $LgBacM_{myx}$ as well as $BacM_{bdv}$, but no PPIs were detected between $SmMglA_{bdv}$ or $SmSar1_{yeast}$ and $LgBacM_{myx}$. Bitlucopt was used as a positive control, while the tagged proteins plus the non-tagged Lg fragment of bitlucopt were used as negative controls. The Y-axis shows the relative light units (RLU), while the bars show the mean and standard deviation calculated based on three biological replicates.

2.4 Discussion

Published data regarding the occurrence of Ras GTPases in bacteria, along with BLAST searches for homologues of MglA (Wuichet and Søgaard-Andersen 2014), were utilized to identify MglA homologues in a variety of phylogenetically diverse bacteria. Similarly, the highly conserved bactofilin domain DUF583 was used as a guide to identify BacM-like bactofilins in a broad range of bacteria. A comparison of these two datasets, identified bacteria that contained homologs for both of these proteins, MglA and BacM, and that therefore were suited candidates for the planned PPI studies. Overall, four bacterial species were selected that represented three classes of the phylum proteobacteria, the beta-proteobacteria *L. mobilis* and *C. fungivorans*, the gamma-proteobacterium *X. bromi*, and the *bdellovibrionota B. bacteriovorus.* No member of the alpha-proteobacteria was included in the selection as this class of bacteria lacks homologues of MglA or BacM.

To investigate potential interactions between the identified MglAs and BacMs of the four bacterial species, their respective genes were cloned into the vanillate-inducible plasmid pMR3679 (Iniesta et al., 2012), bacteria were transformed into the Δ*mglA M. xanthus* strain, and used as constructs for a recently developed luciferase-based PPI assay in *M. xanthus*. This assay had been originally developed for PPIs in *Clostridium difficile* (Paiva et al., 2019) and previously been adapted in the lab for work in *M. xanthus* (Semeijn, 2019). Importantly, the luciferase-based PPI assay addresses a number of shortcomings of the more commonly used *E. coli*- or yeast-based two hybrid PPI assays. In particular due to its sensitivity, the newly developed assay allows the study of PPIs at physiological levels thereby minimizing the risk of inadvertent interactions of highly overexpressed proteins in the confined space of a bacterial cell. In addition, the use of the natural physiological milieu of the bacterium of choice potentially circumvents problems associated with the correct folding or posttranslational modifications of proteins. Importantly, the assay was successfully used in the past to confirm

the interaction between MglA and BacM (Semeijn, 2019) that had been discovered using an *in vitro* pull-down assay (Zuckerman, unpublished).

Using the bitlucopt luciferase-based assay, it was found that MglA and BacM from the *B. bacteriovorus* and *L. mobilis* interacted like MglA and BacM from *M. xanthus*, while no interactions were detected for these two proteins from the other two investigated bacterial species. It's important to note that *B. bacteriovorus* is, like *M. xanthus*. Two additional important findings were made: the SmMglA negative control led to light output in three proteins of the four bacteria, *B. bacteriovorus, L. mobilis,* and *X. bromi.* The reasons for this observation are currently unclear but possibly due to heterologous SmMglA interacting with the endogenous BacM of *M. xanthus* due to their amino acid charges. Additionally, the light output signal for heterologous protein pairs decayed faster in *M. xanthus* than for native protein pairs, indicating that heterologous proteins are recognized by the endogenous proteases of *M. xanthus* and subsequently proteolytically degraded. Overall, these findings suggest that this novel two-hybrid system is a valuable addition to conventional two-hybrid systems in yeast and *E. coli* that have so far been used to study PPIs in *M. xanthus* (Whitworth et al., 2008; Nan et al., 2015). Excitingly, the new assay will allow the critical re-examination of earlier identified PPIs in *M. xanthus* that relied on conventional two-hybrid systems of proteins expression, potentially leading to inadvertent interactions that are physiologically irrelevant due to the above described shortcomings of conventional two-hybrid systems for proteins from *M. xanthus* or other bacteria.

Taking advantage of the bitlucopt assay, we investigated whether the heterologous MglA proteins were capable of complementing the non-motile phenotype of the *ΔmglA M. xanthus* strain, which would suggest that these proteins might have conserved functions and interaction partners in their respective bacterial species. Unfortunately, none of the four MglA proteins

could complement A- or S-motility, indicating that the role of MglA in motility in *M. xanthus* may be a unique feature or that motility-relevant amino acids or protein motifs were absent from the tested MglAs. This holds even true for *B. bacteriovorus*, capable of gliding locomotion (Lambert et al., 2011). However, it is unclear whether this gliding is analogous to the A-motility of *M. xanthus* and relies on similar motor and control proteins.

Next, the bitlucopt assay was utilized to investigate the PPIs between SofG, another Ras-like protein from *M. xanthus*, and the four bactofilins BacM, BacO, BacN, and BacP of this species (Koch et al., 2011; Bulyha et al., 2013). The results of these experiments revealed that SofG positively interacts with BacM, as evidenced by the relatively high measured light output, while no interactions between SofG and BacO, BacP or BacN could be detected. Of note, our findings are in contrast to previously published data that SofG binds to BacP (Bulyha et al., 2013). However, this earlier study used a maltose-binding protein MalE fusion of SofG and His-tagged BacP as interaction partner. Moreover, the interaction assay was done *in vitro* at un-physiological concentrations and therefore would need at least to be repeated using an *in vivo*-based two-hybrid system. Without additional validation it is possible that the published SofG-BacP interaction is an artefact due to the conditions of the used assay. The discovery of the interaction between SofG and BacM is particularly intriguing, as the described polarly arranged "BacP filaments" (Bulyha et al., 2013) look strikingly similar to previously described polarly arranged BacM filaments (Koch et al., 2011), which could indicate that the previously described structures are in fact BacM filaments. Moreover, this new finding may support the idea that BacM has a unique key function as binding partner of small RasGTPases in *M. xanthus*. In this context, it would be interesting to find out whether the third known small RasGTPase of *M. xanthus*, the protein MXAN_2694 also binds to BacM like MglA. SofG plays a role in motility albeit a more limited only S-motility-relevant role through the control of the localisation and assembly of type IV pili (Bulyha et al., 2013). Together these findings provide

clues for the localisation and roles of MglA, SofG, and BacM in *M. xanthus*. The picture that emerges suggests that polarly arranged BacM filaments may help SofG localize to the cell pole where this RasGTPase controls the assembly and activity of type IV pili. Similarly, these BacM filaments may also help localize a portion of the cellular MglA pool to the front cell pole. However, the non-membrane-attached cellular BacM cytoskeleton formed by the N-terminal truncated version of this protein (Koch et al., 2011) appears to also be able to bind MglA. The functional significance of this interaction is currently unclear, but one possible function could be to remove and store excess MglA to prevent it from binding to cellular localisation and to further control the availability of this protein. Overall, the findings presented in this chapter show that one novel highly important and somewhat unexpected function of the cytoskeletal protein BacM is to act as binding partner for the small RasGTPases MglA and SofG in *M. xanthus* and that similar interactions also exists between other bacterial RasGTPase and their cognate bactofilins. Therefore, this study has shed light on the protein-protein interactions involved in the motility of *M. xanthus* and provide insights for future studies to further investigate these interactions and their functions.

In addition, it was previously postulated that the N-terminal region of BacM binds to the cytoplasmic membrane (Deng et al., 2019), which suggests that there exist two separate populations of BacM-associated MglA molecules in the cell. One population that is in close proximity of the cytoplasm membrane binding to the full-length BacM molecules and one that attaches to the N-terminal truncated BacM fibres that are dispersed throughout the cytoplasm. Based on the relative size of the two populations of BacM, the latter one is twofold more abundant suggesting that the majority of MglA is bound to the cytoplasmic pool of BacM, which includes the aforementioned polar filaments (Koch et al., 2011). Interestingly, our PPI studies suggest that the second investigated RasGTPase of *M. xanthus*, SofG also binds to BacM and not as previously shown to BacP, but that the SofG-BacM interaction is only half as

strong as the MglA-BacM interaction. In contrast, despite their conserved DUF583 domain, BacO, P and N did not show any interaction, possibly because they lack the proline-rich C-terminus found in BacM (Koch et al., 2011). In this context, it is interesting to note that the BacM C-terminus region contains two lysine residues (K_{149} and K_{150}), and deletion of this region resulted in the loss of interaction with BacM (Semeijn, 2019). Furthermore, it was confirmed that the interaction between SmSofG and BacM could complement the non-swarming phenotype of the (SA3801) ΔSofG strain, indicating that the functionality of this protein was not compromised by the fusion to the Sm fragment.

Finally, the bitlucopt luciferase was used in *M. xanthus* to examine whether the two Ras-proteins, $MglA_{bdv}$ and $Sar1_{yeast}$ are able to bind to *M. xanthus* BacM. These experiments were based on the high degree of homology of the *B. bacteriovorus* and *M. xanthus* proteins, which e.g. both have C-terminal lysine residues. In addition, both bacterial species have more in common; both are predators that are able to move by gliding motility. Although it is currently unclear whether *B. bacteriovorus* uses the same cellular machinery as *M. xanthus* for this type of motility (Lambert et al., 2011). Similarly, the idea to include Sar1 from S. *cerevisiae* was based on published reports that suggested that this protein can partially complement a *ΔmglA* phenotype in *M. xanthus*. However, no interaction was confirmed between $MglA_{bdv}$ and $BacM_{myx}$ and no light output could be detected. Interestingly, the interactions between $MglA_{bdv}$ and $BacM_{bdv}$ and between $MglA_{myx}$ and $BacM_{myx}$ had been previously demonstrated in *M. xanthus* and were used as positive controls. These results may not be that surprising given the fact that both bacteria are predatory delta-proteobacteria capable of gliding motility (Lambert et al., 2011). More importantly, this phylogenetic closeness is also reflected in the high degree of identity and similarity of their MglA protein sequences (64% identity, 82% similarity). Despite these similarities, however, the two MglAs are not interchangeable indicating that subtle, probably only a few critical amino acids, differences are sufficient to prevent their

binding to the BacM of the other species. The lack of MglB in *B. bacteriovorus* compared to *M. xanthus* could be another reason why their MglAs are not interchangeable (Milner et al., 2014). In contrast, the eukaryotic protein Sar1 from *S. cerevisiae* shares only 24% similarity with $BacM_{myx}$. It was, however, included in these experiments as it had been shown to partially complement a Δ*mglA* phenotype (Hartzell, 1997). Predictably no interaction was found between $Sar1_{yeast}$ and $BacM_{myx}$. This lack of interaction could potentially be explained by their low sequence similarity, particularly in the N- and C-terminal regions, which are possibly crucial for the interaction between RasGTPases and bactofilins. In this context, it is worth mentioning that recent work in the laboratory has cast doubt on the original report about Sar1's ability to complement a *ΔmglA* phenotype in *M. xanthus*. Careful re-examination of the described rescue for example revealed that the reported successful spore formation is not the formation of fruiting body spores but of glycerol spores, which have slightly different shapes. Therefore, the reported complementation has to be viewed with scepticism and the lack of an interaction between $Sar1_{yeast}$ and $MglA_{myx}$ was probably not too surprising.

In summary, the data of this chapter has shown that one novel discovered key feature of bactofilins is their ability to act as binding scaffolds for small Ras-like GTPases in *M. xanthus* and that this feature is conserved across phylogenetically diverse bacteria.

Chapter III: Localization of MglA in *M. xanthus* and *Saccharomyces cerevisiae*

3.1 Introduction

As has been described in the Introduction of the thesis, *M. xanthus* uses two different motility systems, A- and S-motility, simultaneously, to perform unusually complex behaviours such as swarming, hunting, rippling, and fruiting body formation (Zusman et al., 2007). To accomplish these behaviours and to be able to respond to external stimuli in a directed fashion, the cells periodically switch the polarity of their locomotion, a process during which the leading pole of the cell becomes the lagging one and *vice versa*. One major molecular switch enabling these re-orientations is the small Ras-like GTPase MglA, the master regulator of myxobacterial motility (Hartzell, 1997). During re-orientations, MglA interacts with three different types of proteins: the effector proteins, which are required to initiate a specific response; GTPase-activating proteins (GAPs), which stimulate GTP hydrolysis of activated Ras-like proteins, and guanine exchange factors (GEFs), which facilitate the release of GDP from Ras-like proteins (Leonardy et al., 2010). In *M. xanthus*, MglB is the GAP protein of MglA and, like it's cognate Ras-like GTPase essential for motility (Leonardy et al., 2010; Patryn et al., 2010; Miertzschke et al., 2011). In fact, the exclusive localization of MglB at the lagging pole is crucial for properly controlling T4P assembly at the leading pole, as any MglA binding to the lagging pole is promptly converted to its inactive, GDP-bound form and consequently released from the lagging pole. The resulting pole-to-pole oscillations of MglA drive the observed cell reversals (Zhang et al., 2010). Simultaneously, MglA is also a component of lateral clusters that have been termed focal adhesion complexes and that may be generating the power for A-motility (Mignot, 2017). These multiple arrangements and highly dynamic behaviours of MglA defy an easy interpretation of its actual molecular role in these processes. Therefore, understanding the cellular localization of MglA and the conditions under which it occurs is crucial. This will help

understanding the molecular processes that occur during and drive cell reversals, as well as MglA oscillations.

While MglB is the GAP of MglA, the two-protein complex RomR-RomX (RomRX) acts as MglA's GEF (Leonardy et al., 2010; Mercier et al., 2020). Together with MglB, RomRX establishes a polarity axis that determines the localization of MglA, which, in turn, regulates T4P assembly, A-motility, and cell reversals. While the localization and activity of these proteins are stable at any given time, they are highly dynamic to allow cell reversals to occur. These events are induced by the chemosensory (Frz) system, which measures and responds to an unknown internal molecule. Once the chemosensory system is triggered, it starts a cascade of events that eventually lead to a reversal of locomotion. At the start of each reversal, the active GTP-bound form of MglA is localized predominantly at the leading pole, while the majority of MglB and RomRX is localized at the lagging pole. Importantly, although the majority of RomRX is at the lagging pole, a small amount is present at the MglA-occupied front of the cell. This arrangement of RomRX is important, as the protein has been identified to stimulate the localization of both, MglA and MglB to their respective cell poles by forming complexes with these two proteins. Moreover, RomRX also interacts with the output response regulator of the Frz chemosensory system, FrzZ, which initiates and regulates cellular reversals (**Fig. 23)** (Leonardy et al., 2007). While this description accurately captures our current understanding of the cell reversal-related localization of MglA, MglA is also found, i.e., in the focal adhesion complexes. Consequently, the investigation of the precise distribution of MglA in *M. xanthus* is an important first step to understand all aspects of MglA function.

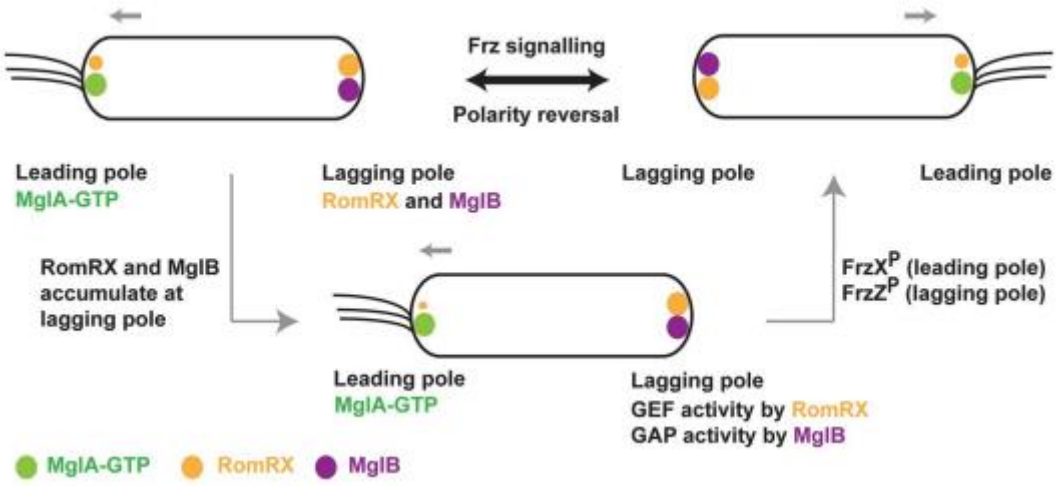

Figure 23: Localization patterns of cell polarity determining proteins in *M. xanthus*.
The diagram illustrates the cellular locations of MgA, MglB, and RomRX in *M. xanthus*. MglA, in the GTP-bound form, is primarily located at the leading pole, whereas MglB and RomRX are at the lagging pole. The polarity reversal resulting from protein re-localization is triggered by a signalling cascade that includes the Frz-signalling proteins. Green, magenta, and orange spheres are used to symbolize MglA, MglB, and RomRX, respectively. The unequal localization of RomR, with a higher concentration at the lagging pole, is depicted by the asymmetric size of the orange spheres at the two poles. FrzX and FrzZ represent the phosphorylated forms of FrzX and FrzZ, respectively. Image from Leonardy et al., 2007.

Various research groups have studied the cellular localization of MglA using different N- or C-terminally fluorescently-tagged versions of the protein (for an overview, see **Table 3**; Patryn et al., 2010; Leonardy et al., 2010; Mauriello et al., 2010b). As described above, the bipolarly arranged RomR plays a key role in cell reversals and A-motility, which is mediated through its asymmetric clusters. Once the larger cluster from the lagging pole starts moving towards the leading pole, this pole switches and becomes the new lagging pole. Probably unsurprisingly, RomR mutant strains do not show cellular reversals (Leonardy et al., 2007). To study the behaviour of MglA during these processes, experiments have been done using YFP-tagged MglA, which partially complemented A-motility defects in a *ΔmglA* background, but failed to restore sporulation. The movement of the labelled MglA followed a helical pattern throughout the cell (Patryn et al., 2010). In contrast, in cells lacking MglB, MglA mostly localized in a bipolar pattern, with few cells showing either a unipolar or diffuse distribution of the protein. In wild-type cells, MglA-YFP was mostly diffuse distributed with few cells

showing a bipolar localization (Baranwal et al., 2019). A major drawback of these studies was that they did not necessarily investigate whether the tagged MglA was rescuing all *ΔmglA*-related defects such as A-motility at the swarm level.

Therefore, the main objective of this part of the project was to generate new tagged versions of MglA that would not interfere with the protein's function and rescue all known *ΔmglA*-related defects. To achieve this, an eYFP-tagged MglA construct was developed that is biologically functional and, therefore, can complement the Δ*mglA* phenotype, including the rescue of A-motility not only on the single-cell but swarm level. This important aspect had not been investigated in previous studies using tagged versions of MglA (**Table 3**). Furthermore, a tetracysteine (TC-) tagged version of MglA was generated. This tag consists in its smallest form of only six amino acids (CCPGCC) and demonstrates a strong affinity for the membrane-permeable biarsenical fluorophores FlAsH and ReAsH, which exhibit low toxicity and can selectively label TC-tagged proteins *in vivo*. Both tagged versions of MglA were investigated for the localization of the protein and its ability to complement A-and S-motility using hard and soft agar.

Finally, the generated eYFP-MglA was introduced into *S. cerevisiae* yeast cells to study the protein's behaviour and cellular localization in a non-bacterial cellular environment. The choice of yeast as host was based on the fact that this eukaryote possesses a small RasGTPase, Sar1, that shares 24% identity and 47% similarity with MglA (Hartzell, 1997). In yeast, Sar1 localizes to the ER membrane and plays a crucial role in protein trafficking from the ER to the Golgi apparatus. Sar1 is able to localize to these membranes through a conformational change that occurs upon GTP-binding. This change exposes an N-terminal amphipathic helix that anchors the protein to ER membrane. As Sar1 is able to partially complement motility and sporulation of the Δ*mglA* phenotype in *M. xanthus* (Hartzell, 1997), it was decided to introduce eYFP-MglA into yeast to study the localization of the bacterial protein in a eukaryotic cell.

Table 3: Differently tagged MglA constructs and their observed motility phenotypes.

MglA-tag construct	Localization	Motility	Study
C-terminal MglA-eYFP tag	Lateral clusters and bipolar distribution	Rescue of A-motility and partial S-motility	Mauriello et al., 2009
C-terminal MglA-eYFP tag	Lateral clusters and bipolar distribution	Rescue of A- and S-motility	Patryn et al., 2010
C-terminal MglA-eYFP tag	Mostly bipolar distribution, with rarer occurrences of unipolar or diffuse cytoplasmic distribution	Not reported	Baranwal et al., 2019
N-terminal MglA-eYFP tag	None	No rescue of A- and S-motility	Patryn et al., 2010
N-terminal MglA-eYFP tag	Diffuse cytoplasmic distribution in some cells and bipolar distribution in other cells	Rescue of A-motility	Leonardy et al., 2010
N-terminal MglA-eYFP tag	Lateral clusters and bipolar distribution	Not reported	Semeijn, 2019

3.2 Materials and Methods

3.2.1 Generation of tagged and truncated versions of MglA

To study the cellular localization and functionality of MglA, various N- and C-terminally tagged, as well as truncated versions of MglA were generated and expressed in an *ΔmglA M. xanthus* background. The N-terminally tagged versions, based on previous work in the laboratory, used a 15 amino acid-long flexible linker between the protein and the tag. This linker, previously shown not to interfere with biological function, fully restored A-motility in *M. xanthus* (Semeijn, 2019). The same linker was employed in combination with eYFP and tetracysteine tags.

Additionally, two truncated versions of MglA were generated. Using the solved X-ray structure of MglA from *T. thermophilus* (**Fig. 24,** Miertzschke et al., 2011), the positions of the α5 helix (residues 175-195) and β0β1 sheets (residues 2-18) in MglA from *M. xanthus* were identified. Two MglA constructs were then generated, each deleting either the N-terminal α5 helix and or C-terminal β0β1 sheets (**Fig. 25**). This approach aimed to provide insight into whether the N- or C-termini are essential for the localization of MglA to the membrane.

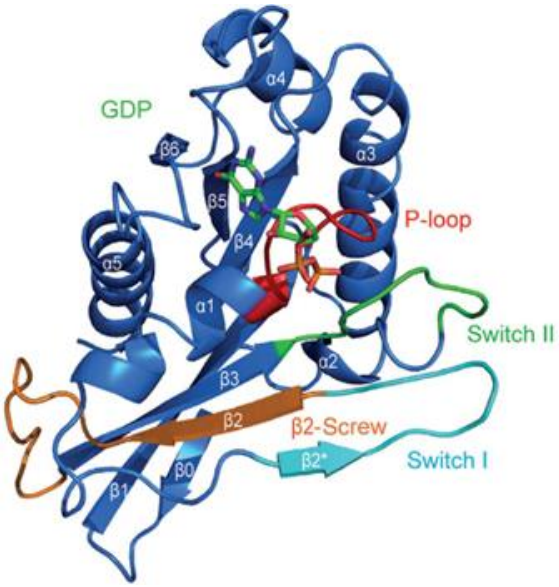

Figure 24: X-ray crystal structure of MglA in complex with GDP.
Schematic representation of the secondary structure of MglA from *T. thermophilus* bound to GDP, showing all α-helices and β-sheets, including the α5-helix and the β0β1-sheets. Image from Miertzschke et al., 2011.

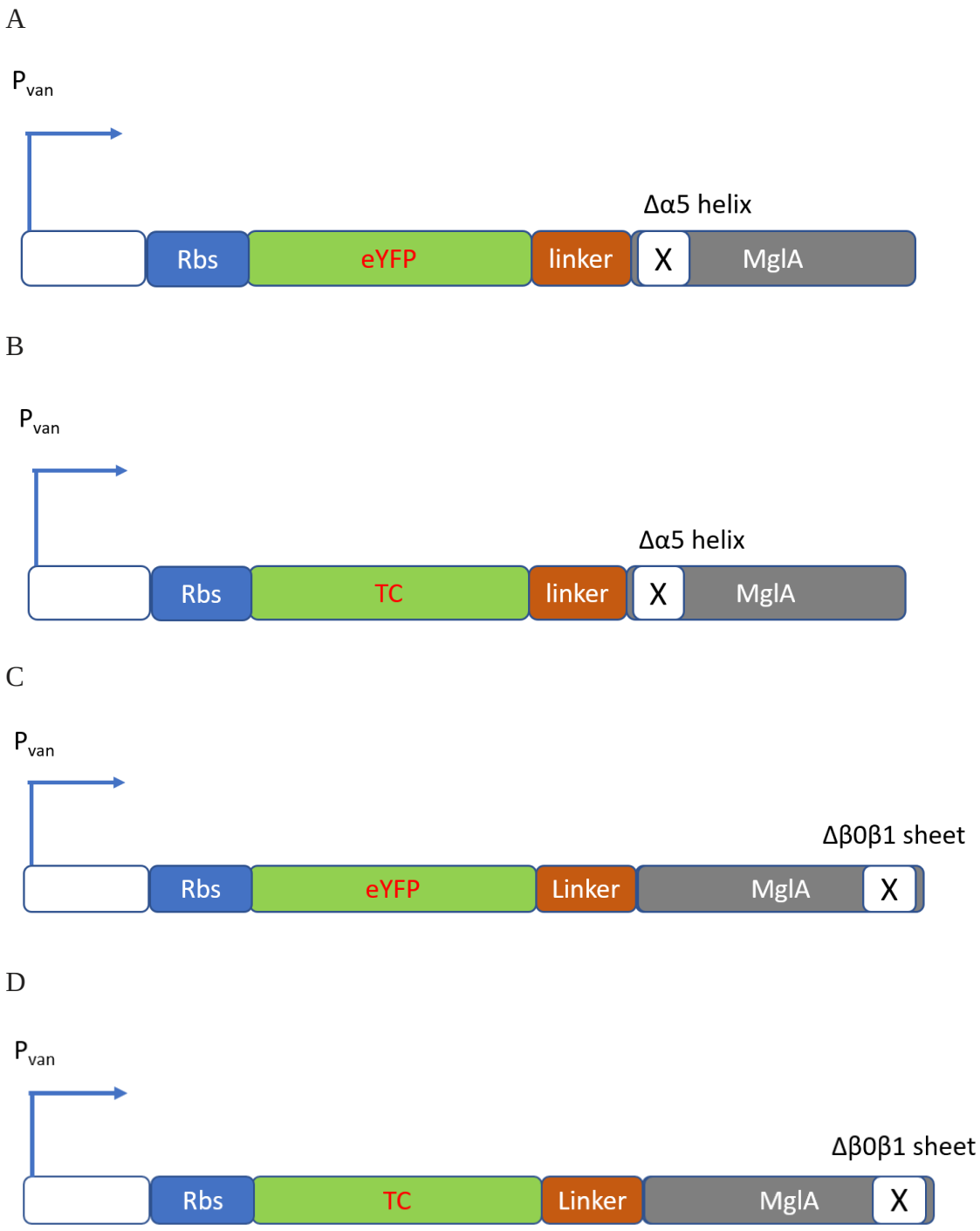

Figure 25: Schematic representation of the plasmids used for the localization studies of eYFP- and TC-tagged MglA.
The membrane localization of MglA was studied using eYFP- and TC-tagged versions of the RasGTPase. The ribosomal binding sites are shown in blue, while the N-terminal *Δ*α5-helix and C-terminal *Δ*β0β1 sheets are shown in grey. The linker region is represented in brown, and the eYFP and TC tags are depicted in green. **(A)** eYFP-MglA$^{\Delta\alpha5\ helix}$, **(B)** TC-MglA$^{\Delta\alpha5\ helix}$, **(C)** eYFP-MglA$^{\Delta\beta0\beta1\ sheets}$, and **(D)** TC-MglA$^{\Delta\beta0\beta1\ sheets}$.

3.2.2 Cloning of tagged versions of MglA

An N-terminal eYFP and TC tags-containing MglA were cloned into the pMR3679 plasmid using the restriction enzymes *NdeI* and *EcoRI*. The gene insert reactions were prepared in a 23.3 µl volume, containing 0.5 µl of each restriction enzyme and 2.3 µl of 10X CutSmart buffer. For plasmid reactions, the volume was 11 µl, with 0.5 µl of each restriction enzyme and 1000 ng of plasmid, and the rest filled with ddH_2O. Incubation of reactions occurred at 37 °C for 30 minutes. *NdeI* and *EcoRI* enzymes required a 100 mM concentration of NaCl for optimal activity. Reactions involving these enzymes were first incubated with the other restriction enzyme, followed by an additional 30-minute incubation with *NdeI* and *EcoRI* after adding 0.58 µl and 1.2 µl of 2 M NaCl to the plasmids and gene inserts, respectively. Recircularization of plasmids was prevented by incubation at 37 °C for 30 minutes with 0.5 µl of shrimp alkaline phosphatase.

The GeneJET Plasmid Miniprep Kit (Thermo Scientific) was used to purify the restriction-digested plasmids, and the GeneJET Gel Extraction Kit (Thermo Scientific) for the digested gene inserts. The Plasmid Miniprep Kit was followed by both DNA purification kits, 21 µl of elution buffer was used instead of 50 µl. DNA concentrations were measured using a nanodrop spectrophotometer.

The ligation reactions were prepared to a volume of 10.5 µl, containing 60 ng of plasmid, 30 ng of gene insert, 1 µl of T4 ligase buffer, and 0.5 µl of T4 ligase enzyme, with the rest of the volume filled with ddH_2O. The ligations were then incubated at room temperature for 10 minutes.

Transformation of chemically competent *E. coli* cells (strain DH5α) from a -80 °C stock involved adding 4 µl of ligation reaction to 50 µl of culture and incubating it on ice for 30 minutes. Afterward, the mixture was heat-shocked in a 43 °C water bath for one minute and

then immediately placed back on ice for 5 minutes. Next, 1 ml of LB liquid media was added, and the culture was incubated at 37 °C for one hour in a gently rotating tube spinner. The cultures were pelleted at 16,000 rpm for one minute using an Eppendorf 5415D benchtop microcentrifuge. The supernatant was discarded, and the remaining liquid was used to resuspend the pellet. The resuspended pellet was then spread on kanamycin (50 µg/ml) LB agar plates to select for transformants.

The inoculated plates were sealed with parafilm, incubated overnight at 37 °C, and then stored at room temperature to slow the growth of colonies to ease picking of individual transformants. For colony PCR reactions, 12.5 µl of DreamTaq polymerase master mix (Thermo Scientific), 11.4 µl of ddH_2O, 0.5 µl of DMSO (final concentration 2%), and 0.25 µl of the forward and reverse primers were mixed together. After the insert had been successfully transformed into DH5α, the plasmid DNA was harvested using a QIAprep spin miniprep kit (Thermo Fisher, 2020). The concentration of the plasmid DNA was measured with a nanodrop spectrophotometer. Subsequently, the plasmid was sent for sequencing, to confirm successful cloning. The plasmid with the insert was transformed into *M. xanthus* using electroporation at a setting of 0.65 volts. After electroporation, 1 ml of CTT medium was added, and the cells were allowed to recover for 4 hours or overnight. Cells were plated on CTT agar plates containing kanamycin.

Table 4: List of *M. xanthus* strains used for MglA localization studies.

Strains	**Expression**	**Reference**
N-terminal full length eYFP-MglA	Δ*mglA M. xanthus*	This study
N-terminal eYFP-tagged Δα5 MglA	Δ*mglA M. xanthus*	This study
N-terminal eYFP-tagged Δβ0β1MglA	Δ*mglA M. xanthus*	This study
N-terminal full-length TC-MglA	Δ*mglA M. xanthus*	This study
N-terminal TC-tagged Δα5 MglA	Δ*mglA M. xanthus*	This study
N- terminus TC-tagged Δβ0β1MglA	Δ*mglA M. xanthus*	This study
N-terminal full-length MglA-TC	Δ*bacM M. xanthus*	This study

Table 5: List of primers used for the cloning experiments of the MglA localization studies.

Plasmid	**Primers Forward and Reverse**	**Sequences 5-3**
pMR3679	MglA forward primer *NdeI*	ATCGC CATATG ATGTCCTTCATCAATTACTCATC
pMR3679	MglA reverse primer *EcoRI*	TATAT GAATTC TCACCACCCTTCTTGAGCTC
pMR3679	MglA forward primer *NdeI*	TATAT CATATG ATGTCCTTCATCAATTAC
pMR3679	MglA reverse primer *EcoRI*	TATAT GAATTC TCAACCACCCTTCTTGAG
pMR3679	BacM forward primer *NdeI*	TATATA CATATG TCTGGTGAGGTCCAC
pMR3679	BacM reverse primer EcoRI	TATATA GAATTC CTACTTCTTCTCGCCACC

3.2.3 Cloning of MglA-eYFP into the yeast *Saccharomyces cerevisiae*

The cloning of MglA-eYFP into yeast was conducted in collaboration with Dr. Ewald Hettema's laboratory at the University of Sheffield. For the cloning procedure, the *pIS04* plasmid was chosen, which contains an N-terminally gfp-tagged *Pex19* gene. This *Pex19* gene is positioned between the yeast *Pex19* endogenous promoter and the PGK1 terminator. The plasmid also contains a URA3 selection marker, facilitating the identification of positive clones using standard uracil-deficient medium (Gietz and Sugino, 1988). To enhance the suitability of the plasmid for the cloning of the *M. xanthus mglA-eyfp* gene, the multiple cloning site (MCS) of the pMR3679 plasmid was introduced. This MCS was chosen because it introduced several useful new restriction sites to the plasmid, with only one of its restriction sites being unsuitable for the planed cloning procedure. To remove this problematic restriction site of the MCS, an initial PCR amplification was performed to successfully mutate this restriction site. Following the modification of the plasmid, the *mglA-eyfp* gene was cloned into the *pIS-04* plasmid using the two restriction enzymes *HindIII* and *EcoRI*. The modified plasmid was then transformed into DH5α *E. coli* cells, using the ampicillin resistance marker for selection. To confirm the successful incorporation of the gene insert, a colony PCR was performed, and colonies with the gene insert were selected. The plasmid was subsequently isolated and sent for sequencing to validate the correct insertion.

Next, BY4741 yeast cells (MATA his3-1 leu2-0 met15-0 ura3-0) (Brachmann et al., 1998) were transformed with the modified plasmid using electroporation. After transformation, the yeast cells were recovered on supplemented medium and then plated on plates lacking uracil. This step allowed for the selection of yeast cells that had successfully taken up the *mglA-eyfp*-containing plasmid, as the plasmid's URA3 selection marker enables growth on uracil-deficient medium.

3.2.4 Fluorescent light microscopy

A Nikon dual-camera inverted wide-field microscope, located in the microscopy facility at the University of Sheffield, was utilized to acquire images of the yeast cells. The equipment comprised a Nikon Ti inverted microscope fitted with a tunable light source for fluorescent microscopy (Luminor SpectraX), operating at a wavelength of 488 nm, and a Dual Andor Zyla sCMOS camera. The microscope was also equipped with a 100x NA oil PH objective and emission filters for visualizing green, red, and blue fluorescent proteins. Before initiate image recording, the microscope's temperature-controlled stage incubation chamber was preheated for 1 to 2 hours at 32 degrees Celsius. Once the temperature of the chamber had stabilized, glass slides with the samples were positioned on the X, Y motorized stag, and a drop of high refractive index (RI 1.518) immersion oil was applied to the objective lens before examining the samples. The time-lapse duration was set to 5-10 minutes with intervals of 10 seconds, while the exposure time was approximately 100 ms for the cells expressing eYFP-tagged proteins. Fluorescent data were acquired using either FITC, DAPI, or TxRED filters, depending on the specific tag of each sample.

In addition to eYFP, the six-amino-acids-long Tetra Cysteine-tag (TC) was also used to label MglA. This tag, with the amino acid sequence CCPGCC, has a strong affinity for the membrane-permeable biarsenical fluorophores FlAsH and ReAsH, allowing pulse-chase experiments that can be used to track the movement of MglA protein clusters inside cells. Finally, images were recorded using the NIS elements software of the camera and then processed using the Fiji-image1.53i software. During processing, maximum intensity projections of the images were produced.

3.2.5 Colony expansion assays on hard and soft agar

The expansions of *M. xanthus* cell colonies were measured on hard (1.5%) and soft (0.5%) agar over a period of 1 to 3 days of growth at a temperature of 32 °C, as described in the Materials and Methods section of Chapter II.

3.3 Results

3.3.1 Investigation of the restoration of A- and S-motility of Δ*mglA* cells using N-terminal eYFP-tagged MglA

Previous work in our laboratory demonstrated that a C-terminal eYFP-tagged MglA, containing a long linker, could fully restore A-motility in a Δ*mglA* mutant at both the single-cell and swarm levels (Semeijn, 2019). However, during Western Blot analysis using an MglA antibody, a band appeared at the height of MglA, suggesting that in some fusion protein, the eYFP tag had been cleaved off. This small amount of cleaved MglA could potentially have restored motility in these cells, casting uncertainty on whether the eYFP-bound MglA is indeed biologically active. Therefore, it was decided to carefully re-examine the localization and biological activity of an N-terminal eYFP-tagged MglA expressed in a Δ*mglA* mutant background. The pMR3679 plasmid was used to control the expression level of the fusion protein with vanillate. This tunable expression level allowed the expression of the tagged MglA to match the native cellular levels of MglA during the experiment. Using this expression setup, colony spreading assay were performed at different concentrations of vanillate to test at which concentration level the colony expansion resembled that of the WT. The results showed that the N-terminal eYFP-tagged MglA was unable to rescue A-motility and colony expansion in the non-motile Δ*mglA* background, independent of the vanillate concentration (**Fig. 26** and **27)**. These data confirmed published results showing that an N-terminal eYFP-labelled MglA containing a 12-amino acid-long linker was unable to restore Δ*mglA* single cell motility (Patryn et al., 2010). Interestingly, the same study showed that a C-terminal construct was able to effectively restore single cell A-motility but only partially swarm expansion and sporulation.

A

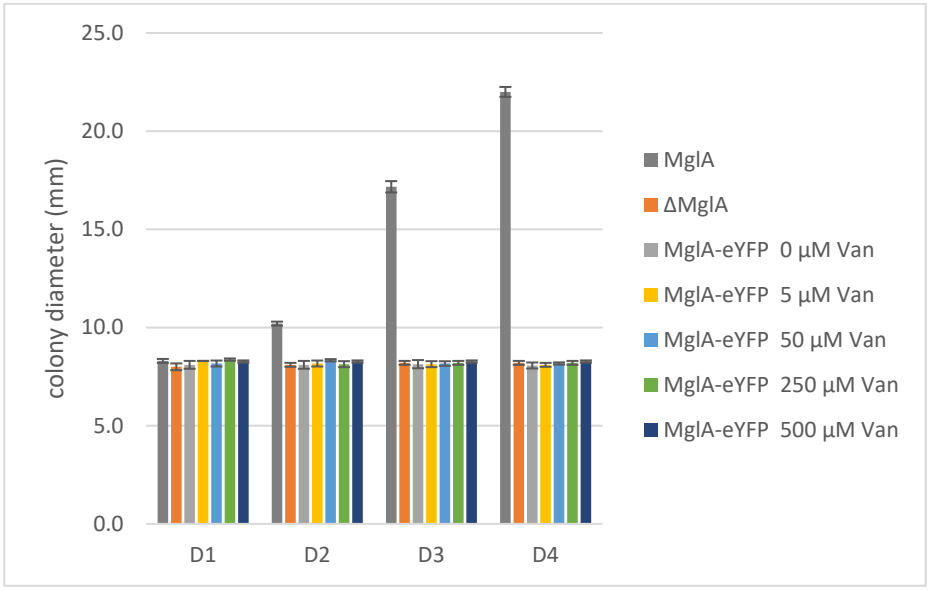

B

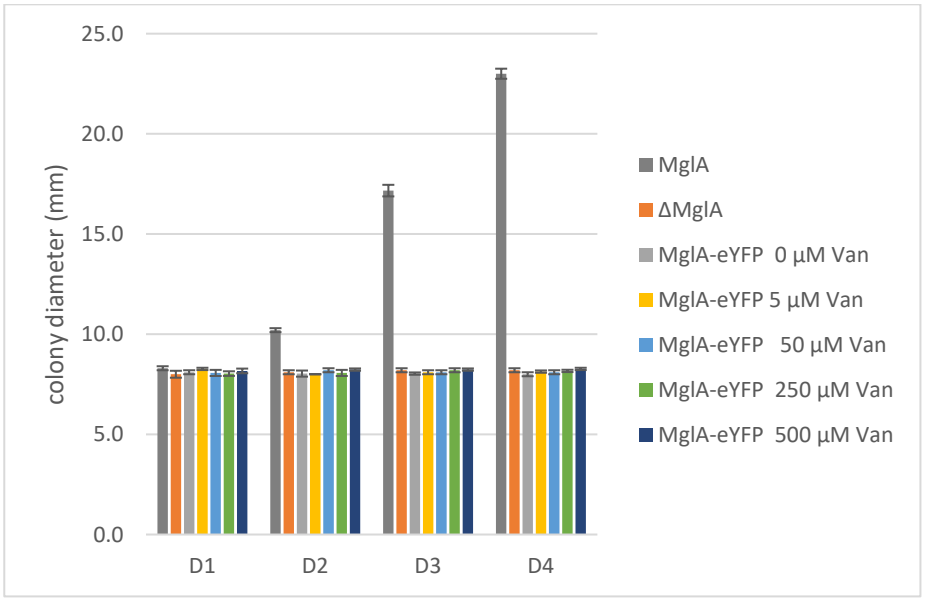

Figure 26: Investigation of A- and S-motility of Δ*mglA* cells expressing different amounts of N-terminal eYFP-tagged MglA in a Δ*mglA* background.
The experiment was conducted on (**A**) hard agar and (**B**) soft agar. The X-axis represents the number of days (D1 to D4) and the Y-axis represents the colony diameter in millimetres, respectively. The strains were unable to restore A- and S-motility in Δ*mglA* cells. The cultures were induced with increasing concentrations of vanillate, and the colony diameters were measured daily. Measurements are shown with the standard deviation based on replicates on each colony per plate.

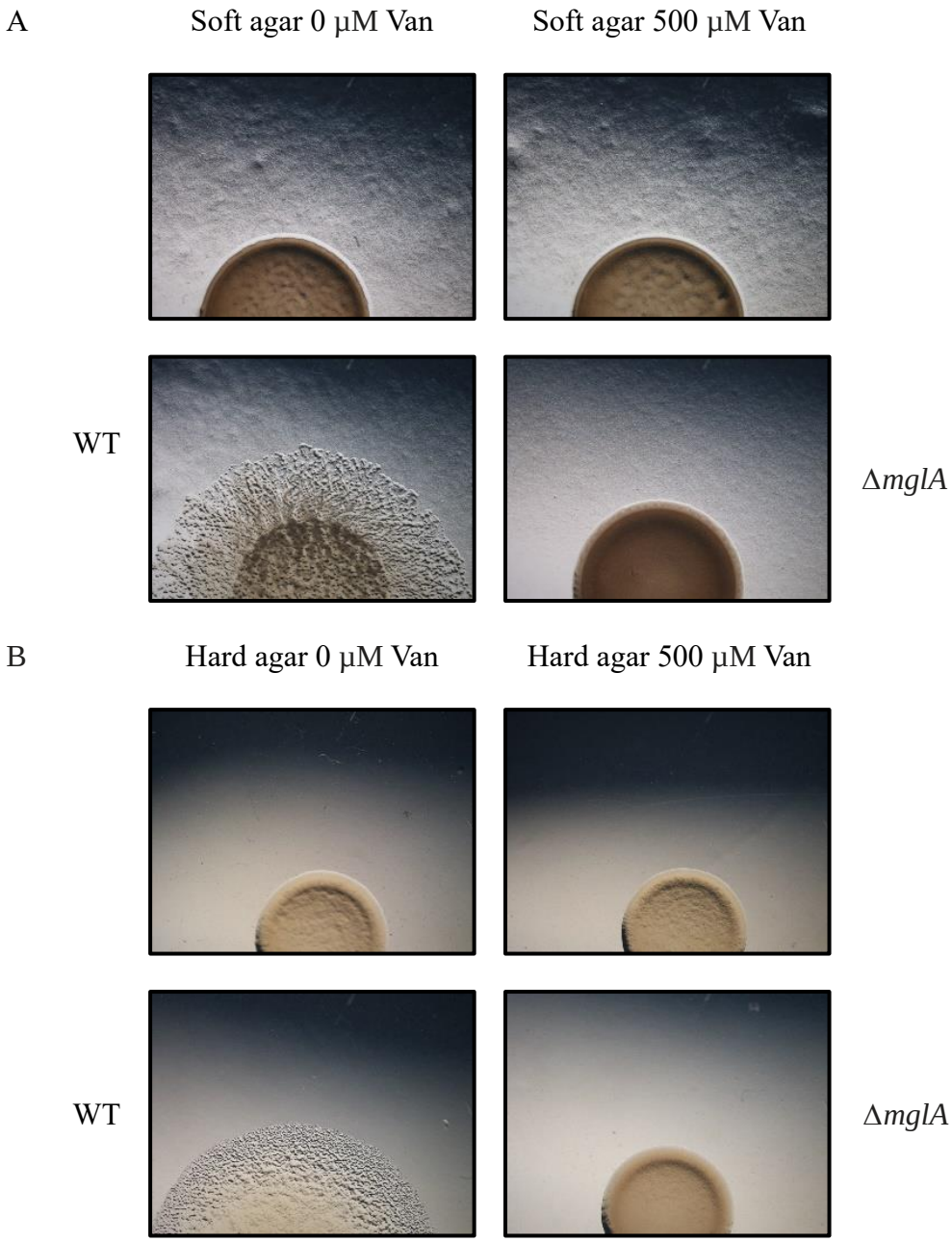

Figure 27: Expansion of Δ*mglA* cell colonies expressing different amounts of eYFP-tagged MglA in a Δ*mglA* background.
eYFP-tagged MglA was expressed at low and high vanillate concentrations in Δ*mglA* cells on soft and hard agar. Each picture represents the expansion of the spotted cells after incubation for four days at 32 °C.

3.3.2 Investigation of the restoration of A- and S-motility using N-terminal eYFP-tagged MglA$^{\Delta\beta0\beta1\text{-sheets}}$

The observed inability of the N-terminal eYFP-tagged MglA construct to complement the Δ*mglA* phenotype could have various reasons. One of these reasons might be the inability of the tagged protein to localize to the membrane. Some Ras proteins undergo post-translational modifications that enable them to localize and bind to membranes. Two common post-translational modifications of Ras proteins are prenylation and palmitoylation, both leading to attachment to membranes. As these modifications are often present close to the N-terminus of Ras-like GTPases, the commonly modified amino acid residues serine and cysteine were identified in this part of the sequence of MglA. In order to investigate their potential role in prenylation and lipidation, and consequently membrane localization, an eYFP-tagged MglA construct was generated that lacked the β0β1-sheets to determine whether their removal would impact the localization of MglA to the membrane.

Like the original eYFP-tagged MglA construct, the newly generated N-terminal eYFP-tagged MglA$^{\Delta\beta0\beta1\text{-sheets}}$ deletion mutant was investigated on both hard and soft agar. Unfortunately, similar to the full-length construct, the removal of the β0β1-sheets did not impact motility, even when grown in the presence of increasing vanillate concentrations. This result indicates that the N-terminal region of MglA may not be involved in the protein's ability to localize to membranes. As before, the WT and the Δ*mglA* mutant strain were used as positive and negative control, respectively (**Fig. 28** and **29**).

A

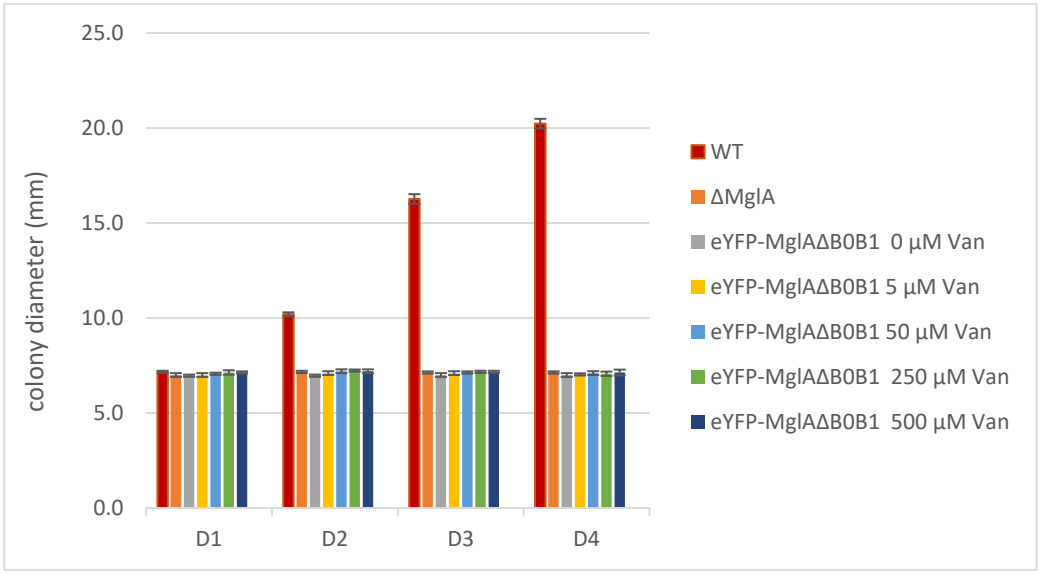

B

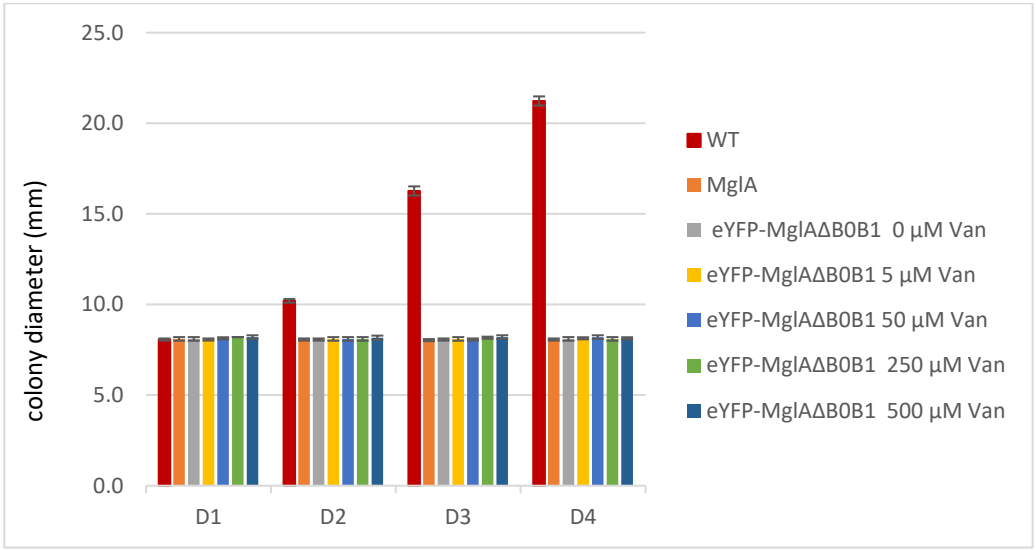

Figure 28: Investigation of A- and S-motility of Δ*mglA* cells expressing different amounts of N-terminal eYFP-tagged MglA$^{\Delta\beta0\beta1\text{-sheets}}$ in a Δ*mglA* background.
The experiment was conducted on **(A)** hard agar and (**B**) soft agar. The X-axis represents the number of incubation days (D1-D4), and the Y-axis shows the colony diameter in millimetres. The strain did not restore motility in the Δ*mglA* background under both conditions. The cultures were induced with increasing concentrations of vanillate, and the colony diameters were measured daily. Measurements are shown with the standard deviation based on replicates on each colony per plate.

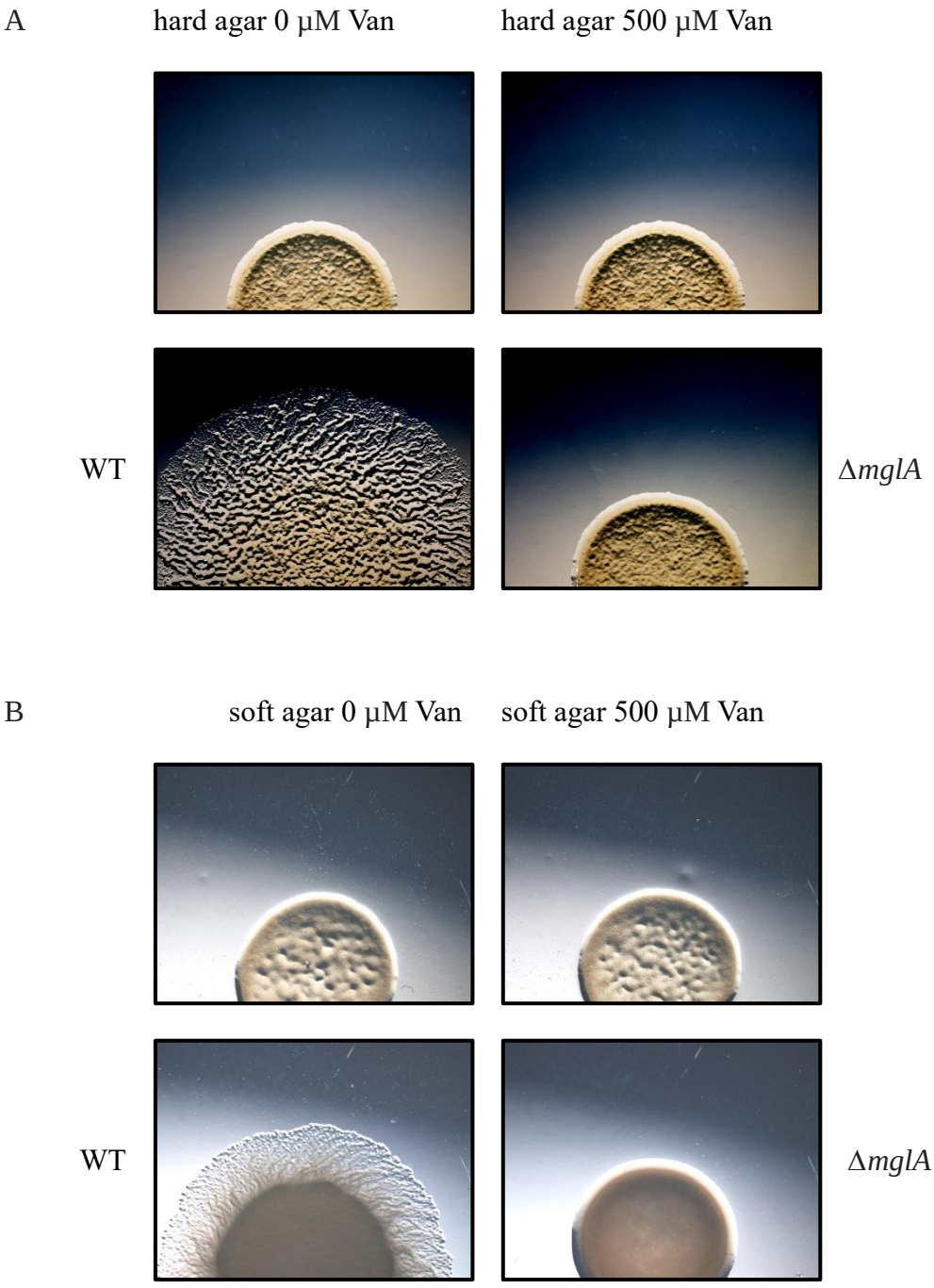

Figure 29: Expansion of Δ*mglA* cell colonies expressing different amounts of eYFP-tagged MglA$^{\Delta\beta0\beta1\text{-sheets}}$ on hard and soft agar.
An eYFP-tagged MglA$^{\Delta\beta0\beta1\text{-sheets}}$ construct was expressed at low and high vanillate concentrations in Δ*mglA* cells on hard and soft agar. Each image represents the expansion of the cell colony after incubation for four days at 32 °C.

3.3.3 Investigation of the restoration of A- and S-motility using an N-terminal eYFP-tagged MglA$^{\Delta\alpha5\ helix}$ construct

Based on the X-ray structure of MglA from *T. thermophilus*, it was suggested that the amphipathic α5 helix might play a role in binding to the membrane (Miertzschke et al., 2011). As this helix is also amphipathic in the *M. xanthus* MglA, an N-terminal eYFP-tagged MglA$^{\Delta\alpha5helix}$ construct was generated and expressed in a Δ*mglA* background. To investigate the ability of the Δα5helix mutant to restore motility in this background, the strain expressing the construct was grown overnight in liquid CTT medium, followed by spotting on soft and hard agar plates in the presence of increasing vanillate concentrations. The colony diameters were measured over a four-day period at 32 °C, and the results were compared with the WT and Δ*mglA* strains, serving as positive and negative controls. Unfortunately, like for the N-terminal eYFP-tagged MglA$^{\Delta\beta0\beta1\text{-sheets}}$ construct, no restoration of motility of the non-motile phenotype of the *ΔmglA* mutant strain was observed, independent of the concentration of added vanillate (**Fig. 30** and **31**).

A

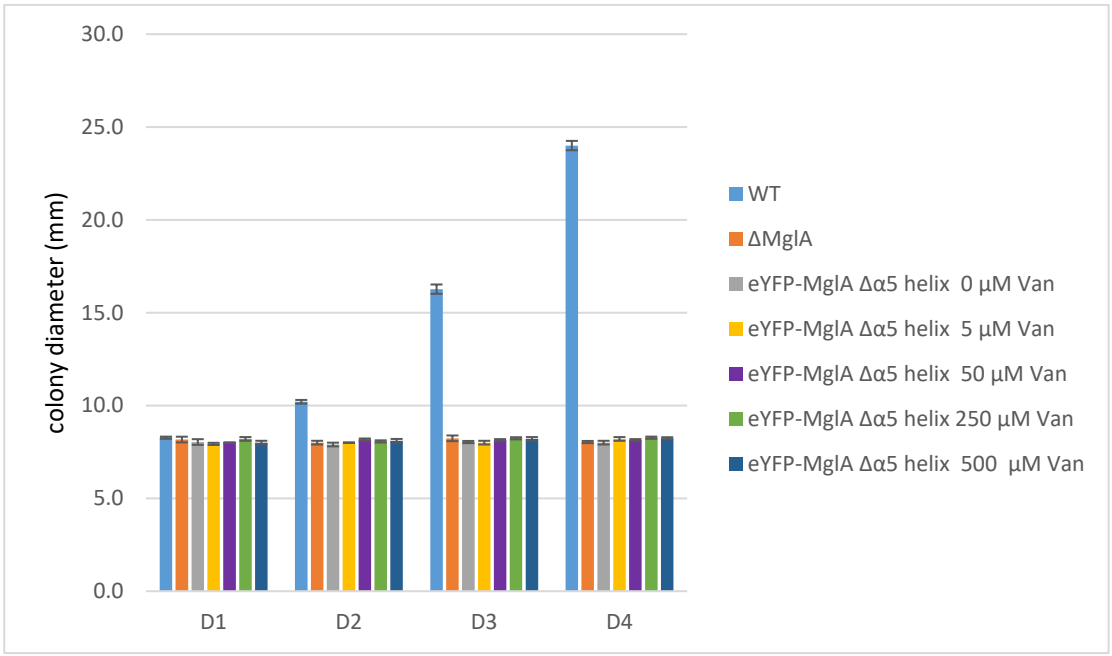

B

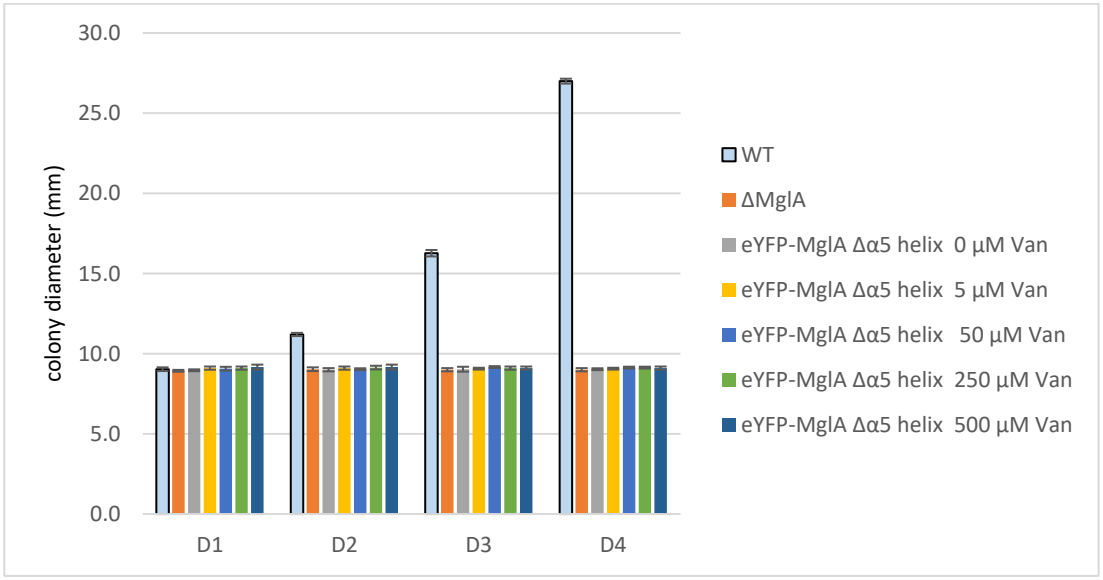

Figure 30: Restoration of A- and S-motility of Δ*mglA* cells expressing different amounts of N-terminal eYFP-tagged MglA$^{\Delta\alpha5\text{-helix}}$ in a Δ*mglA* background.
The motility assays were conducted on (**A**) hard agar and (**B**) soft agar. The X-axis represents the number of days the cells were incubated and the Y-axis shows the diameter of the colony. The strain did not restore motility in the Δ*mglA* cells under both conditions. The cultures were induced with increasing concentrations of vanillate, and the colony diameters were measured daily. Measurements are shown with the standard deviation based on replicates on each colony per plate.

Figure 31: Expansion of Δ*mglA* cell colonies expressing varying amounts of N-terminal eYFP-tagged MglA$^{\Delta\alpha5\text{-helix}}$ on hard and soft agar.
An eYFP-tagged MglA$^{\Delta\alpha5\text{-helix}}$ construct was expressed at low and high vanillate concentrations in a Δ*mglA* background on hard and soft agar. Each image represents the expansion of the cell colony after incubation for four days at 32 °C.

3.3.4 Investigation of the restoration of A- and S-motility using N-terminal TC–tagged MglA$^{\Delta\alpha5\text{-helix}}$ on soft and hard agar

According to the literature, the usage of fluorescent protein tags like eYFP, although convenient and powerful, comes with drawbacks (Leonardy et al., 2010). Due to their sizes, these tags can interfere with the proper folding of the fusion partner protein or prevent necessary protein-protein interactions or post-translational modifications to occur. Furthermore, the tag can also be cleaved of in some or most of the fusion protein upon expression as previous work in the laboratory had indicated (Semeijn, 2019). Therefore, it was decided to replace the large eYFP tag with the only 6 amino acid-long Tetra Cysteine (TC) tag. This tag is not only substantially smaller but also shows a high affinity for its fluorescent biarsenical detection reagents HlAsH and ReAsH. Consequently, an N-terminal TC-tagged MglA$^{\Delta\alpha5\text{-helix}}$ construct was generated and overexpressed in *M. xanthus* in a *ΔmglA* background on both soft and hard agar using increasing concentrations of vanillate to increase expression. Unfortunately, the change of the tag did not rescue motility in these cells even after a 4-day period of incubation at 32°C (**Fig. 32** and **33**).

A

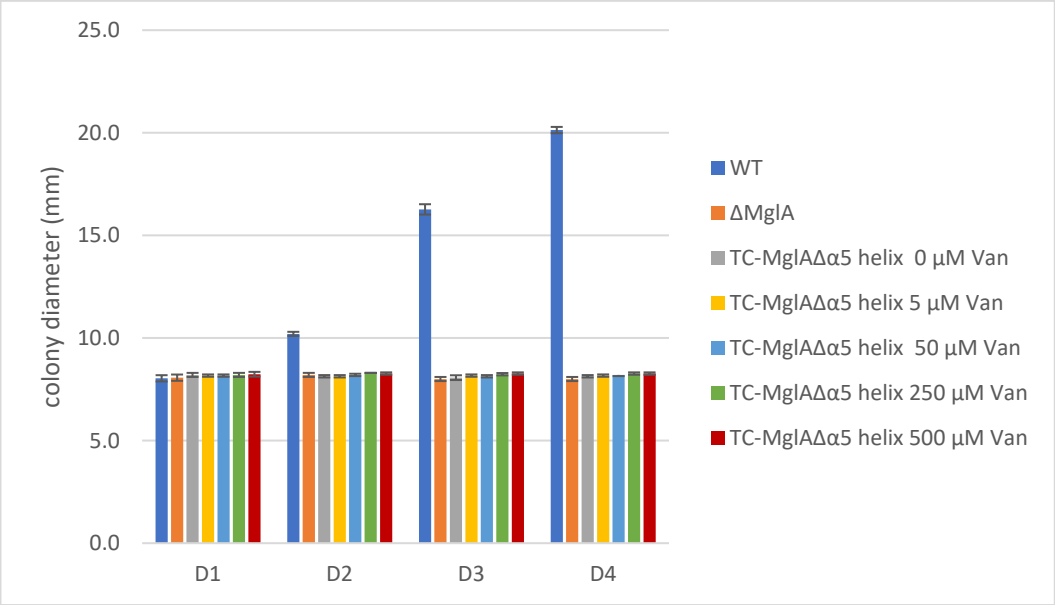

B

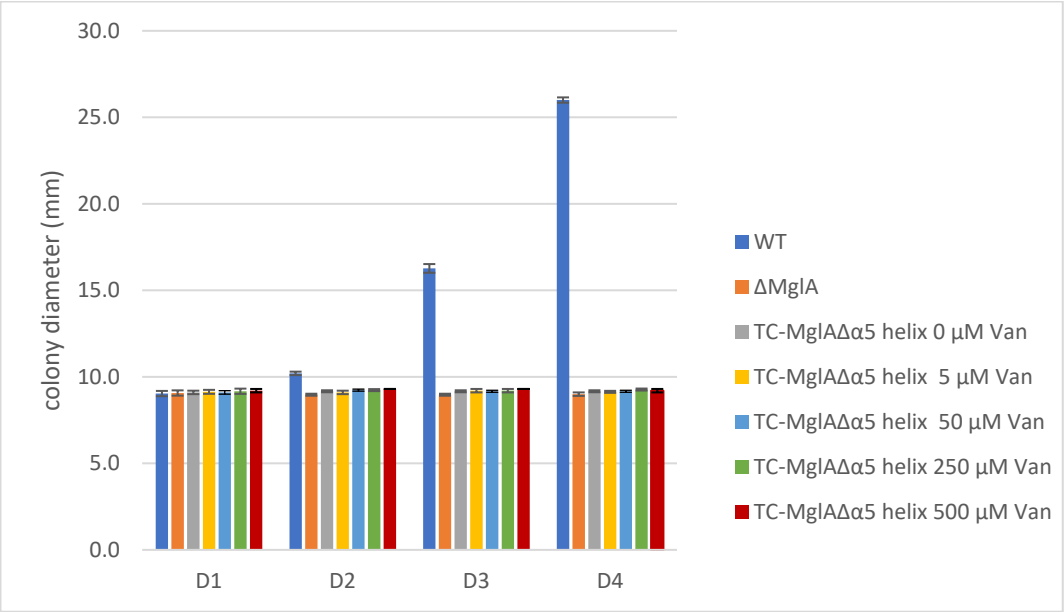

Figure 32: Investigation of A- and S-motility of ΔmglA cells expressing varying amounts of N-terminal TC-tagged MglAΔα5-helix.
The results highlight the fact that the N-terminal TC-tagged MglA$^{\alpha 5\text{-helix}}$ construct is unable to rescue the motility of a Δ*mglA* strain on both (**A**) hard and (**B**) soft agar plates irrespective of the concentration of vanillate. All assays were performed in triplicates and the average of different colonies is shown. Error bars represent standard error.

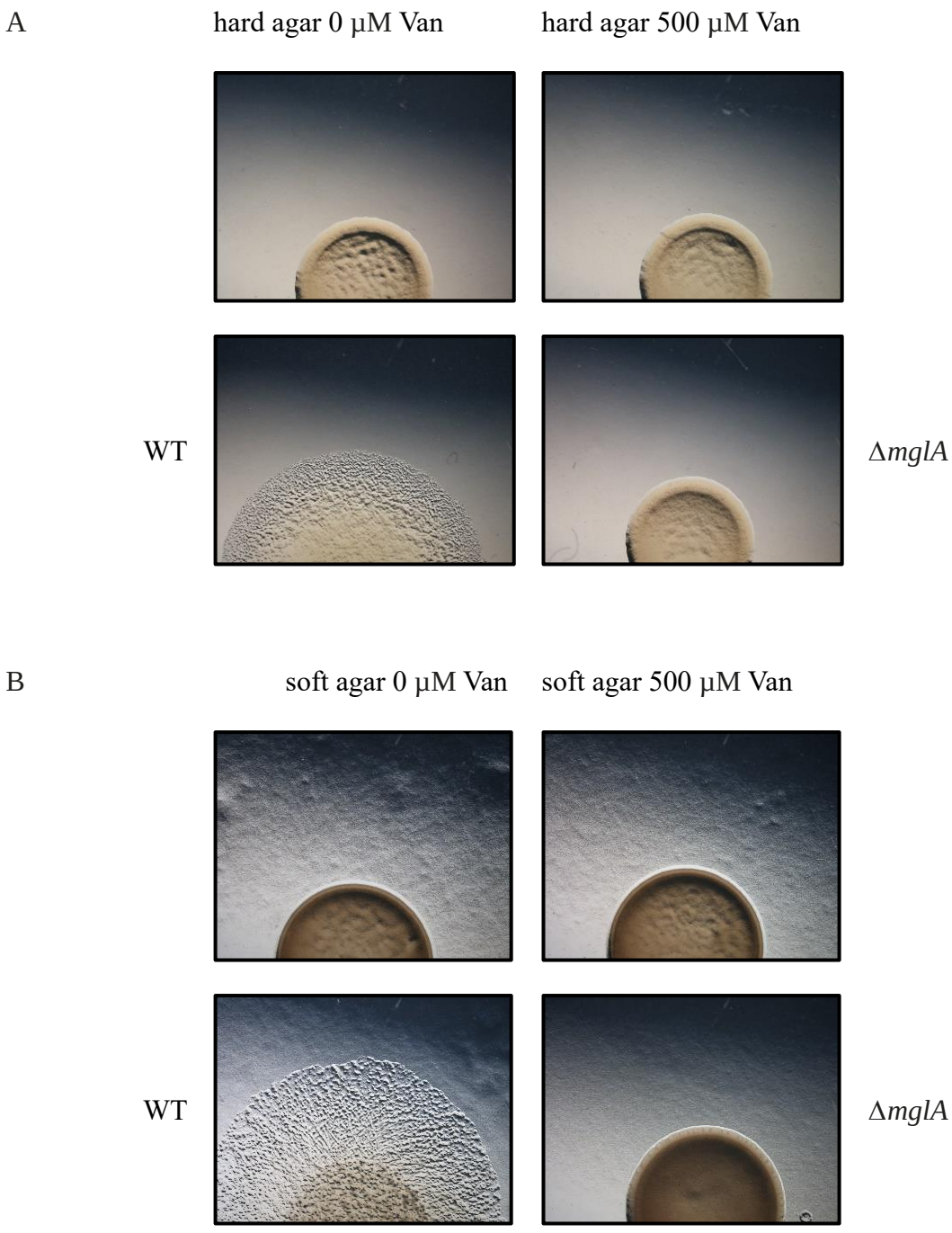

Figure 33: Expansion of Δ*mglA* cell colonies expressing varying amounts of N-terminal TC-tagged MglA$^{\Delta\alpha5\text{-helix}}$ on both hard and soft agar.
Expression of the N-terminal TC-tagged MglA$^{\Delta\alpha5\text{-helix}}$ construct in a Δ*mglA* background did not restore motility on either (**A**) hard or (**B**) soft agar, even after 3 days of growth at 32 °C.

3.3.5 Rescue of A- and S-motility using an N-terminal TC–tagged MglA$^{\Delta\beta0\beta1\text{-sheets}}$ construct

As discussed above in more detail, the idea to remove the β0β1 sheets at the N-terminus of MglA was based on the hypothesis that they may facilitate attachment to the cytoplasmic membrane and therefore, influence the localization of the protein. To test this hypothesis, an N-terminal TC-tagged MglA construct lacking the β0β1-sheets was cloned into the *pMR3679* plasmid, which contains a short linker between the tag and the N-terminus. After transforming the construct into the Δ*mglA* strain, its ability to complement the non-motile phenotype of this strain was tested on both soft and hard agar.

To induce the expression of the construct, the agar contained varying concentration of vanillate, namely, 0, 5, 50, 250 and 500 µM, to determine the optimal concentration required for stimulating motility. Unfortunately, similar to the experiments with the N-terminal TC-tagged MglA$^{\Delta\alpha5\text{-helix}}$ construct, these experiments showed that the construct lacking the two β-sheets was unable to rescue on either soft or hard agar plates **(Fig. 34** and **35)**.

A

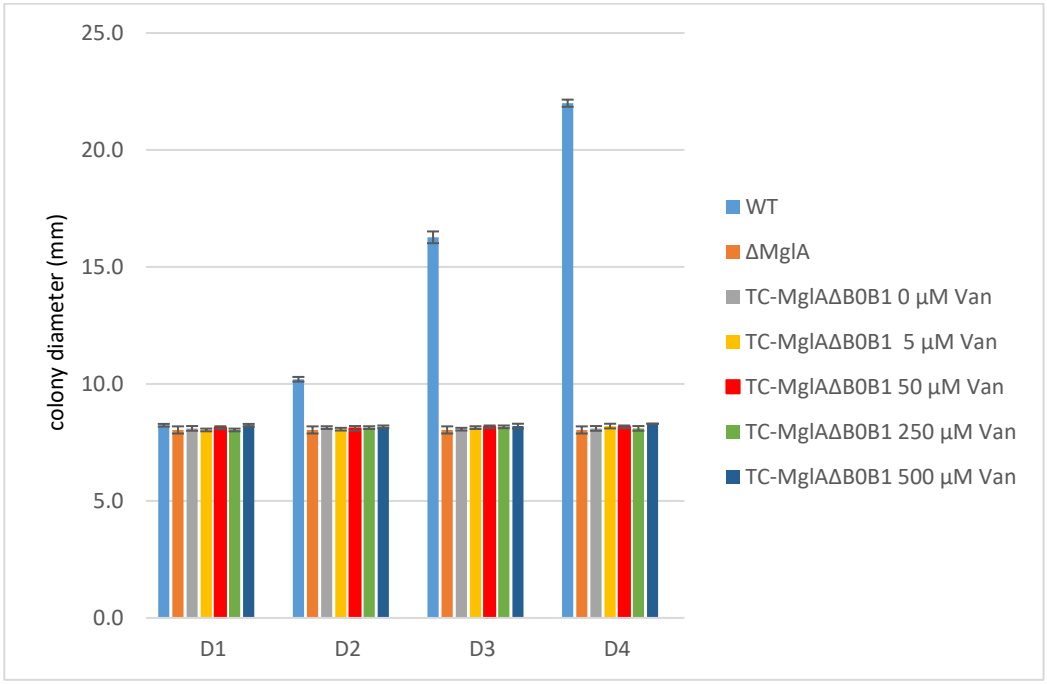

B

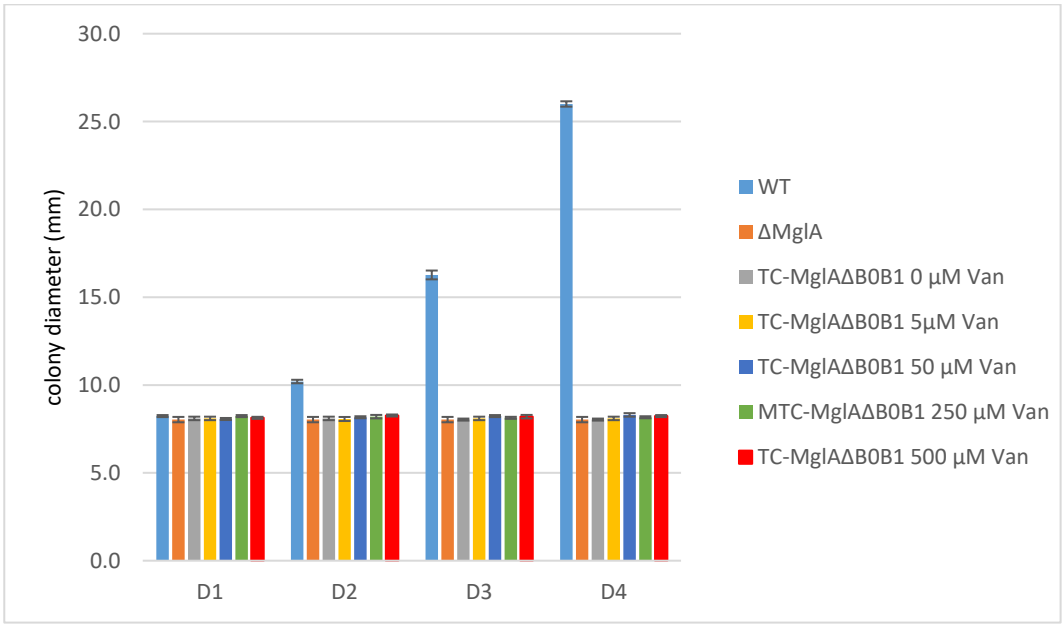

Figure 34: Investigation of A- and S-motility of Δ*mglA* cells expressing varying amounts of N-terminal TC-tagged MglA$^{\Delta\beta0\beta1\text{-sheets}}$ in a Δ*mglA* background.
The results demonstrate that the N-terminal TC-tagged MglA $^{\beta0\beta1\text{-sheets}}$ construct is unable to rescue the motility of an Δ*mglA* strain on both (**A**) hard or (**B**) soft agar irrespectively of the concentration of the inducer vanillate. All assays were performed in triplicates and the average of different colonies is shown. Error bars represent standard error.

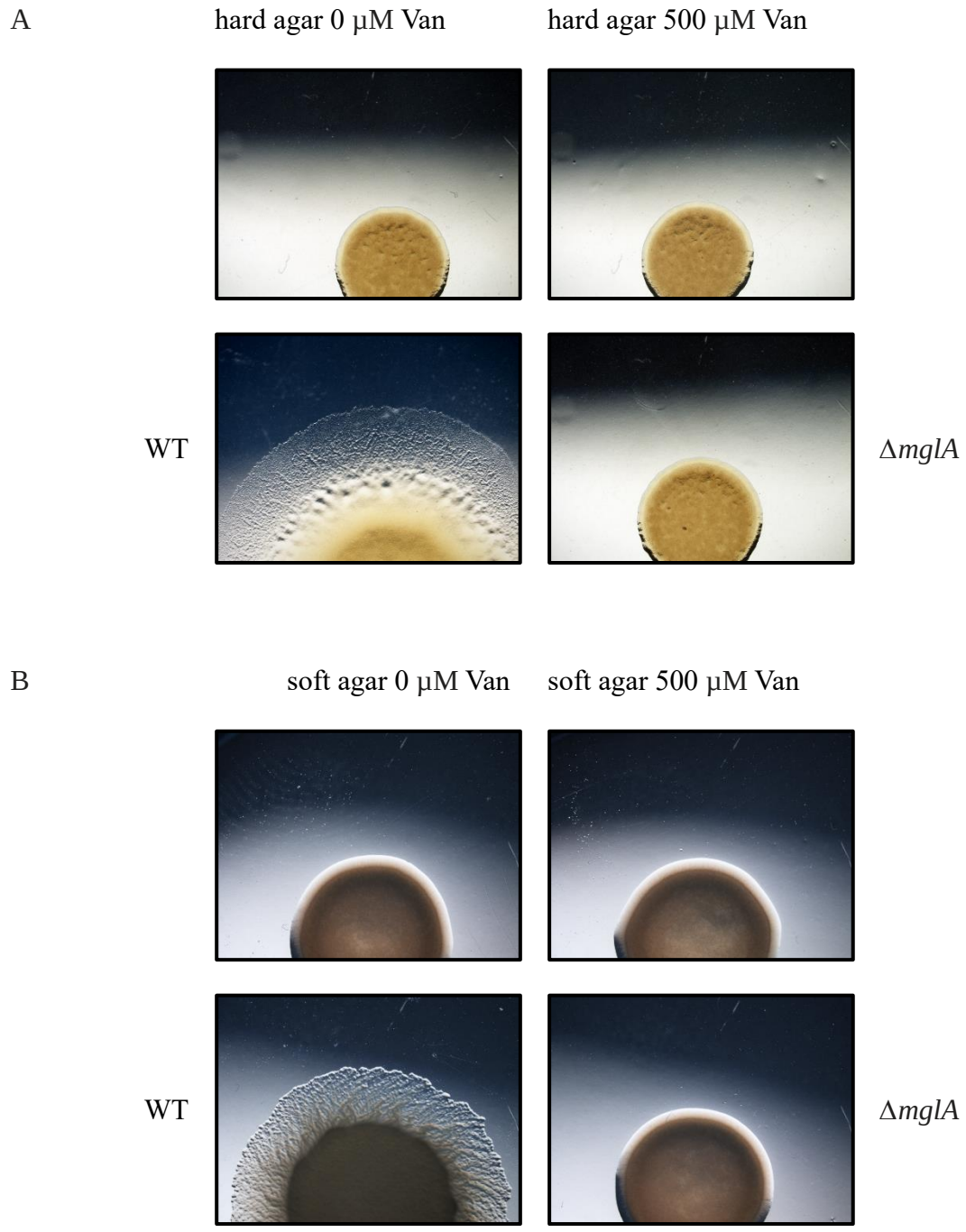

Figure 35: Expansion of Δ*mglA* colonies expressing varying amounts of TC-tagged MglA$^{\Delta\beta0\beta1\text{-sheets}}$ on hard and soft agar.
Expression of TC-tagged MglA$^{\Delta\beta0\beta1\text{-sheets}}$, like the N-terminal TC-tagged MglA$^{\Delta\alpha5\text{-helix}}$, construct in a Δ*mglA* background did not rescue motility on either (**A**) hard or (**B**) soft agar, following 3 days of growth at 32 °C in the presence of 0 or 500 µM vanillate.

3.3.6 Restoration of A- and S-motility using full-length N-terminal TC-tagged MglA

To test whether the size of the chosen tag had any influence on the ability of constructs to rescue motility in a *ΔmglA* background, the eYFP tag was replaced by the much shorter TC-tag, which is only 6 amino acids long. In preliminary experiments, N-terminal TC-tagged MglA$^{\Delta\beta0\beta1\text{-sheets}}$ and TC-tagged MglA$^{\Delta\alpha5\text{-helix}}$ failed to rescue motility. Consequently, a full-length N-terminal TC-tagged MglA construct was generated next. For this purpose, the construct was cloned into the *pMR3679* plasmid with a short linker between the tag and the N-terminus. Similar to the previous experiments, the construct was induced with increasing vanillate concentrations during growth on hard and soft agar plates. Notably, at a vanillate concentration of 500 µM, the full-length TC-tagged MglA rescued A-motility to a level close to that of WT, nearly matching the recorded motility of the positive control. Moreover, this construct also somewhat rescued S-motility during the 4-day growth period at 32 °C, albeit to a much lower degree than A-motility (**Fig. 36** and **37**), indicating that the smaller tag did not interfere with the correct folding of MglA or the potentially necessary post-translational modification of the protein (Weiss et al., 2000). Importantly, the reasons for the difference in the rescue of A- and S-motility are currently not understood.

A

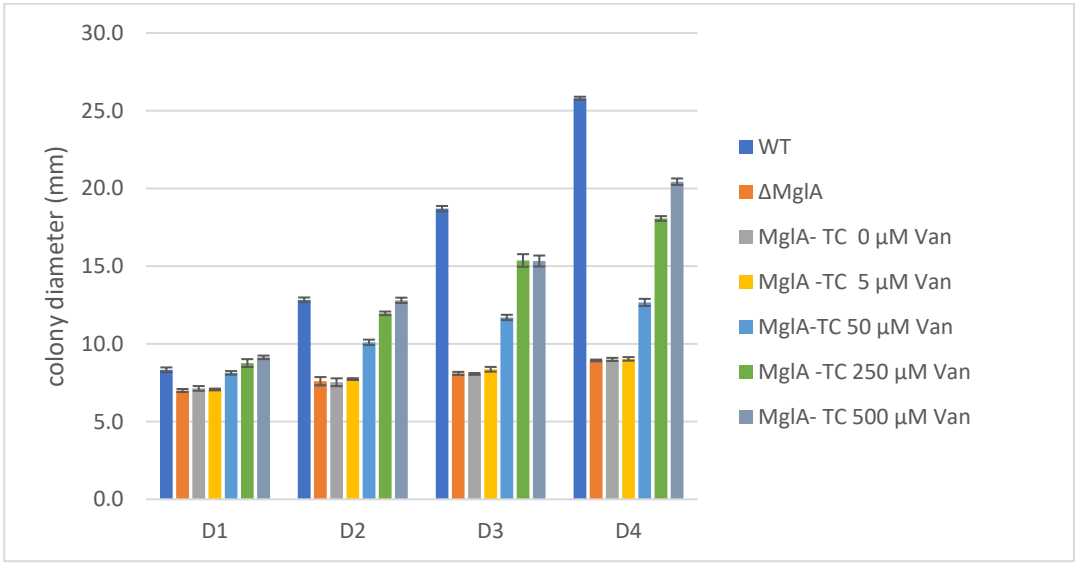

B

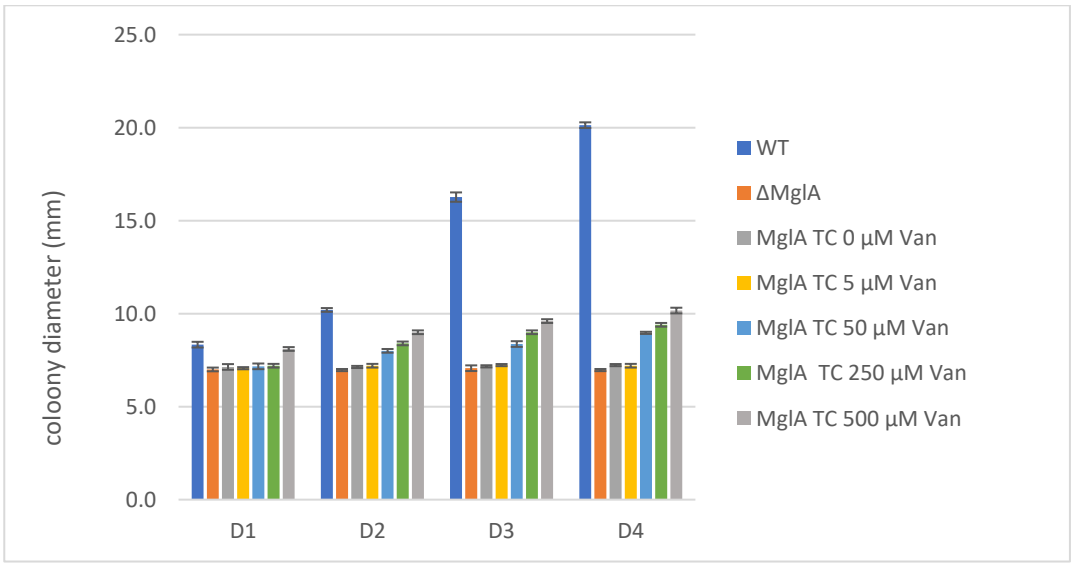

Figure 36: Restoration of A- and S-motility of Δ*mglA* cells expressing varying amounts of full-length N-terminal TC-tagged MglA in a Δ*mglA* background.
The expression of full-length N-terminal TC-tagged MglA in a Δ*mglA* background was able to restore motility of Δ*mglA* cells on **(A)** hard and **(B)** soft agar. The X-axis represents the number of days the cells were incubated and the Y-axis shows the diameter of the colony. Interestingly, the construct restored A-motility substantially better than S-motility. The cultures were induced with increasing concentrations of vanillate, and the colony diameters were measured daily. Measurements are shown with the standard deviation based on replicates on each colony per plate.

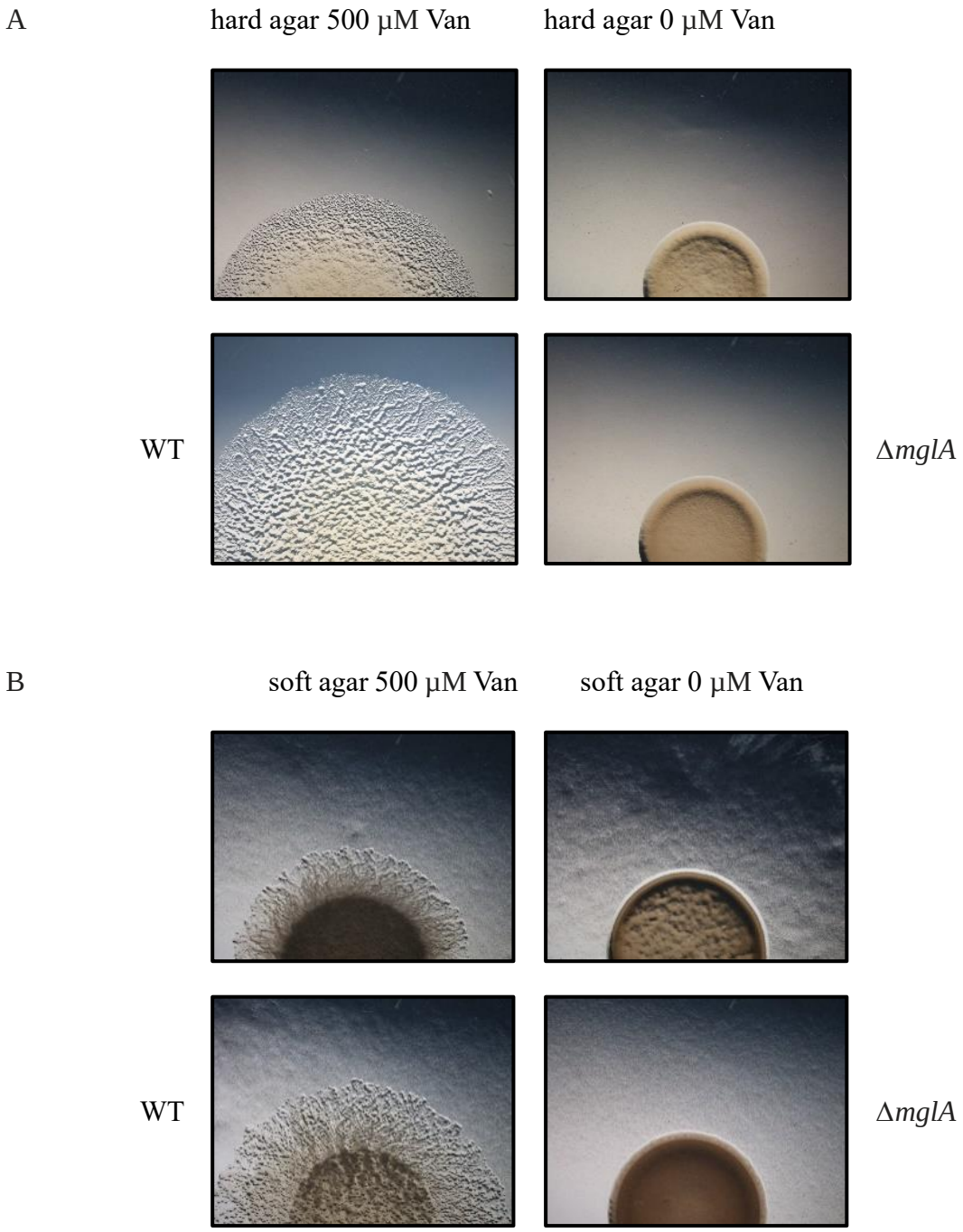

Figure 37: Expansion of Δ*mglA* cell colonies expressing different amounts of full-length TC-tagged MglA on hard and soft agar.
The expression of full-length TC-tagged MglA in a Δ*mglA* background rescues motility on both **(A)** hard and **(B)** soft agar at 32 °C, albeit the degree of rescue is very different. While A-motility is nearly rescued to WT level, the rescue of S-motility is much weaker.

3.3.7 Restoration analysis of A-motility using N-terminal MglA-TC in Δ*bacM*

As previous experiments had shown that the full-length N-terminal TC-tagged MglA was able to rescue motility of an *ΔmglA* strain nearly at wildtype level on hard agar and to a lesser degree on soft agar, we next investigated the rescue of motility of this construct in a Δ*bacM* background. This experiment was based on the results of the luciferase-based protein-protein interaction studies that had shown that the bactofilin BacM and the RasGTPase MglA bind to each other and, therefore, could influence each other's role in motility. Intriguingly, the expression of the full-length N-terminal TC-tagged MglA in the Δ*bacM* strain had the opposite effect from the expression in the Δ*mglA* strain, reducing A-motility on hard agar instead of increasing it. At low concentration of vanillate such as 0, 5 or 50 µM vanillate the cell colonies containing the construct expanded at nearly wild type level, a process that is drastically reduced at higher vanillate concentrations like 250 or 500 µM. The Δ*mglA* and Δ*bacM* strains were used in these experiments as a negative and positive controls, respectively. Overall, these results suggest that the overexpression of the tagged MglA ion the absence of BacM interferes with motility and possible cell viability (**Fig. 38** and **39**).

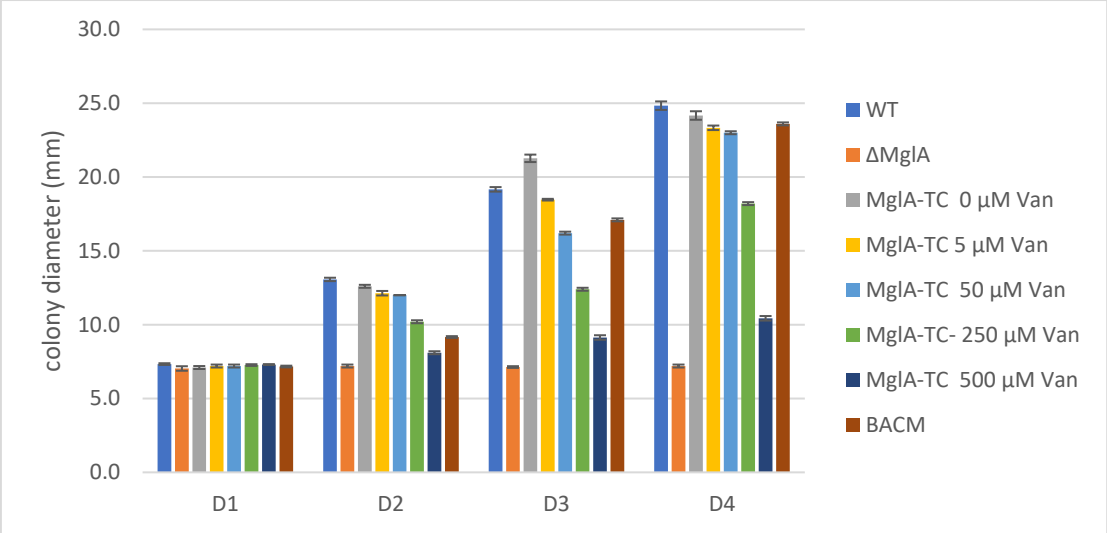

Figure 38: Change of A-motility of Δ*bacM* cells expressing varying amounts of full-length N-terminal TC-tagged MglA on hard agar.
Vanillate-induced increased expression of full-length N-terminal TC-tagged MglA in Δ*bacM* cells reduces A-motility on hard agar. All assays were performed in triplicates and the average of different colonies is shown. Error bars represent standard error.

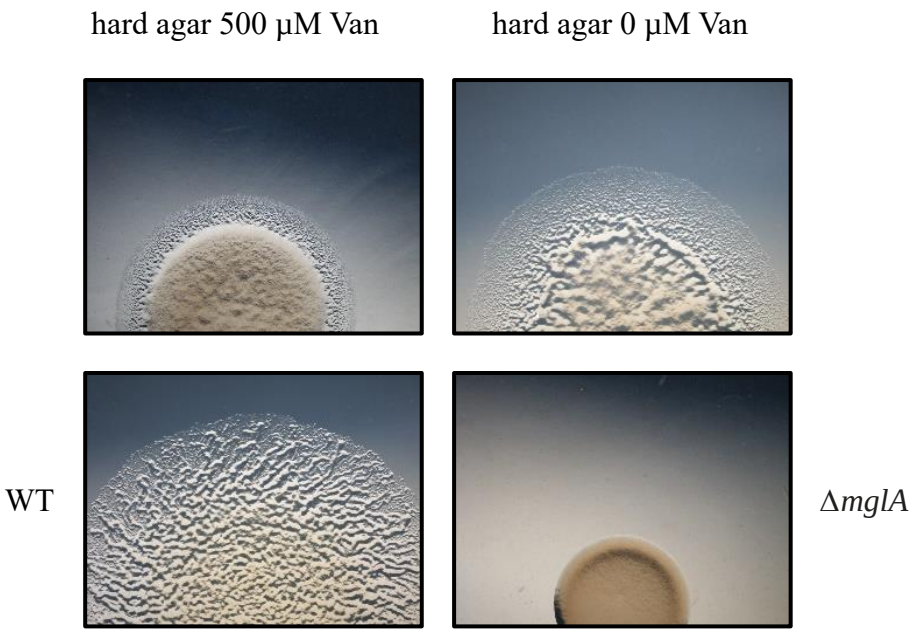

Figure 39: Expansion of Δ*bacM* cell colonies expressing varying amounts of full-length N-terminal TC-tagged MglA on hard agar.
Images of colony expansion were taken after growth for 3 days at 32 °C at different concentrations of vanillate. The induced increased concentration of the tagged MglA reduces A-motility on hard agar.

3.3.8 Fluorescent microscopy localization studies of N-terminal TC-tagged MglA$^{\Delta\beta0\beta1\text{-sheets}}$, TC-tagged MglA$^{\Delta\alpha5\text{-helix}}$, and full-length TC-tagged MglA

Published research has demonstrated that fluorescently labelled MglA, capable of complementing the *ΔmglA* phenotype, exhibits unipolar localized at the leading pole of the cell during locomotion. This suggests that this distribution mirrors the localization of native non-tagged MglA. Importantly, this research has also shown that the choice of the MglA terminus used for tagging significantly influences the localization and degree of complementation (see **Table 3** for a summary of relevant published results). Even more importantly, when considering the degree of complementation, tagged versions of MglA that restore single-cell level A-motility do not necessarily restore A-motility at the swarm level. This makes it imperative to investigate the localization and degree of complementation for each construct (Guzzo et al., 2018; Mercier et al., 2020; Zhang et al., 2021).

Therefore, we decided to investigate the cellular localization and ability to bind to membranes for the following three constructs: The N-terminal TC-tagged MglA$^{\Delta\beta0\beta1\text{-sheets}}$, the N-terminal MglA$^{\Delta\alpha5\ \text{helix}}$, and the full-length TC-tagged MglA strains. For the 3-hour-long investigations on 1.5% CTT hard agar plates, the first two strains were induced using 500 µM vanillate, while the third strain was induced with varying amounts of vanillate. For the first two strains, quite different observations were made (**Fig. 40**). While most of the cells of N-terminal TC-tagged MglA$^{\Delta\beta0\beta1\text{-sheets}}$ showed intracellular fluorescence that was either punctate of diffusely distributed throughout the cells, the N-terminal MglA$^{\Delta\alpha5\ \text{helix}}$ carrying strain often showed no fluorescence at all but exhibited signs of cellular stress instead, with many cells being dead or clearly damaged. In contrast, the cellular localization of the full-length TC-tagged MglA strain mirrored more closely the distribution reported in the literature, with many

cells showing punctate staining either in form of lateral or unipolar clusters, the latter possibly representing MglA clusters at the leading pole where the T4P are located (**Fig. 41**).

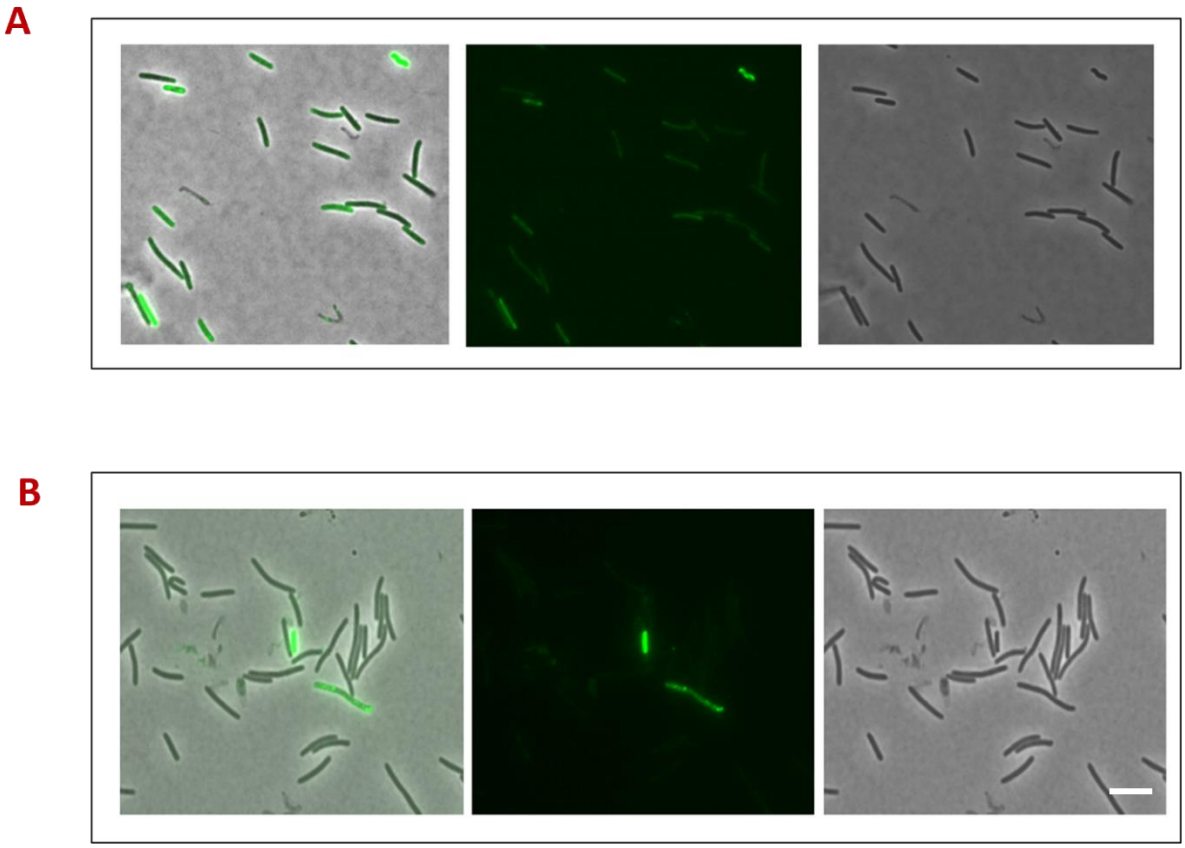

Figure 40: Fluorescence microscopic localization of two variously N-terminal TC-tagged MglA constructs. While many cells show fluorescence in (**A**), the TC-tagged MglA$^{\Delta\beta0\beta11\text{-sheets}}$ construct, most cells in (**B**), the TC-tagged MglA$^{\Delta\alpha5\ helix}$ construct were non-fluorescent and showed signs of cellular stress instead after induction with 500 µM vanillate at 32 °C for 4 days. The rows show from left to right, the fluorescence image, the overlay view, and the phase contrast image. Scale bar = 5 µm.

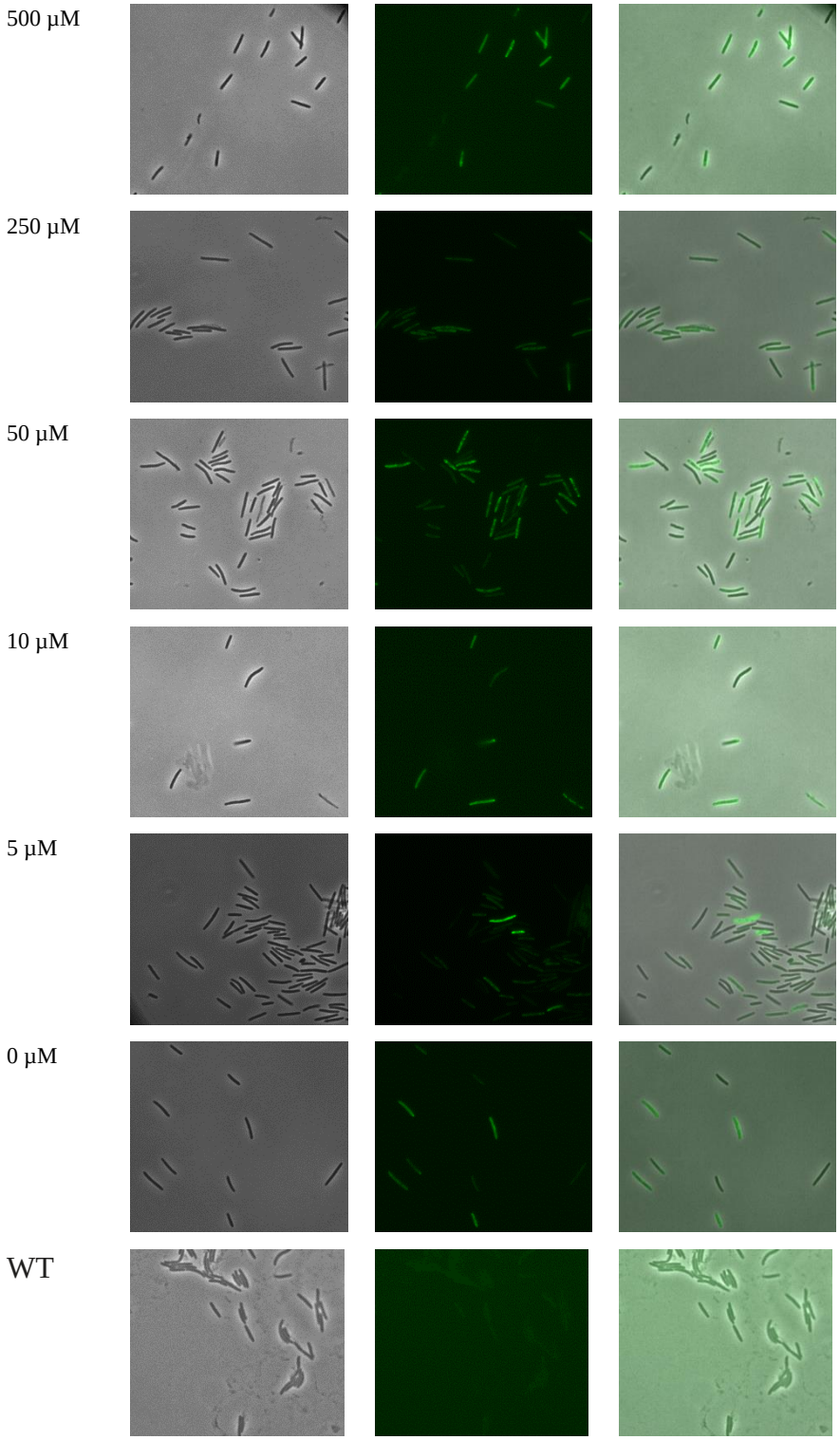

Figure 41: Fluorescence microscopic localization of the full-length N-terminal TC-tagged MglA in a Δ*mglA* background at varying concentrations of vanillate.
Each row shows from left to right: the phase contrast image, the overlay view, and the fluorescence image with the concentrations of vanillate shown in µM. All images were recorded on hard agar after growth for 4 days at 32 °C. The wild type is used as negative control as this strain does not contain any tagged protein that can interact with the added biarsenical fluorophore.

3.3.9 Fluorescence light microscopic localization of *M. xanthus* MglA-eYFP in yeast

Although the central role of MglA in *M. xanthus* motility has been well established more than thirty years ago, the precise role or process the protein in motility plays is still unclear. Interestingly, a landmark paper demonstrated that the Ras GTPase Sar1 from *S. cerevisiae* could partially complement the motility and sporulation defects in the Δ*mglA M. xanthus* strain (Hartzell, 1997). Inspired by these observations, a reverse-engineered experiment was conducted in which MglA was expressed in yeast to investigate its cellular localization to potentially gain new insights into its biological function. Yeast was also chosen because it possesses additional endomembrane systems such as the ER, mitochondria, Golgi apparatus, etc. which differ in lipid composition and curvature.

Surprisingly, MglA-eYFP expressing yeast cells displayed a non-uniform distribution of fluorescence (**Fig. 42**). According to our collaborator Dr. Ewald Hettema, this non-uniform fluorescent distribution is indicative of mitochondrial staining. This somewhat unexpected result could suggest that MglA-eYFP might bind to mitochondrial membranes due to their high content of cardiolipin, a lipid also found in bacterial cytoplasmic membranes, particularly in areas of membrane curvature such as the cell poles, deformations of the cell envelope, and during cell division. Excitingly, this observation could indicate that MglA interacts with cardiolipin either directly or through post-translational modification and, as a consequence, becomes enriched at the cell poles in *M. xanthus* cells.

To record the cellular localization of MglA-eYFP in yeast, the transformed yeast cells were grown overnight in YPD medium and needed relatively long exposed due to the weak fluorescence inside the cells (5 s, binning 1x1, gain 3 s). WT BY4741 yeast cells were used as a negative control (**Fig. 43**).

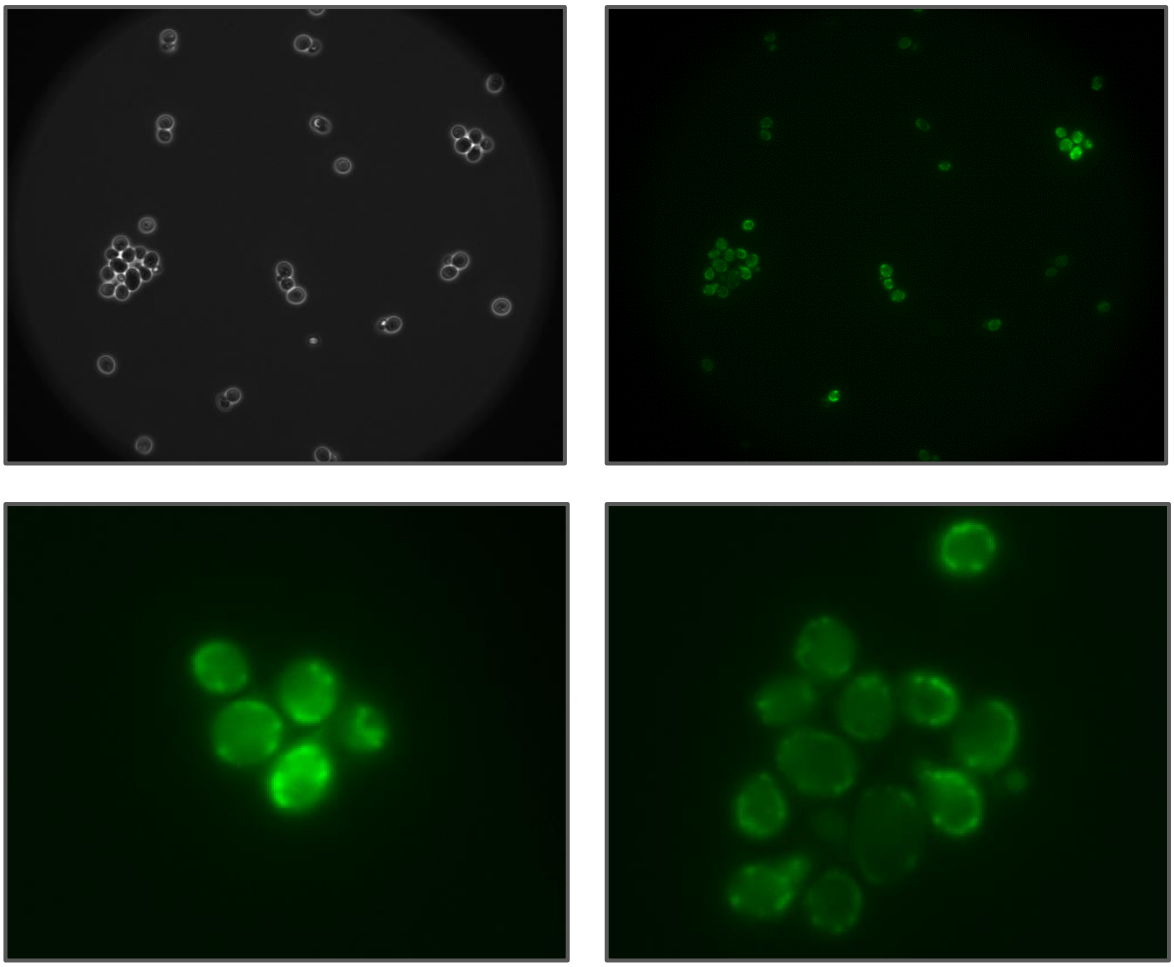

Figure 42: Image of background fluorescence in WT BY4741 yeast control cells on TPM agar. Overnight-grown WT BY4741 yeast cells were spotted onto TPM agar patches. The upper two images show the phase-contrast picture of a number of cells (left) and the corresponding fluorescence image (right). The two images in the lower row show two groups of cells from the upper right fluorescence picture at high magnification (1000x). A relatively long exposure was necessary to capture the weak, diffusely distributed autofluorescence of the cells (5 s, binning 1x1, gain 3s).

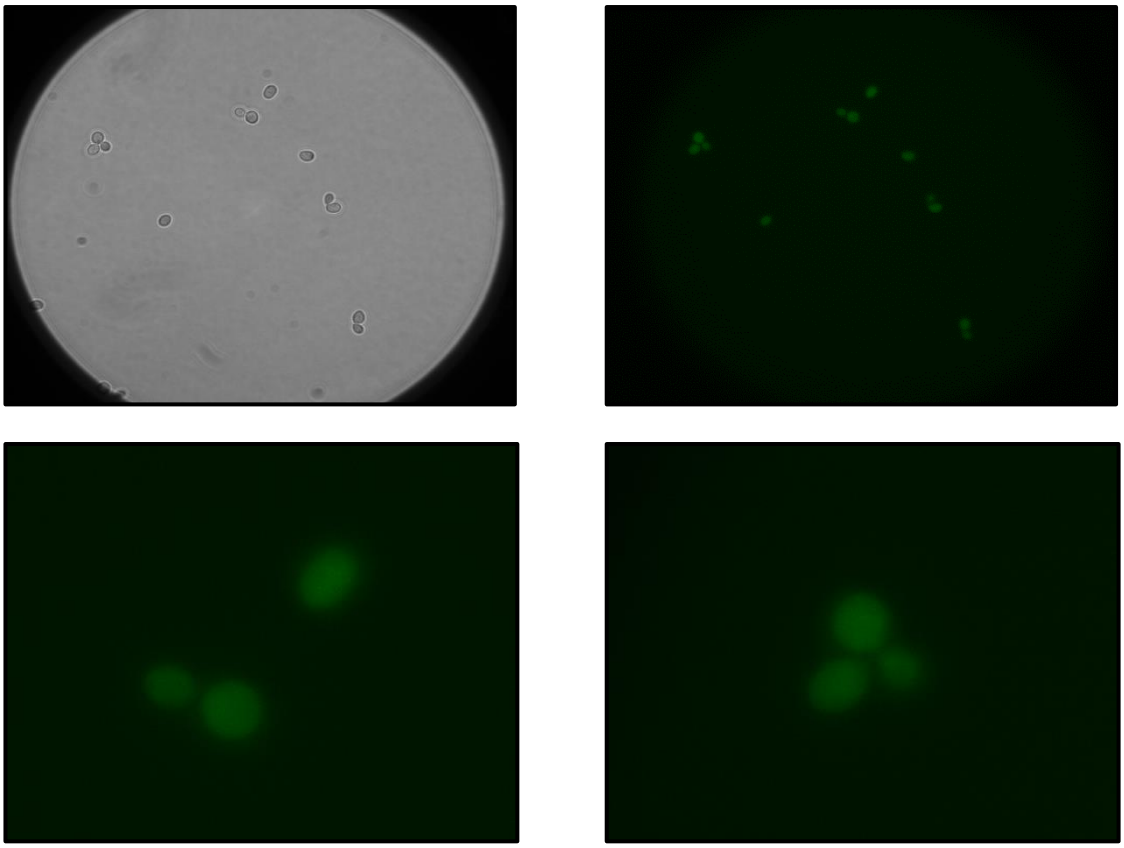

Figure 43: Fluorescent microscopy of the cellular localisation of MglA-eYFP in yeast cells.
WT BY4741 yeast cells containing the pIs-04 plasmid expressing MglA-eYFP were grown overnight in liquid YM1 medium. The upper two images show the phase-contrast picture of several cells (left) and the corresponding fluorescence image (right). The two images in the lower row show two groups of cells from the upper right fluorescence picture at high magnification (1000x). Note, the punctate staining at the periphery of the cells, which is typical for mitochondrial staining. The same long exposure settings (5 s, binning 1x1, gain 3s) were applied as for the control cells to enhance the comparability of the images.

3.4 Discussion

Previously published studies had reported that N- and C-terminally eYFP-tagged MglA can complement the motility of a Δ*mglA M. xanthus* strain (Leonardy et al., 2010; Mauriello, 2010; Patryn et al., 2010). Moreover, these studies showed that the labelled MglA formed unipolar and lateral clusters, believed to be the physiologically active arrangement of the protein in motile cells. Although these results seem encouraging for using fluorescently labelled fusions of MglA to study the cellular localization and behaviour of this small Ras-like GTPase, closer inspections in the lab had revealed that the previously used eYFP fusions of MglA only complemented motility at the single cell level, not at the swarm level. Furthermore, cells expressing the fusion protein versions of MglA showed reduced motility compared to WT cells. Overall, these results indicate that the fluorescently labelled versions of MglA generated and used so far are deficient in their ability to truly complement the Δ*mglA* motility phenotype.

Therefore, the constructs and experiments described in this chapter aimed to generate a fluorescently tagged MglA construct that would behave like native untagged MglA and complement motility at the swarm level, enabling colony spreading. To achieve this, we expressed different tagged versions of MglA using the *pMR3679* plasmid, which allows for tightly controlled expression. Two different tags were tested: the approximately 27 kDa large eYFP tag and the much smaller six amino acid-long TC-tag. Additionally, the length and amino acid composition of the linker between the tags and the MglA protein were modified to identify an optimally suited linker, a feature that is particularly important when using the large eYFP tag. While previous linkers were 12 (Patryn et al., 2010) or 11 aa-long (EFERYASPVGH; Semeijn, 2029), here, a 15 aa-long linker was used that is rich in glycine and serine to provide a high degree of flexibility.

In a previous study in the laboratory, it had been shown that a C-terminally eYFP-tagged MglA was able to rescue A- and S-motility (Semeijn, 2019). Upon induction with 250 µM

vanillate, the moderately expressed MglA-eYFP construct resulted in wild type levels of A- and S-motility in a *ΔmglA* background. Unfortunately, closer inspection of these results by Western Blots indicated that besides the protein band of the fusion protein, the cells also contained an MglA antibody-cross-reacting protein at the size of native MglA, indicating that a small percentage of the fusion protein may have been cleaved during expression. A similar cleavage of the MglA fusion protein had been reported for other constructs in the literature, demonstrating that the observed proteolytic processing of the fusion protein may have interfered with the biological activity and localization of MglA in *M. xanthus* cells (Leonardy et al., 2010). To overcome these issues, it was decided to try using an N-terminally eYFP-tagged MglA instead, a strategy that had been used before (Leonardy et al., 2010; Patryn et al., 2010). Although these previous studies reported issues with the biological activity and localization of the N-terminal eYFP-MglA, we tried to address these by using an inducible expression plasmid combined with a 15 aa-long flexible linker.

Using this novel construct, various strategies were employed to improve the previously obtained results (Leonardy et al., 2010). These strategies included the use of varying concentrations of the inducer vanillate to fine-tune the amount of MglA, as well as using different environmental situations during expression such as growth on soft and hard agar. Unfortunately, for none of these conditions was eYFP-MglA able to rescue motility, likely indicating that the relatively large eYFP tag, even when separated by a long and more flexible linker, interfered with the biological function of MglA. One possible reason for the inconsistency of the experimental results could be the differences in cell preparation methods. In the Patryn study, cells were grown in 0.5% (v/v) methylcellulose TPM broth or placed on TPM 1.5% agar pads (Patryn et al., 2010), whereas in our laboratory, cells were placed on freshly prepared 0.7% or 1.5% CTT agar pads instead, which provided nutrients, allowing the

cells to be metabolically active during the experiment. This metabolic boost may have influenced the expression and localization of the MglA fusion protein.

Other differences resulted from the storage of the pre-made agar pads. Although all agar pads were covered with polyvinyl film to prevent drying, they were stored differently. In particular, the prolonged storage in the fridge at 4°C could have negatively impacted motility by increasing the dryness of the agar pad, which may, in turn, have impacted not only motility but also the intracellular localization of MglA. However, the most important factor influencing the results is certainly the size of the the eYFP tag (27 kDa), which is larger than the tagged protein, MglA (21 kDa). It is for this reason that it was hypothesized that the size of eYFP, even when separated by a linker, interferes with MglA's function. Therefore, the much smaller, only six-amin-acid-long TC tag was used to tag MglA. When expressed in a *ΔmglA* background, TC-tagged MglA was indeed able to rescue motility in these otherwise non-motile cells on both soft and hard agar. Encouragingly, the degree of A-motility observed increased with increasing concentrations of vanillate, matching at the highest concentration the wild type level of motility. Moreover, the rescue of motility for the TC-tagged MglA was also observed on soft agar, indicating that the TC-tagged construct rescued both A- and S-motility. Based on these results, therefore, in general terms, the most promising tags would combine a small tag like TC with a long, highly flexible linker, a result that will be valuable for the design of future tagged versions of MglA.

We next analysed the intracellular localization of the construct using fluorescence light microscopy. Similar to published reports, various intracellular patterns of localization were observed for the TC-tagged MglA. While some cells showed a uniform diffuse distribution of the tagged protein, other cells had punctate staining, including lateral and polar clusters. Interestingly, similar results had been previously described for eYFP-tagged MglA (Patryn et al., 2010), indicating that tagged MglA under physiological conditions forms clusters and

associates with membranes, particularly in the cell's polar regions - a distribution similar to that shown by some eukaryotic Ras-like proteins that are involved in signalling and membrane curvature (Antonny et al., 2005; Booth et al., 2007; Hanna et al., 2016; Liang et al., 2018).

Intriguingly, MglA shares other features with eukaryotic Ras-like GTPases, as it is not only essential for motility but also for establishing cell polarity. To do so, MglA accumulates at the leading pole where the T4P assemble, a process that is influenced by MglA's interaction with its GAP MglB at the lagging pole as well as other motility-related proteins like RomR or MreB (Kaiser, 1991a; Leonardy et al., 2010; Zhang et al., 2010; Mauriello et al., 2010c). Additionally, MglA has also been postulated to be a protein component of the focal adhesion complexes that have been hypothesized to power A-motility (Mignot et al., 2007b; Nan et al., 2010; Sun et al., 2011; Nan et al., 2011). For example, based on protein-protein interaction data, MglA interacts with AglZ, another important focal adhesion complex protein that is essential for A-motility (Yang et al., 2004; Mauriello et al., 2010a). Notably, MglA has been suggested to be more than just a protein component of the focal adhesion complexes, but actively involved in processes that regulate their formation and the generation of propulsive force. To do so, it has been proposed that MglA directly interacts with the Agl-Glt multiprotein machinery of the focal adhesion complexes (Nan, 2017).

Given these different roles and the various cellular localizatios associated with the possible functions of MglA, it is important to understand how MglA might bind to these different cellular targets. Previous work in the lab (Semeijn, 2019) had examined the X-ray structure of MglA and other homolog bacterial Ras-like GTPases for the presence of structural elements possibly accounting for these proteins' abilities to bind to membranes. This study had identified two such structural elements: The amphipathic helix α5 and the N-terminal β0β1 sheets of MglA, with both elements using different mechanisms for membrane attachment. While the amphipathic α5 helix can interact directly with membranes through its hydrophobic

side chains, the β-sheet structures could only indirectly interact as the result of post-translational modifications like lipidations or prenylations - both of which are widespread among eukaryotic Ras-like GTPases. One of the more common lipidation is palmitoylation, while common prenylations include farnesyl or geranylgeranyl isoprenoid moieties that are covalently bound to cysteine or serine residues. Importantly for both of these membrane attachment mechanisms, there exist precedence among eukaryotic Ras-like GTPases. Sar1 of *S. cerevisiae*, a RasGTPase involved in membrane remodelling of the ER and Golgi apparatus uses an amphipathic helix for membrane targeting (Lee et al., 2005; Schwieger et al., 2017), while the GTPases Ras, Rac1 or Rab are all at their N-termini prenylated (Campbell & Philips, 2021). Based on these data, two different MglA constructs were generated, one lacking the α5 helix and the other one lacking the N-terminal β0β1 sheets containing accessible serine and cysteine residues. Unfortunately, neither construct was able to rescue motility of the *ΔmglA* strain. Most likely, this failure was due to the introduced changes to the protein's structure. Furthermore, to achieve rescue of motility, even for constructs that complemented the phenotype, such as the full-length TC-tagged MglA, high levels of expression were essential (250-500 μM vanillate combined with the strong *pilA* promotor). However, at these high concentrations of MglA, the protein may become toxic, which is especially evident in the absence of BacM (Semeijn, 2019). Controlled expression of the constructs also showed that even at the lowest level, no complementation was achieved, likely due to topological consequences of the deleted structural elements that may interfere with MglA's ability to interact with its cognate GAP, MglB, ultimately preventing the necessary MglB-assisted GTP hydrolysis of MglA (Baranwal et al., 2019; Galicia et al., 2019).

As mentioned above, the Sar1 homologue of MglA in yeast, is able to attach to the membrane using its N-terminal amphiphatic helix and, more importantly, is capable of partially complementing a Δ*mglA* phenotype (Hartzell et al., 1997). This observation was the basis for

our hypothesis that MglA may also be capable of either directly binding or attaching to the membrane like Sar1 or indirectly by interacting with another membrane-bound protein (Hanna et al., 2016). One such candidate protein, BacM, had been identified in the lab earlier (Semeijn, 2019). The full-length version of this protein has been reported to bind to membranes using its N-terminal sequence (Deng et al., 2019), a process that may influence membrane curvature as *ΔbacM* mutant strains show defects in their membrane topology (Koch et al., 2011). Membrane attachment of the MglA mutant constructs may also cause reduction in speed as they may influence the formation of focal adhesion complexes, which has been suggested to be important for gliding motility (Pollock et al., 2005; Secko et al., 2006; Mignot, 2007).

The Sar1 experiments also inspired our experiments to express MglA-eYFP in yeast cells. Surprisingly, yeast cells expressing MglA-eYFP displayed a non-uniform distribution of fluorescence staining, identified by our collaborator, Dr Ewald Hettema, as mitochondrial staining. Importantly, the membrane of this eukaryotic cellular compartment is enriched in cardiolipin, a type of lipid not commonly found in other eukaryotic membrane systems. However, most bacterial cytoplasmic membranes contain cardiolipin in varying concentrations. What makes this finding intriguing is the fact that cardiolipin, due to the cone-shape of its head group, specifically enriches in areas of high membrane curvature, most prominently the two cell poles (Galicia et al., 2019). Thus, one possible explanation for the polar localization of MglA would be that this protein specifically interacts with cardiolipins either directly or through post-translational modification. Interestingly, recent research has highlighted the importance of the lipidome of *M. xanthus* in fruiting body formation and spore germination (Ahrendt et al., 2015), a fact that could also play a role in possible lipid or isoprenoid-based post-translational modifications.

Importantly, the interpretation that the eYFP-MglA distribution is indeed caused by the protein's association with mitochondria needs further experimental support. First, the use of mitochondria-specific stains such as MitoTracker could be used to colocalize the eYFP-MglA signal and the distribution of mitochondria. Another approach would be the use of the yeast mutant strain DM that produces spherical mitochondria. Expression of eYFP-MglA in this mutant strain should, therefore, result in fluorescently stained spherical structures. A more specific and telling experiment, however, would be, of course, the use of yeast strains that are defective in the production of cardiolipin, as they would allow for chemically characterizing the MglA-mitochondria interaction in more detail and help confirm our initial hypothesis. Finally, several control experiments have to be done. First and foremost, the empty plasmid would have to be expressed to exclude the possibility that the observed fluorescence is a form of stress-induced auto-fluorescence.

In summary, the data in this chapter have shown that the full-length TC-tagged MglA is the best candidate construct to observe the localization and behaviour of MglA in *M. xanthus* cells as the fusion protein is capable of rescuing A- and S-motility at the single-cell and swarm levels. Moreover, its intracellular localization appears to mirror the behaviour of the untagged protein, forming lateral and polar clusters. Finally, the expression of MglA-eYFP in yeast cells resulted in a non-uniform, possibly mitochondrial staining, hinting at the possibility that MglA may associate with cardiolipins during membrane attachment. However, additional experiments are needed to confirm this hypothesis.

Chapter IV: Complementation of the *M. xanthus ΔmglA* phenotype using homologous and mutated versions of MglA

4.1 Introduction

Although the role of MglA as the master regulator of myxobacterial motility is well established and undisputed, the precise mechanism by which this RasGTPase actually controls both A- and S-motility is currently not well understood. This perplexing discrepancy between our principal understanding of its global function and the near-complete lack of any mechanistical details hampers not only the understanding of MglA's role but also of many cellular functions that are directly or indirectly linked to this RasGTPase, such as cell division, motility, cell reversals, developmental differentiation, and spore formation. To begin unravelling this puzzle, we decided to focus on two crucial questions integral to MglA's function: How does MglA find its cellular localization, and what structural elements and amino acid residues are crucial for MglA's function?

Two cellular structures have been described in the literature where MglA is localized in the cells, the two polar regions and laterally arranged membrane protein complexes termed focal adhesions. These adhesions are located along the length of the cell and have been suggested to be the molecular motors of A-motility (Mignot et al., 2007; Nan, 2017).

As for its protein interaction partners, at least four proteins have so far been described and confirmed through protein-protein interaction assays: the GAP MglB, the RomRX complex, MreB, and AglZ. The latter, initially proposed as the actual motor of A-motility, is now believed to be involved in the signalling process connecting the Frz chemosensory system to cell reversals (Nan, 2017). Importantly, work in our lab has cast doubt on one of those four

proteins, MreB, whose binding to MglA could not be confirmed using a novel luciferase-based two-hybrid assay in *M. xanthus.* Instead, recent work in the lab has added another cytoskeletal protein, BacM, to the list (Koen, 2019*)*. Unfortunately, with the exception of MglB (Miertzschke et al., 2011), no molecular data exist detailing the interactions of these proteins with MglA. This makes it virtually impossible to judge which parts of the RasGTPase are important for each interaction and, by extension, the functions of MglA.

No plausible model has been suggested about how MglA precisely localizes to the cell pole other than that its interaction with MglB and RomRX results in a dynamic unequal polar distribution, with the majority of MglA localizing to the leading pole. However, how MglA localizes to the cell poles in the first place is a bit of a mystery. Several scenarios exist: hydrophobic or amphiphilic elements of the protein itself could anchor it to the membrane preferentially at areas with high curvature. Secondly, the protein could be post-translationally lapidated or prenylated, which could localize it to the membrane, although not necessarily to the poles. Thirdly, MglA could interact with one or more polarly arranged protein(s), or fourth, it could specifically interact or bind to cardiolipin, a lipid that, due to the geometry of its head group, is highly enriched at areas of membrane curvature.

The latter idea is supported by the findings of this thesis, indicating that upon expression in yeast, MglA-eYFP results in mitochondrial staining (see Chapter III), specifically within cellular organelles possessing cardiolipin-enriched membranes. However, these new data do not exclude the possibility that any of the other three scenarios may be utilized. Possibly, the most likely scenario among the three would involve post-translational modification, as this method of membrane attachment and cellular localization is common among RasGTPases. One such prevalent modification is lipidation, with palmitoylation and myristoylation particularly often found in mammalian Ras proteins (Campbell and Philips, 2021). Notably, lipidations can

occur more than once in a protein. For example, during palmitoylation, one or two palmitoyl acyl chains are covalently bound to cysteine residues, thereby stepwise increasing membrane affinity and tracking (Sanders et al., 2015; Ahearn et al., 2018). Structurally, lipidations and other membrane-anchoring modifications, such as prenylations often occur at the N- and C-termini, as these sequence elements are often particularly accessible, thereby facilitating the modification as well as the binding to the membrane of the RasGTPase (Messina et al., 2019). As our work on the third scenario, the potential use of the amphiphilic helix α5 did not show any noticeable effect, we concentrated in this part of the project on the investigation of the role of potentially post-translationally modified residues and their effect on MglA function.

The second avenue of investigation in this part of the project involved the potential identification of sequence elements that are crucial for MglA's function. Although the identification of the above mentioned four interaction partners, MglB, RomRX, BacM, and AglZ, are informative, they do not shed directly light on the question how MglA controls motility as none of them is a part of the A- or S-motors far as we know. Therefore, we decided to approach this problem by using highly homologous and mutated versions of MglA to try identifying critical structural elements or sequences in the protein that can complement the *ΔmglA* phenotype and restore motility and colony expansion. To do so, a comprehensive database search was conducted to identify prokaryotic and eukaryotic Ras-like proteins that showed high sequence identity and similarity to MglA. Based on their conservation and previous use in complementation studies (Fremgen et al., 2010), we selected the following proteins for our experiments: Sar1 (*S. cerevisiae*), $MglA_{C.\ torosa}$ (*C. torosa, Ostracoda*), $MglA_{bdv}$ (*B. bacteriovorus*), $MglA_{stigm}$ (*S. aurantiaca*), and SofG (*M. xanthus*), and investigated their ability to complement the *ΔmglA* phenotype either by themselves or upon mutations. The goal of this part of the project was to potentially identify critical amino acids or sequence elements

of MglA that play a role in the protein's function in motility, fruiting body formation, sporulation, and protein interaction, thereby trying to deepen our understanding of MglA.

4.2 Materials and Methods

4.2.1 Bioinformatic identification and analysis of MglA homologues

Homologues of *M. xanthus* MglA were identified in the National Centre for Biotechnology Information (NCBI) database using the Basic Local Alignment Search Tool for proteins (BLASTp) with the amino acid sequence of MglA as a reference. Subsequently, the identified sequences were aligned using the CLUSTALW programme and arranged in order of similarity to MglA, starting with the closest match and proceeding to the least similar amino acid sequence. Both pro-and eukaryotic sequences of Mgl-like RasGTPases were used for the alignment.

4.2.2 Generation of mutant versions of *M. xanthus* MglA

Standard genetic techniques were employed to introduce two single point mutations within the N-terminal amino acid sequence of MglA, converting the two cysteine residues Cys_{13} and Cys_{23} into serine residues. These replacements were introduced to investigate whether these cysteines are post-translationally modified in MglA and may impact motility. Although these cysteine residues in MglA are not conserved across species and their specific functions are unknown, they appear to be part of structural elements that interact with the GAP MglB based on X-ray data (Kanade et al., 2019). To test if these residues are essential for MglA-controlled motility, a *ΔmglA M. xanthus* strain was complemented with the serine-containing construct, and the motility phenotype was compared to a wild-type positive control.

A second set of genetic constructs aimed to investigate the role of the N- and C-termini of MglA in motility. For this purpose, a SofG/MglA hybrid protein was generated by removing all amino acid sequences of SofG that are not aligned with the Ras-like GTPase core of MglA. Then, in the next step, the first and last 13 amino acids, the N- and C-termini, from MglA were

added to the truncated SofG to make the hybrid protein even more MglA-like. The addition of the MglA N- and C-termini was necessary as they play critical roles in MglB-binding and the interaction with other binding partners (Kanade et al., 2019). The genetic construct coding for the final SofG/MglA hybrid protein was introduced into cells lacking MglA to assess whether the hybrid SofG was able to restore motility in this background. For these experiments, the PCR products were digested and then cloned into the *pMR3679* plasmid using the protocols described in Chapter III. A list of all the generated constructs is shown in **Table 4**.

Table 4: List of the generated constructs used for the experiments of Chapter IV.

Strains	**Expression**	**Reference**
mglA$_{bdv}$ Δ*mglA*	*M. xanthus*	This study
mglA$_{stigma}$ Δ*mglA*	*M. xanthus*	This study
sar1 Δ*mglA*	*M. xanthus*	This study
mglA$_{C.\ torosa}$ Δ*mglA*	*M. xanthus*	This study
*mglA sofG*Δ*mglA*	*M. xanthus*	This study
sar1 bacM$_{myxo}$	*M. xanthus*	This study
mglA$_{C.\ torosa}$ *bacM*$_{myxo}$	*M. xanthus*	This study
mglA$_{bdv}$ *bacM*$_{myxo}$	*M. xanthus*	This study
mglA$_{C13S}$	*M. xanthus*	This study
mglA$_{C23S}$	*M. xanthus*	This study

Table 5: List of primers used for the generation of the genetic constructs.

Plasmid	**Description**	**Sequences 5' to 3'**
pMR3679	Sar1 F EcoR1	TATATGAATTCATGGCTGGTTGGGATATTTTTGGT
pMR3679	Sar1 R Mulu	TATATACGCGTTTAAATATATTGAGATAACCATTGG AACGCCTC
pMR3679	*C. torosa* F EcoR1	TATATGAATTC TTGAGCTTTATAAATCTCAAGGAAA AGGTT
pMR3679	*C. torosa* R Mulu	TATATGAATTCATGGAGCTTTATAAATCTCAAGGAA AAGGTT
pMR3679	$MglA_{bdv}$ F Ndel	TATATCATATGTCCTTTATTAACTACAATGCCAA
pMR3679	$MglA_{bdv}$ R Mulu	TATATACGCGTTTACAGAGTCGTTCCGCC
pMR3679	SofG MglA F Ndel	TATATCATATGTCCTTCATCAATTACTCATCCCGCG AAATCAACTGCACCTTGCAACTCA
pMR3679	SofG MglA R Mulu	TATATACGCGTTCAACCACCCTCAGCGCCACCGCGC CCACCACCGCCTCGC
pMR3679	$MglA_{stig}$ F Ndel	TATATCATATGATGTCCTTCATCAATTACTCATCCCG CGAA
pMR3679	$MglA_{stig}$ R Mulu	TATATACGCGTTCAACCACCCTTCTTGAGCTCGGT
pMR3679	MglA (point M) MglA_Nde1_F	TATATCATATGAAATTTCATATGTCCTTCATCAATTA CTCATCCCG
pMR3679	MglA point Nhe1 R	AAATTTGCTAGCTCAGAGCTCGGTGAGGACGAGC
pMR3679	MglA point Nde1 F	TATATCATATGTCCTTCATCAATTACTCATCCCGCG AAATCAACTCCAAGATTGTCTATTACGGGCCCGGGC TCTCCGGG
pMR3679	MglA point Nhe1 R	AAATTTGCTAGCTCAGAGCTCGGTGAGGACGAGCTT
pMR3679-lucif	$Mgla_{bdv}$ lucif F KpnI	TATATGGTACC ATGTCCTTTATTAACTACAATGCCAA
pMR3679-lucif	$MglA_{bdv}$ lucif R BglII	TATAT AGATCT TTACAGAGTCGTTCCGCC
pMR3679-lucif	Sar 1luciferase F KpnI	TATAT GGTACC ATGGCTGGTTGGGATATTTTT
pMR3679-lucif	Sar 1luciferase R BglII	TATATAAGATCT TTAAATATATTGAGATAACCATTGGAACGC

4.2.3 Developmental assays

Precultures for developmental assays were grown overnight in CTT medium until they reached mid-log phase. Subsequently, the cultures were diluted in fresh CTT medium at a cell density of 2×10^7 cells/ml before being transferred to 24-well plates, with each strain set up in triplicates using 1 ml of the liquid start culture (Hodgkin and Kaiser, 1979). The cells were incubated for 24 hours at 32 °C to reach a density of approximately 4×10^8 cells/ml (~0.8 OD_{600}), before the CTT medium was replaced by TPM (10 mM Tris-HCl, pH 7.6, 1 mM K_2PO_4, 8 mM $MgSO_4$) to starve the cells.

To start the developmental assay, the cells were harvested at 4,600 × g using a tabletop centrifuge, washed once with TPM before being resuspended in fresh TPM at a final density of $4x10^8$ cells/ml. Drops of 10 µl of the cell suspension were placed onto TPM agar plates and left to dry under the biosafety hood for twenty minutes. Following this, the plates were sealed with parafilm and incubated at 32 °C for three days to allow the cells to aggregate and form fruiting bodies. Images of fruiting bodies were recorded using a stereomicroscope equipped with a digital camera.

To detect and image individual spores, a dissection needle was used to transfer a small cell aggregate or fruiting body onto a glass slide. After placing a cover slip onto the sample, gentle pressure was applied to spread the material to release the spores, which were imaged using a stereo or light microscope.

4.2.4 Glycerol spore formation

To induce glycerol spore formation, actively growing cell cultures in liquid CTT medium at the mid-log phase were exposed to glycerol at a final concentration of 0.5 M. After the addition of glycerol, the cells were further incubated at 32 °C with continuous shaking for at least an hour or until the conversion of the vegetive rod-shaped cells to egg-shaped glycerol spores was complete (Dworkin and Gibson, 1964). Moreover, in experiments aimed at capturing the conversion process in detail, samples were imaged using a light microscope over a total period of 24 hours at intervals of 0, 30, 40, 60, 80 minutes, concluding with a final observation at the end of the 24 hours.

4.2.5 Growth curves

To record growth curves for individual *M. xanthus* strains, precultures were grown in CTT medium overnight at 32 °C on a rotary shaker at 200 rpm until the OD_{600} reached a value of 0.5-0.6. Each overnight culture was freshly inoculated in triplicates in 25 ml CTT medium at an initial OD_{600} of 0.05, and 50 µM vanillate was added to the cultures to induce protein expression. Subsequently, the cultures were grown for a total time of 54 hours, and the cell density was measured at OD_{600} at various intervals using a spectrophotometer (BioRad). More specifically, individual OD_{600} measurements were recorded at the following intervals: TO (time of induction); TA (hour of expression) at 1 h, 2 h, 4 h, 8 h, 16 h, 24 h, 30 h, 38 h, 46 h, and 54 h. At each time point, the average OD_{600} was calculated for each strain using the triplicate cultures, and statistical analysis by two-way ANOVA was conducted using Prism 7 (GraphPad, Inc.).

4.2.6 Live cell imaging

The light microscope set-up for cell imaging was essentially the same as described in Chapter III. Time-lapse videos and still images were captured of individual cells or group of cells to visualize A- and S- motility, while a fluorescence light microscope was used to observe live cells on 1.5% TPM-agarose pads on glass slides. Cells were grown overnight in liquid CTT medium to an OD_{600} of 0.4-0.8. Subsequently, approximately 10 µl of the overnight cultures were placed on top of a freshly prepared hard or soft agar pad on top of a microscope glass slide. Briefly, the agar pads were prepared immediately prior to their use in a glass chamber consisting of two microscope glass slides that were separated by two ethanol-sterilized 22 x 22 mm measuring cover slips functioning as spacer (for a detailed description, see Koch et al., 2011). Molten agarose was then injected with a pipette tip into the narrow space between the two glass slides and left to cool for five minutes. Next, the upper glass slide was carefully removed, leaving the agarose pad on the lower slide behind. The agarose pads have an approximate thickness of 1 mm and a smooth surface due to the contact with the upper glass slide during fabrication.

M. xanthus cells were transferred onto the agarose pads, covered with a cover slip, and the chamber was sealed with a mixture of molten candle wax and vaseline to prevent the samples from drying out. The finished slides containing the inoculated pads were incubated at 32 °C for a minimum of 60 minutes before being examined using a fluorescence microscope at an excitation wavelength of 488 nm.

4.3 Results

4.3.1 Bioinformatic identification and analysis of MglA (MXAN_1925) homologues

The primary amino acid sequence of *M. xanthus* DK1622 MglA (MXAN_1925; retrieved from UniProt at https://www.uniprot.org/uniprotkb/Q1DB04/entry) was used to search the NCBI protein database for homologue protein sequences, retrieving numerous prokaryotic and a few eukaryotic sequences (**Table 6**). The goal of this search and the subsequent alignment analysis of the sequences using CLUSTALW was to identify highly conserved amino acid residues located outside of the GTP-binding sites of these RasGTPases.

The focus on these particular residues was based on the hypothesis that they could conceivably be important for conserved biological functions of MglA that are not directly linked to the binding and hydrolysis of guanine nucleotides. Possible functions include the localization and membrane attachment of MglA, control of motility, fruiting body formation, sporulation, and protein-protein interaction with effector proteins (Komano et al., 1982).

Based on the well-understood biology of RasGTPases, one particular focus was conserved amino acid residues that could be post-translationally modified, such as phosphorylated, lipidated, and prenylated. Serine, threonine, and tyrosine are commonly used for phosphorylation, while cysteine is often the site of lipidation and prenylation, with all three types of post-translational modifications commonly found in eukaryotic RasGTPases.

A total of twelve amino acid positions (2, 13, 17, 18, 23, 46, 85, 88, 105, 116, 140, 180) were identified in the twenty aligned homologues protein sequences (**Fig. 44**) that showed complete or more than 80% conservation for these four amino acids: serine, threonine, tyrosine, and cysteine. Among the identified positions, five (2, 46, 88, 105, and 116) were serine residues, one (179) was a conserved threonine, and four positions (17, 18, 85, and 140) had a conserved tyrosine. Additionally, two conserved cysteine residues at position 13 and 23 were identified.

To better judge whether these residues were accessible for post-translational modifications, their relative location within the atomic structure of MglA (Protein Databank entry PDB ID: 5YMX) was investigated. The results indicated that among these 11 conserved positions, serine 2 and 105, cysteine 23, and tyrosine 85 were located in loop regions, while serine 88 and 116, and threonine 180 were found in helical regions, i.e., α2, α3, α5 respectively. All the remaining conserved residues were found in β sheets (**Fig. 44**).

Based on their high degree of conservation of higher than 80%, all of these identified 11 positions are good candidate residues for mutational studies, and it was decided to initially focus on the phosphorylatable residues (**Fig. 44** and **45**). The analyses of these twenty selected sequences also highlighted a number of conserved charged residues such as aspartic acids and lysines, which might play roles in the interaction of MglA with other proteins like BacM and MglB. For each of the mutated residue, the consequences for localization, motility, sporulation, fruiting body formation, and the binding of MglB were investigated using standard assays. Together, these data help to characterize MglA better and to start dissecting which parts of its sequences play roles in which cellular process.

Table 6: MglA homologs are widespread among prokaryote and eukaryote.

Taxonomy	**organism**	**Motility**	**Sporulation**	**Fruiting body**	**MglB protein**	**Amino acid**	**Identity**	**Accession**
Myxococcota	*Myxococcus xanthus* DK 1622. MXAN-1925	Y	Y	Y	Y	195aa	100%	ABF87984.1
Myxococcota	*Corallococcus coralloides* DSM 2259	Y	Y	Y	Y	195aa	90%	WP_014394794.1
Myxococcota	*Stigmatella aurantiaca* DW4/3-1	Y	Y	Y	Y	195aa	97%	>ADO70493.1
Myxococcota	*Corallococcus exiguus*	Y	Y	Y	Y	197aa	97%	>TNV53187.1
Myxococcota	*Pyxicoccus fallax*	Y	Y	Y	Y	195aa	96%	>WP_015347803.
Myxococcota	*Cystobacter ferrugineus*	Y	Y	Y	Y	195aa	94%	>OJH33633.1
Myxococcota	*Archangium primigenium*	Y	Y	Y	Y	195aa	93%	>WP_204493834.

Myxococcota	*Hyalangium minutum*	Y	Y	Y	Y	195aa	53%	>KFE61909.1
Myxococcota	*Melittangiu boletus*	Y	Y	Y	Y	195aa	97%	>WP_095980021.
Myxococcota	*Polyangium fumosum*	Y	Y	Y	Y	196aa	83%	>TKD07389.1
Myxococcota	*Chondromyces apiculatus DSM 436*	Y	Y	Y	Y	196aa	82%	>EYF05872.1
Myxococcota	*Chondromyces crocatus*	Y	Y	Y	Y	196aa	82%	>WP_050434859.
Myxococcota	*Sorangium cellulosum*	Y	Y	Y	Y	196aa	82%	>KYG10128.1
Myxococcota	*Labilithrix sp*	Y	Y	Y	Y	197aa	83%	>MBX3192347.1
Myxococcota	*Minicystis rosea*	Y	Y	Y	Y	196aa	82%	>APR82908.1
Myxococcota	*Nannocystis exedens*	Y	Y	Y	Y	195aa	78%	>PCC70950.1
Myxococcota	*Labilithrix luteola*	Y	?	N	?	198aa	81%	WP_146648292.1
Myxococcota	*Anaeromyxobacter dehalogenans*	N	Y	N	Y	195aa	87%	ABC83399.1

Bdellovibrionia	*B. bacteriovorus HD100*	Y	N	N	N	197aa	(64%)	CAE81098.1
Deinococci	*T. thermophilus*	Y	N	?	Y	196aa	(62%)	AP008226.1
Proteobacteria-delta	*Geobacter sp. AOG2*	Y	Y	Y	Y	195aa	82%	NP_951161.1
Deinococci	*Deinococcus radiodurans*	N	N	N	Y	196aa	61%	NP_294577.1
Chloroflexia	*Chloroflexus aurantiacus*	Y	Y	Y	Y	195aa	53%	YP_001635661.1
Ostracoda	*Cyprideis torosa*	N	N	N	N	273aa	46%	CAD7236820.1
Saccharomycetes	*Saccharomyces cerevisiae*	N	N	N	N	190aa	24%	NP_015106.1

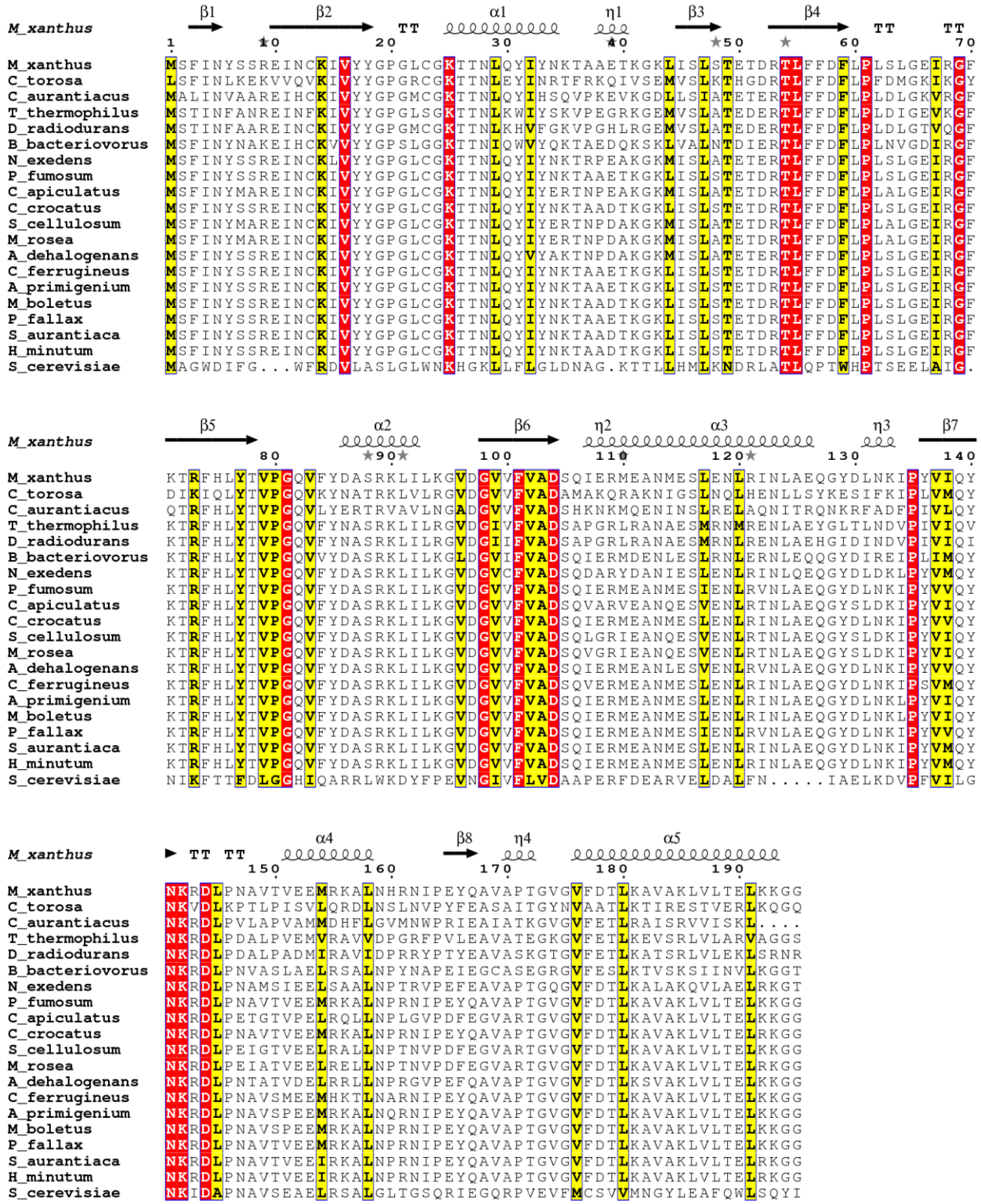

Figure 44: Alignment of twenty selected MglA homologues.
A set of twenty candidate sequences representing various prokaryotes and eukaryotes shows the high degree of conservation among MglA homologues. The amino acid positions correspond to *M. xanthus* MglA, while the information about the secondary structure of the proteins is provided above the sequence alignment.

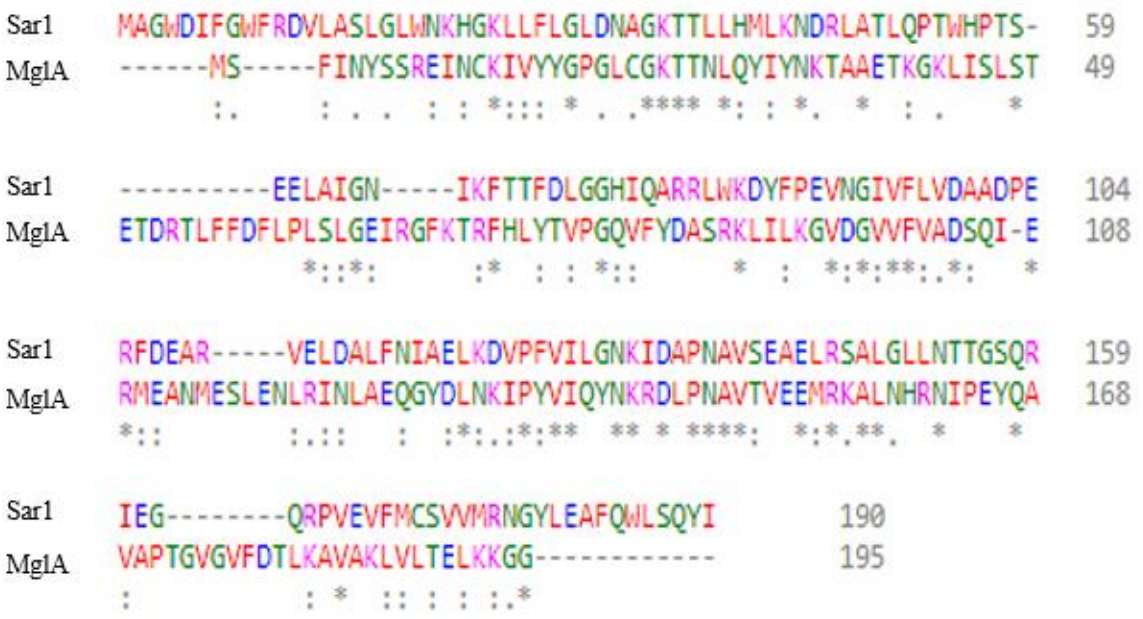

Figure 45: Pairwise alignment of MglA and Sar1 from *S. cerevisiae*.
Sar1 shares 24% identity with MglA, including its conserved GTP-binding site. However, Sar1 exhibits no similarity in amino acids typically subject to post-translational modifications, such as serine, threonine, tyrosine, and cysteine.

4.3.2 Complementation of A- and S-motility in Δ*mglA* cells expressing *S. cerevisiae* Sar1

In a landmark study, it was reported that the RasGTPase Sar1 from the yeast *S. cerevisiae* could partially rescue the motility and spore formation defects of an *M. xanthus ΔmglA* mutant strain (Hartzell, 1997). To further investigate this, a *sar1ΔmglA* construct was generated, cloned into the *pMR3679* plasmid, and subsequently expressed in a *ΔmglA* background using increasing concentrations of vanillate. Upon induction with vanillate, the morphology of overnight grown cells, their ability to move on 1.5% hard agar and 0.5% soft agar, as well as the expansion of cell colonies on the different agar concentrations, was measured (**Fig. 46**, **47** and **48**). Our results showed that there was no discernible morphological change in *ΔmglA* cells expressing Sar1. Moreover, the *sar1ΔmglA* construct failed to restore motility of *ΔmglA* cells on both hard and soft agar even after a four-day-long incubation at 32 °C at the highest concentration of vanillate. Under these conditions, the motility and colony expansion of the *sar1ΔmglA* construct was identical to the *ΔmglA* cells, indicating that Sar1 in our experiments did not rescue motility and colony expansion as had been previously described (Hartzell, 1997).

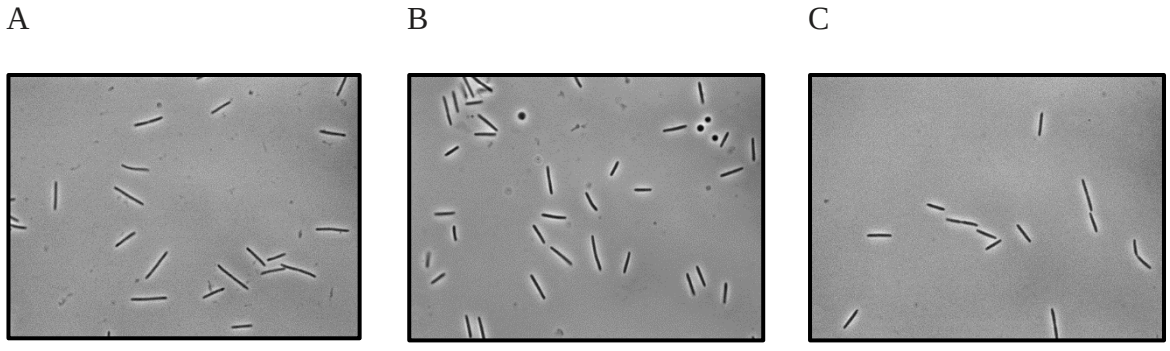

Figure 46: Morphology of Sar1-expressing *ΔmglA M. xanthus* cells.
(**A**) Cell morphology of *M. xanthus* sar1Δ*mglA* cells after induction with 500 µM vanillate, showing wild-type morphology. **(B)** Represents the morphology of the *ΔmglA* parental strain, and (**C**) that of the WT.

A

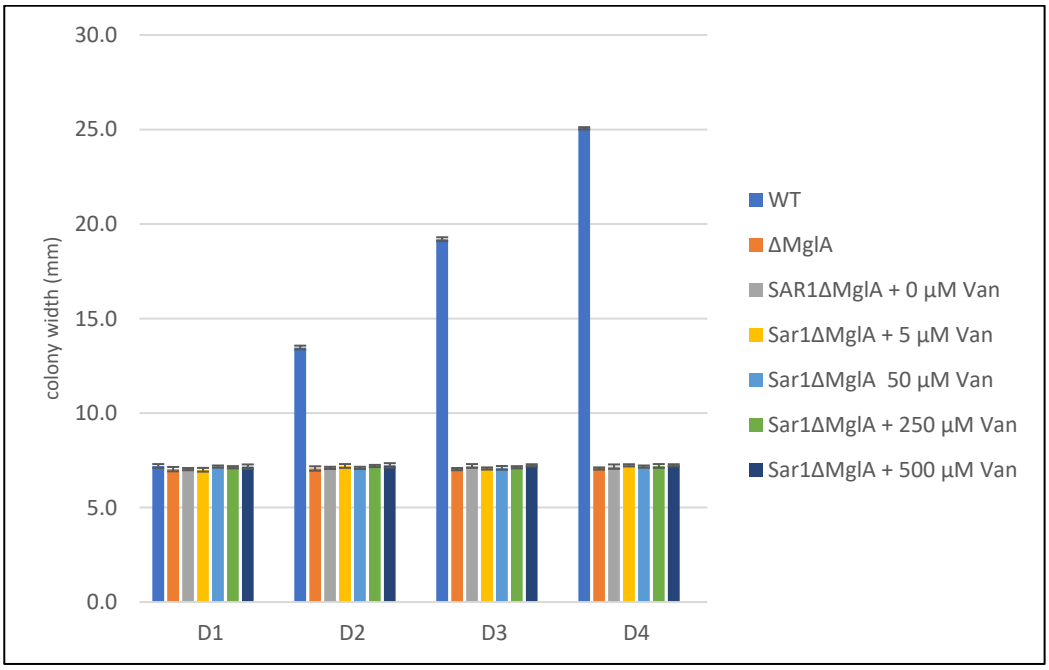

B

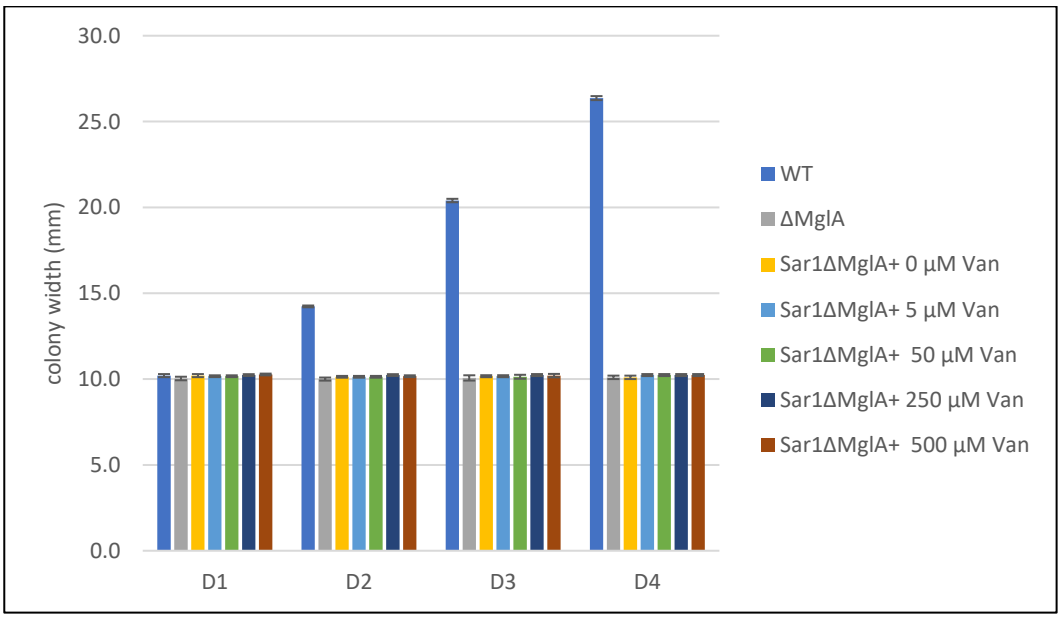

Figure 47: Investigation of A- and S-motility in Δ*mglA* cells expressing varying levels of Sar1.
The X-axis represents the time of incubation in days, and the Y-axis shows the diameter of the colonies in mm. The measurements show that the *sar1ΔmglA* construct did not restore motility of the *ΔmglA* phenotype on (**A**) hard agar and (**B**) soft agar, even in the presence of increasing concentrations of vanillate. Colony diameters were measured daily over a four-day period. Each measurement of the colony diameters was done in triplicate, and the error bars represent the standard deviation of the measurements.

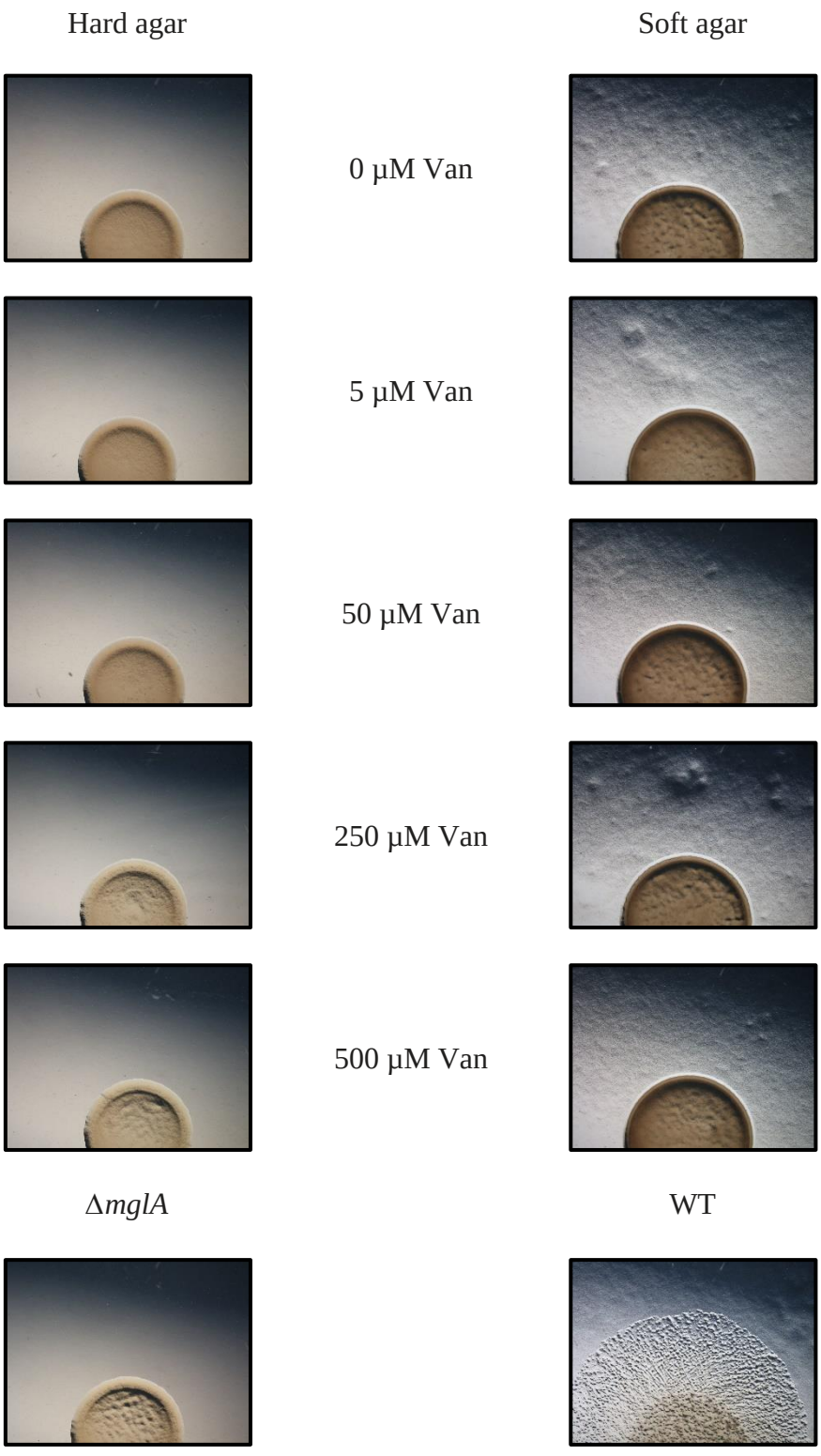

Figure 48: Expansion of Δ*mglA* cell colonies expressing varying levels of Sar1.
The images show that the *sar1ΔmglA* construct did not restore cell colony expansion of the *ΔmglA* phenotype on hard and soft agar, even at increasing concentrations of vanillate. Colony expansion were measured after 3 days of growth at 32 °C in the presence of varying concentrations of vanillate.

4.3.3 Fruiting body formation of *M. xanthus* Δ*mglA* cells expressing Sar1

As described earlier, Hartzell's study (1997) reported that the RasGTPase Sar1 from *S. cerevisiae* can partially rescue the spore formation defect of an *M. xanthus ΔmglA* mutant. Therefore, we were interested in investigating the influence of Sar1 on fruiting body and spore formation in the presence of increasing concentrations of vanillate. Cells containing the *sar1ΔmglA* construct were grown in CTT plus vanillate until reaching a density of $4x10^8$ cells/ml. The cells were then harvested, washed with TPM, and spotted onto 1.5% TPM hard agar plates containing varying amounts of vanillate. After incubation for three days at 32 °C, no aggregation or fruiting body formation was observed. This lack of aggregation is likely due, in part, to the fact that the *sar1ΔmglA* construct cannot rescue the motility necessary for aggregation (**Fig. 49**). Given the strain's inability to rescue motility, it was unsurprising that an increasing concentration of vanillate had no effect. Consequently, we decided to investigate the *sar1ΔmglA* cells' ability to form glycerol spores, which could explain the previously reported observation of a rescue of sporulation by Sar1 (Hartzell, 1997).

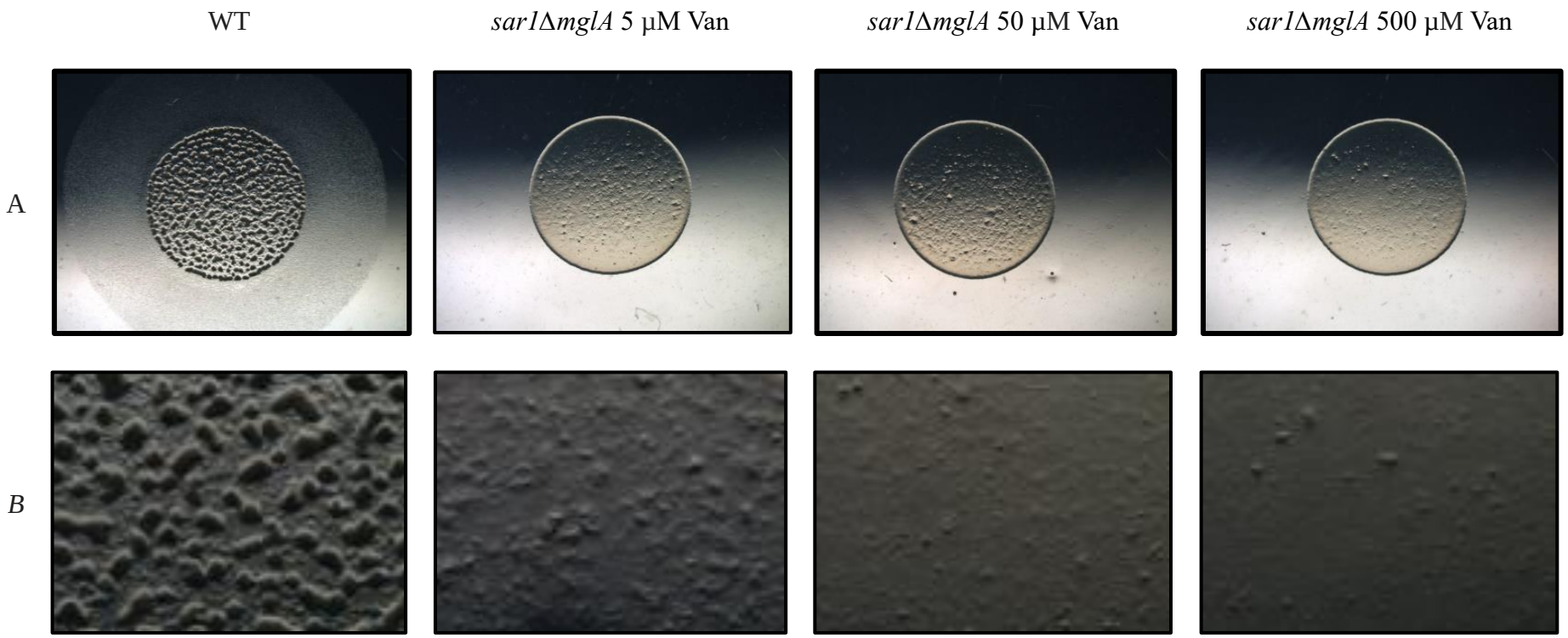

Figure 49: Formation of fruiting bodies of *sar1*Δ*mglA* cells at varying vanillate concentrations.
A) The upper row of images displays *sar1ΔmglA* cell spots in the presence of 5, 50, and 500 µM vanillate. Note that only wild-type cells, as shown in the left image are capable of fruiting body formation. Since *sar1ΔmglA* does not complement motility, no peripheral rod cells swarm around the initial spot of cells. **B**) The lower row shows 2x magnified areas of the corresponding images in the upper row. The cells were imaged after 48 hours on TPM agar.

4.3.4 Glycerol spore formation of *M. xanthus sar1ΔmglA* cells

To determine whether the *sar1ΔmglA* cells form glycerol spores, the cells were grown at 32°C overnight in CTT medium containing either 5 or 500 µM vanillate to induce Sar1 expression. Upon reaching mid-log phase, glycerol was added to the cultures at a final concentration of 0.5 M, and the cells were grown for an additional two hours. Samples were removed from the cultures and observed under the light microscope. The results of this experiment showed that vanillate-induced *sar1ΔmglA* cells appear to form glycerol spores rather than fruiting body spores. This interpretation is supported by the observation that the resulting spores lacked thick spore coats, a structural hallmark of fruiting body spores. Additionally, these spores exhibited an egg-shaped morphology rather than a spherical one, resembling the glycerol spores described in the literature (Dworkin and Gibson, 1964). Images of the spores were captured at different times using a light microscope equipped with phase contrast. The *ΔmglA* and wild-type strains were used as controls, respectively (**Fig. 50** and **51**).

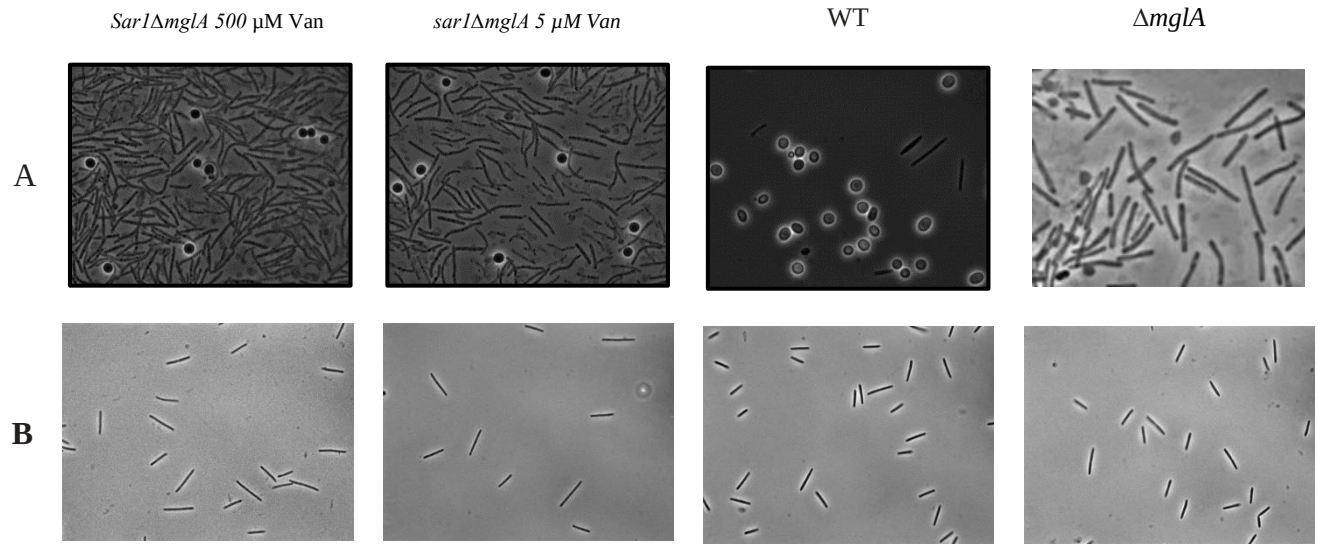

Figure 50: Formation of glycerol spores by *sar1ΔmglA* cells.
A) Upon induction with 5 or 500 µM vanillate, the *sar1ΔmglA* cells form glycerol spore-like entities, resembling those seen in *ΔmglA* cells, but exhibiting slight differences from wild type (WT) glycerol spores. **B)** Images of the respective vegetative cells reveal that induction with vanillate has no discernible impact on cell shape.

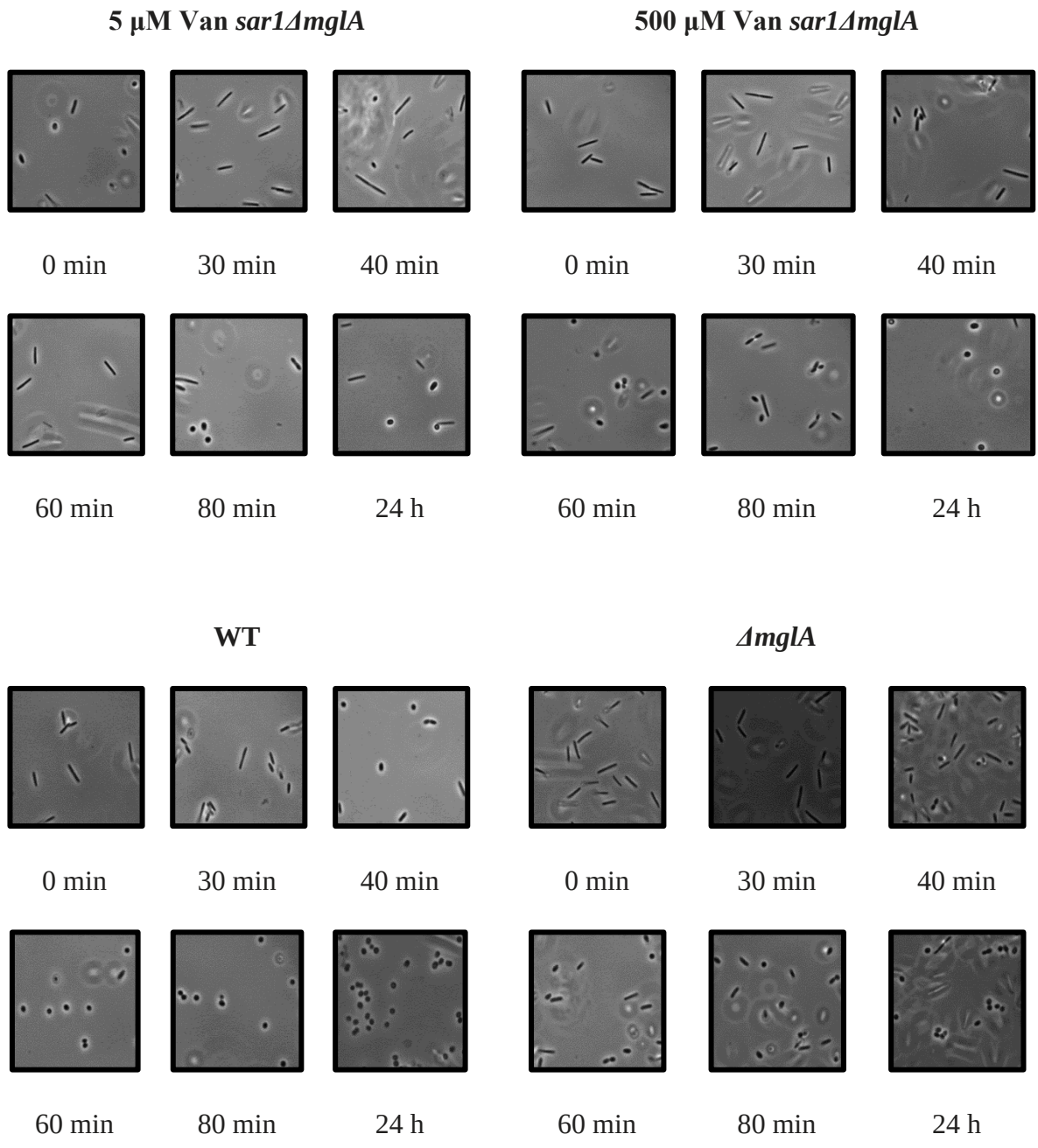

Figure 51: Morphological comparison of glycerol spore formation of *sar1ΔmglA*, WT, and *ΔmglA* cells. Upon glycerol induction, all three strains, *sar1ΔmglA* at 5 and 500 µM vanillate, WT (DK1622), and *ΔmglA* - form glycerol spore-like entities. While biochemical and structural studies have characterized the glycerol spores of WT cells, no such investigations have been conducted on the glycerol spore-like entities of the *sar1ΔmglA* and *ΔmglA* cells. Consequently, it remains unclear whether the oval-shaped entities are identical to the glycerol spores observed in WT cells.

4.3.5 Complementation of A- and S-motility in Δ*mglA cells* using the MglA homologue from the ostracod *Cyprideis torosa*

The bioinformatic investigation of MglA homologues revealed that a Ras-like GTPase from the eukaryotic ostracod *C. torosa* shares 29% identity with MglA of *M. xanthus*. Consequently, we decided to investigate the ability of this ostracod homologue to rescue motility in the non-motile *ΔmglA* strain. Therefore, the *mglA*$_{C.torosa}$ *ΔmglA* construct was expressed, and the morphology of the vegetative cells investigated to determine whether the expression of the construct would have any discernible impact on the cell's shape (**Fig. 52)**. After that, cell motility and swarm expansion were investigated on both 1.5% hard and 0.5% soft agar (**Fig. 53** and **54**). To determine whether the level of MglA$_{C.\ torosa}$ expression matters, we used three different vanillate concentrations in these experiments: 5, 50 and 500 µM. Unfortunately, the *mglA*$_{C.\ torosa}$ *ΔmglA* construct did not complement the non-motile phenotype of the *ΔmglA* cells under any of these circumstances, even after incubation for four days at 32 °C.

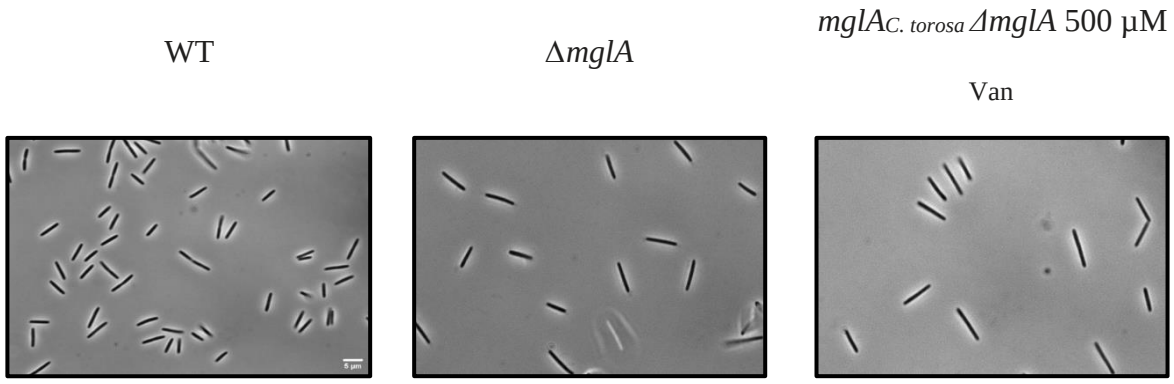

Figure 52: Morphology of *ΔmglA M. xanthus* cells expressing the *mglA*$_{C.\ torosa}$ *ΔmglA* construct.
Vegetative *mglA*$_{C.\ torosa}$ *ΔmglA M. xanthus* cells were grown in the presence of 500 µM vanillate to induce expression of the ostracod MglA homologue. No discernible impact on the cell's morphology was detected. Images of the WT and *ΔmglA* vegetative cells are provided for comparison.

A

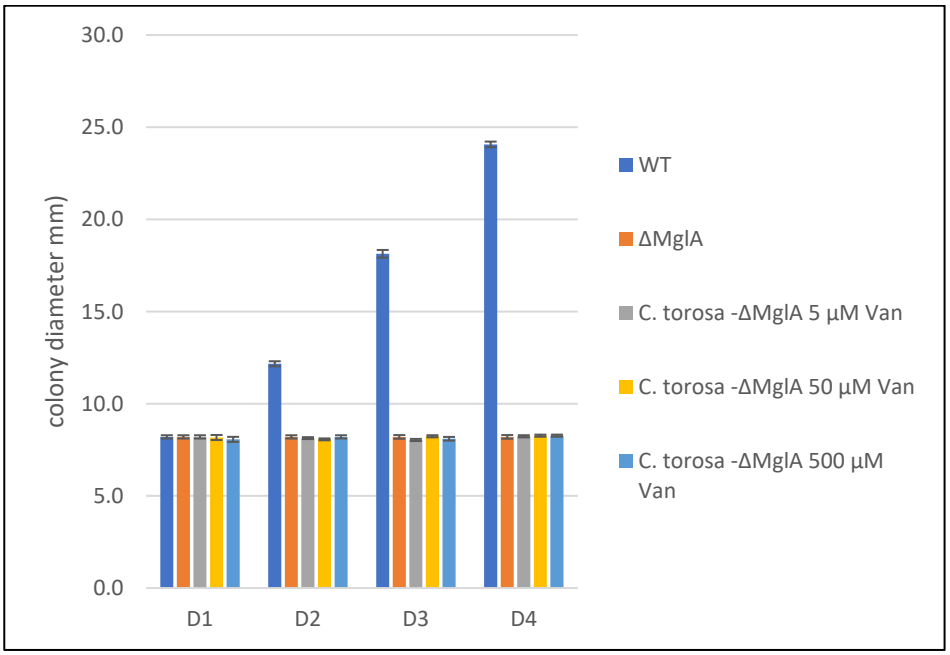

B

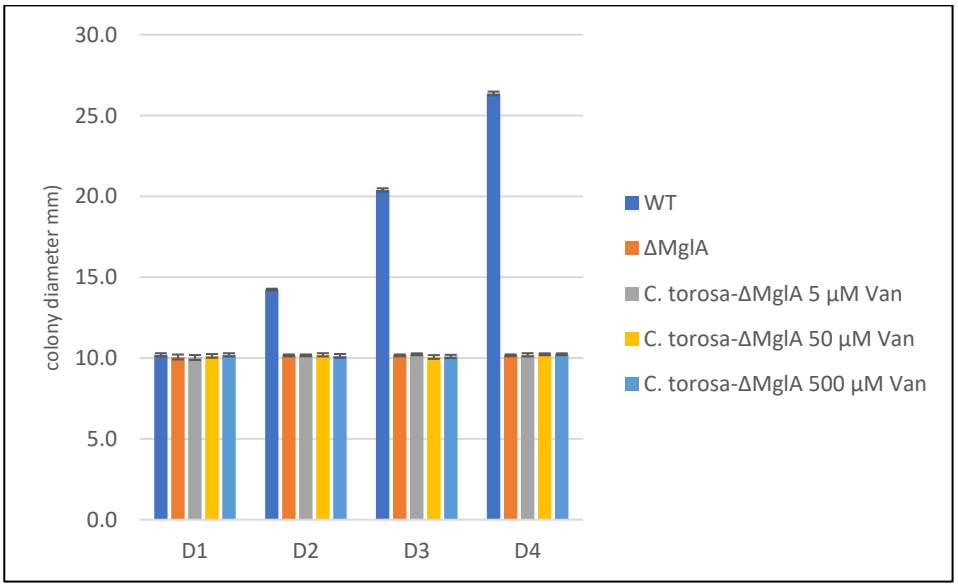

Figure 53: Investigation of A- and S-motility of Δ*mglA* cells expressing MglA$_{C.\ torosa}$ at different vanillate concentrations.
The expression of MglA$_{C.\ torosa}$ in *ΔmglA* cells did not restore A- or S-motility. The X-axis shows the number of days, while the Y-axis represents the diameter of the colonies in millimetre. Experimental data from triplicate measurements on **(A)** hard and **(B)** soft agar using increasing concentrations of vanillate are shown. Colony diameters were measured daily for four days. The error bars represent the standard deviation based of the colony diameter measurements.

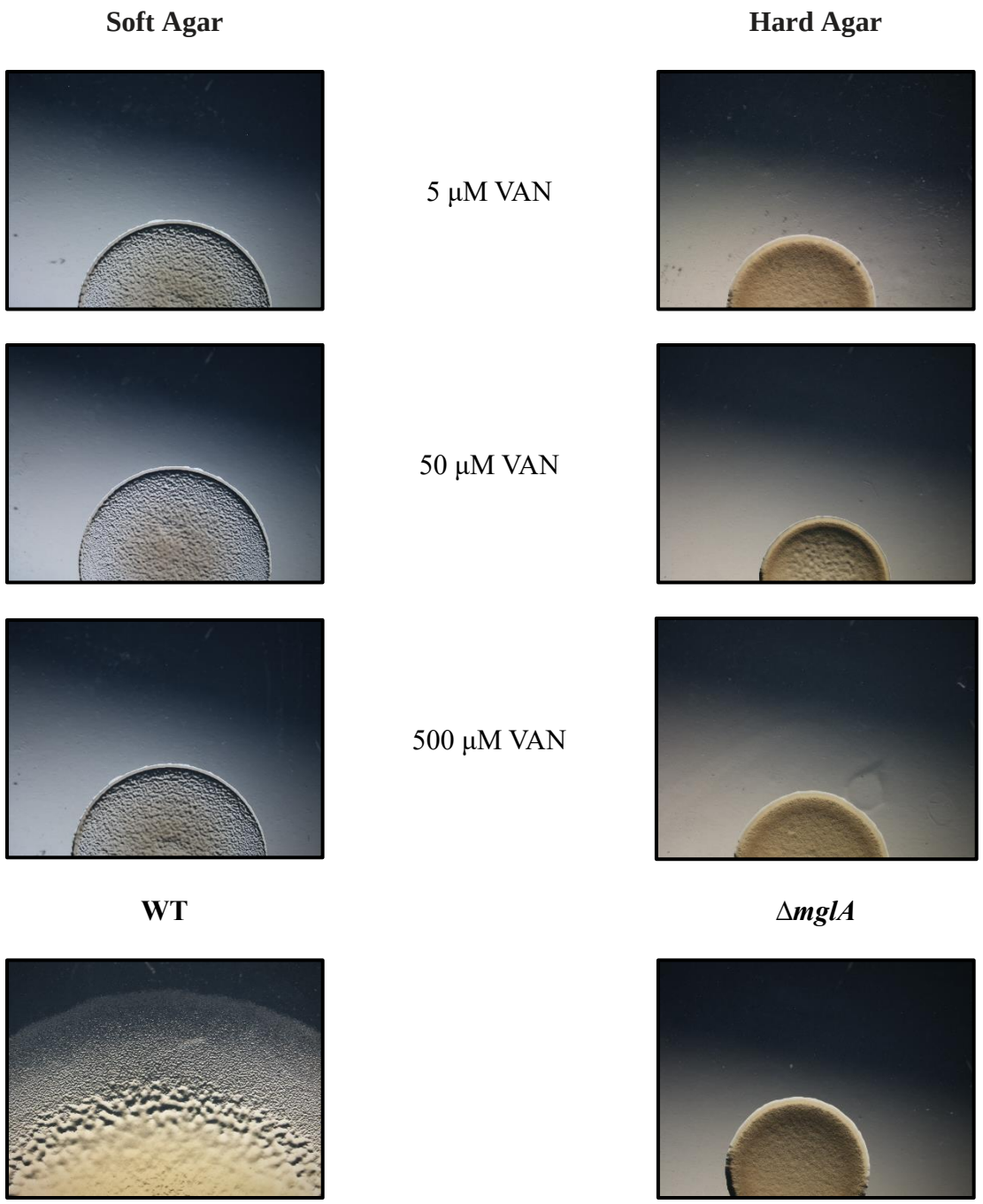

Figure 54: Expansion of Δ*mglA* cell colonies expressing MglA$_{C.\ torosa}$ at different vanillate concentrations on hard and soft agar.
The experiment was conducted on both hard and soft agar and revealed that MglA$_{C.\ torosa}$ did not rescue colony expansion. Images were captured after three days of growth at 32 °C, while the expression was induced using different concentrations of vanillate.

4.3.6 Fruiting body formation of Δ*mglA* cells expressing MglA$_{C.\ torosa}$

The fact that the ostracod *C. torosa* possesses an MglA homologue is surprising, given the vast evolutionary separation between this aquatic eukaryote and the soil bacterium *M. xanthus* (Heip, 1976). After testing the ability of MglA$_{C.\ torosa}$ to complement motility in a *ΔmglA M. xanthus* strain, we next assessed the protein's ability to complement fruiting body formation in this genetic background. For this purpose, *M. xanthus* cells containing the *mglA*$_{C.\ torosa}$*ΔmglA* construct were grown in the presence of varying concentrations of vanillate to induce the expression of MglA$_{C.\ torosa}$. The cells were then spotted on TPM agar containing the same concentrations of vanillate and incubated at 32 °C for three days. However, similar to the results observed for motility, none of the tested vanillate concentrations enabled the formation of fruiting bodies, indicating that the ostracod MglA$_{C.\ torosa}$ protein was unable to complement the *ΔmglA* fruiting body formation defect in *M. xanthus* (**Fig. 55**).

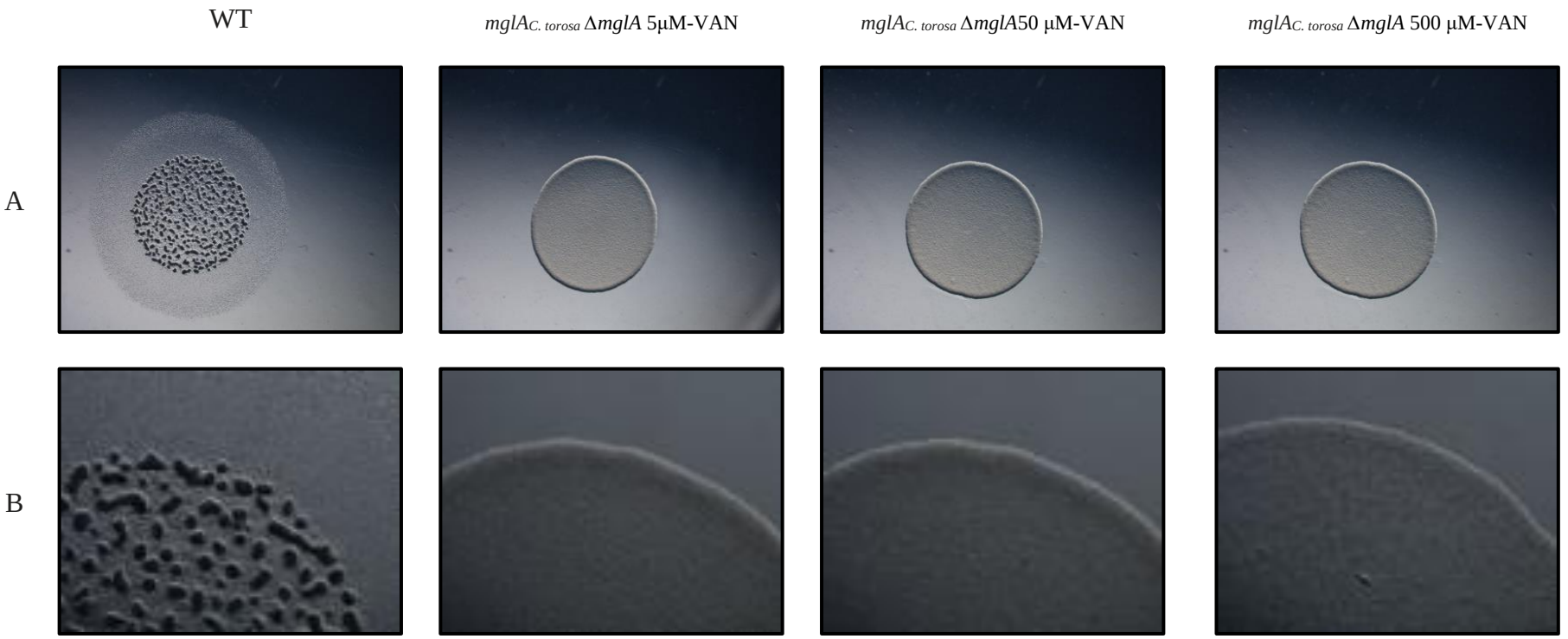

Figure 55: Formation of fruiting bodies of *M. xanthus* cells containing the *mglA*$_{C.\ torosa}$ Δ*mglA* construct.
A) The upper row of images depicts *mglA*$_{C.\ torosa}$ Δ*mglA* cell spots induced with increasing concentrations of vanillate. Only the wild-type, shown in the left image, is capable of forming fruiting bodies, whereas the mutant strain is not. **B)** The lower row of images shows 2x magnified areas of the corresponding images in the upper row. All cells were imaged on TPM agar after 48 h at 32 °C.

4.3.7 Growth curve of vanillate-induced *sar1* Δ*mglA M. xanthus* cells

To investigate whether the expression of Sar1 in a *ΔmglA* background affects the growth of the protein-expressing cells, growth curves were recorded (**Fig. 56**). Four different strains were compared: the 500 µM vanillate-induced *sar1 ΔmglA* strain, the uninduced *pMR3679 ΔmglA* strain, the wild-type, and the *ΔmglA* strain. The graph shows that the wild-type and the *ΔmglA* strain grow equally well in CTT medium. In contrast, the high-level expression of Sar1 in the presence of 500 µM vanillate significantly impacts cell growth. Surprisingly, the uninduced *pMR3679 ΔmglA* construct affect cell growth even more than the Sar1-expressing one. The reasons for this more severe restriction of growth are currently unclear.

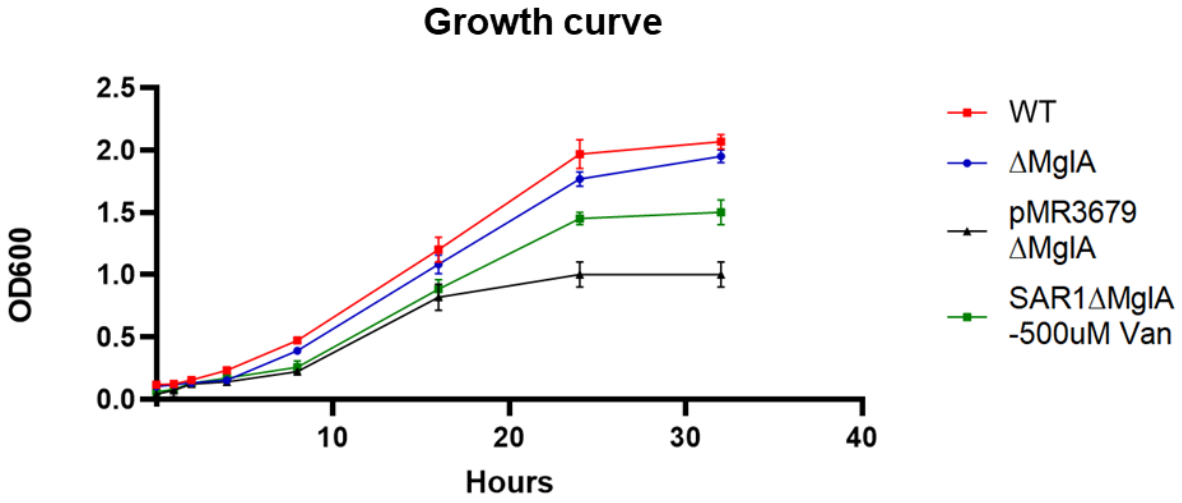

Figure 56: Growth curve of cells containing the *sar1* Δ*mglA* construct.
The expression of Sar1 in *ΔmglA* cells results in a reduced growth rate compared to both wild-type (WT) and *ΔmglA* cells. Sar1 expression was induced at high level (500 µM vanillate) during the experiment. Interestingly, the non-induced plasmid had the most pronounced impact on the cells' growth rate.

4.3.8 Cell length measurements of *sar1* Δ*mglA* and *mglA*$_{C.\ torosa}$ Δ*mglA* cells

Next, we measured the length of cells containing either the *sar1* Δ*mglA* or the *mglA*$_{C.\ torosa}$ Δ*mglA* construct and compared them with the WT cell length to determine whether the expression of these two MglA homologues had any impact on cell length. The results show that there was no significant difference in the lengths of *sar1 ΔmglA* (6.3 ± 1.0 µm), *mglA*$_{C.\ torosa}$ *ΔmglA* (6.2 ± 1.1 µm), *ΔmglA* (5.9 ± 1.2 µm), and the WT cells (5.8 ± 1.0 µm) (**Fig. 57**).

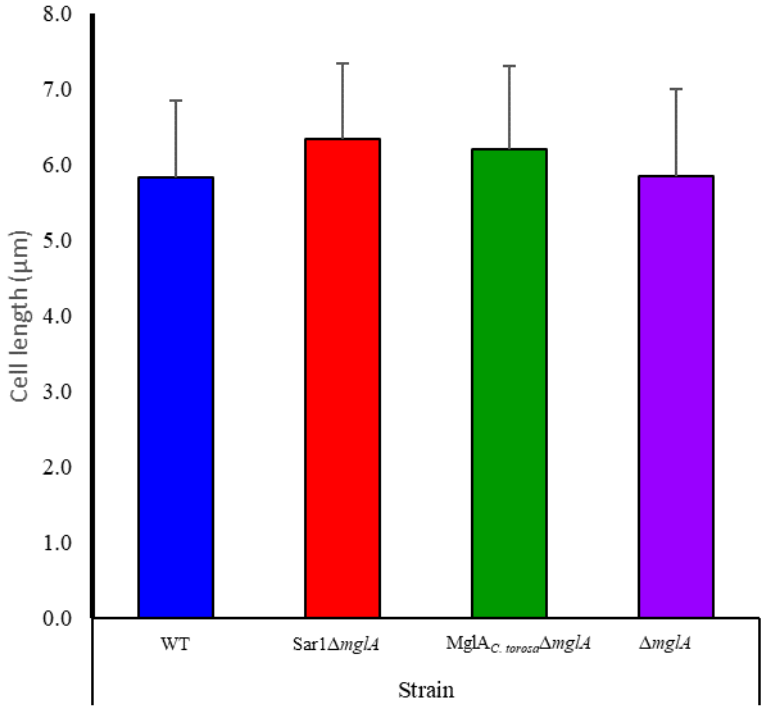

Figure 57: Cell length measurements of *sar1* Δ*mglA* and *mglA*$_{C.\ torosa}$ Δ*mglA* cells.
All cells were incubated in CTT liquid medium overnight, and the average length of cells was determined using a light microscope. For each strain, 500 randomly selected cells were measured, and the mean and standard deviation were plotted. The measurements showed no significant differences in cell length between the four strains.

4.3.9 Complementation of A- and S-motility in Δ*mglA* cells expressing MglA$_{bdv}$

It has been reported that MglA from *B. bacteriovorus*, in contrast to the homologue protein from *M. xanthus*, appears not to control the limited gliding motility that this bacterium exhibits. Instead, MglA$_{bdv}$ critically controls the bacterium's ability to invade its prey and

reduces T4P formation (Milner et al., 2014). Nonetheless, the high sequence identity (64%) with MglA of *M. xanthus* prompted us to investigate whether $MglA_{bdv}$ can complement the non-motile phenotype of *ΔmglA* cells. Similar to other such experiments, an *mglA*$_{bdv}$ *ΔmglA* construct was generated, cloned into *ΔmglA* cells, and expressed using increasing concentrations of vanillate. However, the results showed that expressing $MglA_{bdv}$ had no effect on the cell's morphology and did not restore motility on hard and soft agar plates (**Fig. 58** and **59**). Moreover, the construct also did not restore the spreading of these colonies even at the highest concentration of vanillate, a result that can easily be seen when comparing wild-type and *ΔmglA* cells with the complemented cells (**Fig. 59** and **60**). Each colony was spotted in triplicate, and the diameter of the colonies was measured for four days.

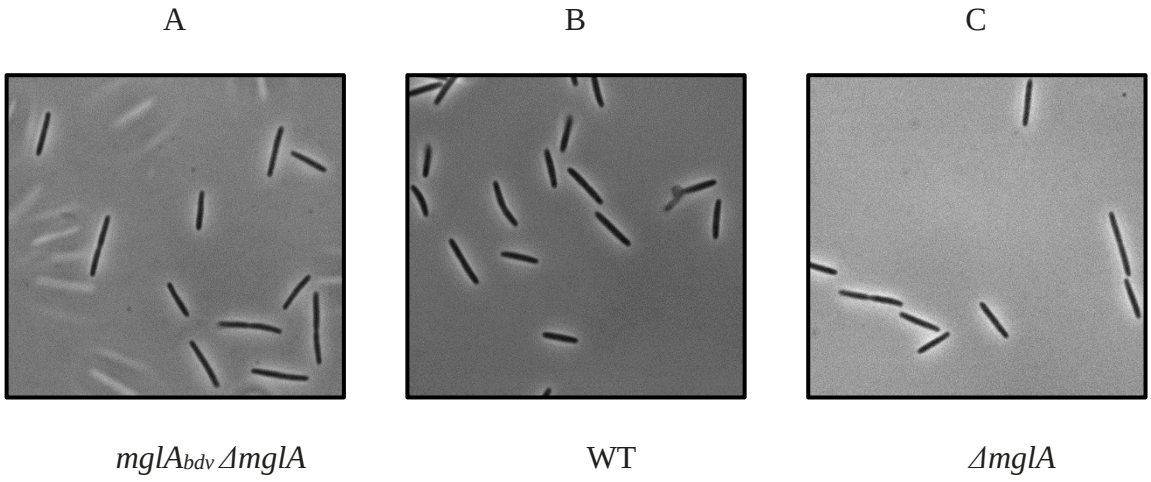

Figure 58: Morphology of *ΔmglA* cells expressing $MglA_{bdv}$.
The light microscopic images of (**A**) *mglA*$_{bdv}$*ΔmglA* cells induced by 500 µM vanillate, (**B**) wild type cells, and (**C**) *ΔmglA cells* show no discernible morphological differences indicating that the expression of $MglA_{bdv}$ has no influence on the cell's morphology. The average cell diameter is approximately 0.5 µm for all cell types.

A

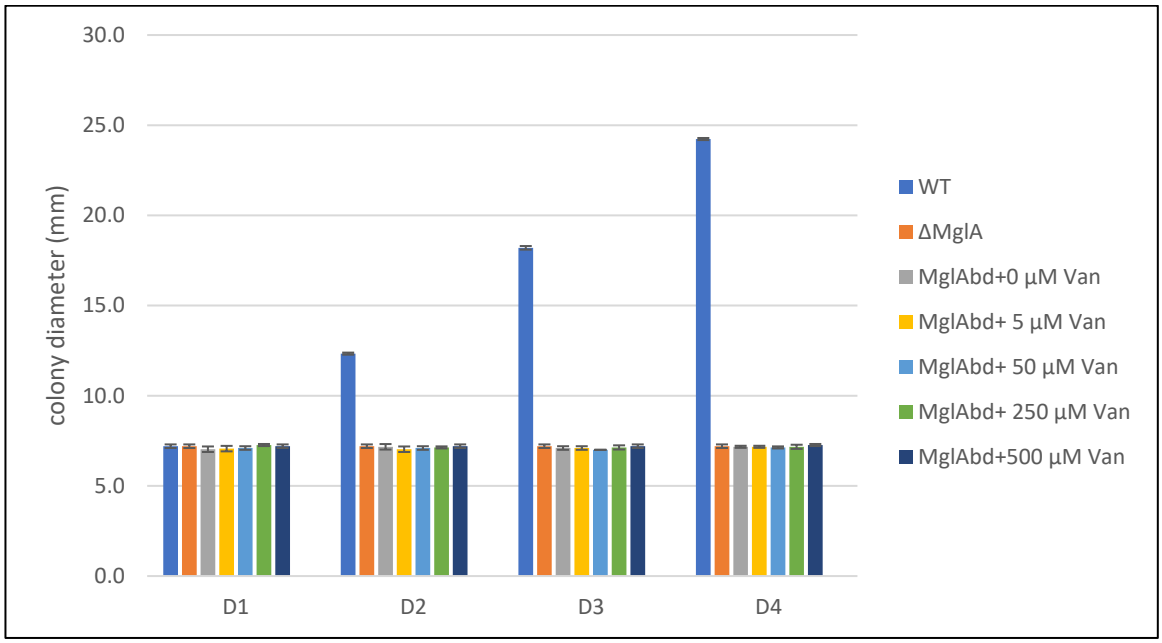

B

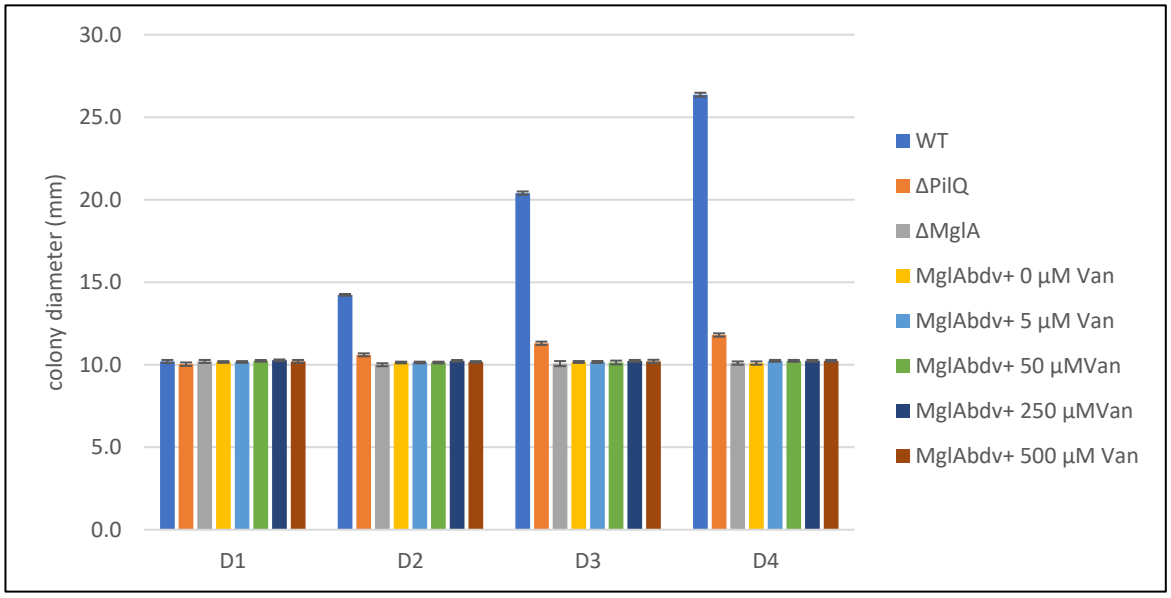

Figure 59: Investigation of A- and S-motility of Δ*mglA* cells expressing varying levels of MglA$_{bdv}$.
The X-axis represents the number of days post inoculation, and the Y-axis represents the colony diameter in mm. The measurements were conducted on **(A)** hard and **(B)** soft agar containing increasing concentrations of vanillate. Colony diameters were measured daily during a four-day period. Each measurement was done in triplicate, and the error bars represent the standard deviation of the measurements.

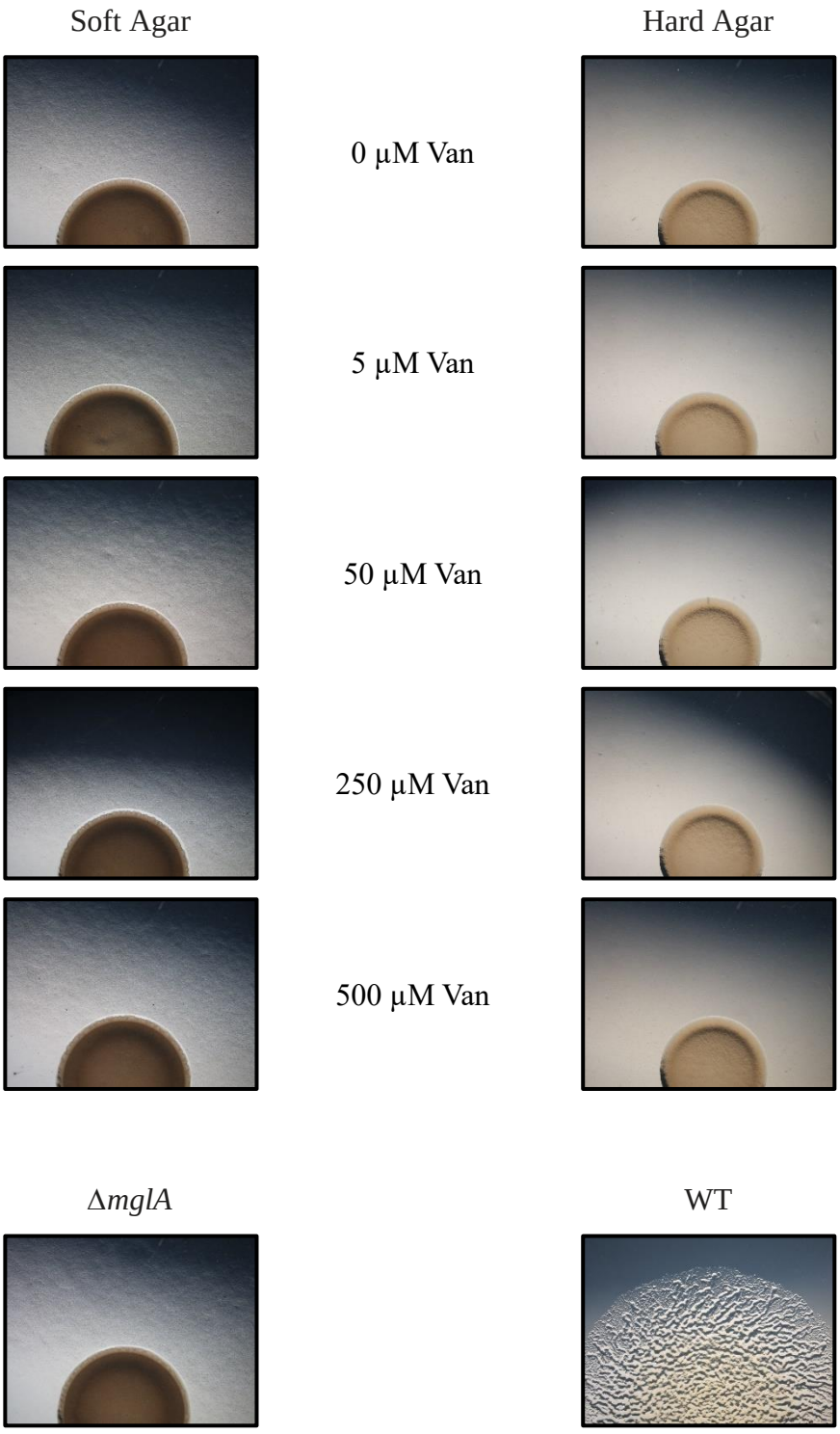

Figure 60: Expansion of Δ*mglA* cell colonies expressing various amounts of $MglA_{bdv}$.
The $mglA_{bdv}$ *ΔmglA* strain failed to expand or rescue motility on hard and soft agar after induction with 0, 5, 50, 250 and 500 µM vanillate following three days of growth at 32°C.

4.3.10 Fruiting body formation of $MglA_{bdv}$-expressing *ΔmglA* cells

Both *B. bacteriovorus* and *M. xanthus* are Gram-negative bacteria that exhibit A- and T4P-driven S-motility. Additionally, these bacteria share a predatory lifestyle. In a previous study, it was found that $MglA_{bdv}$ interacts with *M. xanthus*' BacM in a luciferase-based protein-protein interaction assay (Semeijn, 2019). Therefore, we aimed to investigate whether the expression of $MglA_{bdv}$ in *ΔmglA M. xanthus* cells could restore fruiting body formation.

TPM-washed cells were spotted in triplicate on TPM agar containing increasing amounts of vanillate and incubated for three days at 32°C. Our results indicated that $MglA_{bdv}$ was unable to complement fruiting body formation in the *ΔmglA* mutant (**Fig. 61**) and, moreover, failed to produce fruiting body spores.

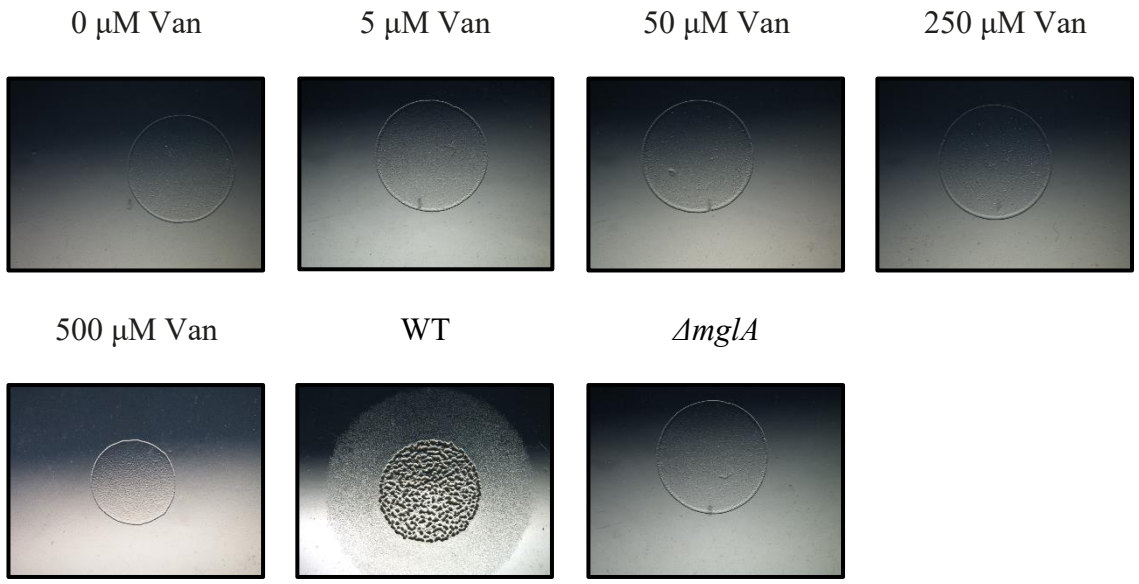

Figure 61: Fruiting body formation of Δ*mglA* cells expressing $MglA_{bdv}$.
The images from left to right show spots of $MglA_{bdv}$-expressing *ΔmglA* cells at increasing concentrations of vanillate. Even at the highest concentration of the inducer, no aggregation or fruiting body formation occurs. The WT and the *ΔmglA* strain were used as positive and negative controls, respectively.

4.3.11 Expression of a SofG-MglA hybrid protein in Δ*mglA* cells

The RasGTPases MglA and SofG of *M. xanthus* share 42% primary sequence identity, including highly characteristics features shared by all Ras-like proteins. Additionally, both proteins play a role in *M. xanthus* motility and interact with the same GAP, MglB (Kanade et al., 2020). Based on the observation that the N- and C-termini of MglA are important for the protein's interaction with GEFs, GAPs, and effector proteins, we decided to replace the thirteen N- and C-terminal amino acids of SofG with the corresponding residues from MglA in an attempt to make SofG more MglA-like (**Fig. 62**). This newly created SofG-MglA hybrid protein was then expressed in the *ΔmglA* strain using varying concentrations of vanillate to test whether the modified protein could rescue the motility defect of these cells (**Fig. 63** and **64**). However, even after growth for four days at 32 °C, the hybrid SofG-MglA protein was unable to restore motility in the *ΔmglA* phenotype and simultaneously failed to allow colony expansion when compared to WT.

Figure 62: Schematic representation of the SofG-MglA hybrid protein.
The hybrid protein was created by substituting the first and last thirteen amino acids of SofG with those from MglA, resulting in a variant of SofG that is more MglA-like.

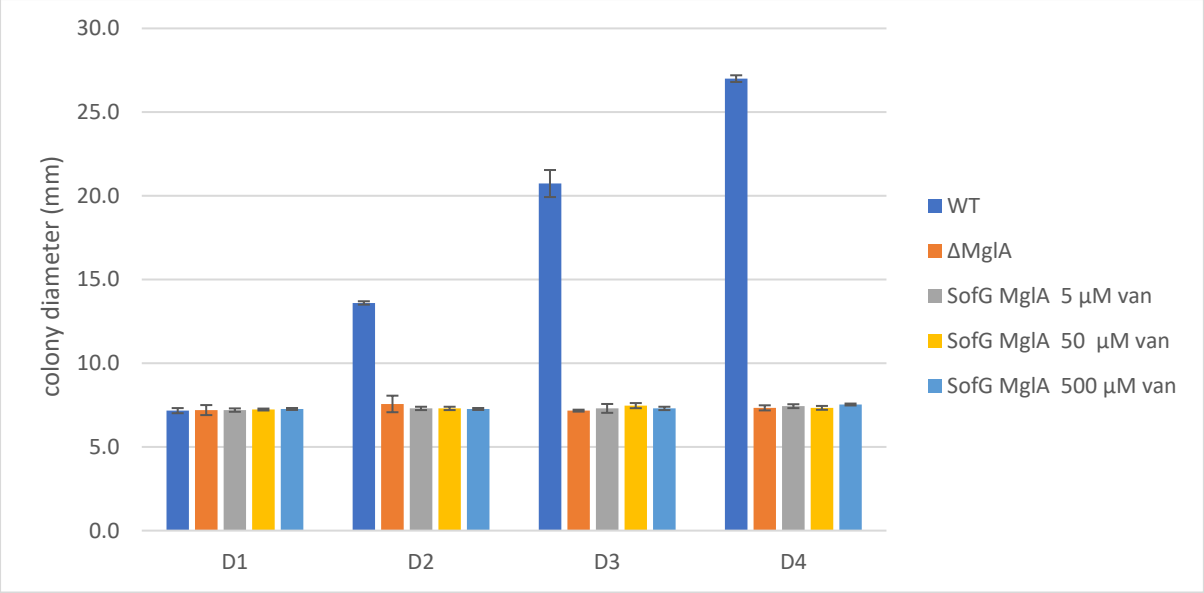

Figure 63: Investigation of A-motility of Δ*mglA* cells expressing varying amounts of SofG-MglA.
Expression of the SofG-MglA hybrid protein did not restore A-motility in Δ*mglA* cells on hard agar, even in the presence of increasing concentrations of vanillate. The X- and Y-axis represent the number of days of the experiment and the colony diameters in mm, measured daily for four days, respectively. Each measurement was conducted in triplicate, and the error bars represent the standard deviation of the measurements.

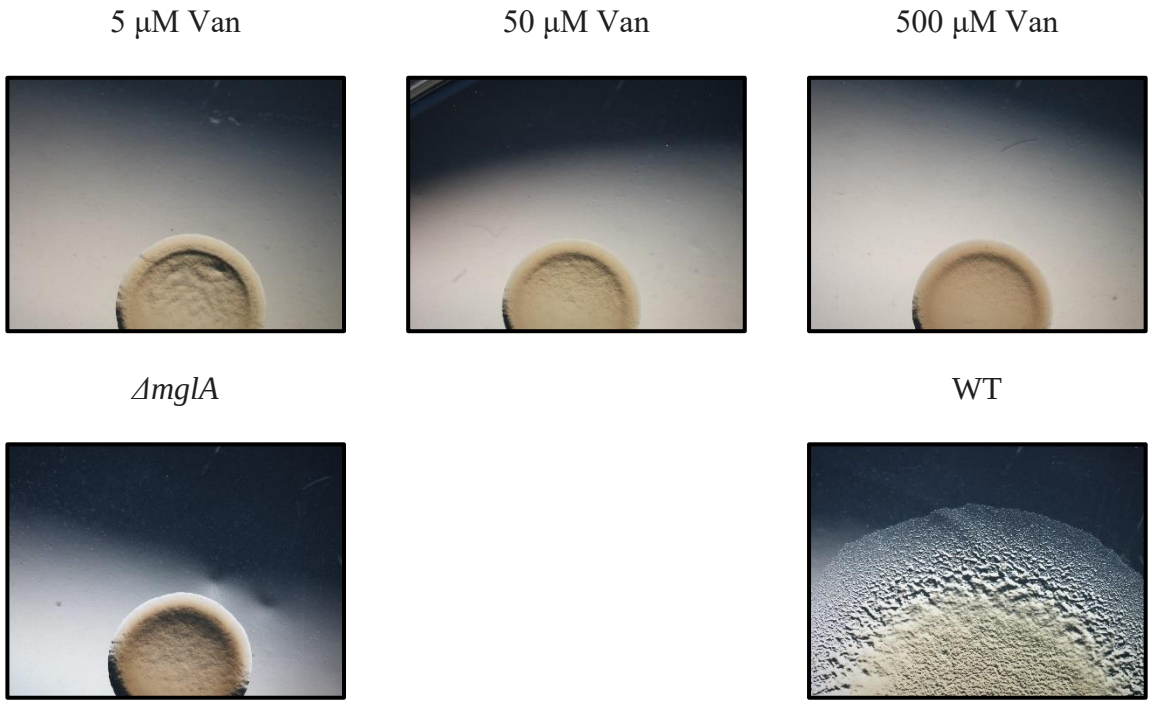

Figure 64: Expansion of Δ*mglA* cells expressing the SofG-MglA hybrid protein on hard agar.
The *sofG-mglA ΔmglA* strain was induced with low (5 µM), middle (50 µM), and high (500 µM) concentrations of vanillate. The cells were grown on 1.5% hard agar for 3 days at 32 °C but failed to expand or show signs of motility. The *ΔmglA* and WT strains were used as negative and positive controls, respectively.

4.3.12 Expression of variously mutated MglAs in Δ*mglA* cells

As previously described, many, if not most, eukaryotic RasGTPases are post-translationally modified and, therefore, it is likely that prokaryotic RasGTPases may also be modified. Therefore, we investigated the importance of commonly modified amino acid residues such as cysteine (i.e., prenylated). We mutated two cysteine residues, C13 and C23, located near the N-terminus of MglA, to serine residues, resulting in MglA-C13S-C23S. Next, we expanded our investigation of C-terminal residues and their potential role in protein-protein interactions with effectors, GAPs, and GEDs or cellular localization. To investigate these potential roles, we removed the last four C-terminal amino acids, creating MglA-del4. Finally, a third mutant, MglA-del2, was generated, in which we removed the last two terminal glycine residues (**Fig. 65**).

Figure 65: Schematic representation of the three different MglA mutants.
(**1**) MglA-C13S-C23S: the two cysteines at position 13 and 23 were replaced by serine. (**2**) MglA-del4: deletion of the four C-terminal amino acids, KKGG. (**3**) MglA-del2: lack of the last two C-terminal glycine residues.

4.3.12.1 Investigation of A-motility in MglA mutants, MglA-C13S-C23S, MglA-del4, and MglA-del2

Previous studies have shown that the N- and C-terminal regions of MglA play a role in motility (Patryn et al., 2010). To test the newly generated MglA mutants (MglA-C13S-C23S, MglA-del4, and MglA-del2) and investigate whether these changes in MglA would restore motility in the *ΔmglA* background, all three constructs were cloned into the *pMR3679* plasmid, transformed into *ΔmglA* cells, and grown overnight in vanillate-containing CTT medium at 32 °C. All three constructs were tested on hard agar plates, and the expansion of the colonies was measured for four days at 32 °C. The results showed that all three MglA mutants were able to rescue motility and colony expansion on hard agar, indicating that the mutated amino acid residues did not interfere with the physiological function of MglA in these processes (**Fig. 66** and **67**). Moreover, the change of the two cysteines to serine residues also had no discernible impact on motility and colony expansion in *ΔmglA* cells, potentially indicating that these cysteines are either not post-translationally modified or that the modification plays no role in the two investigated biological functions of MglA.

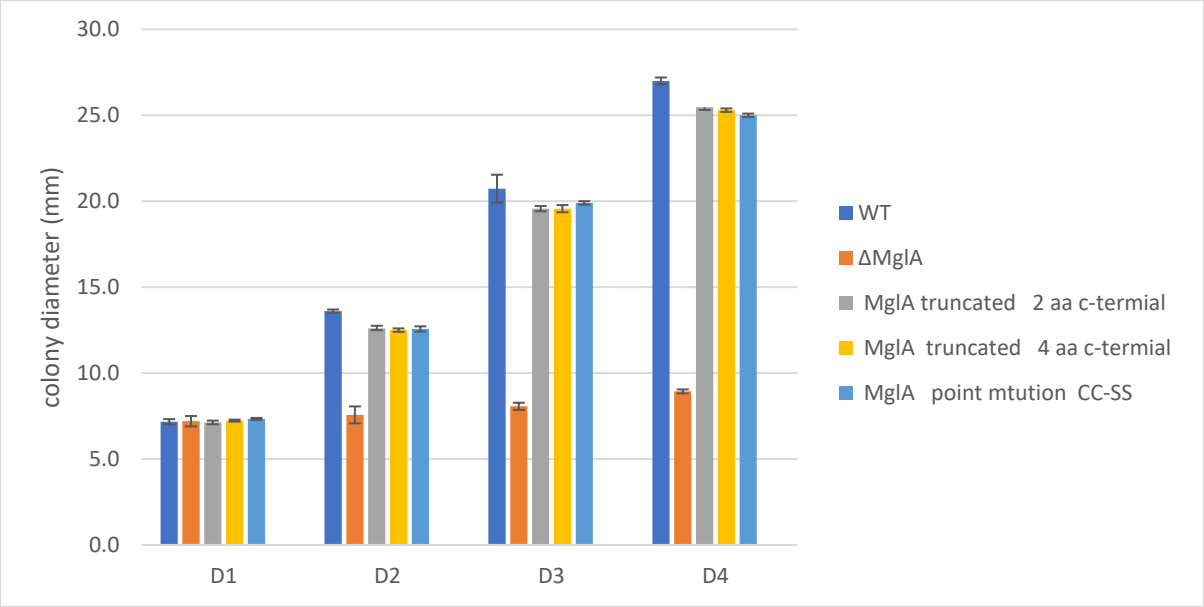

Figure 66: Investigation of A-motility of Δ*mglA* cells expressing various MglA mutants.
The expression of all three MglA mutants - MglA-C13S-C23S, MglA-del4, and MglA-del2 - in *ΔmglA* cells restored A-motility on hard agar at the concentration of vanillate used. The X-axis represents days, and the Y-axis shows the diameter of the cell spots in millimetres. Colony diameters were measured daily, and all the data represent the results of triplicate measurements, with error bars indicating the standard deviation.

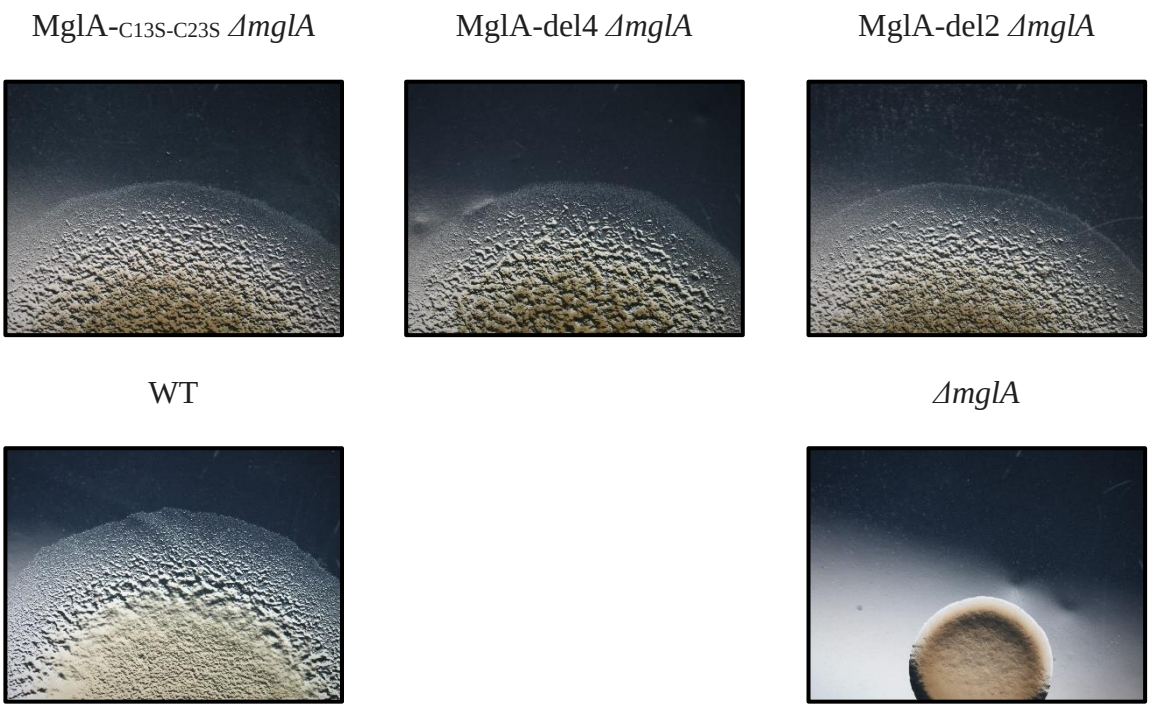

Figure 67: Expansion of Δ*mglA* cell colonies expressing various MglA mutants on hard agar.
All three MglA mutants successfully restored motility on hard agar plates after three days of growth in the presence of vanillate. The WT and the *ΔmglA* strains were employed as positive and negative controls, respectively.

4.3.13 Complementation of A-motility and colony expansion in Δ*mglA* cells expressing $MglA_{Stigm}$

The myxobacterium *S. aurantiaca* serves as a model organism for studying the formation of highly complex, branched fruiting bodies. During these studies, numerous techniques were developed, many of which are now widely adopted in the myxobacteria research community (Gerth & Reichenbach, 1978). Despite the distinct shapes of the fruiting bodies of *S. aurantiaca* (branched tree-like) and *M. xanthus* (hay stack-shaped), the two species exhibit astonishing similarities. These similarities extend to the sequences of their MglAs, which are 99% identical, differing only at five amino acid positions (four conservative replacements and one non-conservative proline to histidine substitution at position 160). This high degree of conservation of MglA in these two species prompted us to investigate whether $MglA_{stigm}$ could rescue motility and colony expansion in a *ΔmglA* background. To test this hypothesis, the *$mglA_{stigm}$ ΔmglA* construct was cloned into *pMR3679,* transformed into *ΔmglA,* and induced with increasing concentrations of vanillate. Unsurprisingly, given their high sequence identity, $MglA_{stigm}$ was able to rescue motility and colony spreading of *ΔmglA* cells. However, several interesting observations were made. First, the level of complementation directly correlated with the amount of $MglA_{stigm}$, as low vanillate concentrations resulted in lower motility and expansion. Somewhat surprisingly, even at the highest vanillate concentration (500 µM), complete complementation to WT level for both motility and expansion was not achieved **(Fig. 68** and **69**). This could either indicate that the amount of $MglA_{stigm}$ was still too low or that the *Stigmatella* protein is not as efficient at interacting with the cognate partner proteins in *M. xanthus*. As usual, the WT and *ΔmglA* strain were used as positive and negative controls, respectively.

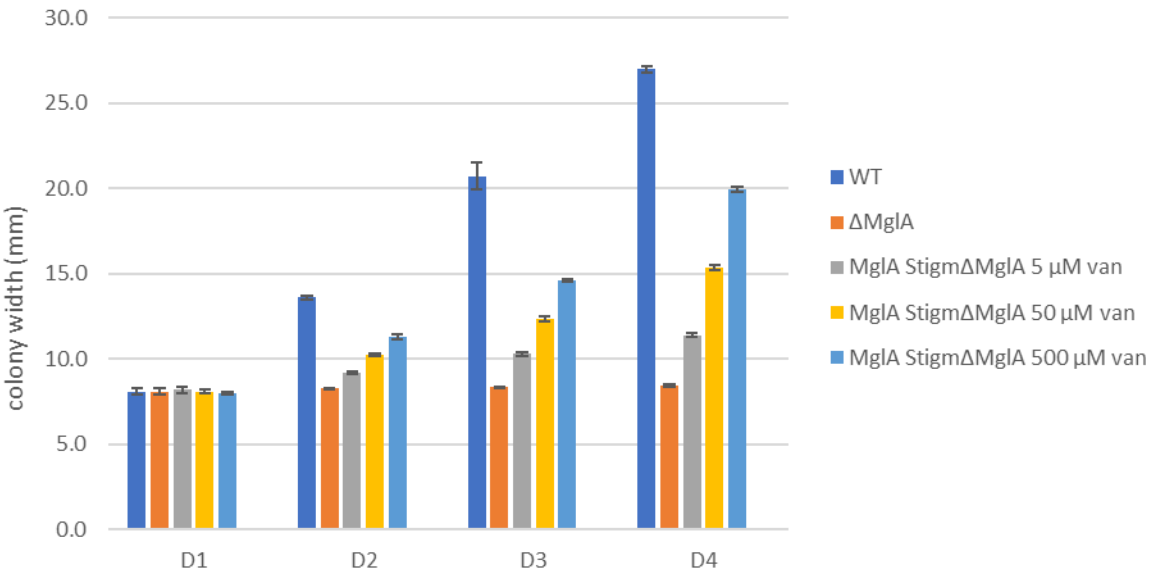

Figure 68: Investigation of A-motility of Δ*mglA* cells expressing MglA$_{stigm}$.
Expression of MglA$_{stigm}$ in the *ΔmglA* strain restores A-motility on hard agar. Moreover, the degree of restoration is vanillate concentration-dependent, reaching nearly wild-type levels at the highest concentration (500 µM). The X-axis represents the days, and the Y-axis displays the colony diameter, which was measured daily for a total of four days. Experiments were performed in triplicate, and the error bars show the standard deviation.

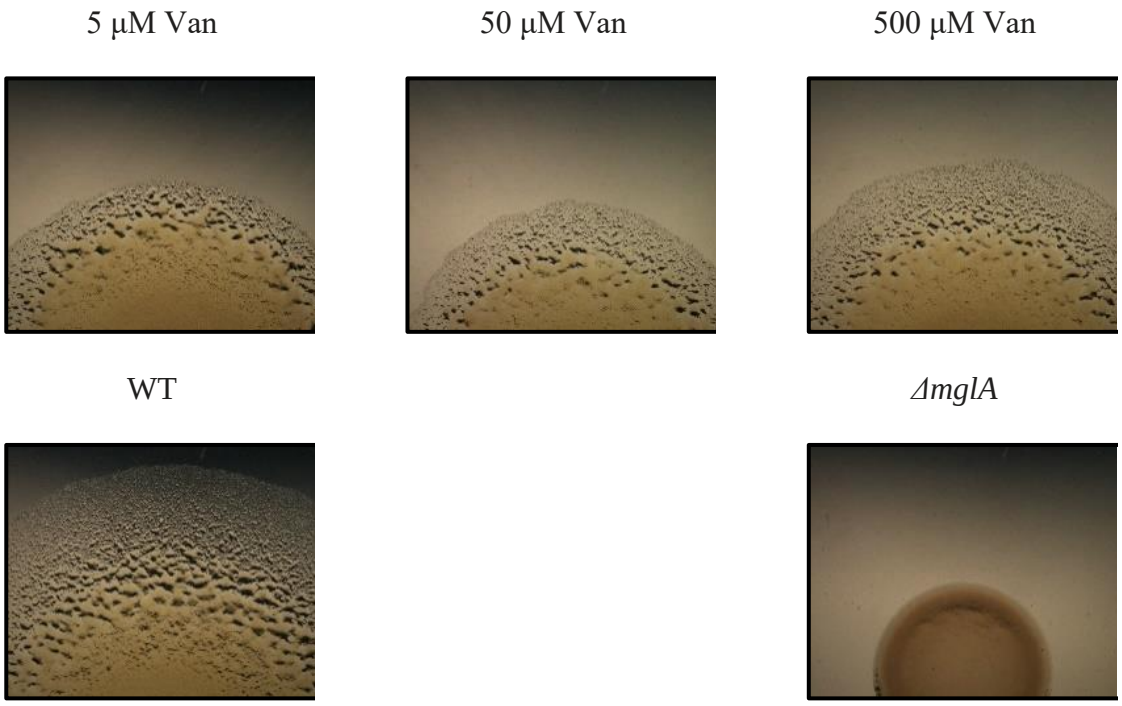

Figure 69: Expansion of Δ*mglA* cell colonies expressing varying amounts of $MglA_{stigm}$.
The expression of $MglA_{stigm}$ in the Δ*mglA* background restores motility and colony expansion. It is noteworthy that the width of the thin edges of the colonies becomes wider with increasing concentrations of vanillate, reaching wild-type levels at 500 μM vanillate. The Δ*mglA* strain was used as the negative control.

4.4 Discussion

Many, if not most, eukaryotic RasGTPases undergo post-translational modifications, with phosphorylation, lipidation, and prenylation being the most common forms. While no reports describe post-translational modifications in known bacterial RasGTPase, their occurrence is likely given their prevalence in eukaryotic counterparts. These modifications play a crucial role in regulating the activities of these important molecular signalling and control proteins (Grangeasse, et al., 2000). Notably, a former lab member observed a slight molecular weight difference between *E. coli*-overexpressed and *M. xanthus* isolated MglA in SDS PAGE, suggesting that this important myxobacterial control protein may be post-translationally modified (Semeijn, unpublished).

Four amino acid residues - serine, threonine, tyrosine for phosphorylations, and serine, cysteine for lipidations and prenylations - are commonly used for attachment of these post-translational modifications. Phosphorylations often act as molecular on or off switches, while lipidations and prenylations are more permanent and usually enable RasGTPases to attach to membranes, thereby determining their cellular localization. Prenylations and lipidations like palmitoylation and myristoylation are particularly widespread forms of modifications in Ras proteins (Campbell and Philips, 2021). Consequently, our investigation focused on determining whether the N-terminal serine and cysteine residues at the β0β1sheets of MglA are lipidated or prenylated, allowing the protein to attach to membranes. These regions, being variable and surface-exposed, are not only ideal for post-translational modifications but also crucial for protein-protein interactions with effector proteins, GAPs or GEFs.

To explore potential post-translational modifications, we compiled a large dataset of MglA homologues from prokaryotic organisms, including two eukaryotic sequences: Sar1 from *S. cerevisiae* and $MglA_{C.\ torosa}$ from the tiny aquatic crustacean *C. torosa*. Sar1 was chosen based on its use in complementation experiments of *ΔmglA M. xanthus* cells (Hartzell, 1997),

and $MglA_{C.\ torosa}$ showed the highest identity score among all analysed eukaryotic RasGTPases with MglA (46% *vs*. only 24% with Sar1). Confirming post-translational modifications in MglA would significantly impact our understanding of bacterial RasGTPase and *M. xanthus* biology, including cell polarity, regulation of cell reversals, molecular motor activity, etc.

When selecting amino acid residues for mutational studies, two factors were considered: their degree of conservation and their relative position within the solved X-ray structure of MglA. Conservation usually indicates functional or structural importance, and the relative position within the protein's architecture influences accessibility, crucial for protein-protein interactions and membrane binding mediated by lipidation and prenylation. In fact, many RasGTPases, such as Rho, Rhb, and Ras, are post-translationally modified, following these principles, as all three contain cysteine-rich regions at the C-terminus that can be modified with lipids (Paduch et al., 2001). Moreover, Arf proteins contain an N-terminal glycine residue that is modified with the unsaturated fatty acid, myristic acid (Moss and Vaughan, 1995). However, post-translational modification is not universally found in RasGTPases; for example, Ran does not contain any post-translationally modified amino acids (Ren et al., 1995).

Based on our bioinformatic analysis, we focused on mutating particular amino acids that could play a role in MglA function and modification, and on identifying homologous protein candidates capable of substituting for *M. xanthus* MglA. The first such closely related candidate protein tested was the $MglA_{stigm}$ from *S. aurantiaca*, which is 99% identical to MglA, differing by only five amino acid residues. These differences include four conservative replacements and one non-conservative proline-histidine substitution at position 160. Notably, $MglA_{stigm}$ was able to rescue motility in a *ΔmglA M. xanthus* strain, an outcome that was probably not too surprising, given the close relatedness of these two organisms. Both *S. aurantiaca* and *M. xanthus* not only belong to the same phylogenetic group, *Myxococcota*, but

have similar-sized genomes of approximately 9.4 Mbp displaying a high degree of synteny (Chen et al., 1990; Neumann et al., 1992).

Next, we tested $MglA_{bdv}$ from *B. bacteriovorus*, possessing 82% sequence similarity and 64% identity to MglA. Interestingly, despite this relatedness (Fremgen et al., 2010), $MglA_{bdv}$ was unable to rescue motility and colony expansion in *M. xanthus ΔmglA* cells even at high concentrations of the inducer vanillate (500 μM). Possible reasons could be the lack of the GAP, MglB, an important partner of MglA, and the fact that MglA in *B. bacteriovorus* appears to be involved in prey invasion rather than gliding motility (Milner et al., 2014). $MglA_{bdv}$ also failed to complement fruiting body formation and spore production, which is less surprising as *Bdellovibrio*, albeit being a predatory bacterium, does not form fruiting bodies (Ferguson, 2014). Intriguingly, $MglA_{myxo}$ and $BacM_{bdv}$ from *B. bacteriovorus* interacted with each other in a luciferase-based protein-protein interaction assay (see Chapter II). However, the reverse binding of $MglA_{bdv}$ to $BacM_{myxo}$ could not be confirmed, showing that there are subtle, not yet understood differences which control the interactions of bactofilins and RasGTPases.

Based on our improved understanding of MglA, we next reexamined the published report that Sar1 from *S. cerevisiae* was able to partially complement sporulation without fruiting body formation and motility after the occurrence of a secondary mutation "*rpm*" (**r**estoration of **p**artial **m**otility) in the *sar1ΔmglA* background (Hartzell, 1997). As the identity and location of the secondary *rpm* mutation were not disclosed in the publication, we focused on the complementation of spore formation by inducing Sar1 expression in *ΔmglA* cells using increasing concentrations of vanillate. While unsurprisingly, no rescue of motility or fruiting body formation *per se* was observed, we did find after starvation individual spore-like cells among the vegetative rod-shaped cells that became, over a period of 24 h, the dominant cell type, confirming the reported observation. However, closer inspection revealed that these

spore-like cells exhibited subtle differences compared with the spores found inside of mature fruiting bodies. In particular, the rescued spores were egg-shaped rather than round and less refractive in phase contrast, indicating that the characteristic thick multi-layered spore coat was missing, strongly suggesting that the spore-like cells were more akin to glycerol spores than fruiting body spores (Hartzell, 1997). Importantly, additional experiments, including electron microscopy of thin sections of the formed spores and biochemical investigations, would need to be performed to confirm that the rescued spores are indeed *bona fide* glycerol spores. Additional experiments would also need to address the more important discovery in the Hartzell paper, namely that the *rpm* secondary mutation can compensate for the loss of MglA complementing both motility and fruiting body formation. The important open issue is how *rpm* restores these phenotypes and what role, if any, Sar1 plays in the process. MglA and Sar1 share a high degree of identity in their G1-G5 structural motifs, although they only share 24% identity overall (Miertzschke et al., 2001).

Given the fact that our bioinformatic search had discovered a eukaryotic RasGTPase, $MglA_{C.torosa}$, that has 46% identity with MglA, nearly double the amount of Sar1, we decided to repeat our motility, colony expansion, and fruiting body formation complementation experiments with this RasGTPase. Unfortunately, the *C. torosa* $MglA_{C.torosa}$ also proved unsuccessful in complementing any of these three phenotypes of *M. xanthus ΔmglA* cells, even at the highest concentration of vanillate. One interesting question in this context is why an aquatic ostracod like *C. torosa* possesses a prokaryotic-like MglA homologue (Marco-Barba et al., 2012). As ostracods feed on detritus and bacteria, the crustacea may have acquired the gene simply from its food. However, it cannot be completely ruled out that the database sequence may actually originate from an endosymbiotic or gut bacterium of *C. torosa*.

Based on our results, it appeared that even relatively closely related MglAs are unable to complement the *ΔmglA* phenotype and that a previous report about the yeast protein Sar1 being

able to do so may have misinterpreted the finding of spore-like cells as proof that Sar1 can complement fruiting body spore formation in the absence of an actual fruiting body. However, our data show that the observed spores are most likely glycerol spores and not fruiting body spores questioning the ability of Sar1 to complement any aspect of the *ΔmglA* phenotype.

Because of these results, we then decided to investigate the contribution of molecular features of MglA more directly, by mutating or changing the protein's sequence and testing the ability of the mutant MglAs to complement the *ΔmglA* phenotype. One focus of these experiments was to test the possibility that MglA, like most eukaryotic RasGTPases, is post-translationally modified. The rationale for selecting these amino acid residues was threefold, they needed to be conserved, accessible, and modifiable.

The first two amino acid residues investigated were the two conserved cysteines located near the protein's N-terminus, C13 and C23, which could undergo either lipidation or prenylation. Unfortunately, no effect was found when these residues were replaced by serine. Therefore, we next removed the last two or four C-terminal amino acids and tested the effect of those changes – again, with no detectable consequence for the *ΔmglA* phenotype. Although these changes did not result in new insights into the function of the investigated sequence elements, there are many more conserved residues that could be important for the regulation or function of MglA, particularly highly conserved phosphorylatable amino acids, like the five serine (2, 46, 88, 105, and 116), four tyrosine (17, 18, 85, and 140), and one threonine (179) residues.

A second avenue of research that we followed was the idea to use the *M. xanthus* RasGTPase, SofG, and transform it into a SofG-MglA hybrid protein by replacing the N- and C-terminal thirteen amino acids of SofG with those of MglA. The choice of SofG was made because it is one of three *M. xanthus* RasGTPases, but in contrast to MXAN_2495, the third one, SofG has been characterized and is necessary for T4 pili-driven S-motility, a function that

partially overlaps with that of MglA, which controls both A- and S-motility (Bulyha *et al*., 2013). Moreover, recent research in the lab has shown that SofG, like MglA, interacts with the bactofilin BacM (Semeijn, 2019), not BacP as had been previously reported (Bulyha *et al*., 2013), again indicating that MglA and SofG have more in common than simply being myxobacterial RasGTPases. Unfortunately, despite these changes and the functional relatedness, the generated SofG-MglA hybrid protein was unable to restore motility and colony expansion in *ΔmglA* cells, indicating that more alterations of the SofG sequence are necessary to achieve this goal.

During this project, a number of amino acid residues and sequences, such as the N- and C-terminus, have been investigated to identify functionally critical amino acids of MglA. Identifying such amino acids will start providing the basis for dissecting how and with which proteins MglA interacts, eventually revealing the molecular function of this important myxobacterial GTPase. Paradoxically, although we know that MglA controls A- and S-motility, it is currently completely unclear how the protein accomplishes this task.

Another related important aspect is the question, whether MglA is post-translationally modified. The experiment mutating the two N-terminally located cysteines did not reveal any noticeable effect. However, as discussed above, there are many more conserved, particularly phosphorylatable amino acids that could be modified. The reason identifying any post-translation modification is crucial is that it could potentially offer an explanation for a molecular conundrum: MglA localizes and interacts at the same time in the cell with multiple cellular structures and proteins, yet we know virtually next to nothing about how this complex spatial distribution is achieved. Among the structures that MglA associates with are the polar regions of the cells and the focal adhesion complexes. The protein partners, besides the obvious candidates, such as MglB and RomRX, also include BacM, which itself appears to exist in two

forms, a less abundant full-length cytoplasmic membrane-associated form and a shorter N-terminally cleaved cytoplasmic version.

Post-translational modifications could be the solution of this molecular puzzle. For example, a simple phosphorylation of MglA would double the existing variants of this protein in the cell, as each GTP- and GDP-bound form could be phosphorylated or unphosphorylated. Yet, another unsolved question is where MglA fits in the complex signalling hierarchy that controls cell reversals. It is known that this process starts with the Frz proteins, but so far, no direct link between any Frz protein and MglA has been discovered, leaving the question unanswered how the input and output modules of cell reversals are connected. Although the thesis has not attempted to address these questions, the described experiments and results provide a solid foundation for future additional work that may reveal the overall molecular function of MglA.

Chapter V: Discussion and Conclusion

The goal of this study was to better understand the interaction between MglA and bactofilins, cytoskeletal proteins, and to investigate the localization, structure, and function of MglA itself. MglA (MXAN_1925) is one of the three non-ribosomal Ras-like GTPases of *M. xanthus*, with SofG (MXAN_6703) and MXAN_2495 being the other two. Importantly, MglA has long been recognized as the only protein of *M. xanthus* that controls both A- and S-motility. This means that *ΔmglA* cells show neither single-cell nor cell group motility. How MglA accomplishes this feat is less well understood, in part due to unclear nature of the A-motility motor and the absence of any direct link or binding of MglA to known S-motor proteins.

Some time ago in our laboratory, pull-down experiments revealed that MglA binds to the bactofilin BacM. This interaction was recently confirmed in a PhD thesis using a novel luciferase-based protein-protein two-hybrid system (Seemijn, 2019). This thesis also revealed that MglA does not bind to MreB, as had been previously published using an *in vitro* overexpression-based interaction assay (Mauriello et al., 2010). Intriguingly, SofG, one of the other two *M. xanthus* RasGTPases, had been reported to bind to the bactofilin BacP, indicating that interactions between RasGTPases and bactofilins may be an important novel feature of these two classes of bacterial proteins (Bulyha et al., 2013).

To investigate whether the interaction between MglA-like RasGTPases and bactofilins is more broadly conserved among prokaryotes, we used bioinformatics to identify bacteria that, like *M. xanthus*, possessed MglA-BacM-like pairs of these two classes of proteins. Four bacteria that represented highly divers phyla were eventually selected, and their MglA-BacM pairs were cloned into *ΔmglA M. xanthus* to test any luciferase-detectable interactions. MglA-BacM pairs from two of the four bacteria, *Leptothrix mobilis* and *Bdellovibrio bacteriovorus*, showed interactions of the same magnitude as MglA-BacM. As for the other two organisms,

Collimonas fungivorans and *Xanthomonas bromi*, *M. xanthus* may have been the wrong expression host due to the vast phylogenetic difference between the two *Pseudomonadota* and this *Myxococcota* (Waite et al., 2020). Consequently, the interaction assays would need to be repeated using an *E. coli*-based two-hybrid system instead. We also re-investigated the interaction between SofG and BacP and found that inside *M. xanthus* they appear not to interact. Instead, SofG binds BacM, which means that there exists an intriguing link between SofG and MglA, as they appear to bind to the same bactofilin.

Next, we decided to investigate the cellular localization of MglA to better understand how its distribution may correlate with the different cellular processes it controls. However, before conducting those studies, a suitable fluorescently labelled and, therefore, detectable construct of MglA was needed. In the literature, numerous such constructs have been described, which differ with respect to the location and the nature of the tag, as well as the linker between the tag and the protein (see **Table 3**). Although a number of studies have "successfully" used eYFP-tagged N- or C-terminal versions for MglA localization studies, our work indicated that none of these versions truly complemented the *ΔmglA* phenotype, as motility was only restored at the single-cell but not colony level. Therefore, we decided to use a TC-tagged MglA construct possessing a long highly flexible linker between MglA and the six-amino-acid-long CCPGCC tag. Although, this tag is less sensitive than the eYFP tags, it allowed us to visualize the same intracellular distribution of MglA that has been described in the literature, a large unipolar cluster at the leading pole and smaller lateral clusters along the length of the cells, confirming this arrangement in fully complemented cells. While the unipolar cluster is involved in regulating cell polarity and T4P assembly and activity (Bulhya et al., 2013), the lateral clusters have been interpreted to represent focal adhesions, multi-protein complexes that may be A-motility motor complexes (Mignot, 2007). Consequently, MglA is located at cellular sites that have been suggested to be also the sites of the A- and S-motility motors. Despite this

virtually identical spatial arrangement, no direct interactions between any known A- or S-motility motor protein and MglA has been documented, leaving the question unanswered how the protein controls the activity of these two different motor systems. The only currently well understood aspect of MglA localization is the observed unipolar cluster at the leading pole. This cluster is the consequence of the dynamic interplay between RomRX, MglB, and MglA, which prevents MglA localization at the lagging pole (Leonardy, 2010; Zhang, 2010; Szadkowski et al., 2019).

More than twenty years ago, a study was published that reported that Sar1 from the yeast *S. cerevisiae* can complement one defect of the *ΔmglA* phenotype, spore formation (Hartzell, 1997). Although we could indeed detect spore-like cells in the *sar1ΔmglA* strain, a critical evaluation of these "spores" revealed that they possess all the hallmarks of glycerol spores, casting doubt on the original interpretation of partial complementation. Nonetheless, based on these previous experiments, we decided to express MglA-eYFP in *S. cerevisiae* to study its localization in a non-prokaryotic organism possessing complex multiple membrane systems of various compositions and curvatures. Surprisingly, yeast cells expressing MglA-eYFP displayed a non-uniform distribution of fluorescence staining, which matched mitochondrial staining. Although more experiments are needed to confirm the mitochondrial straining, including co-staining with MitoTracker dye or the use of yeast mitochondrial mutant strains, these results are highly interesting as mitochondrial membranes are enriched for cardiolipin (Paradies et al., 2014). Cardiolipin is also commonly present in bacteria and accumulates, due to its cone-shaped head group, at areas with high membrane curvatures like the cell poles (Galicia et al., 2019). This result points to the exciting possibility that MglA may localize to the cell poles through its interaction with cardiolipin. Interestingly, lipid-directed membrane association is also utilized by Sar1. During this process Sar1 inserts its N-terminal amphipathic helix into the outer membrane leaflet to initiate membrane deformation. This process

simultaneously lowers the rigidity of the membrane, while at the same time increasing membrane curvature (Settles et al., 2010). Cardiolipin-directed membrane association of MglA could very similar lower membrane rigidity while simultaneously increasing curvature. Although this hypothesis is potentially highly informative for our overall understanding of MglA activity, membrane-association *per se* does not easily explain the protein's control of the A- and S-motility motors. Moreover, direct interactions of RasGTPases *via* hydrophobic or amphipathic structural elements are not the only form of membrane targeting used by members of the RasGTPase superfamily. Another widely used mechanism is the use of post-translational modifications such as lipidations or prenylations. For example, the Ras protein from the rat sarcoma virus has a highly homologous approximately 164 amino acid-long G domain, followed by the C-terminal hypervariable region, ending in the tetrapeptide CAAX motif (Spoerner et al., 2001). During the post-translational modification of the motif, the endoplasmic endopeptidase Rce1 mediates cleavage of the C-terminal three amino acids of the motif, while farnesyl transferase attaches a farnesyl group to the now accessible cysteine residue (Spoerner et al., 2001; Ahearn et al., 2018). In fact, all four isoforms of Ras - H-Ras, K-Ras4A, K-Ras4B, and N-Ras - are modified by farnesyl transferases, while Ras and Rho family proteins are modified by geranylgeranyl transferase 1 (Ahearn et al., 2018). These modifications transform these otherwise globular hydrophilic proteins into peripheral membrane proteins, providing affinity for phospholipid bilayer through the prenylation of the C-terminal cysteine (Campbell and Philips, 2021; Wright and Philips, 2006). Consequently, we explored the possibility that MglA, like these RasGTPases, may be post-translationally modified. Therefore, bioinformatic database searches and sequence alignments were used to identify highly conserved solvent-accessible cysteine and serine residues that could be post-translationally modified. Unfortunately, our investigations into the two conserved cysteine residues of MglA failed to produce data that would reveal the presence of a post-translational modification. Therefore,

other experiments, such as mass spectrometry or radioactive labelling experiments, would have to be done to clarify whether MglA, like so many other RasGTPases, is modified or not.

Overall, this data has substantially broadened our understanding of MglA and its interaction with the cytoskeletal protein bactofilins. Although the mechanism by which MglA controls A- and S-motility is still elusive, the newly gained insight into the biology of this key RasGTPase will help to eventually unravel the control mechanism for motility. In extension, this understanding will contribute to our knowledge of other phenomena, including cell division, polarity, reversals, fruiting body formation, and sporulation.

References

Adkins, J. (2020, March 11). Deep-sea shrimps are covered in organs that see light. *Florida International University News*. https://news.fiu.edu/2020/deep-sea-shrimp-are-covered-in-organs-that-see-light.

Ahearn, I., Zhou, M., & Philips, M. R. (2018). Posttranslational modifications of Ras proteins. *Cold Spring Harbor Perspectives in Medicine*, *8*(11), 1–18. https://doi.org/10.1101/cshperspect.a031484.

Ahrendt, T., Wolff, H., & Bode, H. B. (2015). Neutral and phospholipids of the *Myxococcus xanthus* lipodome during fruiting body formation and germination. *Applied and Environmental Microbiology*, *81*(19), 6538–6547. https://doi.org/10.1128/AEM.0153715.

Anand, B., Verma, S. K., & Prakash, B. (2006). Structural stabilization of GTP-binding domains in circularly permuted GTPases: Implications for RNA binding. *Nucleic Acids Research*, *34*(8), 2196–2205. https://doi.org/10.1093/nar/gkl178.

Antonny, B., Bigay, J., Casella, J. F., Drin, G., Mesmin, B., & Gounon, P. (2005). Membrane curvature and the control of GTP hydrolysis in Arf1 during COPI vesicle formation. *Biochemical Society Transactions*, *33*(4), 619–622. https://doi.org/10.1042/BST0330619.

Argos, P. (1990). An investigation of oligopeptides linking domains in protein tertiary structures and possible candidates for general gene fusion. *Journal of Molecular Biology*, *211*(4), 943–958. https://doi.org/10.1016/0022-2836(90)90085-Z.

Baranwal, J., Lhospice, S., Kanade, M., Chakraborty, S., Gade, P. R., Harne, S., Herrou, J., Mignot, T., & Gayathri, P. (2019). Allosteric regulation of a prokaryotic small Ras-like GTPase contributes to cell polarity oscillations in bacterial motility. *PLoS Biology*, *17*(9), 1–30. https://doi.org/10.1371/journal.pbio.3000459.

Barr, F., & Lambright, D. G. (2010). Rab GEFs and GAPs. *Current Opinion in Cell Biology, 22*(4,) 461–470. https://doi.org/10.1016/j.ceb.2010.04.007.

Barrios-Rodiles, M., Ellis, J., Blencowe, B. & Wrana, J. (2017). LUMIER: A discovery tool for mammalian protein interaction networks. *Methods in Molecular Biology, 1550,* 137–148. https://doi.org/10.1007/978-1-4939-6747-6_11.

Bernards, A., & Settleman, J. (2004). GAP control: Regulating the regulators of small GTPases. *Trends in Cell Biology*, *14*(7), 377–385. https://doi.org/10.1016/j.tcb.2004.05.003.

Bishop, A. L., & Hall, A. (2000). Rho GTPases and their effector proteins. *Biochemical Journal*, *348*(2), 241–255. https://doi.org/10.1042/0264-6021:3480241.

Blümer, J., Rey, J., Dehmelt, L., Maze, T., Wu, Y. W., Bastiaens, P., Goody, R. S., & Itzen, A. (2013). RabGEFs are a major determinant for specific Rab membrane targeting. *Journal of Cell Biology*, *200*(3), 287–300. https://doi.org/10.1083/jcb.201209113.

Booth, I. R., Edwards, M. D., Black, S., Schumann, U., & Miller, S. (2007). Mechanosensitive channels in bacteria: Signs of closure? *Nature Reviews Microbiology*, *5*(6), 431–440. https://doi.org/10.1038/nrmicro1659.

Bos, J. L., Rehmann, H., & Wittinghofer, A. (2007). GEFs and GAPs: Critical elements in the control of small G proteins. *Cell*, *129*(5), 865-77. https://doi.org/10.1016/j.cell.2007.05.018.

Boureux, A., Vignal, E., Faure, S., & Fort, P. (2007). Evolution of the Rho family of Ras-like GTPases in eukaryotes. *Molecular biology and evolution, 24*(1), 203–16. https://doi.org/10.1093/molbev/msl145.

Brachmann, C. B., Davies, A., Cost, G. J., Caputo, E., Li, J., Hieter, P., & Boeke, J. D. (1998). Designer deletion strains derived from *Saccharomyces cerevisiae* S288C: a useful set of

strains and plasmids for PCR-mediated gene disruption and other applications. *Yeast*, *14*(2), 115-132. https://doi.org/10.1002/(sici)1097-0061(19980130)14:2%3C115::aid-yea204%3E3.0.co;2-2.

Braun, P., Tasan, M., Dreze, M., Barrios-Rodiles, M., Lemmens, I., Yu, H., Sahalie, J. M., Murray, R. R., Roncari, L., & De Smet, A.-S. (2009). An experimentally derived confidence score for binary protein-protein interactions. *Nature Methods*, *6*(1), 91–97.

Britton, R. A. (2009). Role of GTPases in bacterial ribosome assembly. *Annual Review of Microbiology*, *63*, 155–176. https://doi.org/10.1146/annurev.micro.091208.073225.

Buchanan, S. G. S. C., & Gay, N. J. (1996). Structural and functional diversity in the leucine-rich repeat family of proteins. *Progress in Biophysics and Molecular Biology*, *65*(1–2), 1–44. https://doi.org/10.1016/s0079-6107(96)00003-x.

Bulyha, I., Hot, E., Huntley, S. and Søgaard-Andersen, L. (2011). GTPases in bacterial cell polarity and signalling. *Current Opinion in Microbiology*, *14*, 726-733.

Bulyha, I., Lindow, S., Lin, L., Bolte, K., Wuichet, K., Kahnt, J., van der Does, C., Thanbichler, M., & Søgaard-Andersen, L. (2013). Two small GTPases act in concert with the bactofilin cytoskeleton to regulate dynamic bacterial cell polarity. *Developmental Cell*, *25*(2), 119–131. https://doi.org/10.1016/j.devcel.2013.02.017.

Cabeen, M., T., Charbon, G., Vollmer, W., Born, P., Ausmees, N., Weibel, D., B., & Jacobs-Wagner C. (2009). Bacterial cell curvature through mechanical control of cell growth. *EMBO Journal* 28(9), 1208-1219. doi: 10.1038/emboj.2009.61.

Campbell, S. L., & Philips, M. R. (2021). Post-translational modification of RAS proteins. *Current Opinion in Structural Biology*, *71*, 180–192. https://doi.org/10.1016/j.sbi.2021.06.015.

Carney, D. S., Davies, B. A., & Horazdovsky, B. F. (2006). Vps9 domain-containing proteins: Activators of Rab5 GTPases from yeast to neurons. *Trends in Cell Biology*, *16*(1), 27–35. https://doi.org/10.1016/j.tcb.2005.11.001.

Chang, Y. W., Rettberg, L. A., Treuner-Lange, A., Iwasa, J., Søgaard-Andersen, L., & Jensen, G. J. (2016). Architecture of the type IVa pilus machine. *Science*, *351*(6278), aad2001. https://doi.org/10.1126/science.aad2001.

Chen, H., Keseler, I. M., & Shimkets, L. J. (1990). Genome size of *Myxococcus xanthus* determined by pulsed-field gel electrophoresis. *Journal of Bacteriology*, *172*(8), 4206–4213. https://doi.org/10.1128/jb.172.8.4206-4213.1990.

Cherfils, J., & Zeghouf, M. (2013). Regulation of small GTPases by GEFs, GAPs, and GDIs. *Physiological Reviews*, *93*(1), 269–309. https://doi.org/10.1152/physrev.00003.2012.

Cock, J. M., Sterck, L., Ahmed, S., Allen, A. E., Amoutzias, G., Anthouard, V., Artiguenave, F., Arun, A., Aury, J., Badger, J. H., Beszteri, B., Billiau, K., Bonnet, E., Bothwell, J. H., Bowler, C., Boyen, C., Brownlee, C., Carrano, C. J., Charrier, B., Cho, G. Y., & Wincker, P. (2012). The *Ectocarpus* genome and brown algal genomics: The Ectocarpus genome consortium. *Advances in Botanical Research*, *64*, 141-184. https://doi.org/10.1016/B978-0-12-391499-6.00005-0.

Colicelli, J. (2004). Human RAS superfamily proteins and related GTPases. *Science's STKE : Signal Transduction Knowledge Environment*, *2004*(250), 1–32. https://doi.org/10.1126/stke.2502004re13.

Copenhagen, K., Alert, R., Wingreen, N. S., & Shaevitz, J. W. (2021). Topological defects promote layer formation in *Myxococcus xanthus* colonies. Nature Physics, 17(2), 211-215. https://doi.org/10.1038/s41567-020-01056-4.

De Wet, J. R., Wood, K. V, DeLuca, M., Helinski, D. R., & Subramani, S. (1987). Firefly luciferase gene: structure and expression in mammalian cells. *Molecular and Cellular Biology*, *7*(2), 725-737. https://doi.org/10.1128/mcb.7.2.725-737.1987.

Deng, X., Gonzalez Llamazares, A., Wagstaff, J. M., Hale, V. L., Cannone, G., McLaughlin, S. H., Kureisaite-Ciziene, D., & Löwe, J. (2019). The structure of bactofilin filaments reveals their mode of membrane binding and lack of polarity. *Nature Microbiology*, *4*(12), 2357–2368. https://doi.org/10.1038/s41564-019-0544-0.

Dixon, A. S., Schwinn, M. K., Hall, M. P., Zimmerman, K., Otto, P., Lubben, T. H., Butler, B. L., Binkowski, B. F., Machleidt, T., & Kirkland, T. A. (2016). NanoLuc complementation reporter optimized for accurate measurement of protein interactions in cells. *ACS Chemical Biology*, *11*(2), 400–408. https://doi.org/10.1021/acschembio.5b00753.

Drin, G., & Antonny, B. (2010). Amphipathic helices and membrane curvature. *FEBS Letters*, *584*(9), 1840–1847. https://doi.org/10.1016/j.febslet.2009.10.022.

Dworkin, M., & Gibson, S. M. (1964). A system for studying microbial morphogenesis: Rapid formation of microcysts in *Myxococcus xanthus*. *Science*, *146*(3641), 243–244. https://doi.org/10.1126/science.146.3641.243.

El Andari, J., Altegoer, F., Bange, G., & Graumann, P. L. (2015). *Bacillus subtilis* bactofilins are essential for flagellar hook-and filament assembly and dynamically localize into structures of less than 100 nm diameter underneath the cell membrane. *PLOS ONE*, *10*(10), e0141546.

Etienne-Manneville, S., & Hall, A. (2002). Rho GTPases in cell biology. *Nature, 420*(6916), 629–635. https://doi.org/10.1038/nature01148.

Fan, F., Binkowski, B. F., Butler, B. L., Stecha, P. F., Lewis, M. K., & Wood, K. V. (2008).

Novel genetically encoded biosensors using firefly luciferase. *ACS Chemical Biology*, *3*(6), 346–351.

Feig, L. A. (1999). Tools of the trade: use of dominant-inhibitory mutants of Ras-family GTPases. *Nature Cell Biology*, *1*(2), E25–E27. https://doi.org/10.1038/10018.

Fremgen, S. A., Burke, N. S., & Hartzell, P. L. (2010). Effects of site-directed mutagenesis of *mglA* on motility and swarming of *Myxococcus xanthus. BMC Microbiology*, *10*, 295. https://doi.org/10.1186/1471-2180-10-295.

Galicia, C., Lhospice, S., Varela, P. F., Trapani, S., Zhang, W., Navaza, J., Herrou, J., Mignot, T., & Cherfils, J. (2019). MglA functions as a three-state GTPase to control movement reversals of *Myxococcus xanthus. Nature Communications*, *10*(1), 1–12. https://doi.org/10.1038/s41467-019-13274-3.

Gerth, K., & Reichenbach, H. (1978). Induction of myxospore formation in *Stigmatella aurantiaca* (Myxobacterales). *Archives of Microbiology*, *117*(2), 173–182. https://doi.org/10.1007/bf00402305.

Gerwert, K., Mann, D., & Kötting, C. (2017). Common mechanisms of catalysis in small and heterotrimeric GTPases and their respective GAPs. *Biological Chemistry*, *398*(5–6), 523–533. https://doi.org/10.1515/hsz-2016-0314.

Gietz, R. D., & Akio, S. (1988). New yeast-*Escherichia coli* shuttle vectors constructed with in vitro mutagenized yeast genes lacking six-base pair restriction sites. *Gene*, *74*(2), 527-534.

Girardi, E., Chane-Woon-Ming, B., Messmer, M., Kaukinen, P., & Pfeffer, S. (2013). Identification of RNase L-dependent, 3′-end-modified, viral small RNAs in Sindbis virus-infected mammalian cells. *mBio*, *4*(6), e00698-13. https://doi.org/10.1128/mBio.00698-

13.

Goitre, L., Trapani, E., Trabalzini, L., and Retta, S. F. (2014). The Ras superfamily of small GTPases: the unlocked secrets. *Methods in Molecular Biology*, *1120*, 1–18. https://doi.org/10.1007/978-1-62703-791-4_1.

Goldman, B. S., Nierman, W. C., Kaiser, D., Slater, S. C., Durkin, A. S., Eisen, J. A., Ronning, C. M., Barbazuk, W. B., Blanchard, M., Field, C., Halling, C., Hinkle, G., Iartchuk, O., Kim, H. S., Mackenzie, C., Madupu, R., Miller, N., Shvartsbeyn, A., Sullivan, S. A., Vaudin, M., Wiegand, R., & Kaplan, H. B. (2006). Evolution of sensory complexity recorded in a myxobacterial genome. *Proceedings of the National Academy of Sciences of the United States of America*, *103*(41), 15200–15205. https://doi.org/10.1073/pnas.0607335103.

Graumann, P. L. (2004). Cytoskeletal elements in bacteria. *Current Opinion in Microbiology*, *7*(6), 565-571. https://doi.org/10.1016/j.mib.2004.10.010.

Guzzo, M., Murray, S. M., Martineau, E., Lhospice, S., Baronian, G., My, L., Zhang, Y., Espinosa, L., Vincentelli, R., Bratton, B. P., Shaevitz, J. W., Molle, V., Howard, M., & Mignot, T. (2018). A gated relaxation oscillator mediated by FrzX controls morphogenetic movements in *Myxococcus xanthus*. *Nature Microbiology*, *3*(8), 948–959. https://doi.org/10.1038/s41564-018-0203-x.

Hall, M. P., Unch, J., Binkowski, B. F., Valley, M. P., Butler, B. L., Wood, M. G., Otto, P., Zimmerman, K., Vidugiris, G., MacHleidt, T., Robers, M. B., Benink, H. A., Eggers, C. T., Slater, M. R., Meisenheimer, P. L., Klaubert, D. H., Fan, F., Encell, L. P., & Wood, K. V. (2012). Engineered luciferase reporter from a deep-sea shrimp utilizing a novel imidazopyrazinone substrate. *ACS Chemical Biology*, *7*(11), 1848–1857. https://doi.org/10.1021/cb3002478.

Hampf, M., & Gossen, M. (2006). A protocol for combined *Photinus* and *Renilla* luciferase quantification compatible with protein assays. *Analytical Biochemistry*, *356*(1), 94–99.

Han, C. W., Jeong, M. S., & Jang, S. B. (2017). Structure, signalling and the drug discovery of the Ras oncogene protein. *BMB Reports*, *50*(7), 355–360. https://doi.org/10.5483/BMBRep.2017.50.7.062.

Hanna, M. G., Mela, I., Wang, L., Henderson, R. M., Chapman, E. R., Edwardson, J. M., & Audhya, A. (2016). Sar1 GTPase activity is regulated by membrane curvature. *Journal of Biological Chemistry*, *291*(3), 1014–1027. https://doi.org/10.1074/jbc.M115.672287.

Harms, A., Treuner-Lange, A., Schumacher, D., & Søgaard-Andersen, L. (2013). Tracking of chromosome and replisome dynamics in *Myxococcus xanthus* reveals a novel chromosome arrangement. *PLoS Genetics*, *9*(9). https://doi.org/10.1371/journal.pgen.1003802.

Hartzell, P. L. (1997). Complementation of sporulation and motility defects in a prokaryote by a eukaryotic GTPase. *Proceedings of the National Academy of Sciences of the United States of America*, *94*(18), 9881–9886. https://doi.org/10.1073/pnas.94.18.9881.

Hartzell, P., & Kaiser, D. (1991). Function of MglA, a 22-kilodalton protein essential for gliding in *Myxococcus xanthus*. *Journal of Bacteriology*, *173*(23), 7615–7624. https://doi.org/10.1128/jb.173.23.7615-7624.1991.

Heasman, S. J., & Ridley, A. J. (2008). Mammalian Rho GTPases: New insights into their functions from in vivo studies. *Nature Reviews Molecular Cell Biology*, *9*(9), 690–701. https://doi.org/10.1038/nrm2476.

Heip, C. (1976). The life-cycle of *Cyprideis torosa* (Crustacea, Ostracoda). *Oecologia*, *24*(3), 229–245.

Herrmann, C. (2003). Ras-effector interactions: After one decade. *Current Opinion in Structural Biology*, *13*(1), 122–129. https://doi.org/10.1016/S0959-440X(02)00007-6

Hodgkin, J., & Kaiser, D. (1979). Genetics of gliding motility in *Myxococcus xanthus* (Myxobacterales): Two gene systems control movement. *MGG Molecular & General Genetics*, *171*(2), 177–191. https://doi.org/10.1007/BF00270004.

Homma, Y., Hiragi, S., & Fukuda, M. (2021). Rab family of small GTPases: an updated view on their regulation and functions. *FEBS Journal*, *288*(1), 36–55. https://doi.org/10.1111/febs.15453.

Hutchings, J., Stancheva, V., Miller, E. A., & Zanetti, G. (2018). Subtomogram averaging of COPII assemblies reveals how coat organization dictates membrane shape. *Nature Communications*, *9*(1). https://doi.org/10.1038/s41467-018-06577-4.

Iniesta, A. A., García-Heras, F., Abellón-Ruiz, J., Gallego-García, A., & Elías-Arnanz, M. (2012). Two systems for conditional gene expression in *Myxococcus xanthus* inducible by isopropyl-β-d-thiogalactopyranoside or vanillate. *Journal of Bacteriology*, *194*(21), 5875–5885. https://doi.org/10.1128/JB.01110-12.

Inouye, S., Watanabe, K., Nakamura, H., & Shimomura, O. (2000). Secretional luciferase of the luminous shrimp *Oplophorus gracilirostris*: cDNA cloning of a novel imidazopyrazinone luciferase. *FEBS Letters*, *481*(1), 19–25. https://doi.org/10.1016/s0014-5793(00)01963-3.

Islam, S. T., Alvarez, I. V., Saïdi, F., Guiseppi, A., Vinogradov, E., Sharma, G., Espinosa, L., Morrone, C., Brasseur, G., Guillemot, J. F., Benarouche, A., Bridot, J. L., Ravicoularamin, G., Cagna, A., Gauthier, C., Singer, M., Fierobe, H. P., Mignot, T., & Mauriello, E. M. F. (2020). Modulation of bacterial multicellularity via spatio-specific polysaccharide secretion. *PLoS Biology*, *18*(6). https://doi.org/10.1371/journal.pbio.3000728.

Jaber, N., Dou, Z., Chen, J. S., Catanzaro, J., Jiang, Y. P., Ballou, L. M., Selinger, E., Ouyang, X., Lin, R. Z., Zhang, J., & Zong, W. X. (2012). Class III PI3K Vps34 plays an essential role in autophagy and in heart and liver function. *Proceedings of the National Academy of Sciences of the United States of America*, *109*(6), 2003–2008. https://doi.org/10.1073/pnas.1112848109.

Jang, H., Abraham, S. J., Chavan, T. S., Hitchinson, B., Khavrutskii, L., Tarasova, N. I., Nussinov, R., & Gaponenko, V. (2015). Mechanisms of membrane binding of small GTPase K-Ras4B farnesylated hypervariable region. *Journal of Biological Chemistry*, *290*(15), 9465–9477. https://doi.org/10.1074/jbc.M114.620724.

Jenkins, C., Samudrala, R., Andersont, I., Hedlund, B. P., Petroni, G., Michailova, N., Pinel, N., Overbeek, R., Rosati, G., & Staley, J. T. (2002). Genes for the cytoskeletal protein tubulin in the bacterial genus *Prosthecobacter*. *Proceedings of the National Academy of Sciences of the United States of America*, *99*(26), 17049–17054. https://doi.org/10.1073/pnas.012516899.

Jia, S., Peng, J., Gao, B., Chen, Z., Zhou, Y., Fu, Q., Wang, H., & Zhan, L. (2011). Relative quantification of protein-protein interactions using a dual luciferase reporter pull-down assay system. *PLoS One*, *6*(10), e26414.

Jiang, S. Y., & Ramachandran, S. (2006). Comparative and evolutionary analysis of genes encoding small GTPases and their activating proteins in eukaryotic genomes. *Physiological Genomics*, *24*(3), 235–251. https://doi.org/10.1152/physiolgenomics.00210.2005.

Kaimer, C., & Zusman, D. R. (2013). Phosphorylation-dependent localization of the response regulator FrzZ signals cell reversals in *Myxococcus xanthus*. *Molecular Microbiology*, *88*(4), 740–753.

Kaiser D. (1979). Social gliding is correlated with the presence of pili in *Myxococcus xanthus*. *Proceedings of the National Academy of Sciences of the United States of America*, *76*(11), 5952–56. https://doi.org/10.1073/pnas.76.11.5952.

Kanade, M., Birjeet, N., Lagad, S., Baranwak, J., & Gayathri, P. (2019). Dual specificity of a prokaryotic GTPase-activating protein (GAP) to two small Ras-like GTPases in *Myxococcus xanthus*. *FEBS Journal 288*(5), 1565-1585. doi: 10.1111/febs.15513.

Kanade, M., Chakraborty, S., Shelke, S. S., & Gayathri, P. (2020). A distinct motif in a prokaryotic small Ras-like GTPase highlights unifying features of Walker B motifs in P-loop NTPases. *Journal of Molecular Biology*, *432*(20), 5544–5564. https://doi.org/10.1016/j.jmb.2020.07.024.

Karbstein, K. (2007). Role of GTPases in ribosome assembly. *Biopolymers*, *87*(1), 1–11. https://doi.org/10.1002/bip.20762.

Karl, D. M. (1978). Occurrence and ecological significance of GTP in the ocean and in microbial cells. *Applied and Environmental Microbiology*, *36*(2), 349-355. https://doi.org/10.1128/aem.36.2.349-355.1978.

Keane, R., & Berleman, J. (2016). The predatory life cycle of *Myxococcus xanthus*. *Microbiology (United Kingdom)*, *162*(1), 1–11. https://doi.org/10.1099/mic.0.000208.

Keilberg D., & Søgaard-Andersen L. (2013). Regulation of bacterial cell polarity by small GTPases. *Biochemistry*, *53*(12), 1899–1907. https://doi.org/10.1021/bi500141f.

Keilberg, D., Wuichet, K., Drescher, F., & Søgaard-Andersen, L. (2012). A response regulator interfaces between the Frz chemosensory system and the MglA/MglB GTPase/GAP module to regulate polarity in *Myxococcus xanthus*. *PLoS Genet*, *8*(9), e1002951. https://doi.org/10.137°C1/journal.pgen.1002951.

Khovidhunkit, W., Kim, M. S., Memon, R. A., Shigenaga, J. K., Moser, A. H., Feingold, K. R., & Grunfeld, C. (2004). Effects of infection and inflammation on lipid and lipoprotein metabolism: Mechanisms and consequences to the host. *Journal of Lipid Research*, *45*(7), 1169–1196. https://doi.org/10.1194/jlr.R300019-JLR200.

Kjeldgaard, M., Nyborg, J., & Clark, B. F. (1996). The GTP binding motif: variations on a theme. *FASEB journal*, *10*(12), 1347–1368.

Klöpper, T. H., Kienle, N., Fasshauer, D., & Munro, S. (2012). Untangling the evolution of Rab G proteins: implications of a comprehensive genomic analysis. *BMC Biology*, *10*, 71. https://doi.org/10.1186/1741-7007-10-71.

Kobe, B., & Deisenhofer, J. (1994). The leucine-rich repeat: a versatile binding motif. *Trends in Biochemical Sciences*, *19*(10), 415–421. https://doi.org/10.1016/0968-0004(94)90090-6.

Koch, M. K., Mchugh, C. A., & Hoiczyk, E. (2011). BacM, an N-terminally processed bactofilin of *Myxococcus xanthus*, is crucial for proper cell shape. *Molecular Microbiology*, *80*(4), 1031–1051. https://doi.org/10.1111/j.1365-2958.2011.07629.x.

Komano, T., Brown, N., Inouye, S., & Inouye, M. (1982). Phosphorylation and methylation of proteins during *Myxococcus xanthus* spore formation. *Journal of Bacteriology*, *151*(1), 114–118. https://doi.org/10.1128/jb.151.1.114-118.1982.

Komatsu, M., Takano, H., Hiratsuka, T., Ishigaki, Y., Shimada, K., Beppu, T., & Ueda, K. (2006). Proteins encoded by the conservon of *Streptomyces coelicolor* A3(2) comprise a membrane-associated heterocomplex that resembles eukaryotic G protein-coupled regulatory system. *Molecular Microbiology*, *62*(6), 1534–1546. https://doi.org/10.1111/j.1365-2958.2006.05461.x.

Kroos, L., Hartzell, P., Stephens, K., & Kaiser, D. (1988). A link between cell movement and gene expression argues that motility is required for cell-cell signaling during fruiting body development. *Genes & Development*, *2*(12a), 1677–1685. https://doi.org/10.1101/gad.2.12a.1677.

Kuhn, H., Küster, H., & Requena, N. (2010). Membrane steroid-binding protein 1 induced by a diffusible fungal signal is critical for mycorrhization in *Medicago truncatula*. *New Phytologist*, *185*(3), 716–733. https://doi.org/10.1111/j.1469-8137.2009.03116.x.

Kühn, J., Briegel, A., Mörschel, E., Kahnt, J., Leser, K., Wick, S., Jensen, G. J., & Thanbichler, M. (2010). Bactofilins, a ubiquitous class of cytoskeletal proteins mediating polar localization of a cell wall synthase in *Caulobacter crescentus*. *EMBO journal*, *29*(2), 327–339. https://doi.org/10.1038/emboj.2009.358.

Lambert, C., Fenton, A. K., Hobley, L., & Sockett, R. E. (2011). Predatory *Bdellovibrio* bacteria use gliding motility to scout for prey on surfaces. *Journal of Bacteriology*, *193*(12), 3139–3141. https://doi.org/10.1128/JB.00224-11.

Lee, M. C. S., Orci, L., Hamamoto, S., Futai, E., Ravazzola, M., & Schekman, R. (2005). Sar1p N-terminal helix initiates membrane curvature and completes the fission of a COPII vesicle. *Cell*, *122*(4), 605–617. https://doi.org/10.1016/j.cell.2005.07.025.

Leipe, D. D., Wolf, Y. I., Koonin, E. V., & Aravind, L. (2002). Classification and evolution of P-loop GTPases and related ATPases. *Journal of Molecular Biology*, *317*(1), 41–72. https://doi.org/10.1006/jmbi.2001.5378.

Leonardy, S., Miertzschke, M., Bulyha, I., Sperling, E., Wittinghofer, A., & Søgaard-Andersen, L. (2010). Regulation of dynamic polarity switching in bacteria by a Ras-like G-protein and its cognate GAP. *The EMBO Journal*, *29*(14), 2276–2289. https://doi.org/10.1038/emboj.2010.114.

Leventis, R., & Silvius, J. R. (1998). Lipid-binding characteristics of the polybasic carboxy-terminal sequence of K-*ras*4B. *Biochemistry*, *37*(20), 7640–7648. https://doi.org/10.1021/bi973077h.

Li, G., & Marlin, M. C. (2015). Rab family of GTPases. *Methods in Molecular Biology*, *1298*, 1-15. https://doi.org/10.1007/978-1-4939-2569-8_1.

Li, G., & Segev, N. (2012). Ypt/Rab GTPases and Intracellular Membrane Trafficking: an Overview. In G. Li, & N. Segev (Eds), *Rab GTPases and Membrane Trafficking* (pp. 3-17). Bentham Science Publishers. https://doi.org/10.2174/978160805365011201010003.

Li, Y., Sun, H., Ma, X., Lu, A., Lux, R., Zusman, D., & Shi, W. (2003). Extracellular polysaccharides mediate pilus retraction during social motility of *Myxococcus xanthus*. *Proceedings of the National Academy of Sciences of the United States of America*, *100*(9), 5443-5448. https://doi.org/10.1073/pnas.0836639100.

Liang, Y. L., Khoshouei, M., Deganutti, G., Glukhova, A., Koole, C., Peat, T. S., Radjainia, M., Plitzko, J. M., Baumeister, W., Miller, L. J., Hay, D. L., Christopoulos, A., Reynolds, C. A., Wootten, D., & Sexton, P. M. (2018). Cryo-EM structure of the active, G_s-protein complexed, human CGRP receptor. *Nature*, *561*(7724), 492–497. https://doi.org/10.1038/s41586-018-0535-y.

Long, K. R., Yamamoto, Y., Baker, A. L., Watkins, S. C., Coyne, C. B., Conway, J. F., & Aridor, M. (2010). Sar1 assembly regulates membrane constriction and ER export. *Journal of Cell Biology*, *190*(1), 115–128. https://doi.org/10.1083/jcb.201004132.

Lonhienne, T.G., Forwood, J.K., Marfori, M., Robin, G., Kobe, B., & Carroll, B. J. (2009) Importin-beta is a GDP-to-GTP exchange factor of Ran: implications for the mechanism of nuclear import. *Journal of Biological Chemistry*, *284*(34), 22549-58. https://doi.org/10.1074/jbc.M109.019935.

Lorenz, W. W., Cormier, M. J., O'Kane, D. J., Hua, D., Escher, A. A., & Szalay, A. A. (1996). Expression of the *Renilla reniformis* luciferase gene in mammalian cells. *Journal of Bioluminescence and Chemiluminescence, 11*(1), 31–37. https://doi.org/10.1002/(SICI)1099-1271(199601)11:1<31::AID-BIO398>3.0.CO;2-M.

Lorenz, W. W., McCann, R. O., Longiaru, M., & Cormier, M. J. (1991). Isolation and expression of a cDNA encoding *Renilla reniformis* luciferase. *Proceedings of the National Academy of Sciences of the United States of America*, *88*(10), 4438–4442. https://doi.org/10.1073/pnas.88.10.4438.

Lowry, R. C., Milner, D. S., Al-Bayati, A. M. S., Lambert, C., Francis, V. I., Porter, S. L., & Sockett, R. E. (2019). Evolutionary diversification of the RomR protein of the invasive deltaproteobacterium *B. bacteriovorus*. *Scientific Reports*, *9*(1), 1–15. https://doi.org/10.1038/s41598-019-41263-5.

Marco-Barba, J., Ito, E., Carbonell, E., & Mesquita-Joanes, F. (2012). Empirical calibration of shell chemistry of *Cyprideis torosa* (Jones, 1850) (Crustacea: Ostracoda). *Geochimica et Cosmochimica Acta, 93*, 143–163. https://doi.org/10.1016/j.gca.2012.06.019.

Markova, S. V, Golz, S., Frank, L. A., Kalthof, B., & Vysotski, E. S. (2004). Cloning and expression of cDNA for a luciferase from the marine copepod *Metridia longa*: a novel secreted bioluminescent reporter enzyme. *Journal of Biological Chemistry*, *279*(5), 3212–3217. https://doi.org/10.1074/jbc.M309639200.

Mauriello, E. M. F. (2010). Cell polarity/motility in bacteria: Closer to eukaryotes than expected? *EMBO Journal, 29*(14), 2258–2259. https://doi.org/10.1038/emboj.2010.144.

Mauriello, E. M. F., Mouhamar, F., Nan, B., Ducret, A., Dai, D., Zusman, D. R., & Mignot, T. (2010). Bacterial motility complexes require the actin-like protein, MreB and the Ras homologue, MglA. *EMBO Journal*, *29*(2), 315–326.

https://doi.org/10.1038/emboj.2009.356Memon, A. R. (2004). The role of ADP-ribosylation factor and SAR1 in vesicular trafficking in plants. *Biochimica et Biophysica Acta, 1664*(1), 9-30. https://doi.org/10.1016/j.bbamem.2004.04.005.

Mauriello, E. M., Mignot, T., Yang, Z., & Zusman, D. R. (2010). Gliding motility revisited: how do the myxobacteria move without flagella? *Microbiology and Molecular Biology Reviews*, *74*(2), 229-249. https://doi.org/10.1128/MMBR.00043-09.

Mercier, R., Bautista, S., Delannoy, M., Gibert, M., Guiseppi, A., Herrou, J., Mauriello, E. M. F., & Mignot, T. (2020). The polar Ras-like GTPase MglA activates type IV pilus via SgmX to enable twitching motility in *Myxococcus xanthus*. *Proceedings of the National Academy of Sciences of the United States of America*, *117*(45), 28366–28373. https://doi.org/10.1073/pnas.2002783117.

Messina, S., De Simone, G., & Ascenzi, P. (2019). Cysteine-based regulation of redox-sensitive Ras small GTPases. *Redox Biology*, *26*, 101282. https://doi.org/10.1016/j.redox.2019.101282.

Miertzschke, M., Koerner, C., Vetter, I. R., Keilberg, D., Hot, E., Leonardy, S., Søgaard-Andersen, L., & Wittinghofer, A. (2011). Structural analysis of the Ras-like G protein MglA and its cognate GAP MglB and implications for bacterial polarity. *EMBO Journal*, *30*(20), 4185–4197. https://doi.org/10.1038/emboj.2011.291.

Mignot, T. (2007). The elusive engine in *Myxococcus xanthus* gliding motility. *Cellular and Molecular Life Sciences*, *64*(21), 2733–2745. https://doi.org/10.1007/s00018-007-7176-x.

Mignot, T., Shaevitz, J. W., Hartzell, P. L., & Zusman, D. R. (2007). Evidence that focal adhesion complexes power bacterial gliding motility. *Science*, *315*(5813), 853–856. https://doi.org/10.1126/science.1137223.

Milner, D. S., Till, R., Cadby, I., Lovering, A. L., Basford, S. M., Saxon, E. B., Liddell, S., Williams, L. E., & Sockett, R. E. (2014). Ras GTPase-like protein MglA, a controller of bacterial social-motility in myxobacteria, has evolved to control bacterial predation by *Bdellovibrio*. *PLoS Genetics*, *10*(4). https://doi.org/10.1371/journal.pgen.1004253.

Mishra, A. K., & Lambright, D. G. (2016). Invited review: Small GTPases and their GAPs. *Biopolymers*, *105*(8), 431–448. https://doi.org/10.1002/bip.22833.

Moon, S. Y., & Zheng, Y. (2003). Rho GTPase-activating proteins in cell regulation. *Trends in Cell Biology*, *13*(1), 13–22. https://doi.org/10.1016/S0962-8924(02)00004-1.

Müller, M. P., & Goody, R. S. (2018). Molecular control of Rab activity by GEFs, GAPs and GDI. *Small GTPases*, *9*(1–2), 5–21. https://doi.org/10.1080/21541248.2016.1276999.

Mulloy, J. C., Cancelas, J. A., Filippi, M.-D., Kalfa, T. A., Guo, F., & Zheng, Y. (2010). Rho GTPases in hematopoiesis and hemopathies. *Blood*, *115*(5), 936–947. https://doi.org/10.1182/blood-2009-09-198127.

Nakajima, Y., Kobayashi, K., Yamagishi, K., Enomoto, T., & Ohmiya, Y. (2004). cDNA cloning and characterization of a secreted luciferase from the luminous Japanese ostracod, *Cypridina noctiluca*. *Bioscience, Biotechnology, and Biochemistry*, *68*(3), 565–570. https://doi.org/10.1271/bbb.68.565.

Nakayama, K., & Katoh, Y. (2018). Ciliary protein trafficking mediated by IFT and BBSome complexes with the aid of kinesin-2 and dynein-2 motors. *Journal of Biochemistry*, *163*(3), 155–164. https://doi.org/10.1093/jb/mvx087.

Nan, B. (2017). Bacterial gliding motility: rolling out a consensus model. *Current Biology*, *27*(4), R154–R156. https://doi.org/10.1016/j.cub.2016.12.035.

Nan, B., & Zusman, D. R. (2011). Uncovering the mystery of gliding motility in the

myxobacteria. *Annual Review in Genetics, 45*, 21-39.

Nan, B., Bandaria, J. N., Guoa, K. Y., Fan, X., Moghtaderi, A., Yildiz, A., Zusman, D. R., & Greenberg, E. P. (2015). The polarity of myxobacterial gliding is regulated by direct interactions between the gliding motors and the Ras homolog MglA. *Proceedings of the National Academy of Sciences of the United States of America*, *112*(2), E186–E193. https://doi.org/10.1073/pnas.1421073112.

Nan, B., Mauriello, E. M. F., Sun, I. H., Wong, A., & Zusman, D. R. (2010). A multi-protein complex from *Myxococcus xanthus* required for bacterial gliding motility. *Molecular Microbiology*, *76*(6), 1539–1554. https://doi.org/10.1111/j.1365-2958.2010.07184.x.

Neumann, B., Pospiech, A., & Schairer, H. U. (1992). Size and stability of the genomes of the myxobacteria *Stigmatella aurantiaca* and *Stigmatella erecta*. *Journal of Bacteriology*, *174*(19), 6307–6310. https://doi.org/10.1128/jb.174.19.6307-6310.1992.

Neumann, B., Pospiech, A., & Schairer, H. U. (1993). A physical and genetic map of the *Stigmatella aurantiaca* DW4/3.1 chromosome. *Molecular Microbiology*, *10*(5), 1087–1099. https://doi.org/10.1111/j.1365-2958.1993.tb00979.x.

Nie, Z., Hirsch, D. S., & Randazzo, P. A. (2003). Arf and its many interactors. *Current Opinion in Cell Biology*, *15*(4), 396–404. https://doi.org/10.1016/S0955-0674(03)00071-1.

Nordmann, M., Cabrera, M., Perz, A., Bröcker, C., Ostrowicz, C., Engelbrecht-Vandré, S., & Ungermann, C. (2010). The Mon1-Ccz1 complex is the GEF of the late endosomal Rab7 homolog Ypt7. *Current Biology*, *20*(18), 1654–1659. https://doi.org/10.1016/j.cub.2010.08.002.

Paduch, M., Jeleń, F., & Otlewski, J. (2001). Structure of small G proteins and their regulators. *Acta Biochimica Polonica*, *48*(4), 829–850. https://doi.org/10.18388/abp.2001_3850.

Paiva, A.M.O., Friggen, A.H., Qin, L., Douwes, R., Dame, R.T., & Smits, W.K. (2019). The bacterial chromatin protein HupA can remodel DNA and associates with the nucleoid in *Clostridium difficile*. *Journal of Molecular Biology, 431*(4), 653–672. https://doi.org/10.1016/j.jmb.2019.01.001.

Papke, R. L. (2014). Merging old and new perspectives on nicotinic acetylcholine receptors. *Biochemical Pharmacology*, *89*(1), 1–11. https://doi.org/10.1016/j.bcp.2014.01.029.

Paradies, G., Paradies, V., Ruggiero, F. M., & Petrosillo, G. (2014). Oxidative stress, cardiolipin and mitochondrial dysfunction in nonalcoholic fatty liver disease. *World Journal of Gastroenterology*, *20*(39), 14205–14218. https://doi.org/10.3748/wjg.v20.i39.14205.

Park, H.O., & Bi, E. (2007). Central roles of small GTPases in the development of cell polarity in yeast and beyond. *Microbiology and Molecular Biology Reviews*, *71*(1), 48–96. https://doi.org/10.1128/MMBR.00028-06.

Pasqualato, S., Renault, L. & Cherfils, J. (2002). Arf, Arl, Arp and Sar proteins: a family of GTP-binding proteins with a structural device for 'front-back' communication. *EMBO reports*, *3*(11), 1035–1041. https://doi.org/10.1093/embo-reports/kvf221.

Patryn, J., Allen, K., Dziewanowska, K., Otto, R., & Hartzell, P. L. (2010). Localization of MglA, an essential gliding motility protein in *Myxococcus xanthus*. *Cytoskeleton*, *67*(5), 322–337. https://doi.org/10.1002/cm.20447.

Perroy, J., Pontier, S., Charest, P. G., Aubry, M., & Bouvier, M. (2004). Real-time monitoring of ubiquitination in living cells by BRET. *Nature Methods*, *1*(3), 203–208. https://doi.org/10.1038/nmeth722.

Pfeffer S. R. (2013). Rab GTPase regulation of membrane identity. *Current Opinion in Cell*

Biology, *25*(4), 414–419. https://doi.org/10.1016/j.ceb.2013.04.002.

Pogliano, J. (2008). The bacterial cytoskeleton. *Current Opinion in Cell Biology*, *20*(1), 19-27. https://doi.org/10.1016/j.ceb.2007.12.006.

Pollock, C. B., Shirasawa, S., Sasazuki, T., Kolch, W., & Dhillon, A. S. (2005). Oncogenic K-RAS is required to maintain changes in cytoskeletal organization, adhesion, and motility in colon cancer cells. *Cancer Research*, *65*(4), 1244–1250. https://doi.org/10.1158/0008-5472.CAN-04-1911.

Rajagopala, S. V., Titz, B., Goll, J., Parrish, J. R., Wohlbold, K., McKevitt, M. T., Palzkill, T., Mori, H., Finley, R. L., Jr, & Uetz, P. (2007). The protein network of bacterial motility. *Molecular Systems Biology*, *3*(1), 128. https://doi.org/10.1038/msb4100166.

Reinke, R., Krantz, D. E., Yen, D., & Zipursky, S. L. (1988). Chaoptin, a cell surface glycoprotein required for *Drosophila* photoreceptor cell morphogenesis, contains a repeat motif found in yeast and human. *Cell*, *52*(2), 291–301. https://doi.org/10.1016/0092-8674(88)90518-1.

Remy, I., & Michnick, S. W. (2006). A highly sensitive protein-protein interaction assay based on *Gaussia* luciferase. *Nature Methods*, *3*(12), 977–979. https://doi.org/10.1038/nmeth979.

Renault, L., Christova, P., Guibert, B., Pasqualato, S., & Cherfils, J. (2002). Mechanism of domain closure of Sec7 domains and role in BFA sensitivity. *Biochemistry*, *41*(11), 3605–3612. https://doi.org/10.1021/bi012123h.

Repasky, G. A., Chenette, E. J., & Der, C. J. (2004). Renewing the conspiracy theory debate: Does Raf function alone to mediate Ras oncogenesis? *Trends in Cell Biology*, *14*(11), 639–647. https://doi.org/10.1016/j.tcb.2004.09.014.

Ridley, A. J. Rho GTPases and cell migration *Journal of Cell Science,114*(Pt 15), 2713–2722. https://doi.org/10.1242/jcs.114.15.2713.

Rodrigues, M. L., & Pereira-Leal, J. B. (2012) Novel Rab GTPases. In G. Li , & N. Segev (Eds). *Rab GTPases and membrane trafficking* (pp. 155–68). Bentham Science Publishers.

Rojas, A. M., Fuentes, G., Rausell, A., & Valencia, A. (2012). The Ras protein superfamily: Evolutionary tree and role of conserved amino acids. *Journal of Cell Biology*, *196*(2), 189–201. https://doi.org/10.1083/jcb.201103008.

Rudack, T., Xia, F., Schlitter, J., Kötting, C., & Gerwert, K. (2012). The role of magnesium for geometry and charge in GTP hydrolysis, revealed by quantum mechanics/molecular mechanics simulations. *Biophysical Journal*, *103*(2), 293–302. https://doi.org/10.1016/j.bpj.2012.06.015.

Sanders, S. S., Martin, D. D. O., Butland, S. L., Lavallée-Adam, M., Calzolari, D., Kay, C., Yates, J. R., & Hayden, M. R. (2015). Curation of the mammalian palmitoylome indicates a pivotal role for palmitoylation in diseases and disorders of the nervous system and cancers. *PLoS Computational Biology*, *11*(8), 1–20. https://doi.org/10.1371/journal.pcbi.1004405.

Sayyad, W. A., Fabris, P., & Torre, V. (2016). The role of Rac1 in the growth cone dynamics and force generation of DRG neurons. *PLoS One*, *11*(1), e0146842. https://doi.org/10.1371/journal.pone.0146842.

Scheffzek, K., Ahmadian, M. R., Kabsch, W., Wiesmüller, L., Lautwein, A., Schmitz, F., & Wittinghofer, A. (1997). The Ras-RasGAP complex: Structural basis for GTPase activation and its loss in oncogenic ras mutants. *Science*, *277*(5324), 333–338. https://doi.org/10.1126/science.277.5324.333.

Schenck, A., Goto-Silva, L., Collinet, C., Rhinn, M., Giner, A., Habermann, B., Brand, M., & Zerial, M. (2008). The endosomal protein Appl1 mediates Akt substrate specificity and cell survival in vertebrate development. *Cell*, *133*(3), 486–497. https://doi.org/10.1016/j.cell.2008.02.044.

Schlessinger, K., Hall, A., & Tolwinski, N. (2009). Wnt signaling pathways meet Rho GTPases. *Genes and Development*, *23*(3), 265–277. https://doi.org/10.1101/gad.1760809.

Schmidt, A., & Hall, A. (2002). Guanine nucleotide exchange factors for Rho GTPases: Turning on the switch. *Genes and Development*, *16*(13), 1587–1609. https://doi.org/10.1101/gad.1003302.

Schumacher, D., & Søgaard-Andersen, L. (2017). Regulation of cell polarity in motility and cell division in *Myxococcus xanthus*. *Annual Review of Microbiology*, *71*(1). https://doi.org/10.1146/annurev-micro-102215-095415.

Schweins, T., & Wittinghofer, A. (1994). Structures, interactions and relationships. *Current Biology*, *4*(6), 547–550.

Schwieger, C., Meister, A., Daum, S., Blume, A., & Bacia, K. (2017). Binding of the GTPase Sar1 to a lipid membrane monolayer: Insertion and orientation studied by infrared reflection-absorption spectroscopy. *Polymers*, *9*(11), 1–25. https://doi.org/10.3390/polym9110612.

Seabra, M. C. (1998). Membrane association and targeting of prenylated Ras-like GTPases. *Cellular Signalling*, *10*(3), 167–172. https://doi.org/10.1016/S0898-6568(97)00120-4.

Secko, D. M., Siu, C. H., Spiegelman, G. B., & Weeks, G. (2006). An activated Ras protein alters cell adhesion by dephosphorylating *Dictyostelium* DdCAD-1. *Microbiology*, *152*(5), 1497–1505. https://doi.org/10.1099/mic.0.28709-0.

Semeijn, K. (2019). Cellular and molecular studies of the Ras-like GTPase MglA and its interplay with the bactofilin BacM of *Myxococcus xanthus*. PhD Thesis, The University of Sheffield.

Settles, E. I., Loftus, A. F., McKeown, A. N., & Parthasarathy, R. (2010). The vesicle trafficking protein Sar1 lowers lipid membrane rigidity. *Biophysical Journal*, *99*(5), 1539–1545. https://doi.org/10.1016/j.bpj.2010.06.059.

Shalaeva, D. N., Cherepanov, D. A., Galperin, M. Y., Golovin, A. V., & Mulkidjanian, A. Y. (2018). Evolution of cation binding in the active sites of P-loop nucleoside triphosphatases in relation to the basic catalytic mechanism. *ELife*, *7*, 1–35. https://doi.org/10.7554/eLife.37373.

Sherf, B. A., Navarro, S. L., Hannah, R. R., Wood, K. V., & Promega Corporation. (1996). Dual-Luciferase™ Reporter Assay: An advanced co-reporter technology integrating firefly and *Renilla* luciferase. *Promega Notes Magazine Number 57*, *2*(57), p.02. http://dibernardo.tigem.it/internal-site/files/website/luc_assay.pdf.

Shi W., & Zusman D. R. (1993). The two motility systems of *Myxococcus xanthus* show different selective advantages on various surfaces. *Proceedings of the National Academy of Sciences of the United States of America*, *90*(8), 3378–3382. https://doi.org/10.1073/pnas.90.8.3378.

Shi, C., Fricke, P., Lin, L., Chevelkov, V., Wegstroth, M., Giller, K., Becker, S., Thanbichler, M., & Lange, A. (2015). Atomic-resolution structure of cytoskeletal bactofilin by solid-state NMR. *Science Advances*, *1*(11), e1501087. https://doi.org/10.1126/sciadv.1501087.

Shi, W., & Sun, H. (2002). Type IV pilus-dependent motility and its possible role in bacterial pathogenesis. *Infection and Immunity*, *70*(1), 1–4. https://doi.org/10.1128/IAI.70.1.1-4.2002.

Shimomura, O., Masugi, T., Johnson, F. H., & Haneda, Y. (1978). Properties and reaction mechanism of the bioluminescence system of the deep-sea shrimp *Oplophorus gracilorostris*. *Biochemistry*, *17*(6), 994–998. https://doi.org/10.1021/bi00599a008.

Smirnova, N. A., Haskew-Layton, R. E., Basso, M., Hushpulian, D. M., Payappilly, J. B., Speer, R. E., Ahn, Y. H., Rakhman, I., Cole, P. A., Pinto, J. T., Ratan, R. R., & Gazaryan, I. G. (2011). Development of Neh2-luciferase reporter and its application for high throughput screening and real-time monitoring of Nrf2 activators. *Chemistry and Biology*, *18*(6), 752–765. https://doi.org/10.1016/j.chembiol.2011.03.013.

South, J., Dick, J. T., McCard, M., Barrios-O'Neill, D., & Anton, A. (2017). Predicting predatory impact of juvenile invasive lionfish (*Pterois volitans*) on a crustacean prey using functional response analysis: effects of temperature, habitat complexity and light regimes. *Environmental Biology of Fishes*, *100*, 1155-1165. https://doi.org/10.1007/s10641-017-0633-y.

Spoerner, M., Herrmann, C., Vetter, I. R., Kalbitzer, H. R., & Wittinghofer, A. (2001). Dynamic properties of the Ras switch I region and its importance for binding to effectors. *Proceedings of the National Academy of Sciences of the United States of America*, *98*(9), 4944–4949. https://doi.org/10.1073/pnas.081441398.

Spormann, A. M. (1999). Gliding Motility in Bacteria: Insights from Studies of *Myxococcus xanthus*. *Microbiology and Molecular Biology Reviews*, *63*(3), 621–641. https://doi.org/10.1128/mmbr.63.3.621-641.1999.

Spormann, A. M., & Kaiser, D. (1999). Gliding mutants of *Myxococcus xanthus* with high reversal frequencies and small displacements. *Journal of Bacteriology*, *181*(8), 2593–2601. https://doi.org/10.1128/jb.181.8.2593-2601.1999.

Srikanth, S., Woo, J. S., & Gwack, Y. (2017). A large Rab GTPase family in a small GTPase

world. *Small GTPases*, *8*(1), 43–48. https://doi.org/10.1080/21541248.2016.1192921

Stenmark, H. (2009). Rab GTPases as coordinators of vesicle traffic. *Nature Reviews Molecular Cell Biology*, *10*(8), 513–525. https://doi.org/10.1038/nrm2728.

Stephens, K., Hartzell, P., & Kaiser, D. (1989). Gliding motility in *Myxococcus xanthus:* mgl locus, RNA, and predicted protein products. *Journal of Bacteriology*, *171*(2), 819–830. https://doi.org/10.1128/jb.171.2.819-830.1989.

Sun, M., Wartel, M., Cascales, E., Shaevitz, J. W., & Mignot, T. (2011). Motor-driven intracellular transport powers bacterial gliding motility. *Proceedings of the National Academy of Sciences of the United States of America*, *108*(18), 7559–7564. https://doi.org/10.1073/pnas.1101101108.

Suzuki, C., Nakajima, Y., Akimoto, H., Wu, C., & Ohmiya, Y. (2005). A new additional reporter enzyme, dinoflagellate luciferase, for monitoring of gene expression in mammalian cells. *Gene*, *344*, 61–66. https://doi.org/10.1016/j.gene.2004.09.028.

Swulius, M. T., & Jensen, G. J. (2012). The helical mreb cytoskeleton in *Escherichia coli* MC1000/pLE7 is an artifact of the N-terminal yellow fluorescent protein tag. *Journal of Bacteriology*, *194*(23), 6382–6386. https://doi.org/10.1128/JB.00505-12.

Sycuro, L. K., Pincus, Z., Gutierrez, K. D., Biboy, J., Stern, C. A., Vollmer, W., & Salama, N. R. (2010). Peptidoglycan crosslinking relaxation promotes *Helicobacter pylori*'s helical shape and stomach colonization. *Cell*, *141*(5), 822–833. https://doi.org/10.1016/j.cell.2010.03.046.

Szadkowski, D., Harms, A., Carreira, L. A. M., Wigbers, M., Potapova, A., Wuichet, K., Keilberg, D., Gerland, U., & Søgaard-Andersen, L. (2019). Spatial control of the GTPase MglA by localized RomR–RomX GEF and MglB GAP activities enables *Myxococcus*

xanthus motility. *Nature Microbiology*, *4*(8), 1344–1355. https://doi.org/10.1038/s41564-019-0451-4.

Takai, Y., Sasaki, T., & Matozaki, T. (2023). Small GTP-binding proteins. *Physiological reviews*, *81*(1), 153–208. https://doi.org/10.1152/physrev.2001.81.1.153.

Tannous, B. A., Kim, D.-E., Fernandez, J. L., Weissleder, R., & Breakefield, X. O. (2005). Codon-optimized *Gaussia* luciferase cDNA for mammalian gene expression in culture and *in vivo*. *Molecular Therapy*, *11*(3), 435–443. https://doi.org/10.1016/j.ymthe.2004.10.016.

Thanbichler, M., & Shapiro, L. (2008). Getting organized—how bacterial cells move proteins and DNA. *Nature Reviews Microbiology*, *6*(1), 28-40. 28–40. https://doi.org/10.1038/nrmicro1795.

Thaxter, R. (1892). On the myxobacteriaceæ, a new order of schizomycetes. *Botanical Gazette*, *17*(12), 389–406. https://doi.org/10.1086/326866.

Thiery, S., & Kaimer, C. (2020). The predation strategy of *Myxococcus xanthus*. *Frontiers in Microbiology*, *11*(January), 2. https://doi.org/10.3389/fmicb.2020.00002.

Thompson, E. M., Nagata, S., & Tsuji, F. I. (1989). Cloning and expression of cDNA for the luciferase from the marine ostracod *Vargula hilgendorfii*. *Proceedings of the National Academy of Sciences of the United Stated of America*, *86*(17), 6567–6571. https://doi.org/10.1073/pnas.86.17.6567.

Touchot, N., Chardin, P., & Tavitian, A. (1987). Four additional members of the *ras* gene superfamily isolated by an oligonucleotide strategy: Molecular cloning of YPT-related cDNAs from a rat brain library. *Proceedings of the National Academy of Sciences of the United States of America*, *84*(23), 8210–8214. https://doi.org/10.1073/pnas.84.23.8210.

Treuner-Lange, A., Macia, E., Guzzo, M., Hot, E., Faure, L. M., Jakobczak, B., Espinosa, L., Alcor, D., Ducret, A., Keilberg, D., Castaing, J. P., Gervais, S. L., Franco, M., Søgaard-Andersen, L., & Mignot, T. (2015). The small G-protein MglA connects to the MreB actin cytoskeleton at bacterial focal adhesions. *Journal of Cell Biology*, *210*(2), 243–256. https://doi.org/10.1083/jcb.201412047.

Tzeng, L., & Singer, M. (2005). DNA replication during sporulation in *Myxococcus xanthus* fruiting bodies. *Proceedings of the National Academy of Sciences of the United States of America*, *102*(40), 14428-14433. doi: 10.1073/pnas.0506969102.

Vasa, S., Lin, L., Shi, C., Habenstein, B., Riedel, D., Kühn, J., Thanbichler M., & Lange, A. (2015). β-helical architecture of cytoskeletal bactofilin filaments revealed by solid state NMR. *Proceedings of the National Academy of Sciences of the United States of America, 112*(2), E127-E136. doi: 10.1073/pnas.1418450112.

Veit M, Schmidt MF. (2006) Palmitoylation of influenza virus proteins. *Berliner und Münchner Tierärztliche Wochenschrift*. *119*(3-4), 112-122. PMID: 16573201.

Verhaegen, M., & Christopoulos, T. K. (2002). Recombinant *Gaussia* luciferase. Overexpression, purification, and analytical application of a bioluminescent reporter for DNA hybridization. *Analytical Chemistry*, *74*(17), 4378–4385. https://doi.org/10.1021/ac025742k.

Verstraeten, N., Fauvart, M., Versées, W., & Michiels, J. (2011). The universally conserved prokaryotic GTPases. *Microbiology and Molecular Biology Reviews*, *75*(3), 507–542. https://doi.org/10.1128/mmbr.00009-11.

Vetter, I. R., & Wittinghofer, A. (2001). The guanine nucleotide-binding switch in three dimensions. *Science*, *294*(5545), 1299–1304. https://doi.org/10.1126/science.1062023.

Villalobos, V., Naik, S., & Piwnica-Worms, D. (2007). Current state of imaging protein-protein interactions in vivo with genetically encoded reporters. *Annual Review of Biomedical Engineering*, *9*, 321–349. https://doi.org/10.1146/annurev.bioeng.9.060906.152044.

Vizoso Pinto, M. G., Villegas, J. M., Peter, J., Haase, R., Haas J, Lotz, A. S., Muntau, A. C., & Baiker, A. (2009). LuMPIS–a modified luminescence-based mammalian interactome mapping pull-down assay for the investigation of protein-protein interactions encoded by GC-low ORFs. *Proteomics*, *9*(23), 5303–5308. https://doi.org/10.1002/pmic.200900298.

Waite D. W., Chuvochina M., Pelikan C., Parks D. H., Yilmaz P., Wagner M., Loy A., Naganuma T., Nakai R., Whitman W. B., Hahn M. W., Kuever J., & Hugenholtz P. (2020). Proposal to reclassify the proteobacterial classes *Deltaproteobacteria* and *Oligoflexia*, and the phylum *Thermodesulfobacteria* into four phyla reflecting major functional capabilities. *International Journal of Systematic and Evolutionary Microbiology*, *70*(11), 5972–6016. https://doi.org/10.1099/ijsem.0.004213.

Wang, J., Menon, S., Yamasaki, A., Chou, H. T., Walz, T., Jiang, Y., & Ferro-Novick, S. (2013). Ypt1 recruits the Atg1 kinase to the preautophagosomal structure. *Proceedings of the National Academy of Sciences of the United States of America*, *110*(24), 9800–9805. https://doi.org/10.1073/pnas.1302337110.

Wang, Y., Huynh, W., Skokan, T. D., Lu, W., Weiss, A., & Vale, R. D. (2019). CRACR2a is a calcium-activated dynein adaptor protein that regulates endocytic traffic. *Journal of Cell Biology*, *218*(5), 1619–1633. https://doi.org/10.1083/jcb.201806097.

Ward, M. J., Lew, H., & Zusman, D. R. (2000). Social motility in *Myxococcus xanthus* requires FrzS, a protein with an extensive coiled-coil domain. *Molecular Microbiology*, *37*(6), 1357–1371. https://doi.org/10.1046/j.1365-2958.2000.02079.x.

Weinmann, H., & Ottow, E. (2007) 7.09-Recent development in novel anticancer therapies. In

J. B. Taylor, and D. J. Triggle (Eds.), *Comprehensive Medicinal Chemistry II* (pp. 221–251); Elsevier. https://doi.org/10.1016/B0-08-045044-X/00210-8.

Weiss, V. H., McBride, A. E., Soriano, M. A., Filman, D. J., Silver, P. A., & Hogle, J. M. (2000). The structure and oligomerization of the yeast arginine methyltransferase, Hmt1. *Nature Structural Biology*, *7*(12), 1165–1171. https://doi.org/10.1038/82028.

Wennerberg, K., & Der, C. J. (2004). Rho-family GTPases: It's not only Rac and Rho (and I like it). *Journal of Cell Science*, *117*(8), 1301–1312. https://doi.org/10.1242/jcs.01118.

Wennerberg, K., Rossman, K. L., & Der, C. J. (2005). The Ras superfamily at a glance. *Journal of Cell Science*, *118*(5), 843–846. https://doi.org/10.1242/jcs.01660.

Whitworth, D. E., Millard, A., Hodgson, D. A., & Hawkins, P. F. (2008). Protein-protein interactions between two-component system transmitter and receiver domains of *Myxococcus xanthus*. *Proteomics*, *8*(9), 1839–1842. https://doi.org/10.1002/pmic.200700544.

Widder, E. A. (2010). Bioluminescence in the ocean. *Science*, *704*(5979), 704–708. http://www.sciencemag.org/cgi/doi/10.1126/science.1174269.

Wilson, T., & Hastings, J. W. (1998). Bioluminescence. *Annual Review of Cell and Developmental Biology*, *14*, 197–230. https://doi.org/10.1146/annurev.cellbio.14.1.197.

Wittinghofer, A., & Vetter, I. R. (2011). Structure-function relationships of the G domain, a canonical switch motif. *Annual Review of Biochemistry*, *80*, 943–971. https://doi.org/10.1146/annurev-biochem-062708-134043.

Wolgemuth C., Hoiczyk E., Kaiser D., & Oster G. (2002). How myxobacteria glide. *Current Biology 12*, 369-377. doi: 10.1016/s0960-9822(02)00716-9.

Wood, K.V. 1991. Recent advances and prospects for use of beetle luciferases as genetic

reporters. In P. E. Stanley, & J Kricka (Eds.), *Bioluminescence and Chemiluminescence: Current Status* (pp. 543-546). John Wiley & Sons. https://doi.org/10.1002/bio.1170070108.

Wright, L. P., & Philips, M. R. (2006). CAAX modification and membrane targeting of Ras. *Journal of Lipid Research*, *47*(5), 883–891. https://doi.org/10.1194/jlr.R600004-JLR200.

Wuichet, K., & Søgaard-Andersen, L. (2014). Evolution and diversity of the ras superfamily of small GTPases in prokaryotes. *Genome Biology and Evolution*, *7*(1), 57–70. https://doi.org/10.1093/gbe/evu264.

Yamaguchi, Y., Sakai, E., Okamoto, K., Kajiya, H., Okabe, K., Naito, M., Kadowaki, T., & Tsukuba, T. (2018). Rab44, a novel large Rab GTPase, negatively regulates osteoclast differentiation by modulating intracellular calcium levels followed by NFATc1 activation. *Cellular and Molecular Life Sciences*, *75*(1), 33–48. https://doi.org/10.1007/s00018-017-2607-9.

Yang, R., Bartle, S., Otto, R., Stassinopoulos, A., Rogers, M., Plamann, L., & Hartzell, P. (2004). AglZ is a filament-forming coiled-coil protein required for adventurous gliding motility of *Myxococcus xanthus*. *Journal of Bacteriology*, *186*(18), 6168–6178. https://doi.org/10.1128/JB.186.18.6168-6178.2004.

Yu, R., & Kaiser, D. (2007). Gliding motility and polarized slime secretion. *Molecular Microbiology*, *63*(2), 454-467. doi: 10.1111/j.1365-2958.2006.05536.x.

Zerial, M., & McBride, H. (2001). Rab proteins as membrane organizers. *Nature Reviews Molecular Cell Biology*, *2*(2), 107–117. https://doi.org/10.1038/35052055.

Zhang, L., Ramijan, K., Carrión, V. J., van der Aart, L. T., Willemse, J., van Wezel, G. P., & Claessen, D. (2021). An alternative and conserved cell wall enzyme that can substitute for

the lipid ii synthase murg. *MBio*, *12*(2). https://doi.org/10.1128/mBio.03381-20.

Zhang, Y., Franco, M., Ducret, A., & Mignot, T. (2010). A bacterial ras-like small GTP-binding protein and its cognate GAP establish a dynamic spatial polarity axis to control directed motility. *PLoS Biology*, *8*(7), 1–12. https://doi.org/10.1371/journal.pbio.1000430.

Zhang, Y., Guzzo, M., Ducret, A., Li, Y. Z., & Mignot, T. (2012). A dynamic response regulator protein modulates G-protein-dependent polarity in the bacterium *Myxococcus xanthus*. *PLoS Genetics*, *8*(8). https://doi.org/10.1371/journal.pgen.1002872.

Zhu, G., Chen, J., Liu, J., Brunzelle, J. S., Huang, B., Wakeham, N., Terzyan, S., Li, X., Rao, Z., Li, G., & Zhang, X. C. (2007). Structure of the APPL1 BAR-PH domain and characterization of its interaction with Rab5. *EMBO Journal*, *26*(14), 3484–3493. https://doi.org/10.1038/sj.emboj.7601771.

Zuckerman, D. M., Boucher, L. E., Xie, K., Engelhardt, H., Bosch, J., & Hoiczyk, E. (2015). The bactofilin cytoskeleton protein BacM of *Myxococcus xanthus* forms an extended β-sheet structure likely mediated by hydrophobic interactions. *PLoS ONE*, *10*(3), 1–25. https://doi.org/10.1371/journal.pone.0121074.

Zusman, D. R., Scott, A. E., Yang, Z., & Kirby, J. R. (2007). Chemosensory pathways, motility and development in *Myxococcus xanthus*. *Nature Reviews Microbiology*, *5*(11), 862–872. https://doi.org/10.1038/nrmicro1770.